

# **The impact of tides and mass transfer on the evolution of metal-poor massive binary stars**

Dissertation  
zur  
Erlangung des Doktorgrades (Dr. rer. nat.)  
der  
Mathematisch-Naturwissenschaftlichen Fakultät  
der  
Rheinischen Friedrich-Wilhelms-Universität Bonn

vorgelegt von  
**Pablo Marchant Campos**  
aus  
Santiago, Chile

Bonn 2017

Angefertigt mit Genehmigung der Mathematisch-Naturwissenschaftlichen Fakultät der Rheinischen Friedrich-Wilhelms-Universität Bonn

1. Gutachter: Prof. Dr. Norbert Langer  
2. Gutachter: Prof. Dr. Thomas Tauris

Tag der Promotion: 9.6.2017  
Erscheinungsjahr: 2018

# Abstract

---

Stars more massive than  $10M_{\odot}$ , although few in number compared to objects like our sun, play a very large role in the evolution of the universe. Through strong winds and supernovae they enrich the interstellar medium with heavy elements and provide mechanical feedback on galactic scales. Their large flux of ionizing photons may dominate the reionization of the universe. A thorough understanding of massive stellar evolution is then paramount to our understanding of the universe.

In the last years, observations have established that binary interaction is a fundamental part of the evolution of massive stars, most of which will undergo mass exchange with a nearby companion. In addition, the recent detection of gravitational waves from the merger of two  $\sim 30M_{\odot}$  black holes opens up exciting new possibilities to improve our understanding of the evolution of massive stars. To this purpose, we have extended the open-source stellar evolution code MESA to include the necessary physics to model binary systems. This new version of MESA allows us to explore in detail the parameter space of massive and very massive binary stars.

The first problem we consider involves the evolution of very massive stars orbiting each other with periods of a few days. Owing to tidal locking, both components are fast rotators, which induces large scale mixing throughout their radiative envelopes. The stars then evolve chemically homogeneously, burning all their available nuclear fuel instead of developing a core envelope structure. This modifies their evolution dramatically: Instead of expanding significantly, these stars contract inside their Roche lobes to eventually form a pair of close black holes of similar mass that can merge in less than a Hubble time. For the design sensitivity of advanced LIGO, we expect  $\sim 20 - 900$  detections per year from this channel, with the large uncertainty arising from uncertainties in the chemical evolution of the universe. Owing to a range of very massive stars exploding as pair instability supernovae rather than forming a black hole, we expect to detect a gap in the distribution of black hole masses between  $60M_{\odot}$  and  $130M_{\odot}$ .

Considering similar systems for which the secondary component is significantly less massive, we show that only the more massive star evolves homogeneously to become a black hole. On a longer timescale, the secondary expands and initiates mass transfer to the compact object, which makes it active as an X-ray source. Owing to their large black hole masses (in excess of  $20M_{\odot}$ ), these X-ray binaries would have luminosities characteristic of those of observed ultra-luminous X-ray sources, which are difficult to explain through standard stellar evolution. The occurrence of pair-instability supernovae, just as was the case for binary black holes, produces a gap in black hole masses, which could be observable as a gap in the luminosity distribution of ultra-luminous sources. Our simulations show a strong metallicity dependence, and future X-ray surveys such as eROSITA could potentially test our claims.

Finally, we modelled a large set of binary and single models of massive stars to study the population of objects in the LMC. Under extreme assumptions that minimize the contribution of binaries to our sample, we show that the large observed binary fraction inescapably implies a degeneracy between the predictions of rotational mixing in single stars and mass transfer in binaries. Binaries with low transfer efficiencies explain observed rapidly rotating stars with low nitrogen enrichment at their surfaces, but still undergo mixing and a slight enrichment in nitrogen. Accurate measurements of the abundances of rapid rotators could then provide valuable information on the efficiency of rotational mixing.

Throughout this thesis we have extensively demonstrated the use of detailed stellar evolution models to cover the wide parameter space of single and binary stellar evolution in a statistically significant way. This new capability is certain to enable many new venues of research.

# Contents

---

<b>1</b>	<b>Introduction</b>	<b>1</b>
1.1	Single stars . . . . .	3
1.1.1	Post main-sequence evolution and final fates of stars . . . . .	7
1.1.2	Current developments in the evolution of massive stars . . . . .	9
1.2	Binary stars . . . . .	16
1.2.1	Current observations of massive binaries . . . . .	18
1.2.2	Mass transfer in binary systems . . . . .	20
1.3	The dawn of gravitational wave astronomy . . . . .	22
1.3.1	Identifying the progenitors of merging stellar-mass black holes . . . . .	25
1.4	This thesis . . . . .	27
1.4.1	The formation of merging binary black holes . . . . .	27
1.4.2	Models for ultra-luminous X-ray sources . . . . .	28
1.4.3	The evolution of binaries in the Large Magellanic Cloud . . . . .	28
<b>2</b>	<b>Modules for Experiments in Stellar Astrophysics (MESA): Binaries, Pulsations, and Explosions</b>	<b>29</b>
2.1	Initialization of a Circular Binary System . . . . .	31
2.2	Evolution of Orbital Angular Momentum . . . . .	31
2.2.1	Gravitational Wave Radiation . . . . .	31
2.2.2	Mass Loss . . . . .	32
2.2.3	Spin Orbit Coupling . . . . .	32
2.2.4	Magnetic Braking . . . . .	33
2.3	Mass Transfer from RLOF . . . . .	33
2.3.1	Explicit Methods . . . . .	34
2.3.2	Implicit Methods . . . . .	35
2.4	Effect of Tides and Accretion on Stellar Spin . . . . .	36
2.5	Treatment of Thermohaline Mixing in Accreting Models . . . . .	36
2.6	Numerical Tests . . . . .	37
2.6.1	Gravitational Wave Radiation . . . . .	37
2.6.2	Inefficient Mass Transfer . . . . .	37
2.6.3	Spin Orbit Coupling . . . . .	37
2.6.4	Thermal Response to Mass Loss . . . . .	38
2.7	Period Gap of Cataclysmic Variables . . . . .	39
2.8	Evolution of Massive Binaries . . . . .	41
2.9	Rotating Binaries and the Efficiency of Mass Transfer . . . . .	43
2.10	Description of a Binary Run . . . . .	45

<b>3 A new route towards merging massive black holes</b>	<b>47</b>
3.1 Methods . . . . .	49
3.1.1 Physics implemented in MESA and initial parameters . . . . .	49
3.1.2 Computing massive overcontact systems . . . . .	50
3.2 Results . . . . .	51
3.2.1 Exemplary MOB evolution . . . . .	51
3.2.2 Example grid . . . . .	51
3.2.3 Final binary configurations . . . . .	52
3.2.4 Mass distribution and mass ratios . . . . .	55
3.2.5 Merger delay times . . . . .	56
3.2.6 Observational counterparts . . . . .	58
3.2.7 Spins . . . . .	58
3.2.8 Models up to core collapse . . . . .	59
3.2.9 Explosive mass loss and momentum kicks . . . . .	59
3.3 Merger rates . . . . .	61
3.3.1 Chirp masses and MOB evolution . . . . .	61
3.3.2 Model assumptions for estimating aLIGO detection rates . . . . .	63
3.3.3 Accounting for the star-forming history and the galactic metallicity distribution throughout the Universe . . . . .	63
3.3.4 Resulting predictions for aLIGO detection rates . . . . .	64
3.4 Concluding remarks . . . . .	65
<b>4 Ultra-luminous X-ray sources and neutron-star–black-hole mergers from close very massive binaries at low metallicity</b>	<b>67</b>
4.1 Methods . . . . .	70
4.1.1 The Eddington limit for accretion to a BH . . . . .	73
4.2 Formation of ULXs through CHE . . . . .	74
4.2.1 Mass-ratio dependence . . . . .	76
4.2.2 The impact of metallicity on the properties of ULXs . . . . .	79
4.3 Luminosity distribution function of ULXs . . . . .	81
4.3.1 Luminosity distribution at redshift $z = 0$ . . . . .	85
4.3.2 Galactic $L_X$ – SFR relation at low metallicities . . . . .	87
4.4 Orbital parameters of ULXs formed through CHE . . . . .	87
4.5 NS-BH and BH-BH binaries after a ULX phase . . . . .	91
4.5.1 Rate estimates for NS-BH and BH-BH mergers . . . . .	94
4.6 Conclusions . . . . .	97
<b>5 Surface abundances and spins of massive stars in interacting binary systems</b>	<b>101</b>
5.1 Methods . . . . .	103
5.1.1 Comparison to the models of Brott, de Mink et al. (2011) . . . . .	104
5.1.2 Overshooting limitation . . . . .	107
5.1.3 Rotationally enhanced winds and mass transfer efficiency . . . . .	107
5.1.4 Contact systems . . . . .	111
5.2 Estimating the impact of binaries . . . . .	113
5.2.1 Pre-interaction binaries . . . . .	114
5.2.2 Mergers . . . . .	115
5.2.3 Post-interaction . . . . .	117

5.2.4	Comparing the effect of different assumptions . . . . .	119
5.3	Evolutionary properties of the binary models . . . . .	119
5.4	Rotation and nitrogen enhancement . . . . .	122
5.4.1	Single stars . . . . .	122
5.4.2	Binary stars . . . . .	122
5.4.3	Expected properties of apparent single stars . . . . .	125
5.5	Summary and Conclusions . . . . .	127
<b>6</b>	<b>Outlook</b>	<b>129</b>
<b>A</b>	<b>Dynamical implications of black hole kicks</b>	<b>131</b>
<b>B</b>	<b>Comparison to the standard BH+BH formation scenario</b>	<b>135</b>
<b>C</b>	<b>Grids of binary models leading to ULXs</b>	<b>139</b>
<b>D</b>	<b>Properties of ULXs</b>	<b>151</b>
<b>E</b>	<b>Grids of LMC binary models</b>	<b>157</b>
<b>Acknowledgements</b>		<b>171</b>
<b>Bibliography</b>		<b>173</b>



# CHAPTER 1

---

## Introduction

---

*I always thought they were balls of gas  
burning billions of miles away*

Pumbaa, The lion king

In modern times we have it pretty easy. With just a couple of finger swipes, it only takes a few seconds for us to find our position in the world and the moment of the year to within a precision of meters and seconds respectively. Surely we can figure out many things without such a technological aid; most adults are aware that the duration of a day depends on the season (though you could be forgiven for not knowing that if you live near the equator), and that the Sun sets and rises from more or less west and east respectively. But for any degree of accuracy in measuring time or directions we rely on technology. In the absence of such tools, humanity relied on the stars, which appeared as a fixed set of patterns with an extremely reliable yearly variation. Around the year 3000 BCE the ancient Egyptians awaited for the moment of the year when Sirius became visible just before dawn, which preceded the yearly flooding of the Nile. Homer's "The Odyssey" clearly refers to the usage of the big dipper as a compass. In ancient cultures surrounding the world, the skies are filled with a multitude of heroes and myths, acting as helpful tools to recognize them and as reminders of their importance.

Greek astronomers were satisfied with this picture of the firmament as a fixed and immutable set of patterns. The Aristotelian and Ptolemaic models of the universe differed in their explanations for the motion of the Sun and the planets, but in both the stars were fixed to the inside of a hollow sphere that surrounded it all. One of the strongest arguments for a geocentric universe came from the lack of a yearly modulation in the relative positions of stars, which would result from the yearly movement of the Earth around the Sun. At the time, the upper limits set on this stellar parallax would place the stars in a heliocentric model at extremely far away distances, which were unthinkable back then. Ptolemy's model, recorded in his "Almagest" in the year ~ 150 CE, went on to be the generally accepted one throughout the middle ages. This picture of a static universe slowly changed through the centuries, the oldest record of observation of a supernova, which we now know results from the explosion of a massive star at the end-point of its evolution, was made by Chinese astronomers in 185 CE. The Chinese went on to record



Figure 1.1: Stamp issued by the german federal post office to celebrate the observation of dark lines in the spectrum of the Sun by Joseph Fraunhofer. The upper panel shows the relative intensity of light at different colors, as estimated by Fraunhofer, 1817. By designing precise spectrographs Fraunhofer was able to identify more than 500 hundred distinct dark lines in the solar spectrum, and measured the wavelengths of some of the strongest features observable, which are known as the Fraunhofer lines (marked with upper and lower case letters from A to H in the Figure).

many instances of such guest stars (D. H. Clark and Stephenson, 1982), and the two supernovae events in 1006 and 1054 were observed throughout the world by Chinese, Arab and Japanese astronomers. These new stars would brighten in a timescale of days and take months to fade, but during this time they still remained as fixed points relative to other stars.

It would take many more centuries to observe the relative changes in the position of the stars. In 1718, Edmund Halley took advantage of the historical records present in the “Almagest” to determine that in a period of approximately 1800 years the stars Sirius, Arcturus and Aldebaran had been displaced by almost half a degree (a copy of Halley’s original paper can be found in Aitken, 1942). Improvements in telescope technology brought ever more precise measurements of the positions and the movement of stars, and during the late 18th century William Herschel undertook a massive, decades-long effort to study precisely the proper motions of multiple objects. After careful study, he determined from the motion of a pair of stars, which included Castor in the Gemini constellation, that they formed part of a binary system, orbiting each other as a consequence of their mutual gravitational interaction (Herschel, 1803). The very long orbital period of this system meant that he could only observe a fraction of a full orbit, which he estimated took 342 years in total, not far from the modern value of 420 years (Rabe, 1958). The first measurement of stellar parallax was performed by Friedrich Bessel in 1838 for the star 61 Cygni, from which he concluded concluded that it was located at a distance of approximately 10 light years (Bessel, 1838), about 600 000 times the distance between the Earth and the Sun. Measurements like this had an enormous impact in our understanding of the scale of the universe, but astrometry by itself would prove insufficient to understand the inner workings of stars.

Our main source of information on stars, and the only one at disposal before the 20th century, was the measurement of the light they emit. As methods were devised to separate starlight into its different colors, and perform precise measurements on the resulting spectrum, we started to understand the composition of stars. The first observation of dark lines in the solar spectrum is attributed to William Wollaston in 1802.

Joseph Fraunhofer, who independently discovered these same features, undertook the task of carefully studying and measuring these dark lines (see Figure 1.1). He went on to study stellar spectra, finding that many features present in the Sun could be observed in other stars, as well as additional lines that were not seen in the Sun (Fraunhofer, 1823). Although Fraunhofer recognized that some features of the solar spectrum matched that of ordinary lamps, it was through the work of many scientists, including Léon Foucault, Julius Plücker, Robert Benson and Gustav Kirchhoff, that it was understood that dark lines were produced by the absorption of radiation from elements in the atmosphere of the Sun. By comparison with laboratory spectra, this established the presence in the Sun of elements such as hydrogen, iron and calcium among many others.

After his appointment as the director of the Harvard College Observatory in 1876, Edward Pickering pushed for the use of spectral measurements in the study of stars, and together with a large team of assistants, including Williamina Fleming, Annie Cannon and Antonia Maury, performed a large programme of observation and spectral classification of thousands of stars. This effort lead to the *Henry Draper (HD) Catalogue*, which included the classification of more than 200 000 stellar spectra and was completed in the year 1924. One of the products of this work was the creation of the Harvard classification system for stellar spectra (Cannon and Pickering, 1901), that defined a continuum of spectral types for which different lines and features progressively became more or less prominent. The letters OBAFGKM that they chose for the different types still remain in widespread use, with the sequence from O to M marking a switch from bluer to redder stars. These would play a large role in the development of the theory of stellar structure and evolution. Careful modeling of the physical processes resulting in dark lines also allowed the first measurements of the relative abundances of elements in stellar atmospheres, with the work of Cecilia Payne establishing that stars are mostly composed of hydrogen and helium (Payne, 1925).

## 1.1 Single stars

Owing to their apparent isolation with respect to each other, most of the early theoretical work on stars considered them as isolated objects. Our understanding of the evolution of single stars is typically compressed into five differential equations, each encompassing a clearly defined concept:

- Conservation of mass.
- Balance of forces.
- Energy generation.
- Energy transport.
- Changes in composition.

During the mid and late 19th century, when the theory of stellar structure and evolution slowly started to develop, many of the physical ingredients required to properly describe these processes were not yet known. The issue of energy generation is a prime example of this. In the context of Newtonian mechanics and thermodynamics, a natural explanation for its power source could be the release of gravitational energy as material falls to its surface. Lord Kelvin and Hermann von Helmholtz proposed in 1854 that no such external source was required, but rather the contraction of the Sun under its own gravity could serve this purpose. This implied that the expected timescale of evolution (known as the Kelvin-Helmholtz timescale) for the Sun would be of tens of millions of years, but this would come into conflict with

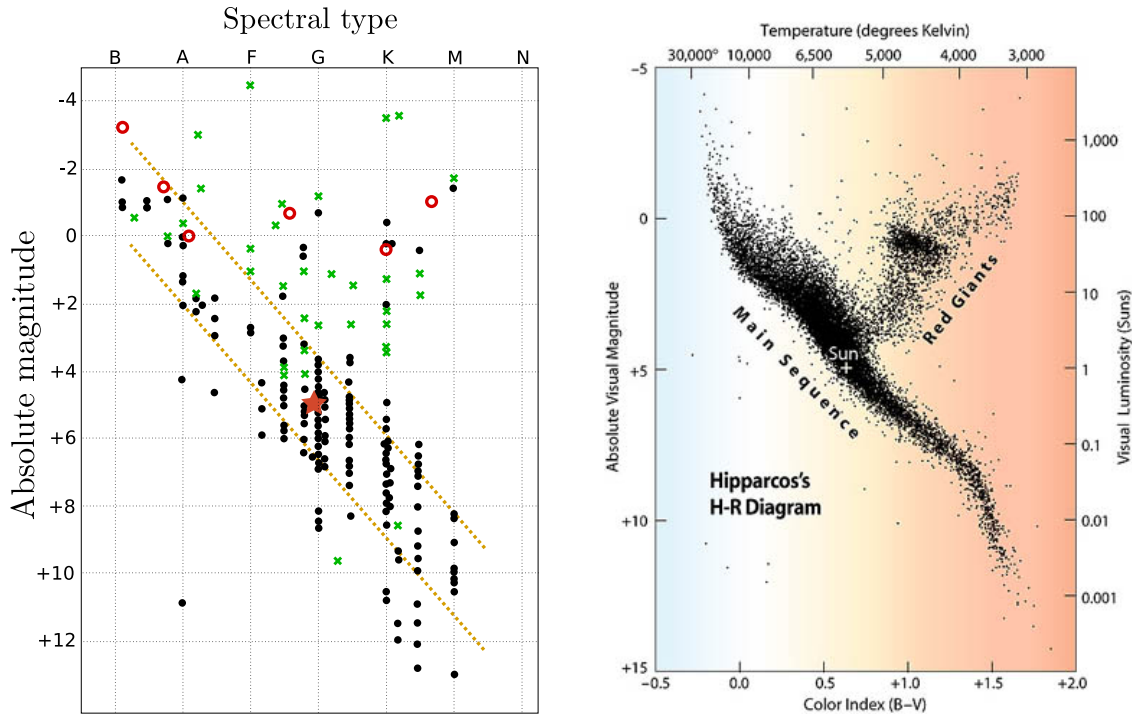


Figure 1.2: (left) Reproduction of the spectral-type vs magnitude plot of Russell (1914) for nearby stars with measured parallaxes at that time. The image has been edited for clarity, including the addition of a red star that marks the approximate position of the Sun. Black dots are for stars where the parallax had a reasonable error (less than 42% of the total), while crosses where for objects with larger errors, which implies a large error in the estimate of their magnitude. Empty circles are averages of values of stars with similar properties, but large errors in their parallaxes. (right) A modern version of this diagram, using data from stars with parallaxes measured by the Hipparcos satellite. In this figure the x-axis is the color-index of each object, which is closely related to their stellar type (Credit: Michael Perryman).

radioactive dating of the age of the earth. An additional energy source, arising from yet unknown physical processes, was required.

Newtonian physics were however appropriate to describe conservation of mass and force balance. As most stars shine steadily through the years with minimal changes in their luminosities, they are expected to be in mechanical equilibrium, with the force of gravity being precisely compensated by the pressure gradient of the fluid. Homer Lane and Robert Emden were among the first that used the correct equations for these concepts which they applied with varying degrees of success to attempt to explain the properties of the Sun (Emden, 1907). It was around this time that Ejnar Hertzsprung and Henry Norris Russell independently developed the color-magnitude and the spectral type-magnitude diagrams respectively (Hertzsprung, 1911; Russell, 1914), two closely related diagrams that paved the way for further theoretical work. Figure 1.2 shows an example of one of the diagrams published by Russell for nearby stars with measured parallaxes, together with a modern rendition of the same diagram using data from the Hipparcos satellite. In this figure, most stars reside in a strip, where stars of bluer spectral types have higher luminosities than the redder ones. Explaining the nature of this strip, which was named the main sequence, and how stars evolved through the Hertzsprung-Russell diagram would be one of the earlier successes in the theory of stellar evolution.

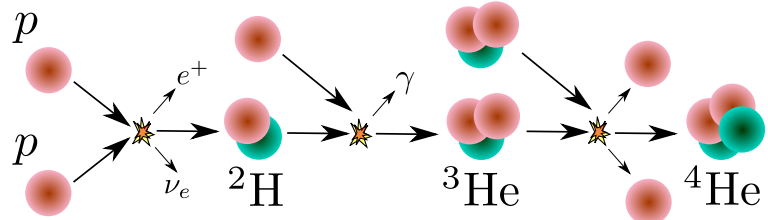
The work of sir Arthur Stanley Eddington was fundamental for this. Earlier on it was believed that

convection, where large blobs of material can travel large distances as is the case with boiling water, could be the main mechanism for energy to be transported outwards from the stellar core, but Karl Schwarzschild showed in 1906 that convection could only happen under very specific conditions. The idea of radiative diffusion, where photons slowly diffused outwards through the opaque material of the star, was first studied by Ralph Sampson (Sampson, 1895), but it was Eddington who pushed strongly for this concept and put it in a firm theoretical ground (Eddington, 1916), as well as describing some of the main sources of opacity. Eddington also correctly guessed that the main source of energy in stars stemmed from the formation of helium from hydrogen atoms. At the time it was thought that helium was formed by four hydrogen atoms bound together with two electrons, but the mass of a helium atom was known to be slightly below that of four hydrogen atoms. The concept of mass-energy equivalence, encapsulated in the formula  $E = mc^2$ , had recently been proposed by Einstein in his special theory of relativity. Considering this, Eddington argued that if hydrogen atoms were in fact merged together to form helium, the energy released by the resulting mass deficiency could potentially power the Sun for much longer than pure gravitational energy as was proposed by Kelvin and Helmholtz (Eddington, 1920). The work of Eddington resulted in the fundamental equations of stellar structure that describe the five concepts listed above, but still required an understanding of the properties of matter at very high temperatures and pressures, as well as the details on how hydrogen could actually be fused into helium.

With further advances in quantum and atomic physics, two distinct processes, depicted in Figure 1.3, were recognized to turn hydrogen into helium. This came during the late 1930s as a result of the work of, among others, Robert Atkinson, Carl von Weizsäcker, Hans Bethe and Charles Critchfield, and the recognition of the importance of weak interactions was fundamental. One of these processes, the proton-proton chain, more-or less resembled the picture of Eddington of putting four hydrogen atoms together. The CNO chain worked instead by adding protons to heavier nuclei until a helium atom is released at one point, using carbon, nitrogen and oxygen as a catalyst for this reaction. The proton-proton chain would be found to operate in low-mass stars, with masses similar or below that of the Sun ( $M \lesssim 1.5M_\odot$  where  $M_\odot$  is the mass of the Sun), while the more massive stars were powered by the CNO chain. With this in place, Fred Hoyle and Raymond Littleton could develop fundamental relationships, known as homology relationships, from which most of the structure of the main sequence in the Hertzsprung-Russel diagram could be well understood. Objects in this band were found to correspond to stars slowly burning hydrogen into helium at their cores, with more massive stars being bluer and significantly brighter than their lower mass counterparts. This increase in brightness was so steep, that the most massive stars would have lifetimes in the order of millions of years, compared to several billion years for stars like our Sun.

The burning of hydrogen was still a finite source of energy, and understanding stellar evolution after the main sequence would prove very challenging. Among the many assumptions made by Eddington in order to compute solutions to the equations of stellar structure, was that of homogeneous evolution, where stars could potentially burn all their hydrogen content thanks to strong mixing through the star, with rotation being a probable candidate as the source of this mixing. This idea fell out of favor as evidence piled up that red giants, the second most prominent feature in the Hertzsprung-Russell diagrams of Figure 1.2, were likely the product of an inhomogeneous structure (Öpik, 1938; Schönberg and Chandrasekhar, 1942). This, together with the introduction of much more complex atomic data which was needed for the development of precise models, resulted in purely analytical methods being insufficient to drive much more progress. As soon as computers became available, astrophysicists started to take full advantage of their potential. In 1952, Schwarzschild together with Alan Sandage performed detailed numerical calculations of stellar evolution in order to estimate the ages of stellar clusters (A. R. Sandage and Schwarzschild, 1952). The computation of stellar models would become a complex industry, with notable contributions at its beginnings from Louis Henyey, Icko Iben, Rudolf Kippenhahn and Robert Christy. The increasing quality of data on opacities and nuclear reactions (lead in part by developments on nuclear

## PP-I chain



## CNO cycle

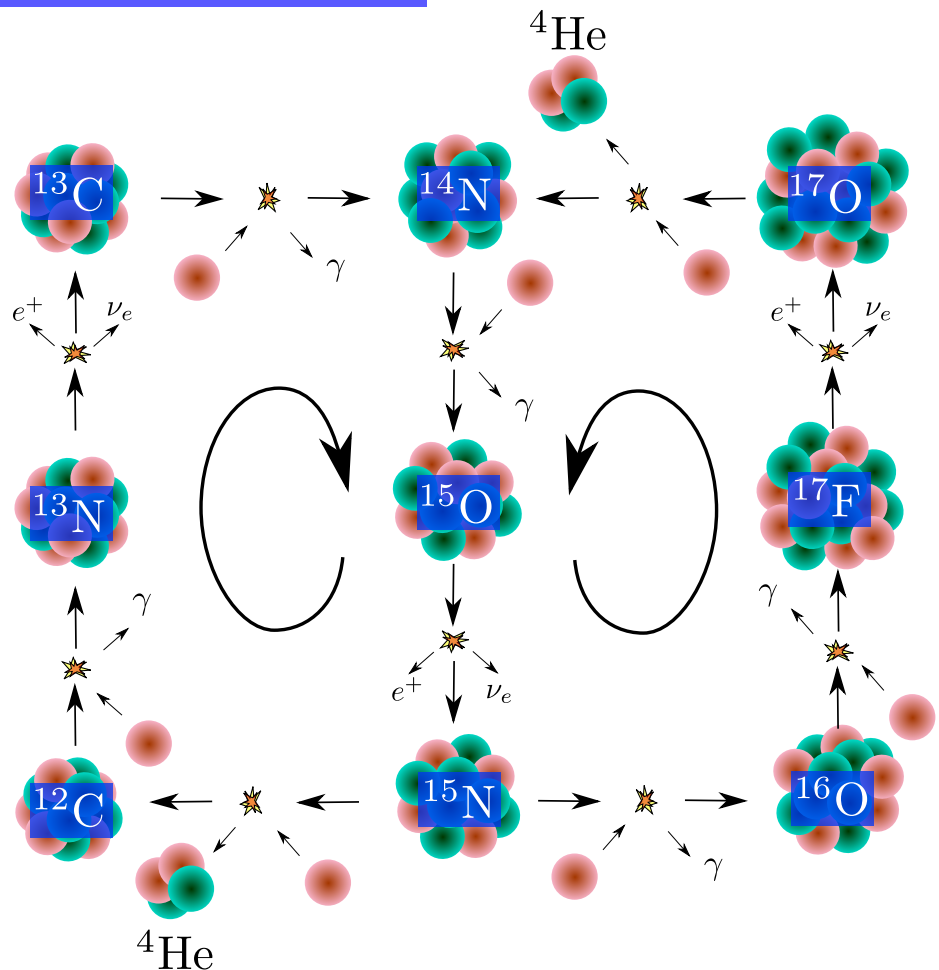


Figure 1.3: Main reactions involved in the proton-proton chain and the CNO cycle. The PP-chain is the main source of energy for low mass stars ( $M \lesssim 1.5M_\odot$ ), while hydrogen burning in more massive stars is dominated by the CNO cycle.

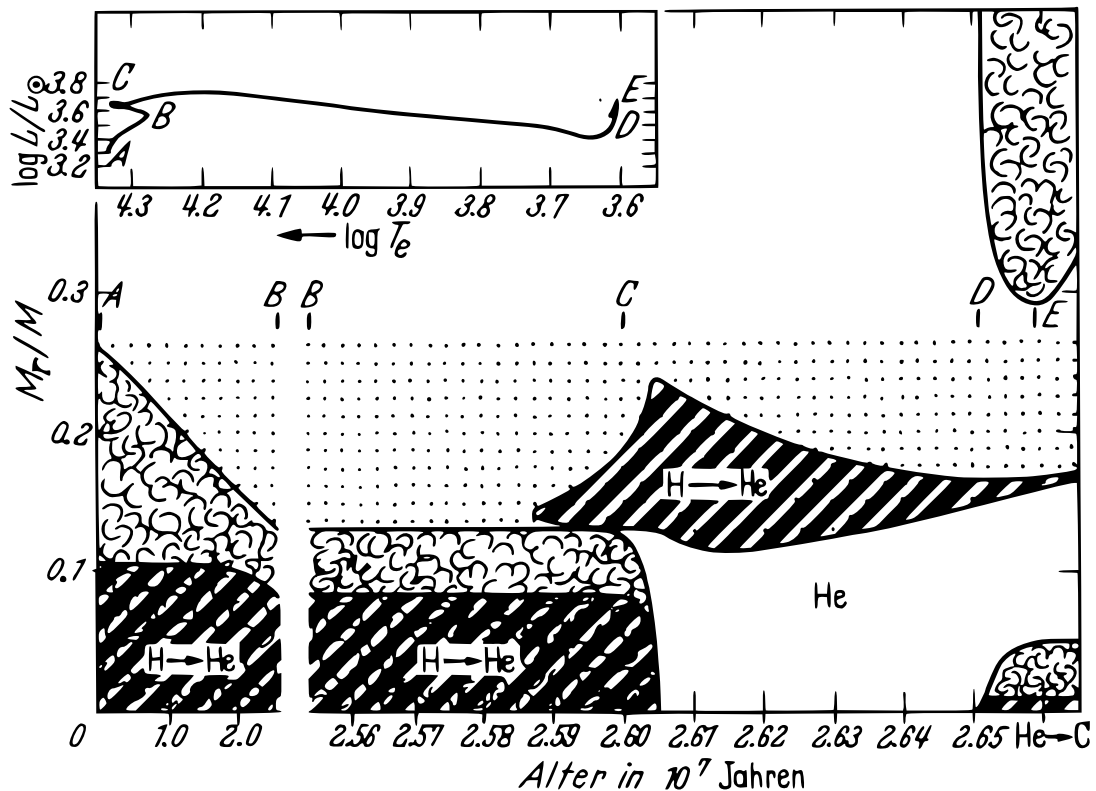


Figure 1.4: Evolution of the inner regions of a  $7M_{\odot}$  star from Hofmeister, Kippenhahn and Weigert (1964b). These diagrams, usually referred to as “Kippenhahn diagrams”, show the structure of a star (as a function of mass coordinate) against time, together with different regions where convective mixing and nuclear burning is occurring. “Cloudy” areas denote regions with convective mixing, while diagonal stripes mark regions where the energy generation rate from nuclear burning exceeds  $10^3 \text{ erg g}^{-1} \text{ s}^{-1}$ . The age of the star is given in units of  $10^7$  years, and the inset shows the evolution of the star in the Hertzsprung-Russell diagram.

weapons), together with exponential increases in computing power, would turn stellar astrophysics into a very precise science.

### 1.1.1 Post main-sequence evolution and final fates of stars

Calculations of stellar evolution, which became commonplace in the second half of the 20th century, are nicely summarized by so-called “Kippenhahn diagrams”, one of which is shown in Figure 1.4 depicting the evolution of a  $7M_{\odot}$  star, where  $M_{\odot}$  is the mass of the Sun. The results of these early simulations turned out to be pretty robust, with most of the fundamental processes described back then remaining in a firm basis up to this day. It was clearly established that stars burned hydrogen into helium in their cores, and after the depletion of this nuclear fuel the resulting helium cores would contract and hydrogen would begin to be burnt in a shell. As this happens, the hydrogen rich envelope would expand in response, resulting in much cooler temperatures and larger radii. These stars would then be the red giants that are observed in the Hertzsprung-Russell diagrams of Figure 1.2. During core hydrogen burning, stars with a mass similar to that of the Sun would have convective outer layers, and a core where radiative diffusion transports energy outwards during core hydrogen burning. Instead stars with masses  $\gtrsim 1.5M_{\odot}$  would have convective cores and radiative envelopes during this phase, as shown in Figure 1.4.

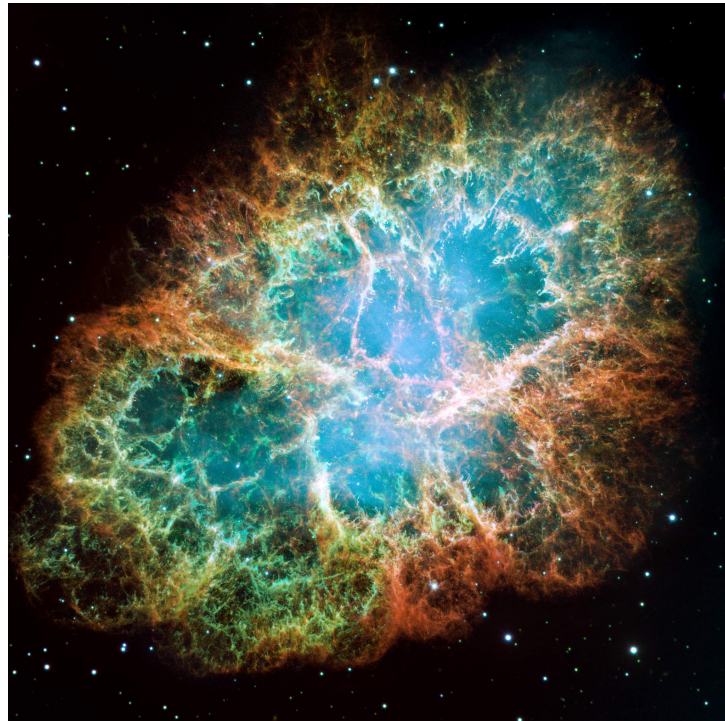


Figure 1.5: The crab supernova remnant, as observed by the Hubble telescope. This object resulted from the explosion of a massive star and was observed by Chinese astronomers in 1056 CE. Credit: NASA, ESA

The stellar model shown in Figure 1.4, although significantly more massive than the Sun and with important differences in its evolution, shares a similar fate at the end of its life. As its core contracts it will eventually start burning helium into carbon and oxygen (the end point in Figure 1.4). After the helium fuel is depleted, the core becomes inert, with stellar winds in the red giant branch slowly removing the outer layers and exposing it. This exposed core is known as a white dwarf (CO white dwarf in particular), and in the absence of an energy source it cools down and becomes less luminous. The first white dwarf discovered, *o*-Eridani, can in fact be seen as a clear outlier with a low magnitude and a spectral type A in the original diagram by Russell (Figure 1.2). Some of these objects were in binary systems, allowing an estimate of their masses, which lead Eddington to conclude that white dwarfs were very dense and compact, containing a mass comparable to that of the Sun but with a size comparable to the Earth (Eddington, 1924). Understanding these objects required further advances in both quantum mechanics and special relativity to describe the behavior of matter at such densities, which led to the conclusion that these stars were supported thanks to the pressure provided by electrons. Accounting for this Subrahmanyan Chandrasekhar discovered that there was a maximum mass to these objects, beyond which the pressure provided by the electrons could not compensate for its gravity (Chandrasekhar, 1931). This maximum mass is about  $1.46M_{\odot}$  and white dwarfs above it would not exist as they would be unstable and collapse under their own gravity.

For masses in excess of  $\sim 10M_{\odot}$ , nuclear burning does not stop at helium, with carbon, neon, oxygen and silicon burning phases occurring one after the other. Eventually, the core of the star is turned into iron, which unlike lighter elements consumes energy when fused into heavier elements. Lacking an energy source, but having a mass in excess of that allowable for a white dwarf, the core collapses, and depending on its mass it results either in a neutron star or a black hole. Neutron stars were first proposed

by Walter Baade and Fritz Zwicky (Baade and Zwicky, 1934a) shortly after the discovery of the neutron, and consist of material with a density comparable to that of atomic nuclei, so dense that an object with the mass of the Sun would have a radius in the order of 10 km! The main motivation of Baade and Zwicky was to explain the energetics of supernovae (a term also proposed by Baade and Zwicky 1934b), the same bright explosions observed nearly a millenia ago by chinese astronomers. If the core of a star would suddenly collapse to such a small radius, an enormous amount of energy would be produced, potentially disrupting the outer layers of the star. This results in beautiful supernovae remnants like the one shown in Figure 1.5, which is the result of the historical supernova observed by the chinese in 1056 CE.

The term “massive star” refers to objects with initial masses above the limit at which supernova can occur, although for high enough masses the star might not be able to form a neutron star. Just as there is an upper limit for the mass of white dwarfs, there is one for neutron stars (which is much more uncertain but expected to be less than  $3M_{\odot}$ ), and beyond this point there is no process capable of halting collapse. The result of this is a black hole, an object so dense that at a given radius called its horizon, even light cannot escape its gravitational pull. The existence of black holes was first proposed in 1783 by John Michell in the context of Newtonian physics, but a proper description required Einstein’s theory of general relativity and the work of Schwarzschild, who in 1916 described the solution to Einstein field equations exterior to a spherical mass distribution. Both Landau (1932) and Eddington (1935) argued against this picture of collapse to a singularity, believing that an additional force should be capable of halting collapse and the formation of an horizon. The issue of collapse was first studied in detail by Oppenheimer and Snyder (1939), but not much work was done until the late 50s (with this early work being summarized by Harrison et al., 1965). It was in this context that John Wheeler first coined the term “black hole” in a lecture in 1968.

### 1.1.2 Current developments in the evolution of massive stars

The general picture described so far had an enormous success in explaining many fundamental aspects of the physical universe. In the context of massive stars, their supernovae explain the synthesis of most of the heavy elements (Burbidge et al., 1957). Neutron stars were discovered by Antony Hewish and Jocelyn Bell owing to the emission of periodic pulses in radio wavelengths (Hewish et al., 1968), while the first black-hole candidates were discovered in binary systems in the early 70s (see Section 1.2 for details). It is now known as well that the high luminosities of massive stars should play an important role in the reionization of the universe (Haiman and Loeb, 1997), and that the energetic feedback of supernovae has a large impact in galactic evolution (Mac Low et al., 2005). Massive stars are usually referred to as “cosmic engines”, owing to the large impact they have in the universe.

Despite our wide knowledge of the inner workings of stars, there are still many unresolved points, and developments in the last few decades have shown important inconsistencies between observations and theory. A particular example of this is the case of supernova 1987A (usually referred to as SN1987A, see McCray 1993 for a review), which resulted from the explosion of a massive star in the Large Magellanic Cloud, a satellite galaxy of the Milky Way. Supernovae are uncommon events in the universe, and one of the reasons SN1987A was so interesting was its proximity, which allowed for an unprecedented case study. One of the expected products of core collapse and the production of a neutron star, was the emission of large amounts of neutrinos. Although a neutron star has not yet been observed at the location of SN1987A, the burst of neutrinos it produced was detected in Earth. However, SN1987A presented a clear difference with stellar models leading to supernovae explosions, as its progenitor star was found in archival data to be a blue supergiant at the moment of its explosion (Sonneborn, Altner and Kirshner, 1987). Instead, the general prediction from simulations of stellar evolution was that such an event would involve progenitors in the red supergiant branch.

Issues involving blue supergiant stars are not only related to the end states of stars though. Relative to the time it takes for a star to deplete hydrogen at its core, the transition from the main sequence to the red giant branch is expected to be a very fast process, making it unlikely to detect objects in between. But observations place a disproportionate amount of objects in this region of the Hertzsprung–Russell diagram (Fitzpatrick and Garmany, 1990; C. J. Evans, Lennon et al., 2006; Larsen et al., 2011). Regarding the ratio of blue to red-supergiants observations show that it increases with metallicity<sup>1</sup>, which is the opposite behaviour to that of stellar models (Langer and Maeder, 1995; Eggenberger, Meynet and Maeder, 2002). Another discrepancy between theory and observations comes from the measurement of stellar masses. For single stars, two different approaches exist for the measurement of stellar masses. Knowing the effective temperature and luminosity of a star, this can be matched to stellar evolution tracks at different masses to produce an “evolutionary” mass estimate. On the other hand, spectroscopic measurements also allow an estimate of the surface gravity of a star, which together with the stellar radius that can be computed from the effective temperature and the luminosity, allow for an independent “spectroscopic” mass estimate. However, these two mass estimates usually differ in a systematic way, with evolutionary estimates resulting in a higher mass than spectroscopic ones, and this constitutes what is known as the mass discrepancy problem (Herrero et al., 1992; Repolust, Puls and Herrero, 2004; Mokiem, de Koter, C. J. Evans et al., 2007; Martins, Mahy et al., 2012).

To sort out these problems, large and unbiased samples of massive stars are required, and in the last decade a significant improvement in this area was provided by the VLT-FLAMES survey (C. Evans et al., 2008) and the VLT-FLAMES Tarantula Survey (VFTS C. J. Evans, W. D. Taylor et al., 2011). The VFTS in particular studied the Tarantula nebula in the Large Magellanic Cloud (pictured in Figure 1.6), acquiring spectra for over 800 massive stars. Several extreme objects are present in this region, including the R136 open cluster which contains the most massive stars known (with estimated masses in excess of  $200M_{\odot}$  Crowther, Schnurr et al., 2010; Crowther, Caballero-Nieves et al., 2016), and the most massive overcontact system known, VFTS352 (Almeida, Sana, de Mink et al., 2015). Binarity, which we discuss in more detail in Section 1.2, has also been recognized to play a fundamental role, with the majority of massive stars being expected to form in a close binary that would undergo some form of interaction.

In the remainder of this Section we summarize some aspects of the evolution of massive stars for which significant uncertainties remain, and have a large impact on the predictions of stellar models. For a recent in-depth review, the reader can refer to Langer (2012).

## Mass loss

Mass loss has come to be recognized as a fundamental process that can significantly alter the evolutionary path that is followed by massive stars (for a recent review, see N. Smith, 2014). In particular, mass loss during the red giant phase can expose the helium core before core-collapse producing a hot and compact Wolf-Rayet star. These objects, which were discovered by Charles Wolf and Georges Rayet in 1864 exhibit strong emission lines in their spectra, which arise from strong optically thick winds which prohibit a direct observation of their surfaces. Figure 1.7 shows the expected phases that stars with different initial masses would follow. As mass loss exposes deeper regions of the star the ashes of different burning processes appear at its surface, resulting on the various WN, WC and WO types. To properly explain these phenomena, stellar evolution models require precise measurements of the mass loss rates of various objects.

The first detection of stellar winds in hot stars came from observations of ultraviolet radiation, which is absorbed by Earth’s atmosphere and thus required high altitude instruments. To do so, Morton (1967)

---

<sup>1</sup> The metallicity  $Z$  of a star describes what fraction of its surface composition consists of elements more massive than helium. Current measurements of the Sun indicate a metallicity of  $Z = 0.0142$  (Asplund et al., 2009)



Figure 1.6: Composite image of the Tarantula nebula in the large magellanic cloud, combining observations of the Hubble space telescope together with ground-based observatories. This region is an active place of star formation that provides us with a large sample of massive stars. Credit: NASA, ESA, ESO, D. Lennon (ESA/STScI), and the Hubble Heritage Team (STScI/AURA)

used a spectrograph on board of a rocket, and obtained the first clear sign of the presence of steady outflows. The physical mechanism driving these winds would be recognized to be the absorption of outgoing photons at specific frequencies by different ions in the atmospheres of these stars, which would provide an outwards acceleration (Lucy and Solomon, 1970; Castor, D. C. Abbott and Klein, 1975). Calculating the strength of these winds self-consistently is to this day extremely difficult, as it requires the careful consideration of thousands of spectral lines of different elements (Vink, de Koter and Lamers, 2001) and is expected to involve complex three-dimensional hydrodynamical phenomena such as clumping (Muijres et al., 2011). As this cannot be done in any practical way in stellar evolution calculations, simpler recipes calibrated to both observation and theory are normally used.

Mass loss rates after the main sequence are much more uncertain. For red supergiants the mechanism driving mass is still unclear (Bennett, 2010). Current estimates display large variations (De Beck et al., 2010; Mauron and Josselin, 2011), with Mauron and Josselin (2011) claiming that the formula of de Jager, Nieuwenhuijzen and van der Hucht (1988) still represents a good fit to the data, albeit with an additional metallicity dependence. At lower masses, for stars that evolve towards the Asymptotic Giant Branch, pulsations and dust formation are expected to play a fundamental role (Willson, 2000). Wolf-Rayet winds have radiation driven winds just as hot main sequence stars do, but are characterized by very high clumping (Moffat et al., 1988; Marchenko et al., 2007). Self-enrichment of carbon and oxygen in the most massive Wolf-Rayet stars can also modify the dependence with metallicity of stellar winds (Vink and de Koter, 2005). Although shorter lived, mass loss in these later phases increases significantly and has a very defining role in the end state of evolution of a star.

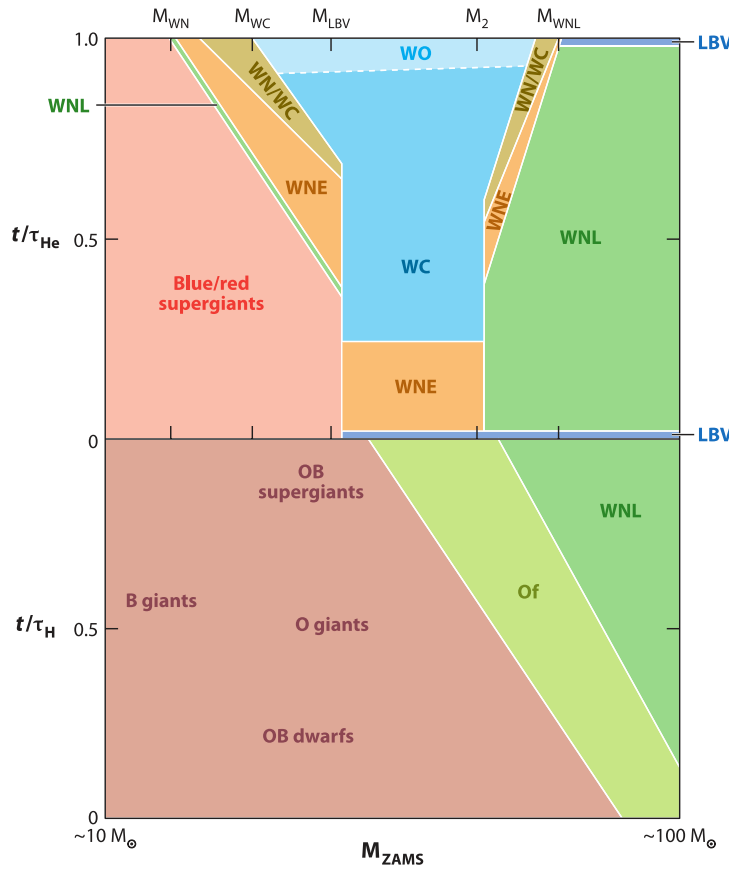


Figure 1.7: Schematic diagram showing the different phases of evolution of massive stars as a function of their initial mass. The lower half of the diagram indicates evolution during the main-sequence, while the upper half shows its evolution during the phase of core helium burning. Objects starting with the letter W denote different types of Wolf-Rayet stars, characterized by the presence of strong emission lines in their spectra which indicate the presence of an optically thick wind. Image reproduced from Langer (2012).

Very massive stars can also evolve to become luminous blue variables, objects that can experience large amounts of mass loss through violent outbursts. This is the case of  $\eta$  Carinae, a luminous blue variable which is estimated to have lost more than  $10 M_{\odot}$  in a violent outburst that was observed in 1827 (N. Smith, Gehrz et al., 2003). The efficiency with which these outbursts can remove mass is poorly constrained, but it is believed to be related to their extreme luminosities, as explained in the following Section.

### Inflation and the Eddington limit

It was first pointed out by Eddington that for very high luminosities, and depending on the opacity of the material through which radiation is diffusing, the force exerted by the outgoing radiation could exceed the gravitational pull of the star (Eddington, 1926). If this happens at some point in the interior of the star, then an inversion in density and gas pressure is required to preserve hydrostatic equilibrium (Joss, Salpeter and Ostriker, 1973). Modern opacity calculations by the OPAL (Iglesias and F. J. Rogers, 1996) and OP projects (Badnell et al., 2005) have shown that iron produces an important opacity peak at

temperatures of around 150 000 K. This effect reduces the efficiency of radiation diffusion in the very outer layers of massive stars, and is expected to result in convectively unstable regions not far from the stellar surface (Cantiello, Langer et al., 2009). For very hot Wolf-Rayet stars this peak is located close to the surface, and is likely related to their high mass loss rates (Gräfener and Hamann, 2008).

Simulations of very massive stars using these updated opacity values exhibit strong inflation, where the Eddington limit is reached at some point inside the envelope which expands significantly in response. At the metallicity of the Large Magellanic Cloud, stars with initial masses above  $40M_{\odot}$  are expected to have some degree of inflation (Sanyal et al., 2015). The extent of this inflation depends in large part in how efficiently can convection transport energy outwards, but mixing-length theory (Böhm-Vitense, 1958), which is the standard theory of convection applied in the calculation of stellar models, breaks down in this regime. Detailed three-dimensional simulations including the physics of radiative transfer show a complex interplay between radiation and gas dynamics, which cannot be captured in a one-dimensional simulation of stellar evolution (Jiang et al., 2015). The approach to the Eddington limit is also believed to be very important in driving strong stellar winds (N. J. Shaviv, 2001; Owocki, Gayley and N. J. Shaviv, 2004; Gräfener, Vink et al., 2011; Bestenlehner et al., 2014), and potentially power the strong outbursts observed in luminous blue variables (Gräfener, Owocki and Vink, 2012; Sanyal et al., 2015).

### Convective mixing

The most efficient mixing process acting in stars is convection. Operating on a dynamical timescale, convectively unstable regions are efficiently mixed and should have an almost homogeneous composition. Except for particular cases, stars barely evolve in a thousand years, but convection involves timescales well below one day. Moreover, convection is inherently a three-dimensional process, while most simulations of stellar evolution use the assumption of spherical symmetry. An approximation is then needed to account for convection, and the one generally used is mixing length theory (Böhm-Vitense, 1958). In regions that are convectively unstable according to the criteria derived by Karl Schwarzschild (which was later refined by Paul Ledoux to account for composition gradients), mixing length theory provides the rate of energy transport without the need to resolve complex hydrodynamical processes. However, this approximation has important shortcomings. To account for detailed observations of the Sun and other stars, a free parameter in the theory has to be calibrated to observations, and this calibration might not be valid under all circumstances (Bonaca et al., 2012). Another important issue is related to the precise location of the convective boundary. Although the Ledoux criterion defines a clear boundary for the instability, blobs of material can overshoot from the convective region into the stable one, extending the zone where material is mixed. This introduces an additional uncertainty which requires a calibration of its own (Torres, Andersen and Giménez, 2010; Brott, de Mink et al., 2011; Stancliffe, Fossati et al., 2015). Such calibrations do not necessarily translate to later phases of evolution, and in particular, recent three-dimensional simulations of the last minutes prior to core-collapse in massive stars show that the detailed properties of convection play an important role in their explosion (Couch and Ott, 2015; Couch, Chatzopoulos et al., 2015; Müller et al., 2016).

### Semiconvective and thermohaline mixing

Regions that are stable to convection might still undergo significant mixing through the processes of semiconvection and thermohaline mixing. These two instabilities, usually referred to as double-diffusive convection, require that displaced blobs of material exchange heat with its surroundings, and thus operate on longer timescales than convection. Semiconvection acts in regions that are unstable in terms of the Schwarzschild criterion, but stable according to the Ledoux criterion (i.e. there is a stabilizing

composition gradient). A linear stability analysis of a fluid under these conditions predicts the occurrence of oscillations with increasing amplitudes (Kato, 1966), though observations of terrestrial environments where this effect takes place and numerical simulations point to the formation of a layered regime, with homogeneous regions undergoing convection separated by thin layers with a steep composition gradient (Zaussinger and Spruit, 2013; Wood, Garaud and Stellmach, 2013). Simulating this process under conditions realistic to stellar interiors is not possible owing to computational limitations, and the actual efficiency of semiconvective mixing remains poorly constrained. Single star models including this effect show that it already plays a role during the late main sequence in massive stars, and can have a large impact during core helium burning phases (Langer, El Eid and Fricke, 1985). The efficiency of semiconvection also has a large impact in predictions of binary stellar evolution (Wellstein and Langer, 1999; Cantiello, Yoon et al., 2007).

Thermohaline mixing is similar, but operates in regions stable to convection which have an outwards increasing mean molecular weight (i.e. helium rich material on top of hydrogen rich material). This is not a common occurrence in single stars, as nuclear burning normally results in a layered structure with the heavier elements located deeper inside. Thermohaline mixing is mostly expected to act when off-center ignition of material happens in semidegenerate cores (Kippenhahn, Ruschenplatt and Thomas, 1980; Siess, 2009), or during mass transfer in binaries, playing a role in both low-mass (Kippenhahn, Ruschenplatt and Thomas, 1980; Stancliffe and Glebbeek, 2008) and massive stars (Wellstein, Langer and Braun, 2001; Petrovic, Langer and Hucht, 2005). Just as with semiconvection, the efficiency of thermohaline mixing is poorly constrained, although observations of low-mass giant stars can provide some insight (Charbonnel and Zahn, 2007; Cantiello and Langer, 2010).

### **Rotational mixing**

The concept of homogeneous evolution driven by rotational mixing, initially used by Eddington as a simplifying assumption, was put forward again by Maeder (1987), who proposed that massive stars could have a bifurcation in their evolution as a consequence of rotational mixing. In fast rotators large scale flows would mix the material in the core that was processed through nuclear reactions throughout the entire star, burning almost the entirety of its hydrogen into helium. After the main sequence, such a homogeneous star would contract and evolve to much higher surface temperatures, producing a Wolf-Rayet star without undergoing a red supergiant phase. Mixing is expected to be stronger in more massive stars, as the increasing importance of radiation pressure reduces the stratification of their radiative envelopes (Yoon, Langer and C. Norman, 2006). The occurrence of chemically homogeneous evolution can potentially lead to very energetic phenomena, such as gamma-ray bursts (Yoon and Langer, 2005; Woosley and Heger, 2006; Yoon, Langer and C. Norman, 2006) and pair-instability supernovae (Yoon, Dierks and Langer, 2012), which we discuss in more detail in the next point.

Current stellar models consider various rotationally induced mixing processes (Heger, Langer and Woosley, 2000), including the formation of magnetic fields from differential rotation in their radiative envelopes due to the Tayler-Spruit dynamo (Spruit, 2002; Heger, Woosley and Spruit, 2005). Angular momentum transport from magnetic fields results in strong coupling and close to rigid body rotation during the main sequence, which matches the observation by Kurtz et al. (2014) of a pulsating main-sequence A-type star. Although there are important uncertainties in the efficiency of these processes, a strong coupling between the cores and envelopes of stars seems to be required to explain the rotation rates of white dwarfs, with models including angular momentum transport from magnetic fields currently providing the best match (Suijs et al., 2008). Recent asteroseismic observations of post main-sequence stars do show an important amount of differential rotation between their cores and envelopes (Beck, Montalban et al., 2012; Beck, Hambleton et al., 2014; Mosser et al., 2012; Deheuvels et al., 2012), but still

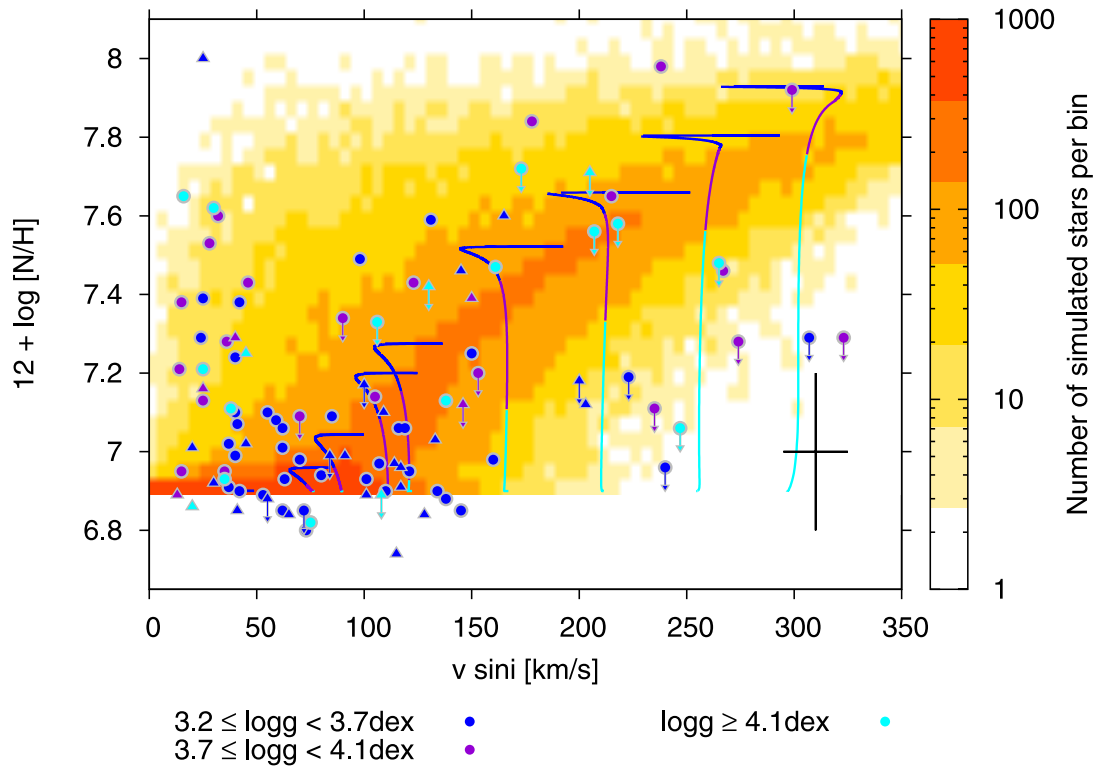


Figure 1.8: Projected rotational velocities and surface nitrogen abundances of B-type stars in the LMC, compared to the predicted distribution from stellar models including rotational mixing. High values of nitrogen are indicative of material that has been processed through the CNO cycle. Compared to stellar models, a large number of slowly rotating and highly enriched stars, and of rapidly rotating unenriched stars is unaccounted for. Figure reproduced from Brott, C. J. Evans et al. (2011).

much lower than what is expected if the core and the envelope would be completely uncoupled. Magnetic fields might not be sufficient to explain the amount of coupling observed, with angular momentum transport through gravity waves being a potential candidate to fill this gap (T. M. Rogers et al., 2013; Fuller et al., 2014).

Even if rotation is not strong enough to produce homogeneous evolution, it is expected to enrich the surfaces of massive stars with the ashes of CNO burning (Maeder and Meynet, 2000; Maeder, 2000), which are characterized by a reduction in carbon and oxygen abundances with a corresponding increase in nitrogen. The observation of rapidly rotating stars with significant amounts of nitrogen enrichment has been considered to be evidence for rotational mixing operating in single stars, but detailed comparisons between models and observations have shown important groups of objects that do not match the theoretical predictions (Hunter et al., 2008; Brott, C. J. Evans et al., 2011; Grin et al., 2016). As evidence accumulates that binary interaction is a fundamental part in the life of massive stars (Sana et al., 2012; Kobulnicky, Kiminki et al., 2014; Almeida, Sana, W. Taylor et al., 2016), the effects of accretion and mergers need to be taken into account.

### Super-luminous supernovae and gamma-ray bursts

Large advances in the field of time-domain astronomy has also resulted in several discoveries, with many transient events being discovered in a regular basis by current surveys such as the Palomar Transient Factory (Rau et al., 2009), Pan-STARRS (Kaiser et al., 2002) and the Dark Energy Survey (Dark Energy Survey Collaboration et al., 2016). One such discovery of particular interest to this thesis is that of super-luminous supernovae, which can reach luminosities more than an order of magnitude higher than regular core-collapse supernovae (Gal-Yam, 2012). Gal-Yam et al. (2009) suggested that one such object could be the result of a pair-instability supernovae, which was proposed as an explosion mechanism for very massive stars by Rakavy and G. Shaviv (1967). In this case, stars that form helium cores in excess of  $\sim 60M_{\odot}$  can become unstable and collapse before oxygen is ignited at their cores. The cause for this is the spontaneous production of electron-positron pairs from photons, which alters the response of the fluid to small perturbations and makes the core unstable. The collapse of these massive cores results in the explosive ignition of oxygen, releasing so much energy that the entire star is disrupted leaving no compact remnant. Stars with less massive cores ( $\sim 30M_{\odot} - 60M_{\odot}$ ) still become unstable, but experience a series of pulsations with mass ejection until finally undergoing core-collapse to a black hole rather than complete disruption (Fraleigh, 1968; Woosley, Blinnikov and Heger, 2007; Woosley, 2016). Stars that develop very massive cores, in excess of  $\sim 130M_{\odot}$ , still undergo core collapse and explosive oxygen ignition, but the released energy is insufficient to unbind the star and complete collapse to a black hole is expected (Wheeler, 1977; Bond, Arnett and Carr, 1984; Heger and Woosley, 2002) A different model, which invokes the rapid spin-down of a highly magnetized proto neutron star (called a magnetar) can also account for the very high energies of super-luminous supernovae, and appears to be favored in terms of detailed comparison to their light curves (Kasen and Bildsten, 2010).

Another family of transient events for which large amounts of data have been acquired in the last decades are gamma-ray bursts (see Piran 2004 for a review). These intense bursts of radiation come mostly in two flavors (Kouveliotou et al., 1993), with short bursts lasting less than two seconds and longer bursts going from a few seconds to a few minutes. The leading theory to explain short gamma-ray bursts invokes the coalescence of a binary neutron star as a result of the emission of gravitational waves (Nakar, 2007), making these a prime candidate for a simultaneous detection of gravitational and electromagnetic waves. For the case of long bursts, these are believed to be one of the products of the end of the life of massive stars, which is supported by the detection of associated supernovae to these events (Hjorth et al., 2003). A potential explanation for this phenomena involves the collapse of a rapidly rotating massive star to a black hole (Woosley, 1993), in which case a massive accretion disk could form instead of direct collapse. Chemically homogeneous evolution in rapidly rotating massive stars appears as a very natural explanation, as this channel of evolution can produce very massive helium cores, while avoiding significant loss of angular momentum during a red supergiant phase (Woosley and Heger, 2006; Yoon, Langer and C. Norman, 2006). As the number of detected super-luminous supernovae has increased comparative studies have shown similarities between the hosts of long gamma-ray bursts and hydrogen poor super-luminous supernovae, possibly indicating a connection between their formation channels (Japelj et al., 2016).

## 1.2 Binary stars

The discovery by Herschel in 1803 of visual binaries allowed a confirmation that the laws derived by Newton in the context of the solar system were valid in a much larger scales. Through the years, many thousands of visual binaries would be detected, with, for example, the *Catalogue of Double Stars within 121° of the North Pole* of Sherburn Wesley Burnham listing 13 665 different systems (Burnham, 1906).

Once it was established that Newtonian gravity properly described these motions, things were turned around so as to use the observed orbits to compute stellar masses. Dynamical mass estimates obtained from the motion of binary stars are of large importance, as they provide (when available) the simplest and cleanest measurement possible. Alternate methods rely on comparing observations to computed stellar models, while dynamical mass measurements in binaries are independent of uncertainties in stellar modeling. However, obtaining the individual masses of a visual binary required knowing the distance to it, and a precise measurement of the individual motion of each star, rather than just their relative motion. Owing to the typically centuries-long orbital periods, and the need of parallax measurements to obtain accurate distances, these measurements could not be done for many systems, with the book *The binary stars* by Robert Grant Aitken listing only 16 such measurements (Aitken, 1935).

Moreover, such visual binaries are physically so far apart from each other that their evolution is completely independent of the presence of a companion. Even when expanding to radii above 100 times that of the Sun when becoming red giants, their orbital separations are much larger, such that their gravitational interaction only modifies their motion through space, but not their structure. The first hint towards the existence of close binaries that could potentially interact during their lifetimes, came from the discovery of eclipsing binaries. In such systems, one component eclipses the other one, producing a periodic decrease in its luminosity. The first system for which this effect was detected was Algol, with John Goodricke reporting in 1783 that approximately every 2 days and 21 hours the brightness of Algol reduced by two magnitudes, with such eclipses lasting a period of 7 hours (Goodricke, 1783). A binary system can only be observed to have eclipses from specific vantage points, and as the orbital separation becomes much larger than the radius of the stars, the chances of this happening become smaller. Because of this, detections of eclipsing systems favor binaries orbiting at periods of the order of days, in large contrast to the periods of centuries typical of visual binaries.

An additional method to detect binary stars would come from the detection of shifts in the frequencies of dark lines in stellar spectra. As the components of a binary orbit each other, they alternately move away and towards an observer depending on the phase at which they are observed. Such displacement shifts the frequencies at which dark lines are observed, moving towards the blue if the object approaches the observer and towards the red if the opposite is the case. It was Pickering that first noticed this for the star Mizar, which showed spectral lines that would appear double every 52 days (Pickering, 1890). This could be interpreted as the simultaneous detection of a blue-shifted and a red-shifted line each coming from one component in a binary system with a period slightly above a 100 days. Such an effect would soon be confirmed for Algol as well, with the periodicity of the line shifts relative to the eclipses following what was expected (Vogel, 1890). Depending on whether lines from one or both components could be observed, the terms SB1 and SB2 (with SB standing for spectroscopic binary) were devised for these binary systems. An SB2 system which also shows eclipses allows for a wealth of information to be extracted from the system.

By the middle of the 20th century, X-ray observations would provide yet another mechanism to detect binary systems. Similar to the case of observations in the ultraviolet, which were required to detect mass loss in hot stars, the atmosphere of the earth is opaque to X-rays and the first observations were performed using rocket-mounted instruments (Giacconi et al., 1962). These early measurements would result in the identification of Sco X-1 as a binary system (Gursky et al., 1966; A. Sandage et al., 1966). With the launch of X-ray observatories such as the *Uhuru* satellite, several such objects would be discovered, for which the power source would be recognized as accretion onto a compact object (see Tauris and van den Heuvel 2006 for a recent review). This allowed for the first evidence of the existence of black holes. Although by definition black holes would emit no light, when present in a binary system and undergoing accretion they can develop hot accretion disks with large X-ray luminosities. The first such object observed was Cygnus X-1 (Bolton, 1972; Webster and Murdin, 1972). Given the uncertainties

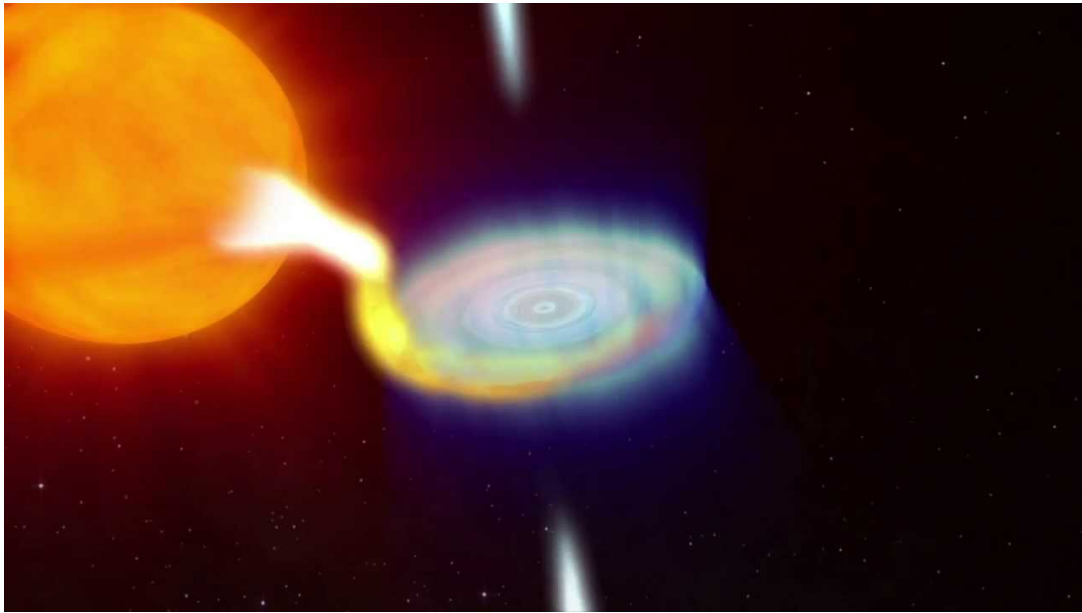


Figure 1.9: Artist impression of the black-hole X-ray binary V404 Cygni. Credit: NASA’s Goddard Space Flight Center.

in dynamical mass estimates, a positive association of these systems as harboring black holes was not made until measurements of V404 Cygni (see Figure 1.9), for which a strict lower limit on the mass of the compact object of  $6.26M_{\odot}$  was established, well above the upper limit for the mass of neutron stars (Casares, Charles and Naylor, 1992). In principle, these observations do not prove the existence of an event horizon, which is the characteristic property of black holes, and for many it is the recent detection of gravitational waves from merging black holes that provides true evidence for this (see Section 1.3).

### 1.2.1 Current observations of massive binaries

In recent times, and through large observational programmes, the importance of binary stars has been well established. The main tools used for this remain the same as old, eclipses and radial velocity variations, but tuned to such precision as to allow the observation of the atmospheres of transiting planets (Charbonneau et al., 2007), while the measurements of radial velocity variations are pushing towards values below  $1 \text{ m s}^{-1}$  (Mayor et al., 2003), which is below the average walking speed of a person. In terms of binary stars, the OGLE project, initially devised to test the existence of dark matter, has studied tens of thousands of eclipsing binaries in the Milky Way (Pietrukowicz et al., 2013), the Large Magellanic cloud (Pietrzyński et al., 2013) and the Small Magellanic Cloud (Pawlak et al., 2013). Most of these contain low-mass stars, as these are inherently more numerous than massive ones.

Spectroscopic studies of massive stars have led to the conclusion that most have a companion which is close enough to undergo some form of interaction during their lifetimes. By carefully accounting for observational biases, Sana et al. (2012) found that more than 70% of O-stars in our galaxy are actually close binary systems that will undergo mass transfer, making binary interaction the rule, rather than the exception, in their evolution (see also Kobulnicky, Kiminki et al. 2014). A similar binary fraction has been measured in the Large Magellanic Cloud (Almeida, Sana, W. Taylor et al., 2016), possibly implying that this result is not strongly dependent on the environment of formation and the metallicity of

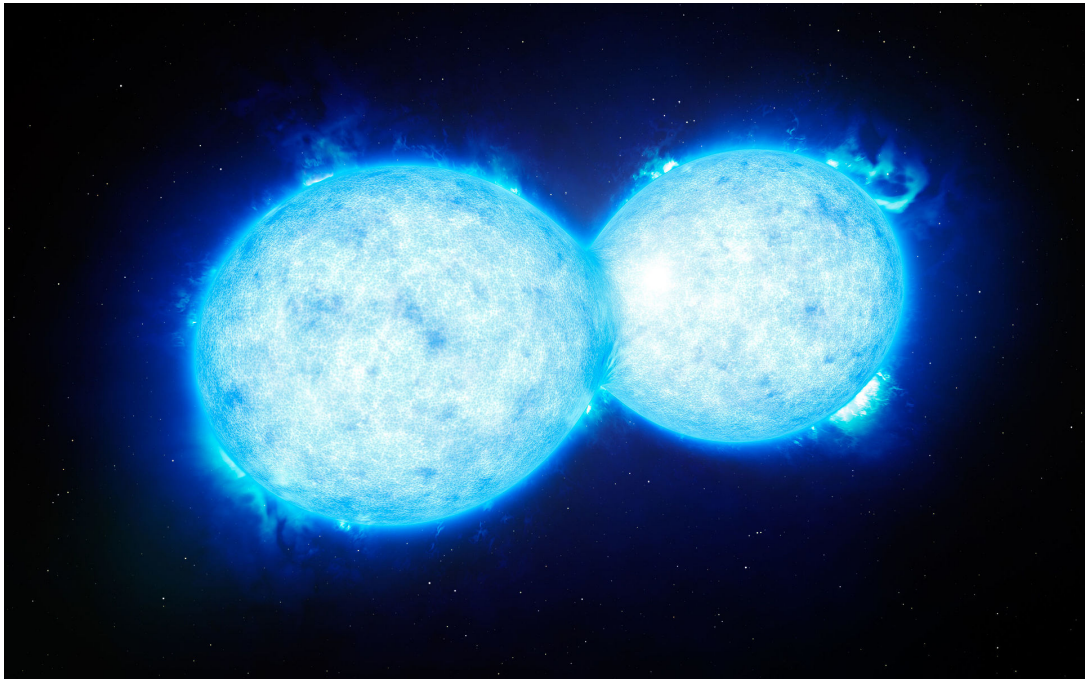


Figure 1.10: Artist impression of VFTS352, the most massive over-contact binary system known to date consisting of two  $30M_{\odot}$  stars with an orbital period of 1.1 days (Almeida, Sana, de Mink et al., 2015). This binary exhibits evidence of rotational mixing, and is expected to evolve towards a stellar merger. Credit: ESO/L. Calçada

the primordial gas from which stars are formed. The dramatic effects that binary interaction can have in the evolution of massive stars are nicely illustrated by the case of VFTS352 (Almeida, Sana, de Mink et al., 2015), the most massive over-contact system discovered so far (see Figure 1.10). This object, detected as part of the VLT-FLAMES Tarantula Survey (C. J. Evans, W. D. Taylor et al., 2011), consists of two  $30M_{\odot}$  stars orbiting each other every 1.1 days, so close to each other that they actually share their outer layers. A large binary fraction difficults the comparison of theoretical models to observation, as a significant fraction of apparently single stars (potentially the majority) are expected to be the products of binary interaction (de Mink, Sana et al., 2014).

With the increasing resolution and sensitivity of X-ray telescopes, it has become possible to study full populations of X-ray binaries in multiple galaxies (see Fabbiano 2006 for a review). One of the most puzzling discoveries from early observations with the Einstein telescope was the detection of extremely bright sources, which assuming isotropic emission would have luminosities well in excess of  $10^{39} \text{ erg s}^{-1}$  (Long and van Speybroeck, 1983). This is problematic, since such high luminosities would imply black holes with masses well above those detected in galactic X-ray binaries. Some argue that these objects could be powered by intermediate mass black holes which would be the seeds for the supermassive black-holes at the center of galaxies (Coleman Miller and Colbert, 2004), but several observations point towards a stellar origin (Grimm, M. Gilfanov and Sunyaev, 2003; Mapelli, Ripamonti et al., 2010; Swartz et al., 2011). A proper understanding of these sources is then likely to provide us with vital information on how massive stellar evolution is modified in environments significantly different from that of our own Galaxy.

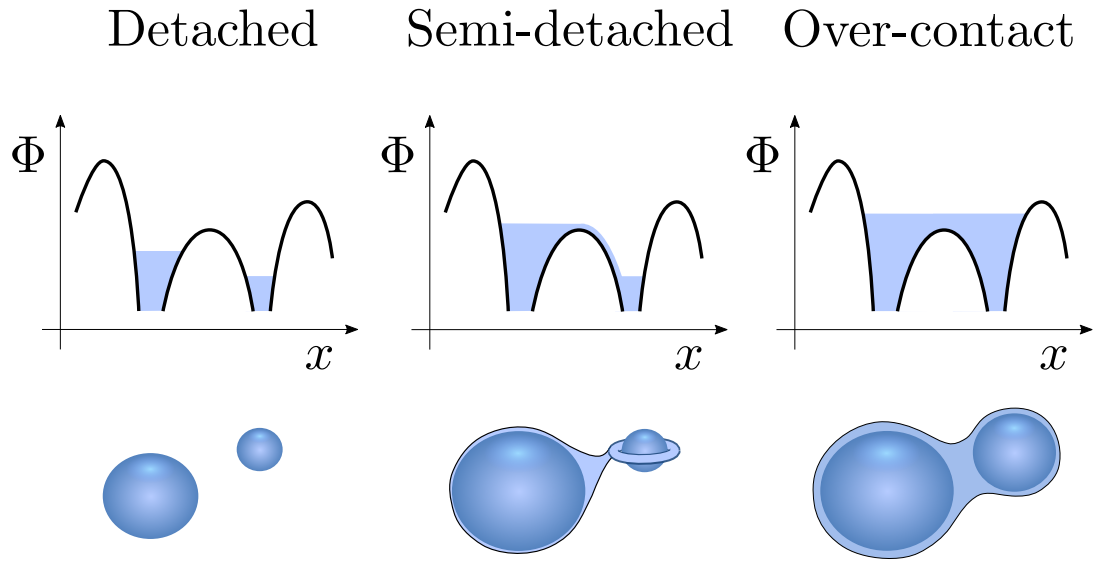


Figure 1.11: Classification of a binary system in terms of the presence or absence of Roche lobe overflow. Shown schematically is the Roche potential as a function of position in the line joining both components. A system where neither of the stars overflows its Roche lobe is called a detached system, while one where one component is overflowing and transferring mass is referred to as semi-detached. If both stars are overflowing their Roche lobes, then the system is called an over-contact binary, which is the case for VFTS352 (see Figure 1.10).

### 1.2.2 Mass transfer in binary systems

The Roche potential, named after the mathematician Édouard Roche, allows one to understand under which conditions a star would initiate mass transfer to a companion. This potential establishes well defined regions, called Roche lobes, within which each component is expected to retain the material it contains. The distinction between detached, semi-detached and over-contact systems considers whether none, one or both components in a binary are filling their Roche lobes (Kopal, 1955), as shown in Figure 1.11. Mass transfer was at the crux of the long-standing Algol paradox, that concerned close binary systems where the less massive component is a Roche lobe filling star which is more evolved than its companion. As stellar lifetimes are shorter for more massive stars, the general expectation was that the more evolved component in a binary system is also the most massive. This was eventually resolved by invoking mass transfer during the main sequence where the originally more massive component would rapidly transfer mass to its companion and invert the mass ratio of the system (Morton, 1960; Paczyński, 1966).

The first simulations of interacting binary systems that followed in detail the evolution of the donor star during mass transfer were pioneered by Kippenhahn and Weigert (1967), with L. Yungelson (1973) studying the evolution of the accreting star as well. Kippenhahn and Weigert (1967) recognized two distinct channels of evolution which they called Case A and Case B. This would be later extended to consider an additional Case C and even a Case D.

- Case A: For binaries that interact during main-sequence evolution, an initial rapid phase of mass transfer (operating on the Kelvin-Helmholtz timescale of the donor) is expected to invert the mass ratio, followed by a semi-detached phase during which the now less massive star keeps transferring mass to its companion, but on the much longer nuclear timescale.

- Case B: After the main sequence, most single stars expand significantly and evolve towards the red giant branch. This expansion stops once helium is ignited, which for a fixed mass ratio defines a range of orbital separations for which Roche lobe overflow would occur during this expansion phase. If mass transfer proceeds stably, then the donor is typically stripped of almost its entire hydrogen envelope, leaving an exposed helium core (see also Smak 1962). In Case A systems, once the donor depletes its central hydrogen, it is also expected to undergo mass transfer until exposing its helium core, a phase commonly referred to as Case AB.
- Case C: After helium depletion, most stars are expected to resume their expansion, allowing for an additional range of orbital periods for which Roche lobe overflow can happen. For higher donor masses, this range becomes much smaller and eventually disappears.
- Case D: Even if a star does not fill its Roche lobe, an important fraction of its wind mass loss could still be captured by its companion. For this to be effective, the wind acceleration region needs to be close to the Roche lobe (Mohamed and Podsiadlowski, 2007).

Owing to the large parameter space involved in binary evolution, there are several uncertain processes that have a large impact in the final outcome of stellar models, and in what follows we list a few of them that are of particular relevance to this work.

### The efficiency of mass transfer

The efficiency of mass transfer in binary systems is not well understood, with observations that clearly favor efficient accretion (Wellstein and Langer, 1999) and others for which the opposite is true (Petrovic, Langer and Hucht, 2005; Ritchie et al., 2012). Even if restricted to Case A evolution a fixed mass transfer efficiency is not appropriate to reproduce observations, which seem to indicate a reduction in accretion efficiency with increasing initial periods (de Mink, Pols and Hilditch, 2007). Just accounting for the accretion of angular momentum Packet (1981) demonstrated that a star needs only to accrete a few percent of its total mass to reach critical rotation. Barring any effect that could feed back angular momentum to the orbit, accretion should be quenched at this point. A potential mechanism that could halt the approach to critical rotation are tides, which owing to their strong dependence with the ratio of the orbital radius to the separation (Zahn, 1975; Zahn, 1977; Hut, 1981) would result in a strong dependence of mass transfer efficiency with orbital separation. Another possibility is that tides act on a wide accretion disk, transporting angular momentum out from the accretor which would allow for efficient mass transfer even after the accretor reaches its critical rotation velocity (Popham and Narayan, 1991). The formation of hot spots produced by the infalling material during accretion could also provide an additional energy source for the ejection of material (van Rensbergen et al., 2008).

### Common envelope evolution

A fundamental aspect of mass transfer is whether or not it can proceed stably. This can be analyzed in terms of mass-radius relationships, that describe how the stellar radius responds to changes in mass, compared to the expected change in the size of the donors Roche lobe (Soberman, Phinney and Heuvel, 1997). If the donor cannot respond fast enough to remain inside its Roche lobe, it might engulf its companion and experience common envelope evolution. If co-rotation is lost, then the secondary would experience viscous drag, leading to an inspiral and potentially a merger. However, if the conditions are right, the release of gravitational energy and angular momentum as the secondary spirals in can unbind the envelope, resulting in a compact binary (Paczynski, 1976; van den Heuvel, 1976). Common envelope

evolution resulting in a successful envelope ejection is the commonly accepted channel for the formation of most tight binaries containing at least one compact object such as X-ray binaries (Tauris and van den Heuvel, 2006) or sources of high frequency gravitational waves (Dominik, Belczynski et al., 2012). Attempts to calibrate the theory had been done for low mass systems (see, eg. Zorotovic, Schreiber, Gänsicke and Nebot Gómez-Morán 2010), but very large uncertainties remain for more massive systems (Taam and Sandquist, 2000; Ivanova et al., 2013).

### Stellar Mergers

Systems that undergo common envelope evolution but fail to eject their envelopes would result in a stellar merger. Also, in close systems undergoing stable and efficient mass transfer, the accreting star can expand significantly resulting in an over-contact binary (Pols, 1994; Wellstein, Langer and Braun, 2001), which is expected to merge for deep contact. This depends strongly on the initial separation of the binary and the ratio between its component masses. Using the distribution of binary parameters of (Sana et al., 2012), de Mink, Sana et al. (2014) concluded that  $\sim 8\%$  of stars are the product of a binary merger, which is conspicuously close to the fraction of OB stars that are magnetic (see, eg. Fossati et al. 2015). The idea that mergers would result in magnetic stars has been proposed by Ferrario et al. (2009) and Wickramasinghe, Tout and Ferrario (2014), and could potentially explain the existence of slowly rotating stars with nitrogen enrichment at their surface. In this case, enrichment could happen during the merger process, with magnetic braking rapidly slowing down the rotation of the star. Smooth-particle-hydrodynamic simulations of mergers have been attempted by Gaburov, Lombardi and S. Portegies Zwart (2008) and Glebbeek et al. (2013), and they show efficient rejuvenation, as well as small fractions of mass being lost during the merger, typically less than a 10% of the total. But it is not clear if this is actually representative of merging binary systems which would undergo a much slower spiral-in.

So far, the only certain observation of a merger event was achieved by Tylenda et al. (2011) for V1309 Sco, which corresponded to the merger of a low mass contact system. The existence of OGLE data for this object previous to its 2008 eruption allowed its detection as an eclipsing binary with a decreasing orbital period. Another event believed to correspond to a merger is V838 Mon (Munari et al., 2002).

## 1.3 The dawn of gravitational wave astronomy

The year 2015 was witness to one of the greatest successes in the history of experimental physics. Following a billion-dollar effort by thousands of researchers through several decades, the twin detectors of the advanced Laser Interferometer Gravitational wave Observatory (aLIGO) detected the merger of two black holes in September 14th of that year (B. P. Abbott et al., 2016a). This detection, which received the name GW150914 for the date of its discovery, is also referred to as “The Event” owing to its groundbreaking nature. Such an outcome was considered unthinkable by Einstein, who predicted the existence of these waves (Einstein, 1916), as their amplitude would be incredibly small. The aLIGO interferometers work by splitting a beam of light into two perpendicular arms of 4 km each, bouncing them from hanging mirrors at the ends to then be superimposed, producing an interference pattern (see Figure 1.12). Incoming gravitational waves modify the structure of space-time, alternately reducing and extending the size of each arm, a difference which can be measured by changes in the resulting interference pattern. The difference in the size of the aLIGO arms produced by GW150914 was smaller than one part in  $10^{20}$ , meaning that each arm changed its length by less than an atomic nucleus! The first observing run of these detectors resulted in an additional observation of merging black holes, GW151226, and an additional event which was of too low significance to be considered as a certain detection,

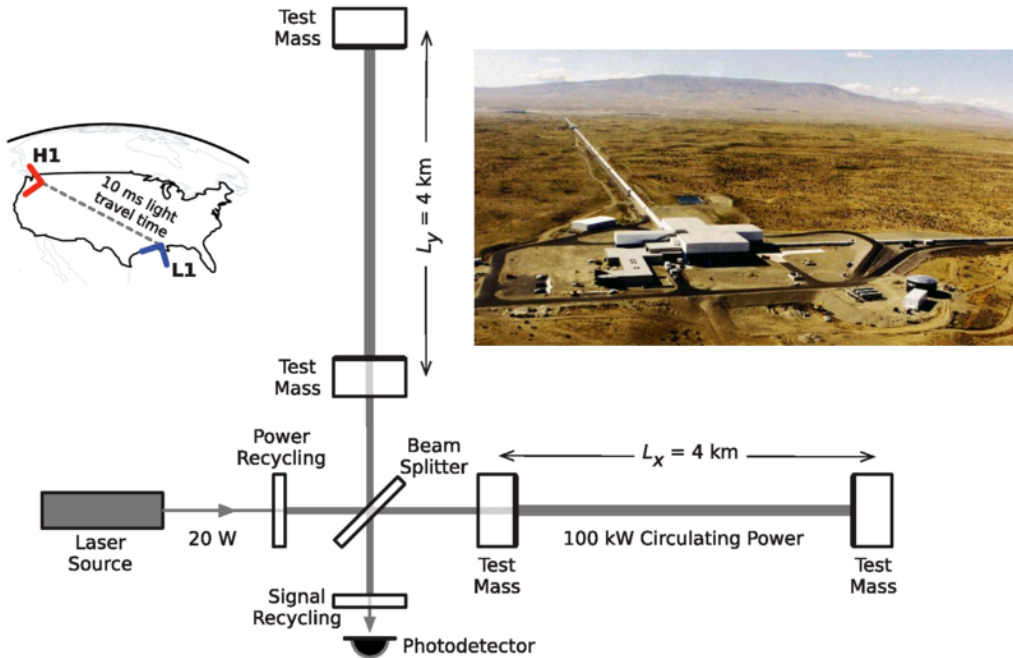


Figure 1.12: Simplified diagram of the LIGO detectors located at Hanford, Washington (pictured) and Livingston Louisiana in the US. The light from a laser source is splitted into two perpendicular beams that travel through two arms with a length of 4 km. Light bounces back an forth at each arm, effectively extending the length travelled by each beam up to 1120km. The two beams are then brought together and made to interfere, allowing the measurement of changes in the relative length of each arm. Image adapted from B. P. Abbott et al. (2016a) and the LIGO website <http://www.ligo.org/>.

LVT151012 (The LIGO Scientific Collaboration et al., 2016a, see Figure 1.13).

Strong evidence in favor of the existence of gravitational waves has existed since the 70s. The observation of the Hulse-Taylor pulsar (Hulse and J. H. Taylor, 1975), a pair of neutron stars orbiting each other every 7.75 hours, showed a decrease in its period that perfectly followed what was expected from the loss of energy due to gravitational waves. But these observations were made entirely based on the detection of radio-waves emitted from the pulses of one of the stars. Instead, the aLIGO detectors measured directly the effect of the incoming gravitational waves in the structure of space-time, opening up a new window for astrophysical observations. For most of its history, astrophysics has mainly relied in the detection of photons emitted at different frequencies by the sources of interest, and gravitational waves present a completely new way to observe the universe. Similar to the case of electromagnetic radiation, gravitational waves do not come in a single flavor. To study the full electromagnetic spectrum very different instruments are required, each covering a range in frequency to which they are sensitive. The aLIGO detectors probe the high-frequency band at which stellar-mass compact objects are expected to emit during a merger event, having the greatest sensitivity in the range 30 – 1000 Hz.

The two most important efforts at the moment to open up new windows of observation for gravitational waves are the evolved Laser Interferometer Space Antenna (eLISA Amaro-Seoane et al., 2012) and the international Pulsar Timing Array (iPTA Manchester and IPTA, 2013), with their sensitivity curves depicted in Figure 1.14. The concept of eLISA is very similar to the LIGO detector, a beam of light is splitted to travel in different directions and then brought back together to interfere. The main difference is the scale of the experiment, this mission would involve spacecraft separated by distances comparable to

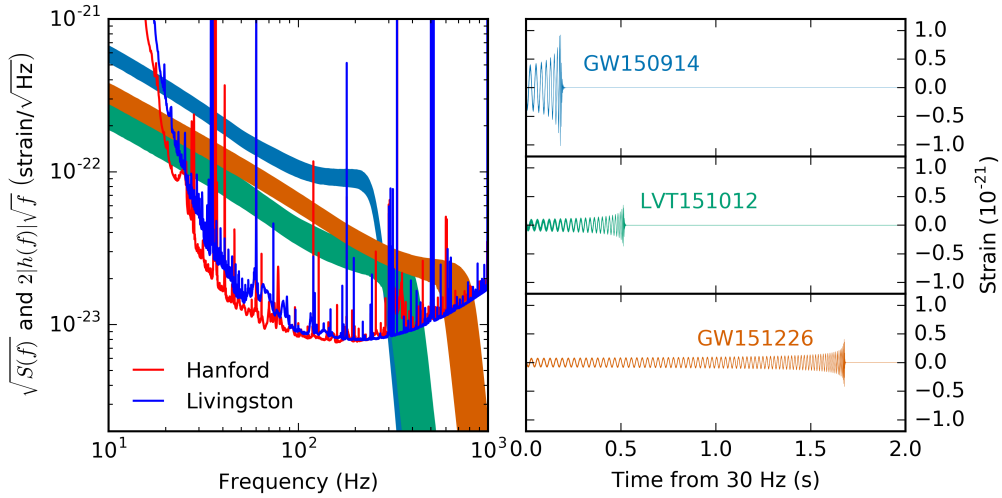


Figure 1.13: Detection of the two gravitational wave sources GW150914 and GW151226, and of the candidate event LVT151012. All of these detections correspond to the merger of black holes with best-fit masses  $36M_{\odot} + 29M_{\odot}$ ,  $14M_{\odot} + 7.5M_{\odot}$  and  $23M_{\odot} + 13M_{\odot}$  respectively. The LIGO detectors measure the strain  $h = \delta L/L$ , which is the relative change in the size of the arms of the detector as a gravitational wave passes through. Figure adopted from (The LIGO Scientific Collaboration et al., 2016a).

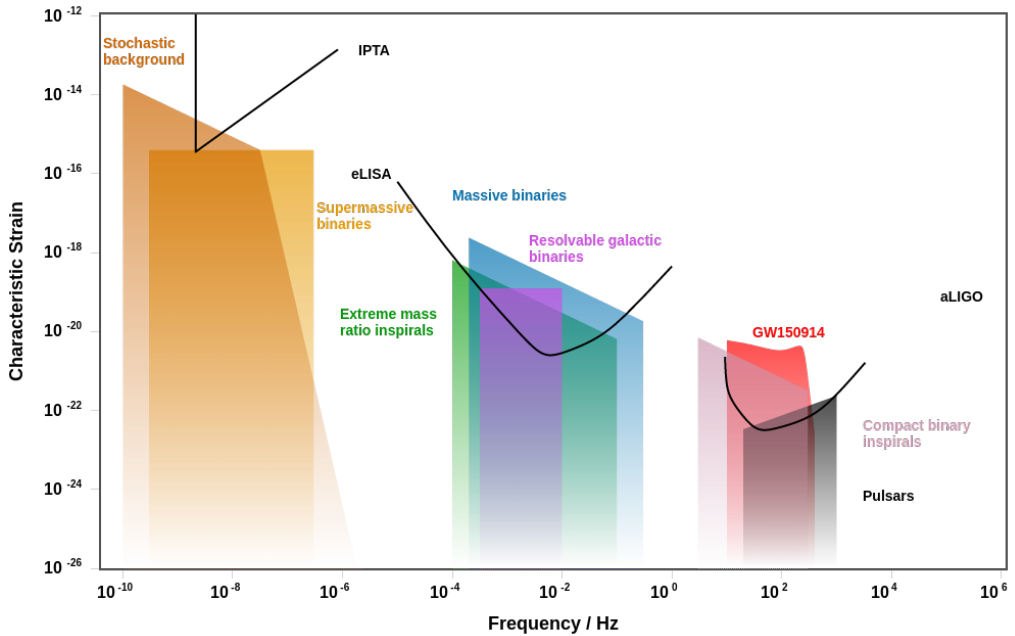


Figure 1.14: Strain sensitivity at different frequencies for different gravitational wave detectors. The strain  $h = \delta L/L$  measures the relative change in length produced by a gravitational wave. Shown are the expected sensitivity curves for the international Pulsar Timing Array (iPTA), the evolved Laser Interferometer Space Antennae (eLISA) and the advanced Laser Interferometer Gravitational wave Observatory (aLIGO). A variety of potential sources are shown, including the detection of GW150914. Image created using the plotter for gravitational-wave sensitivity curves by Moore, Cole and Berry (2015), which can be accessed at <http://rhcole.com/apps/GWplotter/>.

that between the Earth and the Sun. The iPTA in change, relies on the observation and timing of several pulsars for long periods of time. In this case, very-low-frequency gravitational waves would modify the large distance between us and the pulsars, movements that can be detected in terms of small changes in the pulse frequency of these objects. eLISA is expected to launch in 2034, while the iPTA is already in place and taking measurement, and its sensitivity at the lowest frequencies is mainly limited by the length of the period during which data has been acquired. It has been shown that GW150914 would have been detectable by eLISA if it were operating at its design capability (Sesana, 2016).

### 1.3.1 Identifying the progenitors of merging stellar-mass black holes

There are currently three main channels considered to explain the progenitor system of the first black holes detected by aLIGO. These are the dynamical channel involving many-body interactions in globular clusters (S. F. Portegies Zwart and McMillan, 2000), the “classical” common envelope channel (Tutukov and L. R. Yungelson, 1993) and the chemically homogeneous evolution channel (Mandel and de Mink, 2016; Marchant et al., 2016), which is discussed as part of this thesis. These different channels are illustrated in Figure 1.15 and can be briefly described as follows:

- *Dynamical channel:* In a globular cluster, black holes are formed either through single or binary stellar evolution and then segregate towards the center of the cluster. Through many body interactions a black hole binary is formed, and by undergoing multiple scattering interactions with third bodies, the black hole binary becomes more compact and is imparted with a velocity kick. After many interactions, the black hole binary is eventually ejected from the cluster, and in a typical timescale of Gigayears it merges due to the emission of gravitational wave radiation. Different paths of evolution, which include ejection at the moment when the black hole binary forms, are also possible (see, for instance, Rodriguez, Haster et al., 2016).
- *Common envelope channel:* A wide massive binary is formed, with orbital periods of the order of years. After core hydrogen depletion, the more massive star expands to become a red supergiant and undergoes a phase of stable mass transfer, which strips the initially more massive star of its hydrogen envelope. The stripped star then forms the first black hole. When the second star depletes hydrogen at its core and expands, it initiates a phase of unstable mass transfer, with its envelope expanding and engulfing the black hole. Through viscous drag with the envelope, the black hole and the helium rich core of the second star spiral inwards with the release of gravitational energy ejecting the hydrogen envelope. This reduces the orbital period down to the order of tens of days. The second black hole then forms, and the system can undergo a merger through emission of gravitational waves.
- *Chemically homogeneous evolution channel:* A very compact massive binary is formed, with an orbital period  $\sim 0.5 - 2$  days. For sufficiently short periods, such a system is formed in contact, or undergoes a contact phase during its evolution. Due to tidal locking, both stars are rapid rotators, which induces strong mixing through their envelopes an chemically homogeneous evolution. This causes the stars to contract rather than expand, forming a black hole without going through a giant phase. Owing to their rapid rotation, once these objects collapse and form a black hole they could potentially produce a gamma-ray burst as well (Marchant et al., 2016). As with the two previous cases, the resulting black hole binary can then merger through the emission of gravitational waves.

It is interesting to note at this point the words of Bohdan Paczyński when he proposed the possibility of common envelope evolution to form short period binaries containing a white dwarf (Paczynski, 1976):

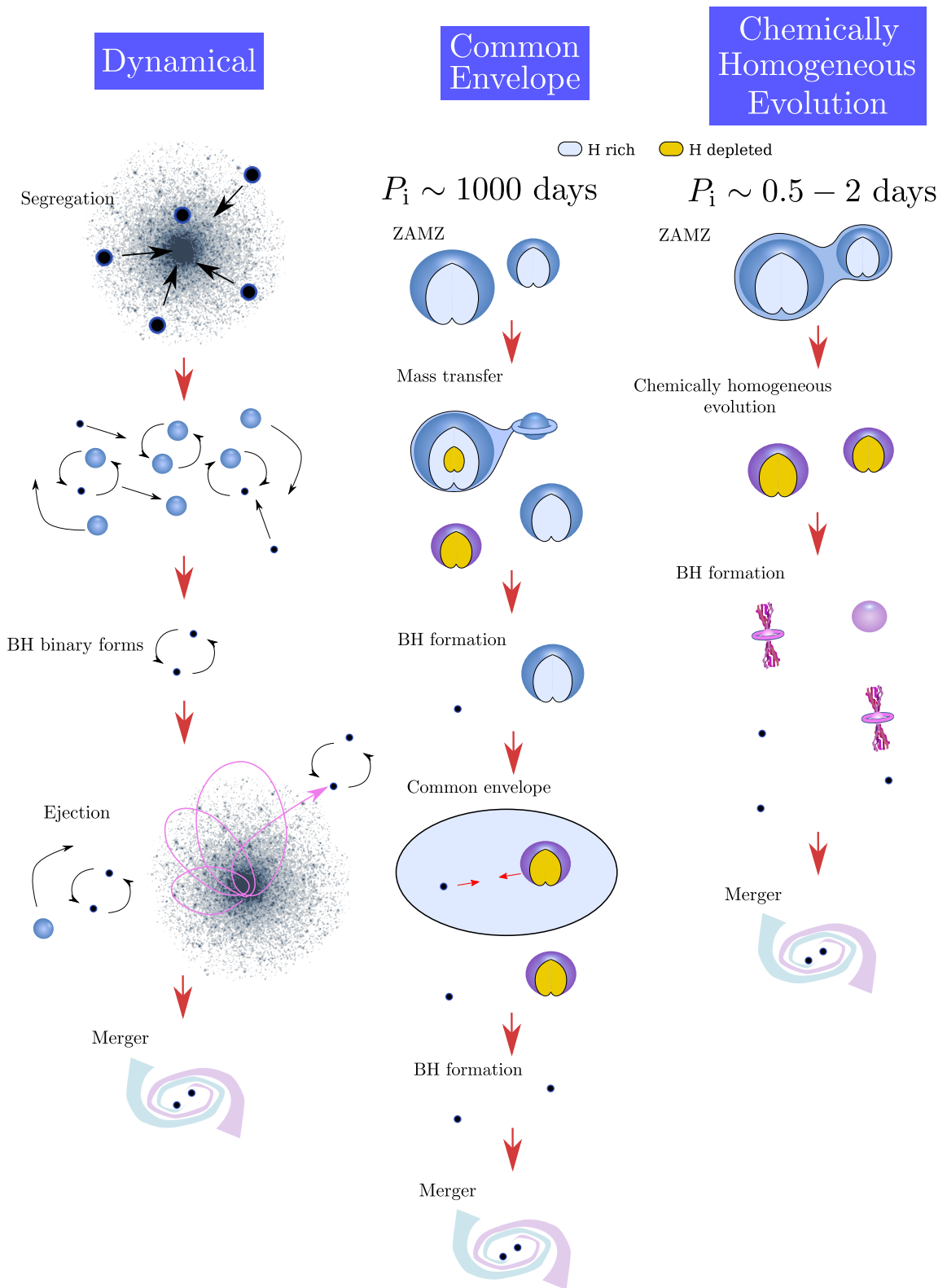


Figure 1.15: Different channels for the formation of merging binary black holes. BH stands for black hole, while ZAMS stand for Zero-Age Main Sequence, which is the starting point of core hydrogen burning in the evolution of a star. See text for details.

*“The two most common suggestions for the origin of novae and dwarf novae do not require a common envelope phase of evolution. According to the first hypothesis, one of the components of a short period binary was always mixed so well that it evolves as a chemically homogeneous star. It becomes a white dwarf without ever being a red giant. I can see no physical process that could account for the complete mixing of a star.”*

It is still not expected that low mass stars resulting in white dwarfs could evolve chemically homogeneously, but in massive and very massive stars it is now believed rotational mixing can indeed produce this outcome.

In particular for GW150914, all three channels discussed can produce such a merger under reasonable assumptions (Belczynski, Holz et al., 2016; Rodriguez, Haster et al., 2016; de Mink and Mandel, 2016), while the low masses of GW151226 can be challenging to explain in terms of chemically homogeneous evolution. However, owing to the relative simplicity of black holes, clear smoking guns that would allow to completely discard a specific formation channel for a single observation are unlikely to be found. Important theoretical uncertainties in all models can be exploited to fit the very finite number of observables of a binary black hole, which are further reduced due to the large degeneracy between measurements of mass ratios and spins (Hannam et al., 2013). Whenever eLISA starts to operate, it will provide an important additional value to our observations, namely the eccentricity of the system (Nishizawa et al., 2016; Breivik et al., 2016). At the high frequencies observable by aLIGO, merging binary black holes are expected to be almost circular, with very small eccentricities that would be undetectable. With increasing sensitivities for ground based detectors, better constraints on the spins of black holes and their relative orientation with the orbit will be obtained. This can also help identify the contribution from different channels of evolution, as the dynamical formation channel predicts that spins should be randomly oriented (Rodriguez, Zevin et al., 2016). As more detection of black hole mergers are announced, their full demographics will need to be considered in order to constrain the different formation scenarios.

## 1.4 This thesis

The work done for this thesis focuses on using detailed stellar simulations to study the impact of binary interaction and rotation in massive stars. For this purpose we have developed the *binary* module for the open-source stellar evolution code Modules for Experiments in Stellar Astrophysics, better known as MESA (Paxton, Bildsten et al., 2011; Paxton, Cantiello et al., 2013; Paxton, Marchant et al., 2015). The *binary* module has been available to MESA users for more than two years, and is actively used by many members of the community. This work was documented in detail in Paxton, Marchant et al. (2015), and is included in this thesis as Chapter 2. Most of the work in this thesis involves the use of this code to model large numbers of detailed stellar evolution models involving the physics of rotation and binary interaction in the evolution of massive stars.

### 1.4.1 The formation of merging binary black holes

In Chapter 3 we model the evolution of very close (orbital periods of just a few days) and very massive binaries (ranging from  $25M_{\odot}$  to  $500M_{\odot}$  for the mass of the primary). Under these conditions the binary components are expected to be tidally locked, resulting in rapid rotation. If both components rotate fast enough, this could induce strong mixing, making them evolve chemically homogeneous and remain compact. A compact black hole binary can then be formed without the need of common envelope evolution or dynamical interactions to reduce the orbital separation. Taking into account the possibility

that binaries could be formed in extremely compact orbits, such that they initiate their main sequences while being in contact, an important number of merging black holes would be produced. For metallicities below  $Z_\odot/10$ , where  $Z_\odot$  is the solar metallicity, we find that nearly  $\sim 1$  merging black hole is formed every  $10^4$  supernovae. The large incidence of contact systems would push the final mass ratios to unity, while the occurrence of pair-instability supernovae should be observable as a gap between  $\sim 60M_\odot$  and  $\sim 130M_\odot$  in the distribution of black hole masses measured by gravitational wave detectors. At its design sensitivity, we expect advanced LIGO to be able to detect between  $\sim 20 - 900$  of these mergers, with the large uncertainty being a product of the uncertainties in the chemical evolution of the universe.

### 1.4.2 Models for ultra-luminous X-ray sources

In Chapter 4 we consider similar systems but with mass ratios far from unity. In this case, we show that only the more massive component undergoes chemically homogeneous evolution and forms a black hole. In a longer timescale, the secondaries evolve normally, expanding and eventually initiating mass transfer. This makes the binary active as a source of X-rays, and given the high black hole masses that can be obtained through this channel, its luminosity would place it in the class of ultra-luminous X-ray sources. By considering model grids at different metallicities, we show that the number of observable ultra-luminous sources increases with decreasing metallicity, until it reaches a peak at a metallicity of  $\log Z = 10^{-4}$ . Similar to the case of binary black holes, the occurrence of pair-instability supernovae produce a gap in black hole masses, which could be observable as a gap in the luminosity distribution of ultra-luminous X-ray sources

After an ultra-luminous phase, the secondary could explode as a supernova, and if it receives a kick in the right direction, it could result in a compact neutron-star-black-hole that would merge in a few gigayears. We estimate the corresponding rate of mergers to be  $r < 0.2 \text{ Gpc}^{-3}\text{yr}^{-1}$ , more than two orders of magnitude below what advanced LIGO is expected to be sensitive to. Although the current generation of gravitational wave detectors would likely not be sensible enough to detect these mergers, third generation observatories like the Big Bang Observatory and the Einstein Telescope could potentially reach the required sensitivity.

### 1.4.3 The evolution of binaries in the Large Magellanic Cloud

Recent observations have established that binary interaction is a dominant process in the evolution of massive stars. To study the impact of binaries in samples of LMC stars, in Chapter 5 we compute grids of both single and binary models including rotation and covering a large range of masses and initial parameters. We choose a set of physical assumptions that minimize the number of binary products in a given sample, which allows us to estimate lower limits on the impact of binarity. We show that even under these extreme assumptions, there is a significant degeneracy between the predictions of rotational mixing and those of binary interaction. The only sample of objects for which the single and the binary population can be clearly distinguished is that of rapidly rotating unenriched stars. Detailed measurements of the abundance of these systems would place important constraints in both rotational mixing and mass transfer efficiency.

## CHAPTER 2

---

# Modules for Experiments in Stellar Astrophysics (MESA): Binaries, Pulsations, and Explosions

---

Bill Paxton, **Pablo Marchant**, Josiah Schwab, Evan B. Bauer, Lars Bildsten, Matteo Cantiello, Luc Dessart, R. Farmer, H. Hu, N. Langer, R.H.D. Townsend, Dean M. Townsley, and F.X. Timmes  
The Astrophysical Journal Supplement Series, Volume 220, Issue 1, id. 15<sup>1</sup>

**ABSTRACT:** We substantially update the capabilities of the open-source software instrument Modules for Experiments in Stellar Astrophysics (MESA). MESA can now simultaneously evolve an interacting pair of differentially rotating stars undergoing transfer and loss of mass and angular momentum, greatly enhancing the prior ability to model binary evolution. New MESA capabilities in fully coupled calculation of nuclear networks with hundreds of isotopes now allow MESA to accurately simulate advanced burning stages needed to construct supernova progenitor models. Implicit hydrodynamics with shocks can now be treated with MESA, enabling modeling of the entire massive star lifecycle, from pre-main sequence evolution to the onset of core collapse and nucleosynthesis from the resulting explosion. Coupling of the GYRE non-adiabatic pulsation instrument with MESA allows for new explorations of the instability strips for massive stars while also accelerating the astrophysical use of asteroseismology data. We improve treatment of mass accretion, giving more accurate and robust near-surface profiles. A new MESA capability to calculate weak reaction rates “on-the-fly” from input nuclear data allows better simulation of accretion induced collapse of massive white dwarfs and the fate of some massive stars. We discuss the ongoing challenge of chemical diffusion in the strongly coupled plasma regime, and exhibit improvements in MESA that now allow for the simulation of radiative levitation of heavy elements in hot stars. We close by noting that the MESA software infrastructure provides bit-for-bit consistency for all results across all the supported platforms, a profound enabling capability for accelerating MESA’s development.

---

<sup>1</sup> The work presented here is adapted from section 2 of this paper which focuses on the modeling of binary stars.

The development of a relatively complete and quantitative picture of stellar evolution is one of the great drivers of astrophysics. On the observational side of this impetus, the *Kepler* (Borucki et al., 2010) and the CoRoT (Baglin et al., 2009) missions continuously monitored more than 100,000 stars in a  $100 \text{ deg}^2$  window with a dynamic range of apparent stellar brightness of  $10^6$ . Highlights include the discoveries that nearly all  $\gamma$  Doradus and  $\delta$  Scuti stars are hybrid pulsators, and the detection of solar-like oscillations in a large sample of red giants (Auvergne et al., 2009; De Ridder et al., 2009; Grigahcène et al., 2010; Bedding et al., 2010; Christensen-Dalsgaard and M. J. Thompson, 2011; Chaplin and Miglio, 2013). The *Dark Energy Survey* is scanning  $5000 \text{ deg}^2$  of the southern sky in 5 optical filters every few days to discover and study thousands of supernovae (e.g., Papadopoulos et al., 2015; Yuan et al., 2015). Building upon the legacy of the *Palomar Transient Factory* (Law et al., 2009), the *intermediate Palomar Transient Factory* conducts a fully-automated, wide-field survey that systematically explores the transient sky with a 90 second to 5 day cadence (Vreeswijk et al., 2014). The forthcoming *Zwicky Transient Facility* will enable a survey more than an order of magnitude faster at the same depth as its predecessors. In its unique orbit the *Transiting Exoplanet Survey Satellite* will have an unobstructed view to scrutinize the light curves of the brightest 100,000 stars with a 1 minute cadence (Ricker et al., 2015). The *Gaia* mission aims to provide unprecedented distance and radial velocity measurements with the accuracies needed to reveal the evolutionary state, composition, and kinematics of about one billion stars in our Galaxy (e.g., Creevey et al., 2015; Sacco et al., 2015). The *Large Synoptic Survey Telescope* will image the entire Southern Hemisphere deeply in multiple optical colors every week with its three billion pixel digital camera, thus opening a new window on transient objects such as interacting close binary systems. (e.g., Oluseyi et al., 2012).

Interpreting these new observations and predicting new stellar phenomena propels the theoretical side, in particular the evolution of the community software instrument Modules for Experiments in Stellar Astrophysics (**MESA**) for research and education. We introduced **MESA** in Paxton, Bildsten et al. (2011) and expanded its range of capabilities in Paxton, Cantiello et al. (2013). This paper describes the major new advances for **MESA** modeling of binary systems.

It has been a little more than 200 years since Herschel (1803) announced, after 25 years of observation, that certain pairs of stars displayed evidence of orbital motion around their common center of mass. Binary systems allow the masses of their component stars to be directly determined, which in turn allows stellar radii to be indirectly estimated. This allows the calibration of an empirical mass-luminosity relationship from which the masses of single stars can be estimated (Torres, Andersen and Giménez, 2010). Recent surveys such as Raghavan et al. (2010) suggest 30% to 50% of solar-like systems in the Galactic disk are composed of binaries, where the binary fraction is higher for more massive stars (Sana et al., 2012; Kobulnicky, Kiminki et al., 2014). As argued by de Mink, Langer et al. (2013), the most rapidly rotating massive stars are expected in binary systems as a consequence of accretion-induced spin-up. Differential rotation has a major impact on the evolution of massive stars (Maeder and Meynet, 2000; Heger, Langer and Woosley, 2000; Heger, Woosley and Spruit, 2005) and for single stars the corresponding physics has been included into **MESA** as described in Paxton, Cantiello et al. (2013). On the other hand very few works that include the physics of differential rotation in binaries have been published (Petrovic, Langer and Hucht, 2005; Cantiello, Yoon et al., 2007). Our improvements to **MESA** now allow for the calculation of differentially-rotating binary stars.

**MESAbinary** is a **MESA** module that uses **MESAstar** to evolve binary systems. It can be used to evolve a full stellar model plus a point mass companion or to simultaneously evolve the structure of two stars. It optionally allows the modeling of systems including stellar rotation, assuming the axis of rotation of each star to be perpendicular to the orbital plane, accounting for the effects of tidal interaction and spin-up through accretion. The implementation of **MESAbinary** benefits from early contributions by Madhusudhan, Justham et al. (2006) and Lin et al. (2011) who modeled mass transfer from a star to a

point mass.

Here we provide an overview of the modelled physical processes for circular binary systems and describe the tests against which we validate `MESAbinary`.

## 2.1 Initialization of a Circular Binary System

A binary system is initialized by specifying the components and either the orbital period  $P_{\text{orb}}$  or separation  $a$ . Each component can be a point mass or a stellar model. The initial model(s) are provided by a saved MESA model or a zero-age main-sequence (ZAMS) specification. For stellar models including rotation, the initial rotational velocities of each component can be explicitly defined, or set such that the star is synchronized to the orbit at the beginning of the evolution. The orbital angular momentum of the system is

$$J_{\text{orb}} = M_1 M_2 \sqrt{\frac{G a}{M_1 + M_2}}, \quad (2.1)$$

where  $M_1$  and  $M_2$  are the stellar masses. Evolution of  $M_1$ ,  $M_2$ , and  $J_{\text{orb}}$  is used to update  $a$  using Equation (2.1). Masses can be modified both by Roche lobe overflow (RLOF) and winds. The total time derivatives of the component masses are given by

$$\dot{M}_1 = \dot{M}_{1,w} + \dot{M}_{\text{RLOF}}, \quad \dot{M}_2 = \dot{M}_{2,w} - f_{\text{mt}} \dot{M}_{\text{RLOF}}, \quad (2.2)$$

where  $M_1$  is the donor mass and  $M_2$  the accretor mass. The stellar wind mass loss rates are  $\dot{M}_{1,w}$  and  $\dot{M}_{2,w}$  (see Paxton, Bildsten et al. 2011 and Paxton, Cantiello et al. 2013) and  $\dot{M}_{\text{RLOF}}$  is the mass transfer rate from RLOF, all defined as negative. The factor  $f_{\text{mt}}$  represents the efficiency of accretion and can be used to limit accretion to the Eddington rate  $\dot{M}_{\text{Edd}}$ .

## 2.2 Evolution of Orbital Angular Momentum

To compute the rate of change of orbital angular momentum, we consider the contribution of gravitational waves, mass loss, magnetic braking, and spin orbit (LS) coupling

$$\dot{J}_{\text{orb}} = J_{\text{gr}} + J_{\text{ml}} + J_{\text{mb}} + J_{\text{ls}} , \quad (2.3)$$

from which the change in orbital angular momentum in one step is calculated as  $\Delta J_{\text{orb}} = \dot{J}_{\text{orb}} \delta t$ , where  $\delta t$  is the timestep. Unless models with stellar rotation are being used, the  $J_{\text{ls}}$  term is equal to zero, and the contribution of the individual spins of each star is not directly considered. On the other hand, the  $J_{\text{mb}}$  term implicitly assumes a strong tide that keeps the orbit synchronized. The simultaneous usage of  $J_{\text{mb}}$  with stellar rotation is not consistent (see Section 2.2.4). We now describe how these terms are computed.

### 2.2.1 Gravitational Wave Radiation

Very compact binaries can experience significant orbital decay due to the emission of gravitational waves. Observations of the Hulse-Taylor binary pulsar over three decades (Weisberg and J. H. Taylor, 2005) and of the double pulsar (Kramer, Stairs et al., 2006a) have tested the predicted effect from general relativity to a high precision. The angular momentum loss from gravitational waves is

$$J_{\text{gr}} = -\frac{32}{5c^5} \left( \frac{2\pi G}{P_{\text{orb}}} \right)^{7/3} \frac{(M_1 M_2)^2}{(M_1 + M_2)^{2/3}}. \quad (2.4)$$

## 2.2.2 Mass Loss

We assume the mass lost in a stellar wind has the specific orbital angular momentum of its star. For the case of inefficient mass transfer, angular momentum loss follows Soberman, Phinney and Heuvel (1997), where fixed fractions of the transferred mass are lost either as a fast isotropic wind from each star or a circumbinary toroid with a given radius:

$$\begin{aligned} j_{\text{ml}} &= \left[ (\dot{M}_{1,w} + \alpha_{\text{mt}} \dot{M}_{\text{RLOF}}) M_2^2 + (\dot{M}_{2,w} + \beta_{\text{mt}} \dot{M}_{\text{RLOF}}) M_1^2 \right] \\ &\quad \times \frac{a^2}{(M_1 + M_2)^2} \frac{2\pi}{P_{\text{orb}}} \\ &\quad + \gamma_{\text{mt}} \delta_{\text{mt}} \dot{M}_{\text{RLOF}} \sqrt{G(M_1 + M_2)} a, \end{aligned} \quad (2.5)$$

where  $\alpha_{\text{mt}}$ ,  $\beta_{\text{mt}}$ , and  $\delta_{\text{mt}}$  are respectively the fractions of mass transferred that is lost from the vicinity of the donor, accretor and circumbinary toroid, and  $\gamma_{\text{mt}}^2 a$  is the radius of the toroid. Ignoring winds, the efficiency of mass transfer is then given by  $f_{\text{mt}} = 1 - \alpha_{\text{mt}} - \beta_{\text{mt}} - \delta_{\text{mt}}$ . When accretion is limited to  $\dot{M}_{\text{Edd}}$ , efficiency of accretion is given by

$$f_{\text{mt}} = \min(1 - \alpha_{\text{mt}} - \beta_{\text{mt}} - \delta_{\text{mt}}, |\dot{M}_{\text{Edd}} / \dot{M}_{\text{RLOF}}|), \quad (2.6)$$

and the additional mass being lost is added to the  $\beta_{\text{mt}} \dot{M}_{\text{RLOF}}$  term in Equation (2.5), i.e., it is assumed to leave the system carrying the specific orbital angular momentum of the accretor.

## 2.2.3 Spin Orbit Coupling

Tidal interaction and mass transfer can significantly modify the spin angular momentum of the stars in a binary system, acting as both sources and sinks for orbital angular momentum. The impact spin-orbit interactions have on orbital evolution depends on the orbital separation and the mass ratio, with the effect being greater for tighter orbits and uneven masses. The corresponding contribution to  $J_{\text{orb}}$  is computed by demanding conservation of the total angular momentum, accounting for losses due to the other  $J_{\text{orb}}$  mechanisms and loss of stellar angular momentum due to winds.

In a fully conservative system, the change in orbital angular momentum in one timestep is  $\delta J_{\text{orb}} = -\delta S_1 - \delta S_2$ , where  $\delta S_1$  and  $\delta S_2$  are the changes in spin angular momenta. This needs to be corrected if mass loss is included, as winds take away angular momentum from the system. If  $S_{1,\text{lost}}$  and  $S_{2,\text{lost}}$  are the amounts of spin angular momentum removed in a step from each star due to mass loss (including winds and RLOF),

$$J_{\text{ls}} = \frac{-1}{\delta t} \left( \delta S_1 + S_{1,\text{lost}} \frac{\dot{M}_{1,w}}{\dot{M}_1} + \delta S_2 + S_{2,\text{lost}} \right), \quad (2.7)$$

where the additional factor for the donor accounts for mass lost from the system, ignoring mass loss due to mass transfer. In the absence of RLOF this equation becomes symmetric between both stars, as then  $\dot{M}_{1,w}/\dot{M}_1 = 1$ .

The form of Equation (2.7) is independent of how tides and angular momentum accretion work, as it is merely a statement on angular momentum conservation. The details of how we model these processes and their impact on the spin of each component are described in Section 2.4.

### 2.2.4 Magnetic Braking

The rotational velocities of low mass stars are strongly correlated with their ages (Skumanich, 1972). This spin-down arises from the coupling of the stellar wind to a magnetic field. If the star is in a binary system and tidally coupled to the orbit, magnetic braking can provide a very efficient sink for orbital angular momentum (Mestel, 1968; Verbunt and Zwaan, 1981). We implement this effect following S. Rappaport, Joss and Verbunt (1983), who assumed the star being braked is tidally synchronized:

$$J_{\text{mb}} = -6.82 \times 10^{34} \left( \frac{M_1}{M_\odot} \right) \left( \frac{R_1}{R_\odot} \right)^{\gamma_{\text{mb}}} \left( \frac{1 \text{ d}}{P_{\text{orb}}} \right)^3 [\text{dyn cm}], \quad (2.8)$$

where in the simplest approximation  $\gamma_{\text{mb}}=4$  (Verbunt and Zwaan, 1981). A similar contribution from the accretor can be included. As tidal synchronization is assumed, this formulation is incompatible with the use of LS coupling.

It is normally assumed that once a star becomes fully convective, the dynamo process that regenerates the field will stop working or at least behave in a qualitatively different manner. Similarly, magnetic fields in stars with radiative envelopes are of a significantly different nature than those seen in stars with convective envelopes, and there is no simple way to predict even the presence of magnetism (Donati and Landstreet, 2009). By default MESAbinary only accounts for magnetic braking as long as the star being braked has a convective envelope and a radiative core, though the process might still operate outside of these conditions.

## 2.3 Mass Transfer from RLOF

Close binary stars are defined as systems tight enough to interact through mass transfer, with the most important mechanism being RLOF. This process is commonly modeled in 1D by considering the spherical-equivalent Roche lobe radius  $R_{\text{RL}}$  of each object (Eggleton, 1983)

$$R_{\text{RL},j} = \frac{0.49 q_j^{2/3}}{0.6 q_j^{2/3} + \ln(1 + q_j^{1/3})} a, \quad (2.9)$$

where  $j$  is the index identifying each star,  $q_1 = M_1/M_2$  and  $q_2 = M_2/M_1$ . This fit is correct up to a few percent for the full range of mass ratios,  $0 < q_j < \infty$ . Mass transfer occurs then when the radius of a star approaches or exceeds  $R_{\text{RL}}$ . Depending on several factors, once a star begins RLOF the ensuing mass transfer phase can proceed on a nuclear, thermal, or dynamical timescale.

The stability of mass transfer is normally understood in terms of mass-radius relationships (e.g., Tout

et al., 1997; Soberman, Phinney and Heuvel, 1997),

$$\zeta_{\text{eq}} = \left( \frac{d \ln R_1}{d \ln M_1} \right)_{\text{eq}}, \quad (2.10)$$

$$\zeta_{\text{ad}} = \left( \frac{d \ln R_1}{d \ln M_1} \right)_{\text{ad}}, \quad (2.11)$$

$$\zeta_{\text{RL}} = \frac{d \ln R_{\text{RL},1}}{d \ln M_1}. \quad (2.12)$$

Here,  $\zeta_{\text{eq}}$  gives the radial response of the donor to mass loss when it happens slowly enough for the star to remain in thermal equilibrium. When mass loss proceeds on a timescale much shorter than the thermal timescale of the star, but still slow enough for the star to retain hydrostatic equilibrium then the radial response will be given by  $\zeta_{\text{ad}}$ . The dependency of the Roche lobe radius on mass transfer is encoded in  $\zeta_{\text{RL}}$ . In general  $\zeta = d \ln R_1 / d \ln M_1$  is a function of  $\dot{M}_{\text{RLOF}}$ , so requiring  $\zeta = \zeta_{\text{RL}}$  will determine the value of  $\dot{M}_{\text{RLOF}}$ . If an overflowing star satisfies  $\zeta_{\text{eq}} > \zeta_{\text{RL}}$ , then it can remain inside its Roche lobe by transferring mass while retaining thermal equilibrium. If on the contrary  $\zeta_{\text{ad}} > \zeta_{\text{RL}} > \zeta_{\text{eq}}$ , mass transfer will proceed on a thermal timescale, while for the extreme case  $\zeta_{\text{RL}} > \zeta_{\text{ad}}$  the star will depart from hydrostatic equilibrium and the process will be dynamical. MESA cannot model common envelope or contact binaries.

MESAbinary provides both explicit and implicit methods to compute mass transfer rates. An explicit computation sets the value of  $\dot{M}_{\text{RLOF}}$  at the start of a step, while an implicit one begins with a guess for  $\dot{M}_{\text{RLOF}}$  and iterates until the required tolerance is reached. The composition of accreted material is set to that of the donor surface, and the specific entropy of accreted material is the same as the surface of the accretor. In models with rotation the specific angular momentum of accreted material is described in Section 2.4.

### 2.3.1 Explicit Methods

MESAbinary implements two mass transfer schemes: the model of Ritter (1988) which we refer to as the Ritter scheme and U. Kolb and Ritter (1990) which we refer to as the Kolb scheme. We use the mass ratio  $q_2$  consistent with the Ritter scheme.

**Ritter scheme:** Stars have extended atmospheres therefore RLOF can take place through the L1 point even when  $R_1 < R_{\text{RL},1}$ . Ritter (1988) estimated the mass transfer rate for this case as

$$\dot{M}_{\text{RLOF}} = -\dot{M}_0 \exp\left(\frac{R_1 - R_{\text{RL},1}}{H_{P,1}/\gamma(q_2)}\right), \quad (2.13)$$

where  $H_{P,1}$  is the pressure scale height at the photosphere of the donor and

$$\dot{M}_0 = \frac{2\pi}{\exp(1/2)} F_1(q_2) \frac{R_{\text{RL},1}^3}{GM_1} \left( \frac{k_B T_{\text{eff}}}{m_p \mu_{\text{ph}}} \right)^{3/2} \rho_{\text{ph}}, \quad (2.14)$$

where  $m_p$  is the proton mass,  $T_{\text{eff}}$  is the effective temperature of the donor, and  $\mu_{\text{ph}}$  and  $\rho_{\text{ph}}$  are the mean molecular weight and density at its photosphere. The two fitting functions are

$$F_1(q_2) = 1.23 + 0.5 \log q_2, \quad 0.5 \lesssim q_2 \lesssim 10. \quad (2.15)$$

and

$$\gamma(q_2) = \begin{cases} 0.954 + 0.025 \log q_2 - 0.038(\log q_2)^2, & 0.04 \lesssim q_2 \leq 1 \\ 0.954 + 0.039 \log q_2 + 0.114(\log q_2)^2, & 1 \leq q_2 \lesssim 20. \end{cases} \quad (2.16)$$

Outside the ranges of validity  $F_1(q_2)$  and  $\gamma(q_2)$  are evaluated using the value of  $q_2$  at the edge of their respective ranges.

**Kolb scheme:** U. Kolb and Ritter (1990) extended the Ritter scheme in order to cover the case  $R_1 > R_{\text{RL},1}$  according to

$$\dot{M}_{\text{RLOF}} = -\dot{M}_0 - 2\pi F_1(q_2) \frac{R_{\text{RL},1}^3}{GM_1} \times \int_{P_{\text{ph}}}^{P_{\text{RL}}} \Gamma_1^{1/2} \left( \frac{2}{\Gamma_1 + 1} \right)^{(\Gamma_1+1)/(2\Gamma_1-2)} \left( \frac{k_B T}{m_p \mu} \right)^{1/2} dP \quad (2.17)$$

where  $\Gamma_1$  is the first adiabatic exponent, and  $P_{\text{ph}}$  and  $P_{\text{RL}}$  are respectively the pressures at the photosphere and at the radius for which  $r_1 = R_{\text{RL},1}$ .

### 2.3.2 Implicit Methods

Explicit schemes exhibit large jumps in  $\dot{M}_{\text{RLOF}}$  unless the timestep is severely restricted. Therefore, if one needs accurate values of  $\dot{M}_{\text{RLOF}}$  and stellar radius, this requires use of an implicit scheme. Implicit schemes also allow the calculation these quantities when there is no general closed form formula for  $\dot{M}_{\text{RLOF}}$ .

These implicit methods use a bisection-based root solve to satisfy  $|f(\dot{M}_{\text{RLOF}})| < \xi$  at the end of the step, where  $\xi$  is a given tolerance. The implicit schemes are then defined by the choice of the function  $f(\dot{M}_{\text{RLOF}})$ . For the Ritter and the Kolb scheme the function is chosen as

$$f(\dot{M}_{\text{RLOF}}) = \frac{\dot{M}_{\text{end}} - \dot{M}_{\text{RLOF}}}{\dot{M}_{\text{end}}}, \quad (2.18)$$

with  $\dot{M}_{\text{end}}$  being the mass transfer rate computed at the end of each iteration.

A different implicit method is also provided. In this case, whenever the donor star overflows its Roche lobe the implicit solver will adjust the mass transfer rate until  $R_1 = R_{\text{RL},1}$  within some tolerance (see e.g., Whyte and Eggleton, 1980; S. Rappaport, Joss and Webbink, 1982; S. Rappaport, Joss and Verbunt, 1983). In this case

$$f(\dot{M}_{\text{RLOF}}) = \frac{2(R_1 - R_{\text{RL},1})}{R_{\text{RL},1}} + \xi, \quad (2.19)$$

and if  $\dot{M}_{\text{RLOF}}$  is below a certain threshold and  $f(\dot{M}_{\text{RLOF}}) < -\xi$  then the system is assumed to detach and  $\dot{M}_{\text{RLOF}}$  is set to zero.

## 2.4 Effect of Tides and Accretion on Stellar Spin

To model tidal interaction we adjusted the model of Hut (1981) to include the case of differentially rotating stars. The time evolution of the angular frequency for each component is

$$\frac{d\Omega_{i,j}}{dt} = \frac{\Omega_{\text{orb}} - \Omega_{i,j}}{\tau_{\text{sync},j}}, \quad \frac{1}{\tau_{\text{sync},j}} = \frac{3}{(q_j r_{g,j})^2} \left(\frac{k}{T}\right)_{c,j} \left(\frac{R_j}{a}\right)^6, \quad (2.20)$$

where  $j = 1, 2$  is the index of each star,  $\Omega_{i,j}$  is the angular frequency at the face of cell  $i$  towards the surface,  $r_{g,j}^2 = I_j/(M_j R_j^2)$  is the radius of gyration (with  $I_j$  being the moment of inertia of each star), and the ratio of the apsidal motion constant to the viscous dissipation timescale,  $(k/T)_{c,j}$ , is computed as in Hurley, Tout and Pols (2002). Similarly to Detmers et al. (2008), we assume constant  $\tau_{\text{sync},j}$  and  $\Omega_{\text{orb}}$  through a step and therefore  $\Delta\Omega_{i,j} = [1 - \exp(-\delta t/\tau_{\text{sync},j})](\Omega_{\text{orb}} - \Omega_{i,j})$ . This extension of Hut's work to differentially rotating stars is not formally derived but merely applies his result for solid body rotators independently to each shell. The formulation of Hut (1981) can be recovered from Equation (2.20), by forcing solid body rotation with a large diffusion coefficient for angular momentum throughout the star. In reality tides would act mostly on the outer layers, and whether the core synchronizes or not depends on the coupling between the core and the envelope.

To compute the specific angular momentum carried by accreted material, we consider the possibility of both ballistic and Keplerian disk mass transfer (e.g., Marsh, Nelemans and Steeghs, 2004; de Mink, Langer et al., 2013). To distinguish which occurs, we compare the minimum distance of approach of the accretion stream (Lubow and Shu, 1975; Ulrich and Burger, 1976)<sup>2</sup>

$$R_{\min} = 0.0425a \left(q_2 + q_2^2\right)^{1/4}, \quad 0.0667 \leq q_2 \leq 15 \quad (2.21)$$

to the radius of the accreting star. When outside the range of validity,  $R_{\min}$  is computed using the value of  $q_2$  at the respective edge. Accretion is assumed to be ballistic whenever  $R_2 > R_{\min}$  and the specific angular momentum is  $(1.7GM_2R_{\min})^{1/2}$ . When  $R_2 < R_{\min}$  the specific angular momentum is taken as that of a Keplerian orbit at the surface  $(GM_2R_2)^{1/2}$ .

## 2.5 Treatment of Thermohaline Mixing in Accreting Models

In stars with radiative envelopes accreted material with a high mean molecular weight is expected to mix inwards due to thermohaline mixing, a process that is very sensitive to the  $\mu$ -gradient (see e.g., Kippenhahn, Ruschenplatt and Thomas, 1980; Cantiello and Langer, 2010). Thermohaline mixing is included in *MESA* (see Paxton, Bildsten et al. 2011). However, as mass with homogeneous composition is added during the accretion process, a jump is produced at the boundary between new and old material. *MESAstar* computes mixing coefficients explicitly at the start of each step, so this results in thermohaline mixing only operating near this boundary, leading to unphysical compositional staircases. To avoid this issue, we artificially soften the composition gradient in the outer  $(\Delta q)_{\text{large}}$  fraction of the star by mass. We do this starting at the surface and homogeneously mixing inwards a region of size  $(\Delta q)_{\text{small}}$ . Then, moving towards the center, the process is repeated at each cell while linearly (with respect to mass) reducing the size of the small mixed region such that it is zero after going  $(\Delta q)_{\text{large}}$  inwards. All the binary models where the accretor is not a point mass are calculated using  $(\Delta q)_{\text{large}} = 0.05$  and  $(\Delta q)_{\text{small}} = 0.03$ .

<sup>2</sup> Note that there is a small typo in the fit given by Ulrich and Burger (1976). The corrected fit given here fits the results of Lubow and Shu (1975) to the 4% accuracy claimed by Ulrich and Burger (1976).

## 2.6 Numerical Tests

Here we describe tests designed to validate the implementation of the physics described in Section 2.2. We check orbital evolution in the presence of gravitational waves and mass loss by comparing to analytical solutions. We also verify total angular momentum conservation in calculations that include the physics of tides and spinup by accretion. To test for the thermal response of stellar models undergoing mass transfer, we compare MESAbinary results to those from the STARS code (Eggleton, 1971; Pols et al., 1995; Stancliffe and Eldridge, 2009).

### 2.6.1 Gravitational Wave Radiation

If gravitational waves are the only source of angular momentum loss and the masses of each component remain constant, Equation (2.3) can be integrated to obtain the time evolution of orbital separation (Peters, 1964). We model a system consisting of a  $0.5 M_{\odot}$  star and a  $0.8 M_{\odot}$  point mass with  $a = 2 R_{\odot}$ . We ignore all effects on the evolution of orbital angular momentum except its loss due to gravitational waves. In 3.5 Gyr the orbital separation of this system reduces to  $a = 1.3 R_{\odot}$ , at which point the  $0.5 M_{\odot}$  star begins mass transfer. We terminate the run at the onset of RLOF. The maximum error in  $a$  is 0.35% relative to the analytical result.

### 2.6.2 Inefficient Mass Transfer

An analytical expression for the evolution of orbital separation can be derived if inefficient mass transfer is the only contribution to the angular momentum evolution (Tauris and van den Heuvel, 2006). We model a  $2.5 M_{\odot}$  main sequence star together with a  $1.4 M_{\odot}$  point mass with an initial orbital separation of  $10 R_{\odot}$ . We choose  $\alpha_{\text{mt}} = 0.03$ ,  $\beta_{\text{mt}} = 0.95$ ,  $\delta_{\text{mt}} = 0.01$  and  $\gamma_{\text{mt}}^2 = 2$ , which give a low mass transfer efficiency of  $f_{\text{mt}} = 0.01$ . Such a system is representative of the evolution of an intermediate mass X-ray binary (IMXB). The model initiates mass transfer just after the end of the main sequence, interrupting the evolution of the star through the Hertzsprung gap and producing a low mass white dwarf (WD) ( $M_{\text{He}} = 0.289 M_{\odot}$ ) with a small amount of hydrogen on its surface. As the WD evolves to the cooling track, it experiences several hydrogen flashes, one of them strong enough to produce an additional phase of RLOF (see Figure 2.1).

Figure 2.2 shows that MESAbinary computes the orbital evolution to a precision of a few parts in  $10^4$ . We run this system using both the Ritter and the Kolb implicit schemes to display that under some circumstances the precise choice of mass transfer scheme does not play a big role in the evolution.

### 2.6.3 Spin Orbit Coupling

We now test angular momentum conservation by ignoring all the mechanisms that remove angular momentum from the binary system. For this purpose we model an  $8 M_{\odot} + 6 M_{\odot}$  binary with rotating components and an initial orbital period of 1.5 days. Due to the short orbital separation we assume the initial spin periods of the two stars are equal to the orbital period. The primary undergoes RLOF during the main sequence, initiating a phase of mass transfer on a thermal timescale. After transferring just  $0.3 M_{\odot}$  the accretor also fills its Roche lobe, producing a contact system. At this point we terminate the evolution.

Figure 2.3 shows that spin angular momentum in both components increases during the pre-interaction phase, which is due to both stars expanding on the main sequence while remaining tidally locked. During Roche lobe overflow, the secondary is rapidly spun-up, reaching nearly 80% of critical rotation before contact. The calculation of total angular momentum requires the summation of different contributions

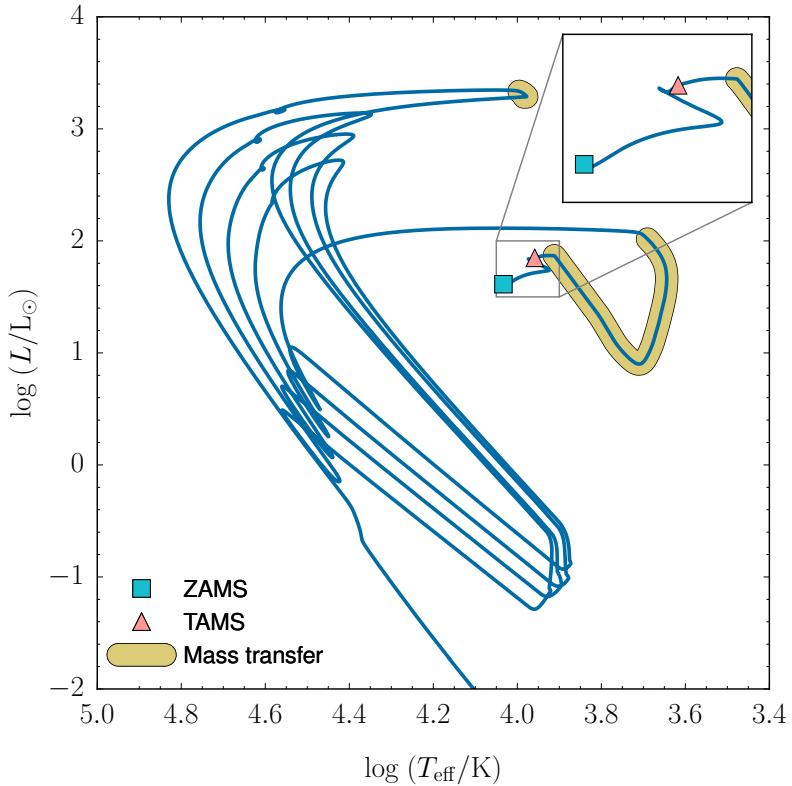


Figure 2.1: Evolution in the HR diagram for a  $2.5 M_{\odot}$  star transferring mass to a  $1.4 M_{\odot}$  point mass, assuming a mass transfer efficiency of 1%. Symbols are shown at zero-age main sequence (ZAMS) and terminal-age main sequence (TAMS), together with parts of the track where RLOF is occurring. The inset shows evolution from ZAMS up to the beginning of the first phase of mass transfer.

(orbital angular momentum and spin of both components). Therefore the maximum accuracy to which we can conserve angular momentum is limited by rounding errors. Figure 2.3 shows that conservation of angular momentum in the run is very close to machine precision.

#### 2.6.4 Thermal Response to Mass Loss

The fate of binary systems depends largely on the precise value of  $\dot{M}$  during an interaction phase, which depends on the thermal response of the donor star to mass loss. For WDs there is a limited range of accretion rates for stable hydrogen burning (Nomoto et al. 2007; Shen and Bildsten 2007). In main sequence binaries the evolution of the accretor radius depends on the mass transfer rate, and expansion during the interaction phase can lead to contact or even a merger (Wellstein, Langer and Braun 2001).

We calculated an  $8 M_{\odot} + 6.5 M_{\odot}$  binary system with an initial orbital period of 1.5 days using both MESAbinary and STARS. To minimize the modeling differences and focus on the thermal response of both components, we use an extremely simplified model that ignores internal mixing (including convective mixing). Under these conditions, the more massive star quickly depletes its central hydrogen and begins shell hydrogen burning, reaching RLOF and undergoing a phase of mass transfer on the thermal timescale. The resulting mass transfer rates are shown in Figure 2.4. The agreement is very

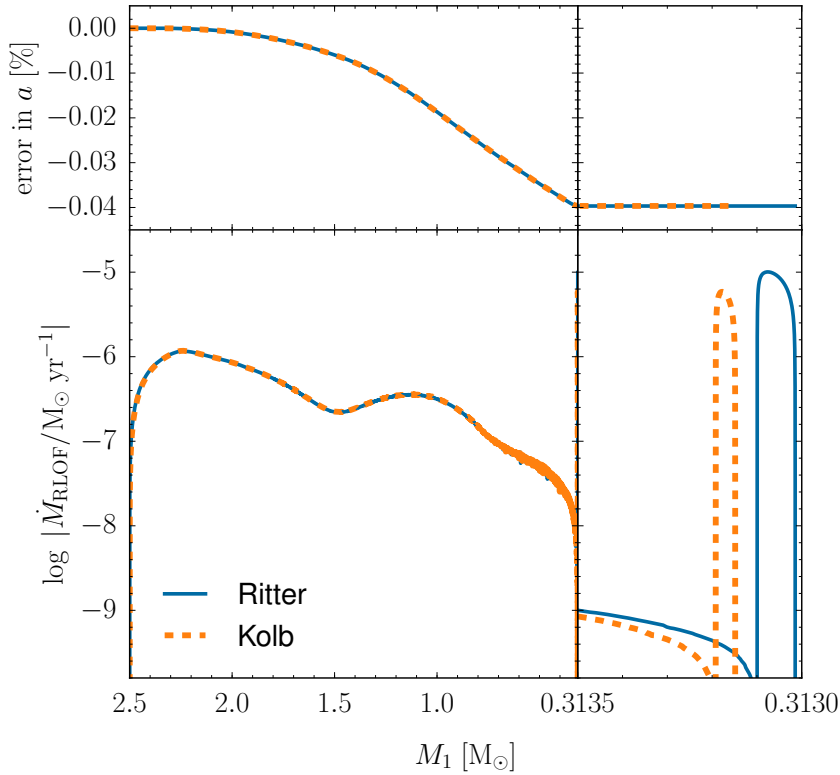


Figure 2.2: Evolution of mass transfer rate from a  $2.5 M_\odot$  to a  $1.4 M_\odot$  point mass, assuming a mass transfer efficiency of 1%. The upper panel shows the difference between the computed orbital separation and the analytical solution while the bottom one displays the evolution of the mass transfer rate, using two different schemes.

good, despite mass transfer rates being computed in slightly different ways. Masses at detachment show a small difference, with the MESAbinary model terminating mass transfer when  $M_1 = 0.952 M_\odot$  while the STARS calculation when  $M_1 = 0.935 M_\odot$ . The figure also shows the change in radius of the accreting star, with two prominent peaks at  $R_2/R_\odot = 4.84, 5.34$  for MESAbinary and  $4.82, 5.28$  for STARS. The larger radius of the MESAbinary model is likely associated to the slightly higher mass transfer rates.

## 2.7 Period Gap of Cataclysmic Variables

Although cataclysmic variables (CVs) span a wide range of periods, observations show a lack of systems in the range  $2 \text{ h} < P_{\text{orb}} < 3 \text{ h}$  (see, for instance, Gänsicke et al., 2009). Such a feature is commonly explained by having an angular momentum loss mechanism “turn off” or become inefficient at some point. The most popular model for such a mechanism is magnetic braking (S. Rappaport, Joss and Verbunt, 1983), as the magnetic field of the donor is assumed to change quickly when the star loses enough mass to become fully convective.

We now compare to the results of Howell, L. A. Nelson and S. Rappaport (2001), who performed a population synthesis study to explore in detail the standard scenario involving magnetic braking. In Figure 2.5 we show the evolution of mass transfer rates and orbital periods for a set of CV models with

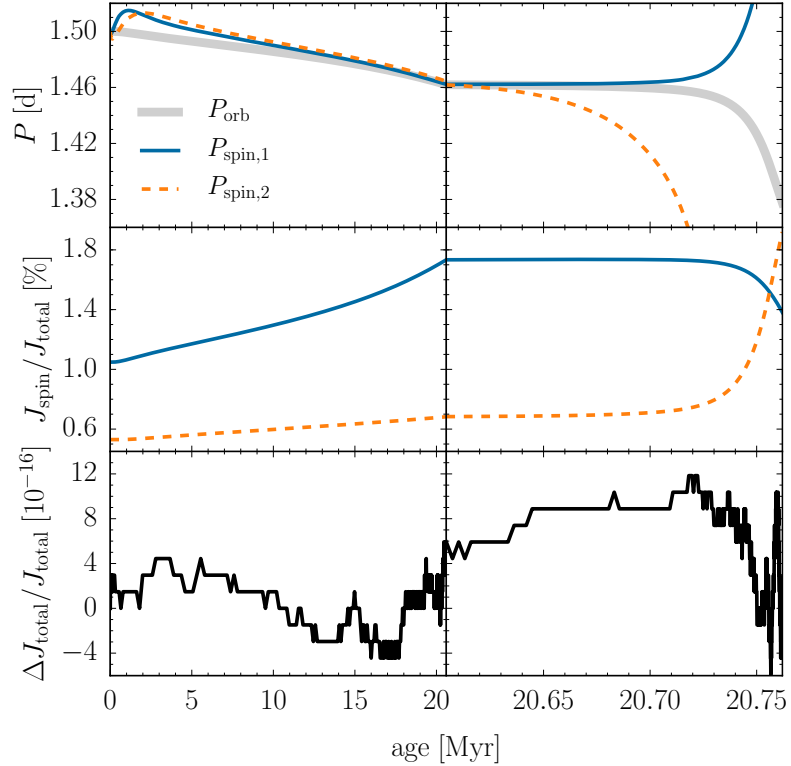


Figure 2.3: Angular momentum evolution in an  $8 M_{\odot} + 6 M_{\odot}$  binary with an initial orbital period of 1.5 days. Left panels show the evolution before the onset of RLOF, while right panels display evolution from the beginning of RLOF until contact, when both components fill their Roche lobe. The fractional error in the total angular momentum is plotted in the bottom panel and is of order machine-precision.

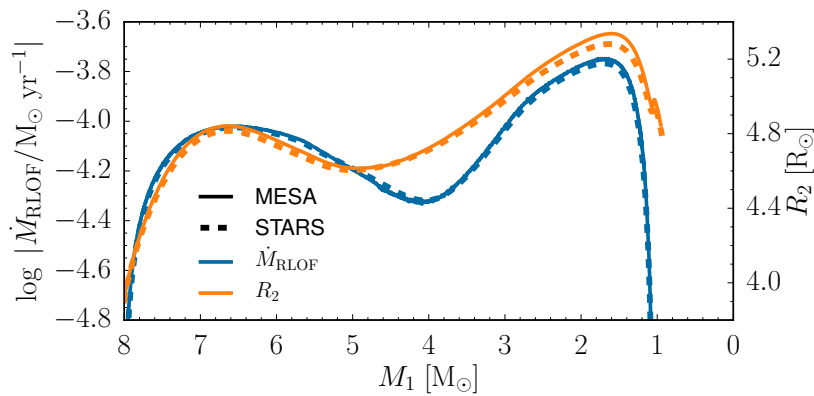


Figure 2.4: Mass transfer rate and accretor radius as computed by MESA and STARS for an  $8 M_{\odot} + 6.5 M_{\odot}$  binary with an initial orbital period of 3 days. All internal mixing processes (including convective mixing) are turned off in the calculations.

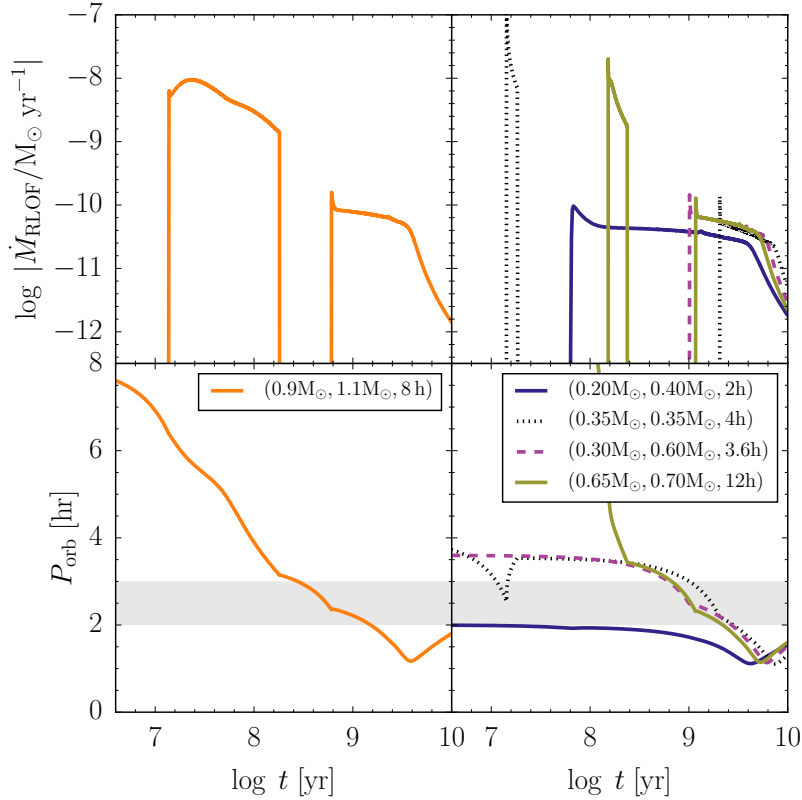


Figure 2.5: Evolution of CV models under the effect of magnetic braking and gravitational wave radiation. For each track the label gives the donor mass, the WD mass, and the initial orbital period respectively. The grey band shows the observed period gap for CVs. These results reproduce figure 1 in Howell, L. A. Nelson and S. Rappaport (2001).

different component masses and orbital periods. We run all models using  $\beta_{\text{mt}} = 1$  and  $\gamma_{\text{mb}} = 3$  and magnetic braking is turned off when the donor star becomes fully convective. As an example the system with a  $0.9 M_{\odot}$  donor (left panel in Figure 2.5) experiences a first phase of mass transfer induced by magnetic braking between  $10^{7.1}$  and  $10^{8.3}$  yr, a non-interacting phase (the gap) between  $10^{8.3}$  and  $10^{8.8}$  yr, and a subsequent phase of mass transfer dominated by gravitational wave radiation, reaching a minimum orbital period of about 1 hour at  $10^{9.6}$  yr. As a comparison, for the same model Howell, L. A. Nelson and S. Rappaport (2001) obtain a first phase of mass transfer between  $10^{7.3}$  and  $10^{8.4}$  yr, the gap occurs between  $10^{8.4}$  and  $10^{8.8}$  yr and a period minimum is reached at  $10^{9.4}$  yr. Figure 2.5 shows that our CV models spend most time away from the observed period gap.

## 2.8 Evolution of Massive Binaries

In massive stars, binary interactions have dramatic effects on the evolution of both components. Kippenhahn and Weigert (1967) introduced the term “case A” to refer to a mass transfer phase occurring in systems tight enough such that RLOF starts during the main sequence. This results in a large amount of mass being transferred on a thermal timescale, followed by a phase of mass transfer that proceeds on the

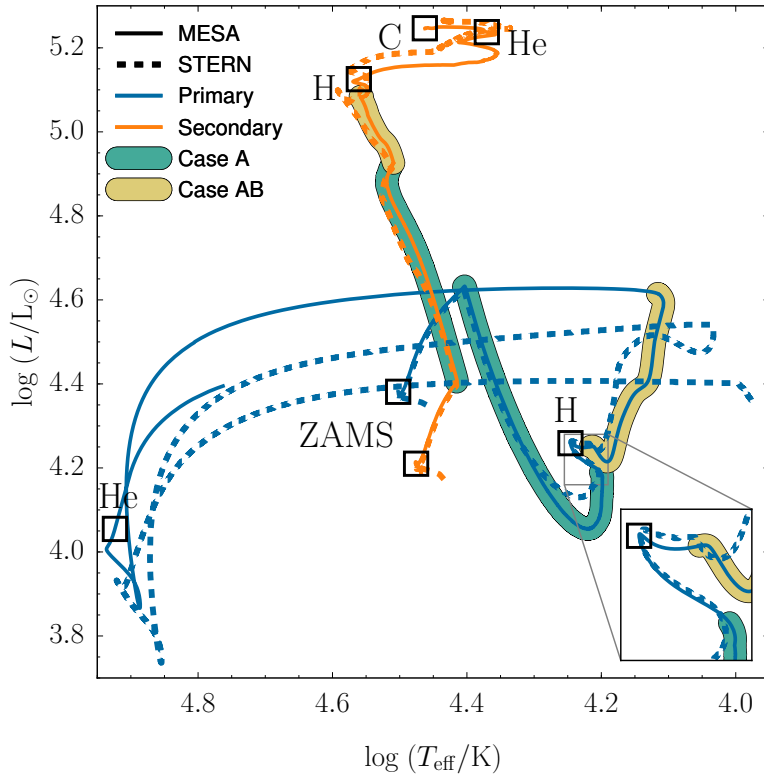


Figure 2.6: Evolution of a  $16 M_{\odot} + 14 M_{\odot}$  system with a 3 day initial orbital period. MESAbinary models are compared to the results of Wellstein, Langer and Braun (2001), which were calculated using the STERN code. The terms primary and secondary are used throughout the evolution to describe the initially more massive and the less massive components, respectively. For each component in the MESAbinary model, squares mark the ZAMS and the depletion of the indicated nuclear fuel in the core.

nuclear timescale until the end of core H-burning. An additional phase of thermal-timescale mass transfer then follows (the so-called “case AB”), which strips the donor and produces an almost-naked helium star.

Here we show that MESAbinary can calculate the evolution of massive interacting binaries. We reproduce one of the models from Wellstein, Langer and Braun (2001), a  $16 M_{\odot} + 14 M_{\odot}$  system with an initial period of 3 days, using the same semiconvection efficiency of  $\alpha_{sc} = 0.01$ . As shown in Figures 2.6 and 2.7 this system experiences case A and AB mass transfer, and the accretor becomes a blue supergiant after core hydrogen depletion. The accretor depletes carbon before its donor.

Figure 2.7 illustrates the prevalence of both thermohaline mixing and semiconvection in the accreting star. Newly accreted material is efficiently mixed inwards by thermohaline mixing. On the other hand the  $\mu$ -gradient formed before interaction prevents the convective core from growing, with the efficiency of semiconvection controlling whether or not the star rejuvenates. Due to the choice of inefficient semiconvection, the core remains small, preventing the star from becoming a red supergiant. The star accretes a large amount of CNO-processed and helium-rich material. After being mixed through the envelope this material results in the surface being nitrogen rich and carbon depleted, with a slight enhancement in helium.

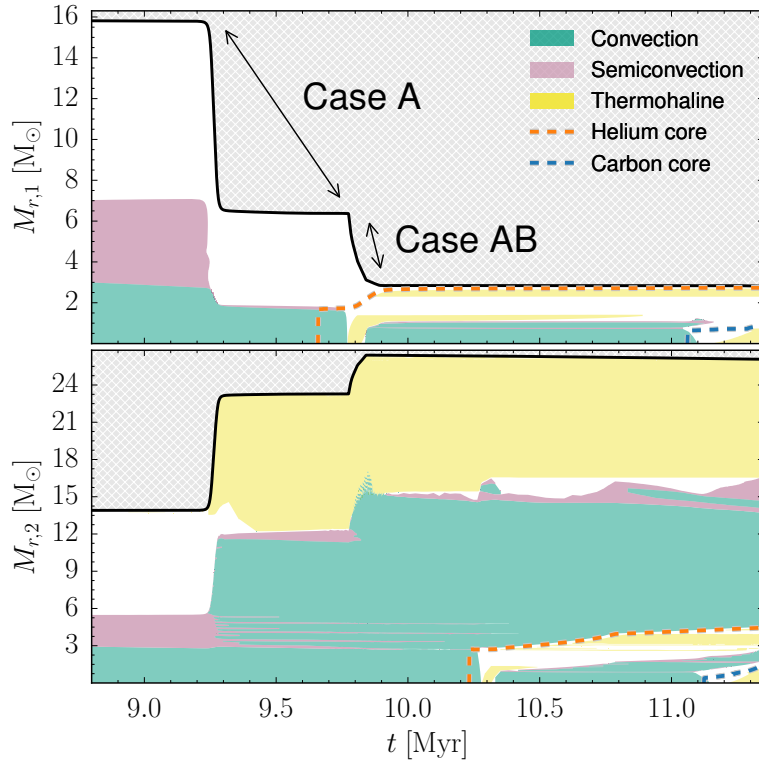


Figure 2.7: Kippenhahn diagram for the evolution of a  $16 \text{ M}_\odot + 14 \text{ M}_\odot$  system with a 3 day initial orbital period. Most of the pre-interaction phase is not shown in this figure. The upper plot shows the evolution of the donor, while the lower plot displays that of the accretor.

## 2.9 Rotating Binaries and the Efficiency of Mass Transfer

The efficiency of mass transfer plays a key role in close binary systems, but the processes by which material is lost from the system are not well-understood. In particular, whenever an accreting star approaches  $\Omega/\Omega_{\text{crit}} = 1$ , it is uncertain whether accretion can continue, one option being the development of a strong wind that prevents accretion (e.g., Petrovic, Langer and Hucht, 2005; Cantiello, Yoon et al., 2007). Whenever  $\Omega/\Omega_{\text{crit}}$  approaches one, we use an implicit method to iteratively reduce  $\dot{M}_2$  until this ratio falls below a threshold.

Tides counteract the effect of spin-up from accretion. Whether or not an accreting object reaches critical rotation depends on the efficiency of tidal coupling. Here we model a  $16 \text{ M}_\odot + 15 \text{ M}_\odot$  binary system including differential stellar rotation, with an initial orbital period of 3 days and assuming initial orbital synchronization. Langer, Wellstein and Petrovic (2003) argue that turbulent processes in the radiative envelope can significantly enhance tidal strength. They model the same system using the simple estimate for the synchronization timescale for a star with a convective envelope given by Zahn (1977),  $\tau_{\text{sync},j} = 1 \text{ yr} \times q_j^2(a/R)^6$ . For our implicit modeling of stellar winds we use a threshold of  $(\Omega/\Omega_{\text{crit}}) = 0.99$ .

Figure 2.8 shows that MESAbinary models using both the Zahn (1977) and Hurley, Tout and Pols (2002) timescales for tidal coupling. These models experience highly non-conservative phases of mass

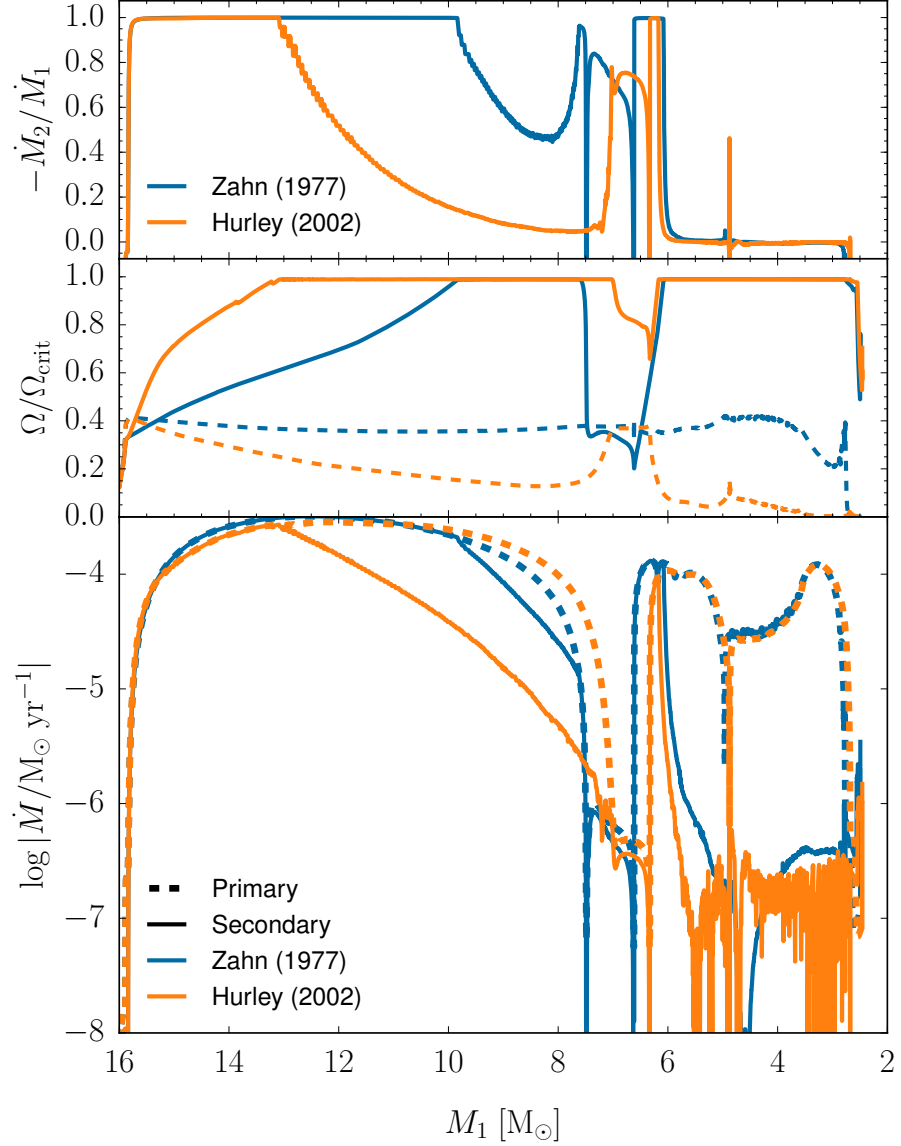


Figure 2.8: Efficiency of mass transfer in a  $16 M_\odot + 15 M_\odot$  binary system including differential rotation. The system is modeled with tides as described by Hurley, Tout and Pols (2002) for radiative envelopes, and also with the simple tidal timescale given by Zahn (1977). The upper panel shows the efficiency of mass transfer, the middle panel the angular frequency of each star in terms of its critical value, while the lower panel shows the evolution of  $\dot{M}$  for both components.

transfer, corresponding to the accreting star evolving very close to critical rotation. In particular during case AB mass transfer the accretor needs to switch from mass accretion to mass loss in order to remain sub-critical. As expected, the system with the tidal timescale from Zahn (1977) has a significantly higher mass transfer efficiency, and during the first phase of RLOF it only experiences a brief period in which the accretor reaches critical rotation. This is in broad agreement with the model by Langer, Wellstein and Petrovic (2003).

## 2.10 Description of a Binary Run

MESAbinary performs each evolution step by independently solving the structure of each component and the orbital parameters, using the same timestep  $\delta t$  for each. This approach differs from STARS, which simultaneously solves for the structure of both stars and the orbit in a single Newton-Raphson solver. Our choice to solve for each star separately gives a significant amount of flexibility and simplicity, as the examples in this paper demonstrate.

The top-level algorithm for evolving a star is described in appendix B1 of Paxton, Cantiello et al. (2013). We modified this algorithm to support the new implementation of binary interactions, which is described in detail in the MESA documentation. Additional timestep limits are imposed in MESAbinary that consider relative changes between the radius and Roche lobe radius of both components, the total orbital angular momentum, the orbital separation, and the envelope mass in the donor.

**Acknowledgements:** It is a pleasure to thank Nilou Afsari, Dave Arnett, Warrick Ball, Ed Brown, Jieun Choi, Joergen Christensen-Dalsgaard, Andrew Cumming, Sebastien Deheuvels, Aaron Dotter, Chris Fryer, Duncan Galloway, Pascale Garaud, Alfred Gautschy, Samuel Jones, Max Katz, Eli Livne, Marcin Mackiewicz, Chris Mankovich, Casey Meakin, Broxton Miles, Ehsan Moravveji, Kevin Moore, Eliot Quataert, Jeremy Sakstein, Richard Stancliffe, Willie Strickland, Anne Thoul, and Joris Vos. We also thank the participants of the 2013 and 2014 MESA Summer Schools for their willingness to experiment with new capabilities.

This project was supported by NSF under the SI<sup>2</sup> program grants (ACI-1339581, ACI-1339600, ACI-1339606) and NASA under the TCAN program grants (NNX14AB53G, NNX14AB55G, NNX12AC72G). The work at UC Santa Barbara was also supported by the NSF under grants PHY 11-25915, AST 11-09174, AST 12-05574. J.S. is supported by the NSF Graduate Research Fellowship Program under grant DGE 11-06400. L.D. acknowledges financial support by the “Agence Nationale de la Recherche” under grant ANR-2011-Blanc-SIMI-BS56-0007. D.T. acknowledges support under HST-GO-12870.14-A from the Space Telescope Science Institute, which is operated by the Association of Universities for Research in Astronomy, Inc., for NASA, under contract NAS 5-26555. R.H.D.T. acknowledges resources provided by of the University of Wisconsin-Madison Advanced Computing Initiative. F.X.T. acknowledges support from the Simons Foundation.



## CHAPTER 3

---

# A new route towards merging massive black holes

---

**Pablo Marchant**, Norbert Langer, Philipp Podsiadlowski, Thomas M. Tauris and Takashi J. Moriya  
Astronomy & Astrophysics, Volume 588, id.A50

**ABSTRACT:** With recent advances in gravitational-wave astronomy, the direct detection of gravitational waves from the merger of two stellar-mass compact objects has become a realistic prospect. Evolutionary scenarios towards mergers of various double compact objects generally invoke so-called common-envelope evolution, which is poorly understood and leads to large uncertainties in the predicted merger rates. Here we explore, as an alternative, the scenario of massive overcontact binary (MOB) evolution, which involves two very massive stars in a very tight binary that remain fully mixed as a result of their tidally induced high spin. While many of these systems merge early on, we find many MOBs that swap mass several times, but survive as a close binary until the stars collapse. The simplicity of the MOB scenario allows us to use the efficient public stellar-evolution code MESA to explore it systematically by means of detailed numerical calculations. We find that, at low metallicity, MOBs produce double-black-hole (BH+BH) systems that will merge within a Hubble time with mass-ratios close to one, in two mass ranges, about  $25 \dots 60 M_{\odot}$  and  $\gtrsim 130 M_{\odot}$ , with pair-instability supernovae (PISNe) being produced at intermediate masses. Our models are also able to reproduce counterparts of various stages in the MOB scenario in the local Universe, providing direct support for the scenario. We map the initial binary parameter space that produces BH+BH mergers, determine the expected chirp mass distribution, merger times, and expected Kerr parameters, and predict event rates. We find typically one BH+BH merger event for  $\sim 1,000$  core-collapse supernovae for  $Z \lesssim Z_{\odot}/10$ . The advanced LIGO (aLIGO) detection rate is more uncertain and depends on the cosmic metallicity evolution. From deriving upper and lower limits from a local and a global approximation for the metallicity distribution of massive stars, we estimate aLIGO detection rates (at the aLIGO design limit) of  $\sim 19 - 550 \text{ yr}^{-1}$  for BH-BH mergers below the PISN gap and of  $\sim 2.1 - 370 \text{ yr}^{-1}$  above the PISN gap. Even with conservative assumptions, we find that aLIGO will probably soon detect BH+BH mergers from the MOB scenario. These could be the dominant source for aLIGO detections.

Stellar binaries that consist of two stellar remnants so close to each other that they can merge within the Hubble time have been known for a long time. Merging double white dwarf systems are thought to provide one potential channel to produce so-called Type Ia supernovae, which are the main producers of iron and through which the accelerated expansion of the Universe was discovered. Various double neutron star systems have also been found, most importantly the Hulse-Taylor system (Hulse and J. H. Taylor, 1975; Weisberg, Nice and J. H. Taylor, 2010) and more recently the double pulsar PSR J0737-3039 (Burgay et al., 2003; Kramer, Stairs et al., 2006b), whose orbital decay has unambiguously confirmed Einstein’s gravitational wave prediction. Double black hole binaries have not yet been detected, which is obviously difficult since they do not emit electromagnetic radiation. However, because they are the most massive of the double compact binaries, their gravitational-wave radiation would be much stronger than that of white dwarf or neutron star systems.

The evolution of a binary system from the initial stage of two orbiting main-sequence stars to the double compact binary stage is in most scenarios believed to require at least one so-called common-envelope phase. This is essential because stars tend to expand dramatically after their main-sequence evolution, and as an early merging of the binary is to be avoided, a large orbital separation is required to accommodate this. The common-envelope stage is then necessary to shrink the system to a compact final configuration. While the physics of this process is not yet well understood (Ivanova et al., 2013), some observational constraints exist for low-mass binaries (e.g. Han et al. 2003; Zorotovic, Schreiber and Gänsicke 2011). For massive binaries, observational evidence is much scarcer, and the common-envelope process is much less well understood theoretically (Taam and Sandquist, 2000). For double neutron star systems, the increased number of observed systems is beginning to provide some constraints (Kalogera et al., 2004). For double black hole systems, however, the uncertainties are so large that the predicted rates of black hole binaries from the common-envelope channel are uncertain by several orders of magnitude (Abadie, B. P. Abbott, R. Abbott, Abernathy et al., 2010).

A completely different route towards double compact binaries is explored in this paper. It does not involve a common-envelope phase and may work only for very massive stars: it involves the chemically homogeneous evolution of rapidly rotating stars in tidally locked binaries.

The stabilizing effects of entropy and composition gradients usually prevent the efficient mixing of gas once composition gradients have been established. However, the more massive a star is, the less this is the case because of the increased importance of radiation pressure. It has been found that mixing induced by rapid rotation can, in principle, keep massive stars chemically homogeneous throughout core hydrogen burning (Maeder, 1987; Langer, 1992; Heger, Langer and Woosley, 2000). Detailed studies of this type of evolution through large grids of stellar models (Yoon and Langer, 2005; Woosley and Heger, 2006; Brott, de Mink et al., 2011; Köhler et al., 2015; Szécsi et al., 2015) have shown that this only works at low metallicity where strong angular-momentum loss that is due to stellar winds can be avoided, such that the stars remain fully mixed until their core hydrogen is exhausted. Because in this case, rapidly spinning iron cores are produced at the end of the stars’ lives, such single-star models have been suggested as progenitors of long-duration gamma-ray bursts (LGRBs) (Woosley and Heger, 2006; Yoon, Langer and C. Norman, 2006).

Chemically homogeneously evolving stars avoid the strong post-main-sequence expansion because they do not maintain a massive hydrogen-rich envelope. de Mink, Cantiello et al. (2009) therefore suggested that massive close binaries, where rapid rotation and thus chemically homogeneous evolution can be enforced through the tidal interaction of both stars, could evolve towards black holes without ever encountering contact or mass transfer (see also Mandel and de Mink (2016) and Song et al. (2016)).

We here explore the evolution of close binaries with component masses above  $\sim 20 M_{\odot}$  by computing large grids of detailed binary evolution models. For this purpose, we use the publicly available code MESA, which we extended to allow the inclusion of contact binaries with mass-ratios close to one

(Sect. 2). Against our initial expectation, we find that contact-free evolution occurs only very rarely. Instead, when computing the evolution of massive overcontact binaries (MOBs), we find many systems that avoid merging during core hydrogen burning. We compute the final configurations of these binaries in Sect. 3, including the black hole masses, separations, and their mass ratios. In Sect. 4 we discuss the predicted black hole Kerr parameters, potential explosive mass loss and momentum kicks, and the connection of the MOB scenario with long-duration gamma-ray bursts (GRBs) and pair-instability supernovae (PISNe). We discuss event rates and potential LIGO detection rates in Sect. 5 before giving our conclusions in Sect. 6.

## 3.1 Methods

We here provide the first detailed binary stellar evolution models that are followed until the double black hole stage. To obtain these, we applied the MESA code (Paxton, Marchant et al., 2015; Paxton, Cantiello et al., 2013; Paxton, Bildsten et al., 2011), which now includes all the physics required for such calculations, in particular, tidal interactions and differential rotation. We computed about 2000 detailed binary-evolution sequences in six model grids for different initial metallicities and mass ratios, thereby achieving a complete coverage of the relevant parameter space. Our model calculations include the overcontact phase, which occurs in the closest simulated binaries. This constitutes the main channel for providing massive close black hole binaries.

### 3.1.1 Physics implemented in MESA and initial parameters

To model the evolution of our systems, we used the binary module in version r8118 of the MESA code.<sup>1</sup> Opacities were calculated using CO-enhanced opacity tables from the OPAL project (Iglesias and F. J. Rogers, 1996), computed using solar-scaled abundances based on Grevesse, Noels and Sauval, 1996. Convection was modelled using the standard mixing-length theory (Böhm-Vitense, 1958) with a mixing-length parameter  $\alpha = 1.5$ , adopting the Ledoux criterion. Semiconvection was modelled according to Langer, Fricke and Sugimoto, 1983 with an efficiency parameter  $\alpha_{sc} = 1.0$ . We included convective core overshooting during core hydrogen burning following Brott, de Mink et al., 2011. The effect of the centrifugal force was implemented as in Heger, Langer and Woosley, 2000. Composition- and angular-momentum transport due to rotation includes the effects of Eddington-Sweet circulation, secular and dynamical shear instabilities, and the GSF instability, with an efficiency factor  $f_c = 1/30$ . This corresponds to the calibrations of the mixing efficiency in stellar models based on the VLT FLAMES Survey of Massive Stars (Brott, de Mink et al. 2011, and references therein). We included the effect of magnetic fields on the transport of angular momentum as in Petrovic, Langer, Yoon et al., 2005. Tidal effects were implemented as in Hurley, Tout and Pols, 2002 and Detmers et al., 2008 for the case of stars with a radiative envelope. We are not interested in following the nucleosynthesis in detail, therefore we used the simple networks provided with MESA `basic.net` for H and He burning, `co_burn.net` for C and O burning, and `approx21.net` for later phases.

Our implementation of stellar winds follows that of Yoon, Langer and C. Norman, 2006, with mass-loss rates for hydrogen-rich stars (with a surface helium abundance  $Y_s < 0.4$ ) computed as in Vink, de Koter and Lamers, 2001, while for hydrogen-poor stars ( $Y_s > 0.7$ ) we used the recipe of Hamann, Koesterke and Wessolowski, 1995 multiplied by a factor of one tenth. In the range  $0.4 < Y_s < 0.7$ , the rate was interpolated between the two. For both rates we used a metallicity scaling of  $(Z/Z_\odot)^{0.85}$ . We also included the enhancement of winds through rotation as in Heger, Langer and Woosley, 2000, and, when the

<sup>1</sup> The necessary input files to reproduce our results with this MESA version are provided at <http://mesastar.org/>.

rotation rate exceeded a given threshold  $\Omega/\Omega_{\text{crit}} > 0.98$ , we implicitly computed the mass-loss rate required for the rotation rate to remain just below this value.

Whenever one component in the system attempted to overflow its Roche lobe, we implicitly computed the mass-transfer rate necessary for it to remain just within the Roche volume (computed as in Eggleton 1983). The treatment of mass transfer in overcontact systems is described in the following section.

We considered four different metallicities,  $Z_{\odot}/4$ ,  $Z_{\odot}/10$ ,  $Z_{\odot}/20$ , and  $Z_{\odot}/50$ , with  $Z_{\odot} = 0.017$  as in Grevesse, Noels and Sauval, 1996. The helium abundance was set in such a way that it increased linearly from its primordial value  $Y = 0.2477$  (M. Peimbert, Luridiana and A. Peimbert, 2007) at  $Z = 0$  to  $Y = 0.28$  at  $Z = Z_{\odot}$ . For all metallicities, we computed grids for mass-ratios  $q_i = M_2/M_1 = 1$ ; for  $Z_{\odot}/50$ , we also computed grids at  $q_i = 0.9, 0.8$ . The initial orbital periods were chosen from the range ( $P_i = 0.5 - 3.0$ ) days, with an interval of 0.1 days, while the initial primary masses were taken from the range ( $\log M_1/M_{\odot} = 1.4 - 2.7$ ) in intervals of 0.1 dex.

### 3.1.2 Computing massive overcontact systems

Very close binaries may evolve into contact where both binary components fill and even overfill their Roche volumes. The evolution during the overcontact phase differs from a classical common-envelope phase because co-rotation can, in principle, be maintained as long as material does not overflow the L2 point. This means that a spiral-in that is due to viscous drag can be avoided, resulting in a stable system evolving on a nuclear timescale.

As a simple approximation to the modelling of overcontact systems with a 1D code, we considered the photosphere of such an object to lie on a Roche equipotential  $\Phi$  and divided it into two distinct volumes for each star,  $V_1(\Phi)$  and  $V_2(\Phi)$ , separated by a plane crossing through  $L_1$  perpendicular to the line joining both stars. We then associated a volume-equivalent radius with each of these,  $R_1(\Phi)$  and  $R_2(\Phi)$ , with the radii corresponding to the potential at  $L_1$  as the Roche-lobe radius  $R_{\text{RL}}$  of each. When both stars overfill their Roche-lobes, the amount of overflow of one component is a function of the mass ratio, and the amount of overflow of the other component is

$$\frac{R_2(\Phi) - R_{\text{RL},2}}{R_{\text{RL},2}} = F\left(q, \frac{R_1(\Phi) - R_{\text{RL},1}}{R_{\text{RL},1}}\right), \quad (3.1)$$

where the function  $F(q, x)$  must satisfy the conditions  $F(q, 0) = 0$  and  $F(1, x) = x$ . By numerically integrating  $V_1(\Phi)$  and  $V_2(\Phi)$  for different  $q$  ratios and potential values between those at  $L_1$  and  $L_2$ , we found the fit  $F(q, x) = q^{-0.52}x$ , with the Roche-lobe radius computed as in Eggleton, 1983, that approximates  $F(q, x)$  with a few percent error in the range  $0.1 \leq q \leq 1$ . During an overcontact phase, mass transfer is then adjusted in such a way that the amount of overflow from each component satisfies this relationship.

After both stars overflow past the outer Lagrangian point, we expect the system to merge rapidly, either as a result of mass loss from  $L_2$  carrying a high specific angular momentum, or in consequence of a spiral-in due to the loss of co-rotation. We found that, given the volume equivalent radii for the potential at the L2 point  $R_{\text{L2},i}$ , the amount of overflow of the least massive star in a system that reaches  $L_2$  approximately satisfies the relationship

$$\frac{R_{\text{L2},2} - R_{\text{RL},2}}{R_{\text{RL},2}} = 0.299 \tan^{-1}(1.84q^{0.397}) \quad (3.2)$$

with an error smaller than 2% in the range  $0.02 \leq q \leq 1$ . At  $q = 1$  this means that a star needs to expand by up to 1.32 times its Roche-lobe radius before reaching L2, which leaves a significant amount of space

for a binary to survive through an overcontact phase. We note that we ignored the effects of energy and element transfer through the shared envelope for the moment. However, since the systems we model in this work undergo contact as rather unevolved stars with mass ratios not far from one, we expect these effects to be of minor importance for our present study.

It is worth mentioning that VFTS352 is a massive ( $\sim 30 M_{\odot} + 30 M_{\odot}$ ), short-period ( $P_{\text{orb}} = 1.12$  d) overcontact binary that evolves on the nuclear timescale. It has a mass ratio of  $q = 1.008$  and is thought to undergo chemically homogeneous evolution (Almeida, Sana, de Mink et al., 2015). This system therefore provides direct support for the MOB scenario and for our treatment of this phase.

## 3.2 Results

Before examining the wider parameter space, we provide an example of a typical MOB evolution in the following section.

### 3.2.1 Exemplary MOB evolution

We show in Fig. 3.1 the evolutionary tracks of the two components of a  $79 + 64 M_{\odot}$  binary at  $Z = Z_{\odot}/50$  with an initial period of 1.1 d from the zero-age main sequence until core helium exhaustion. This system enters an overcontact phase early during core hydrogen burning, during which it swaps mass back and forth several times. Each time, the mass-ratio becomes closer to one, so that eventually contact is avoided and the system evolves as a detached binary with two stars of about  $71 M_{\odot}$  from this time on.

Core hydrogen burning ends at an effective temperature of  $\log T_{\text{eff}} \simeq 4.9$ , after which both stars contract to even smaller radii. As a result of the different initial evolution, the stars do not evolve exactly synchronously during the late evolutionary stages.

Figure 3.2 illustrates the different evolutionary stages of a typical binary in our grid from the zero-age main sequence (ZAMS) to the black-hole merger stage. While chemically homogeneous evolution is maintained throughout core hydrogen burning, mass is transferred back and forth between the two binary components in a succession of contact stages, which eventually leads to a mass ratio very close to one. During the main-sequence phase and the post-core-hydrogen-burning phase, where both stars are compact detached helium stars, stellar-wind mass loss leads to a widening of the orbit. Because the winds are metallicity dependent (Mokiem, de Koter, Vink et al., 2007; Vink and de Koter, 2005), metal-rich systems are found to widen strongly, which limits the tidal interaction so that the homogeneous evolution may end. Furthermore, if the orbital period is too long, any BH+BH binary that may be produced will not merge in a Hubble time. The depicted case corresponds to a case with a metallicity of  $Z = Z_{\odot}/20$ , which provides a black hole merger after 2.6 Gyr.

### 3.2.2 Example grid

An example of a grid of binary systems is shown in Fig. 3.3 for  $Z = Z_{\odot}/50$  and  $q_i = 1$ . Each rectangle in the plot corresponds to one detailed binary evolution model.

As Fig. 3.3 shows, progenitors of massive double helium stars require initial primary masses above about  $30 M_{\odot}$ , and the range of periods for which they are formed widens with increasing primary mass. This broadening is the consequence of the larger convective cores and stronger winds for the more massive stars; this has a similar effect as the rotational mixing in exposing helium-rich material at the surface (Köhler et al., 2015; Szécsi et al., 2015).

In particular for binaries whose final masses are low enough to avoid the pair-instability regime (i.e. roughly for  $M_f < 60 M_{\odot}$ ; cf. Sects. 3.2.8 and 3.2.9), the parameter space for progenitors is completely

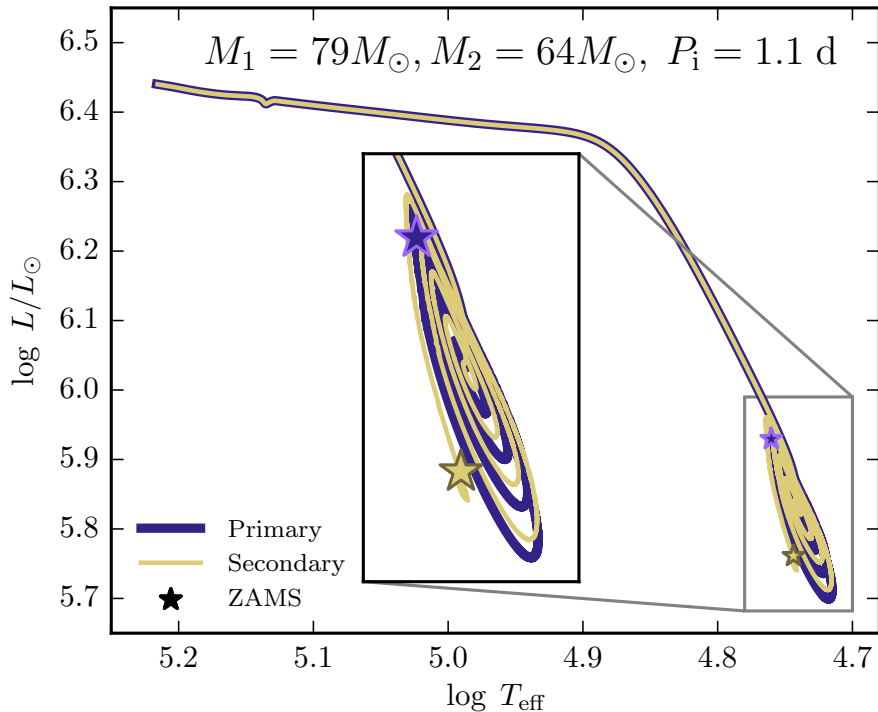


Figure 3.1: Evolutionary tracks of both stars in a MOB in the HR diagram. The initial masses are  $79 M_{\odot}$  and  $64 M_{\odot}$  and the initial orbital period is 1.1 d. Both stars evolve towards nearly equal masses, such that their evolutionary tracks after the overcontact phase become almost identical.

dominated by overcontact systems, many of which come from systems whose periods are so low that they overflow their Roche radii at the ZAMS. Only for initial masses well above  $100 M_{\odot}$  do we find systems that avoid contact throughout their evolution. But even in this mass regime, most systems undergo at least one contact phase.

We stopped all but three (see Sect. 3.2.8) of our binary-evolution models at a time when the stars ended core helium burning since their fate is settled at that time, and the binary orbit will essentially not change any more until the first stellar collapse occurs (third stage in Fig. 3.2).

### 3.2.3 Final binary configurations

Figure 3.4 summarizes the distribution of the final total system masses as a function of their final orbital period for those models in our grid that succeeded in producing close pairs of helium stars. Since the initial binary periods have to be very short to enforce the rapid rotation required for homogeneous evolution, the final properties lie in a narrow strip for each metallicity, but these are distinctly different for different metallicities. For the highest considered masses, this is mainly due to the metallicity dependence of the stellar wind mass loss, which has the effect of widening the systems and reducing the mass of the stars, thus producing systems with longer orbital periods and lower masses at higher metallicity.

Figure 3.4 also indicates the merger times for these systems, assuming that the masses and periods do not change in the black hole formation process (cf. Sect. 3.2.9). All models with  $Z_{\odot}/4$  and all but the

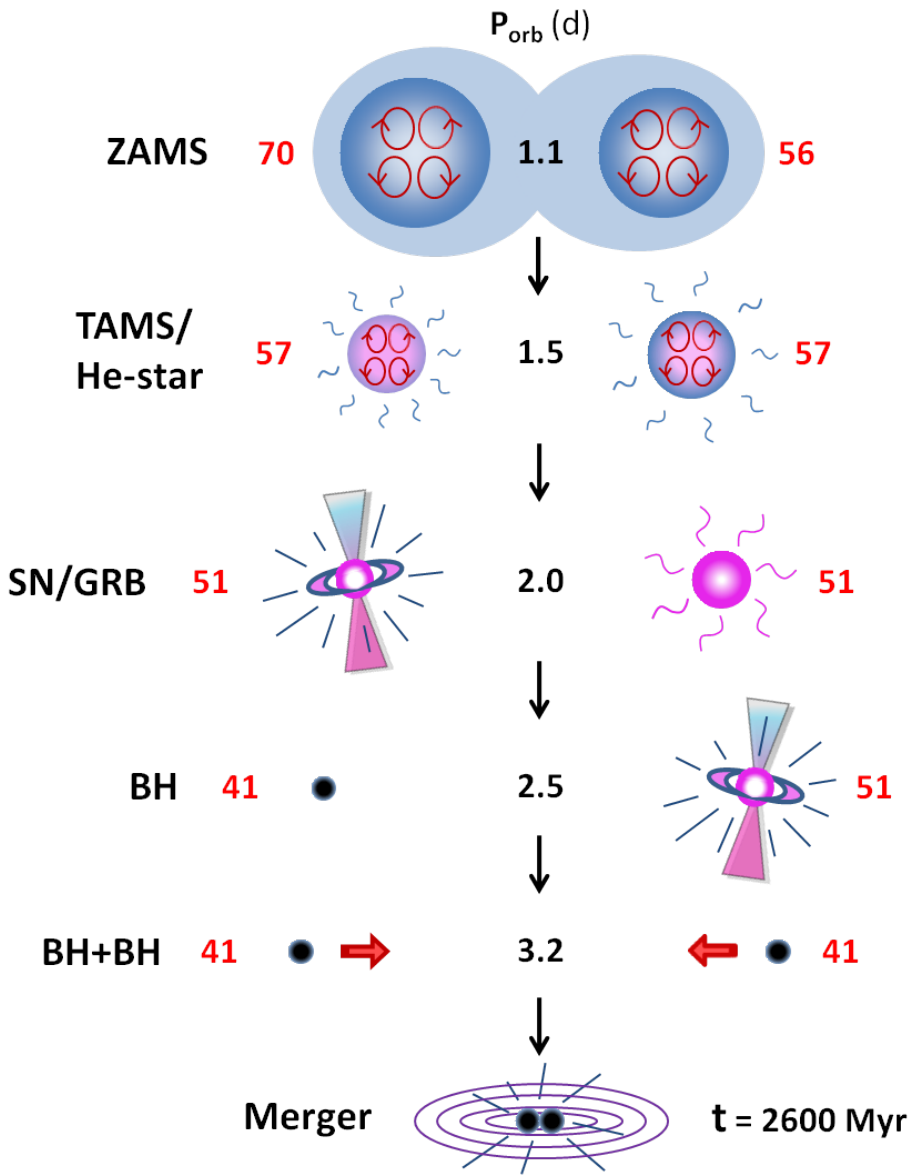


Figure 3.2: Illustration of the binary stellar evolution leading to a BH+BH merger with a high chirp mass. The initial metallicity is  $Z_{\odot}/50$ , the masses of the stars in solar masses are indicated with red numbers, and the orbital periods in days are given as black numbers. A phase of contact near the ZAMS causes mass exchange. Acronyms used in the figure: ZAMS: zero-age main sequence; TAMS: termination of hydrogen burning; He-star: helium star; SN: supernova; GRB: gamma-ray burst; BH: black hole.

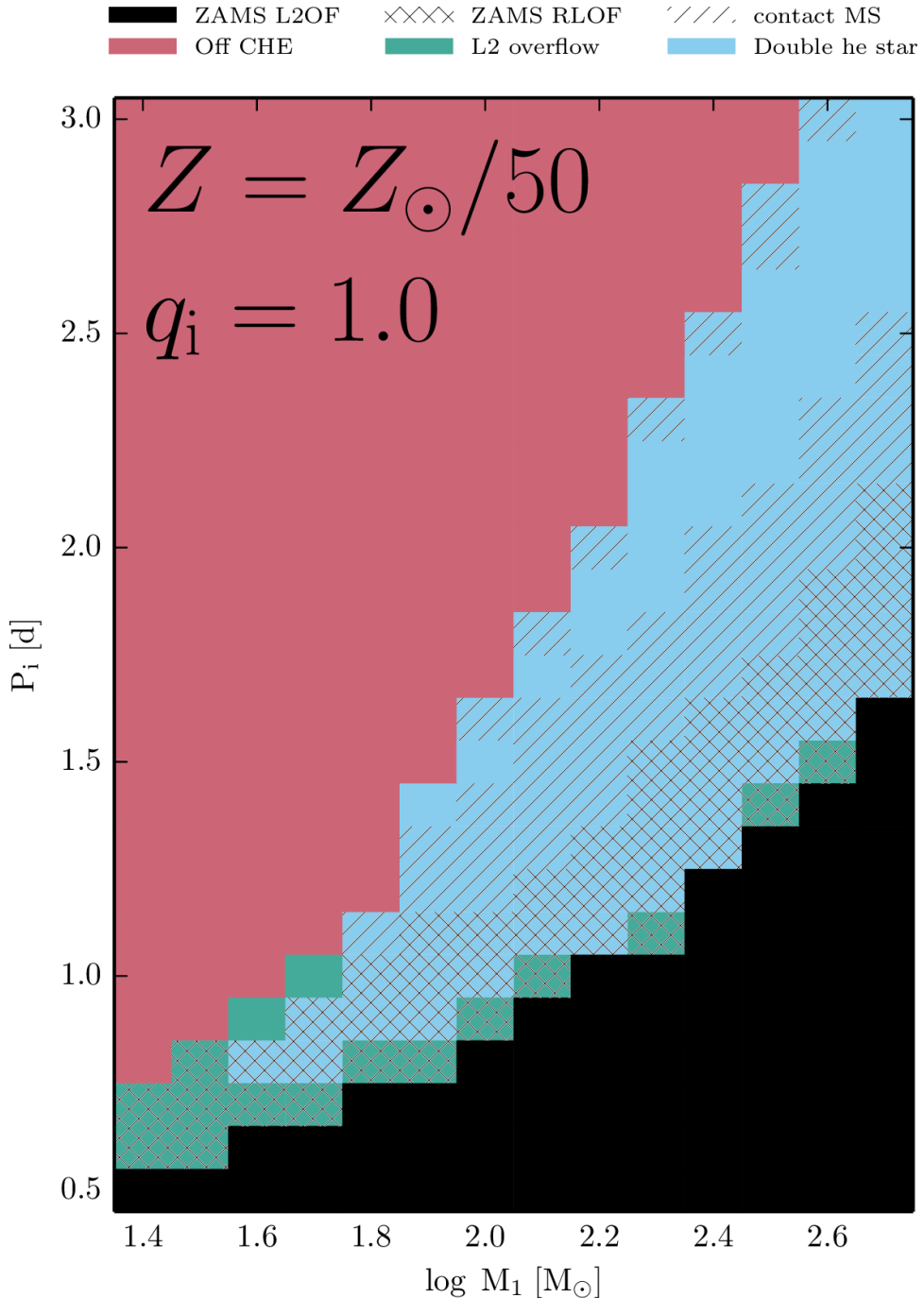


Figure 3.3: Example of a grid of binary systems (initial orbital period versus initial primary mass) with  $Z = Z_\odot/50$  and  $q_i = 1$ . Models that reached a point at which the difference between the surface and central helium abundance in one of the stars exceeds 0.2 are considered not to be evolving chemically homogeneously and their calculation is stopped (pink). The region in which the initial orbital period is small enough as to have L2 overflow at the ZAMS is marked in black, while those systems that reach L2 overflow during the main sequence are marked in green. Systems marked in blue successfully form double helium stars. Single hatching marks systems that experience contact during the main sequence, while doubly hatched systems are in an overcontact phase at the ZAMS.

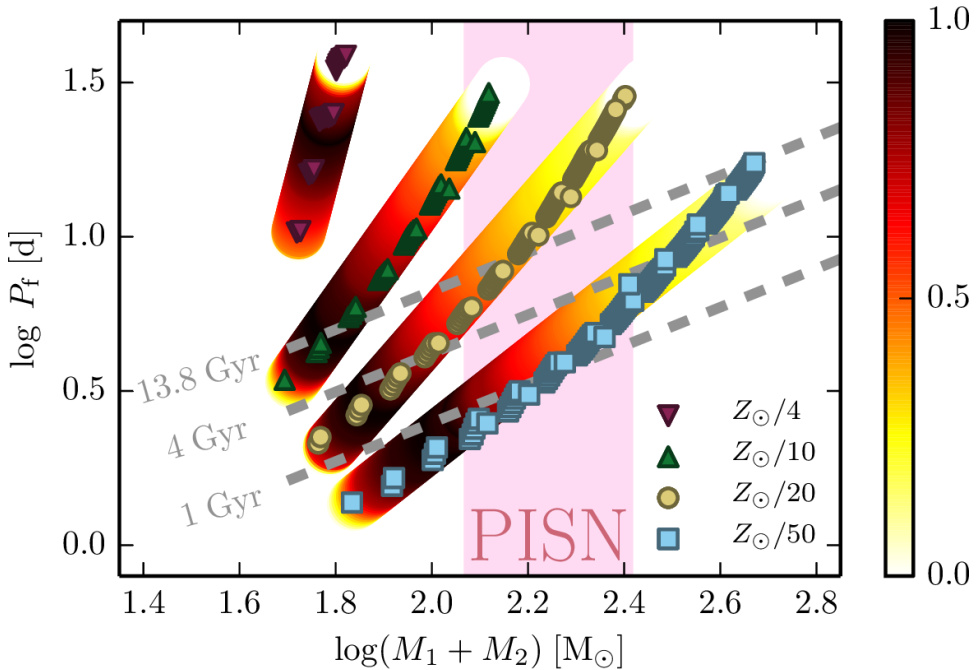


Figure 3.4: Total masses and orbital periods at core helium depletion for systems with  $q_i = 1$  at four different metallicities. Dashed lines show constant merger times assuming direct collapse into a black hole, and the shaded region indicates the mass range at which PISNe would occur, resulting in the total disruption of the stars instead of black hole formation. The coloured bands represent the relative number of objects formed for each metallicity.

lowest mass models with  $Z_\odot/10$  produce binaries that are too wide to lead to black hole mergers within a Hubble time. The more metal-poor models, on the other hand, produce very tight He-star binaries below as well as above the mass regime where pair-instability supernovae (PISNe) are expected to lead to the complete disruption of the stars and not to the formation of black holes (Heger and Woosley, 2002; Chatzopoulos and Wheeler, 2012).

The trend of shorter merger times for lower metallicities is expected to continue towards the lowest metallicities found in the Universe. As stellar wind mass loss becomes increasingly negligible, the initial stellar radii determine the shortest possible orbital periods. As an example, stars of  $60 M_\odot$  have ZAMS radii of  $12 R_\odot$ ,  $10.5 R_\odot$ ,  $10 R_\odot$ , and  $3.5 R_\odot$ , at  $Z = Z_\odot$ ,  $Z_\odot/10$ ,  $Z_\odot/50$ , and  $Z = 0$ , respectively. This implies that the merger times for the lowest metallicities, in particular for Population III stars, become extremely short. While the expected number of such objects is small, this opens the exciting possibility of eventually observing primordial black hole mergers at high redshift.

### 3.2.4 Mass distribution and mass ratios

Figure 3.5 shows the predicted intrinsic chirp mass distribution for BH+BH mergers for our different metallicity grids, again assuming no mass loss in the BH formation process. The most prominent feature is the prediction of a clear gap in this distribution, which occurs because systems that would otherwise populate this gap do not appear since the stars explode as pair-instability supernovae without leaving a stellar remnant. The BH progenitors in the systems above the gap also become pair unstable, but the explosive burning cannot reverse the collapse, which leads straight to the formation of a black hole (Heger and Woosley, 2002; Langer, 2012).

There is a strong general trend towards higher chirp masses with decreasing metallicity. At the lowest metallicity ( $Z = Z_{\odot}/50$ ) we also produce BHs above the PISN gap. While obviously there are fewer of them than BH systems below the gap, they may still be significant because the amplitude of the gravitational-wave signal is a strong function of the chirp mass (cf. Sect. 3.3).

As indicated in Fig. 3.5, the vast majority of merging systems have passed through a contact phase. Since both stars are relatively unevolved when they undergo contact, these contact phases result in mass transfer back and forth until a mass-ratio  $q \simeq 1$  is achieved. This is depicted in Fig. 3.6, where final mass ratios are shown for systems with  $q_i = 0.9$  and  $0.8$  and a metallicity of  $Z = Z_{\odot}/50$ . For each mass ratio, two distinct branches are visible, corresponding to systems that undergo contact and evolve to  $q \simeq 1$ , and systems that avoid contact altogether. Owing to the strong dependence of mass-loss rates with mass, even systems that avoid contact altogether evolve towards  $q = 1$  at high masses.

Mandel and de Mink, 2016 modelled this channel without contact systems and found that many binaries form double BHs from progenitors below the PISN gap, with final mass ratios in the range of 0.6 to 1, reflecting just a small shift from the initial mass ratio distribution as a result of mass loss. However, Mandel and de Mink, 2016 did not perform detailed stellar evolution calculations. They checked whether their binary components underfilled their Roche radii at the ZAMS and then assumed that this will remain so in the course of the quasi-homogeneous evolution of both stars. When considered in detail, however, in particular the more massive and more metal-rich stars undergo some expansion during core hydrogen burning, even on the quasi-homogeneous path (Brott, de Mink et al., 2011; Köhler et al., 2015; Szécsi et al., 2015). This is most likely due to the increase of their luminosity-to-mass ratio and the related approach to the Eddington limit (Sanyal et al., 2015). As a result, the vast majority of the binaries considered by Mandel and de Mink, 2016 enter contact when computed in detail. Therefore, our final mass ratio distribution is much more strongly biased towards  $q = 1$ .

### 3.2.5 Merger delay times

As Fig. 3.4 indicates, the merger delay time, which is the time between the formation of the BH+BH binary and the eventual merger, is a strong function of metallicity, where the merger delay times (at a given BH mass) are systematically shorter for lower metallicity. Figure 3.7 shows the distribution of the merger delay times for the different metallicities in our grids (assuming a uniform metallicity distribution). While the typical delay time is several Gyr, which helps detecting these events at lower redshift (see Sect. 3.3), the delay time can be as short as 0.4 Gyr for BH+BH mergers below the PISN gap at the lowest metallicity.

The decrease in delay times with lower metallicity is not found in the models of Mandel and de Mink (2016), who concluded that no high-redshift mergers are expected. The reason is that they effectively only considered one metallicity, namely the threshold metallicity for chemically homogeneous evolution by Yoon, Langer and C. Norman (2006) of  $Z = 0.004$ . However, the components of lower metallicity binaries are more compact, allowing tighter binaries at zero age, and they have weaker winds, which produces tighter double black hole binaries. Therefore, while Mandel and de Mink (2016) predicted delay times to be longer than 3.5 Gyr, we found up to ten times lower values at our lowest metallicity (Fig. 3.7). Since the shortest delay time depends on the metallicity-dependent stellar radii and stellar radii of massive metal-free stars are smaller than half compared to those at  $Z_{\odot}/50$  (Yoon, Dierks and Langer, 2012; Szécsi et al., 2015), even merger times shorter by orders of magnitude can be expected. Therefore, even though much rarer, we argue that massive BH mergers could occur up to the redshift of Population III stars. If such mergers were detected, it would allow us to probe the evolution of massive stars in the very early Universe.

We also note that if the black holes receive kicks at birth, even higher metallicity systems may merge

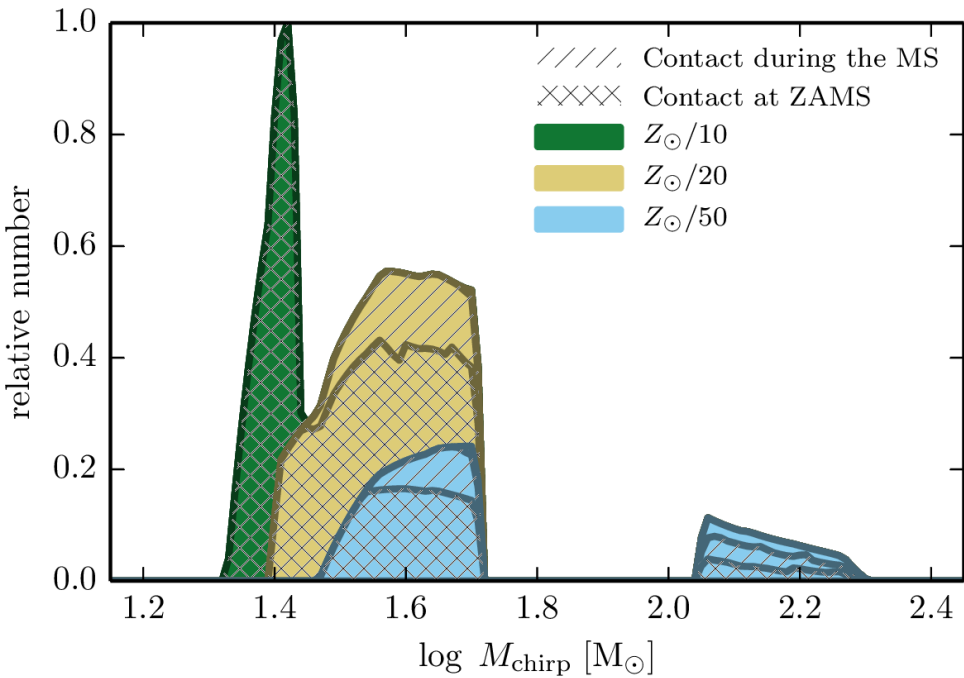


Figure 3.5: Stacked distribution of chirp masses of BH+BH systems formed at different metallicities, so that they merge in less than 13.8 Gyr. The contribution from each metallicity is scaled assuming a flat distribution in  $Z$ . At very short periods, systems are in contact at the ZAMS.

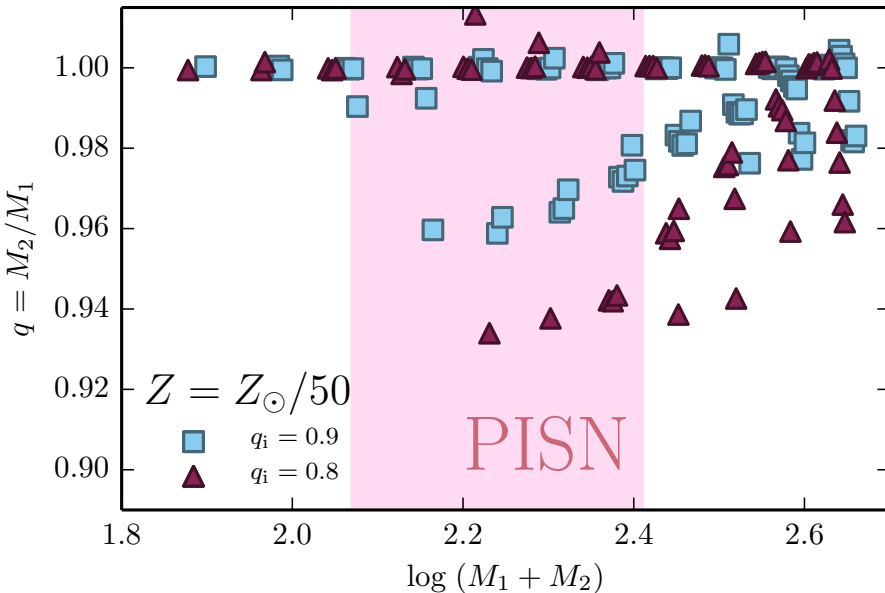


Figure 3.6: Mass-ratios of BH+BH systems resulting from our modelled systems for  $q_i = 0.9$  and  $q_i = 0.8$  and a metallicity of  $Z = Z_\odot/50$  under the assumption that no mass is lost during collapse. The shaded region indicates the limits for the occurrence of PISNe.

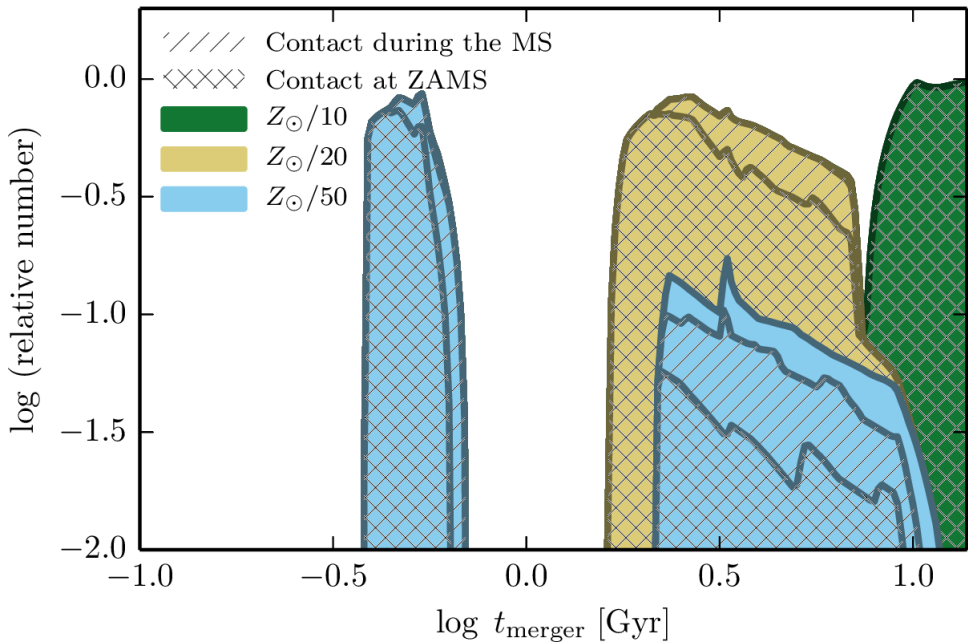


Figure 3.7: Stacked distribution of merger delay times for different metallicities (as indicated). The meaning of the hatching is the same as in Fig. 3.5.

very rapidly if the kick reduces the pericenter distance (see Appendix A).

### 3.2.6 Observational counterparts

Our choice of including models of up to  $500 M_{\odot}$  in our grids is supported by the evidence for stars of such high masses in the LMC (Crowther, Schnurr et al., 2010).

Various evolutionary stages of the MOB scenario are observationally confirmed by massive binary systems in nearby galaxies. As mentioned in Sect. 2, the MOB VFTS352 (Almeida, Sana, de Mink et al., 2015) supports the idea of homogeneous evolution of overcontact binaries, even though it is not expected to lead to a black hole merger because of the rather high metallicity of the LMC (cf. Fig. 3.4). It corresponds to the first stage of our cartoon in Fig. 3.2.

The SMC binary HD 5980 corresponds well to the second stage of Fig. 3.2. It consists of two stars with masses of about  $60 M_{\odot}$  that are both very hydrogen poor, that orbit each other in about 19 d. Koenigsberger et al. (2014) concluded that this system most likely emerged from homogeneous evolution. This system is well recovered in our grid at  $Z_{\odot}/10$ .

Finally, IC10 X-1 and NGC 300 X-1 are binaries that may correspond well to stage 3 of Fig. 3.2. Both have a short orbital period ( $P_{\text{orb}} \approx 1.5$  d for both) and contain very massive black hole primaries ( $> 23 M_{\odot}$  and  $20 M_{\odot}$ ) and similar-mass, hydrogen-free companions ( $\sim 35 M_{\odot}$  and  $26 M_{\odot}$ ; Barnard, J. S. Clark and U. C. Kolb (2008) and Bulik, Belczynski and A. Prestwich (2011)). Both systems have close-matching counterparts in our  $Z_{\odot}/20$  binary-evolution grids, with life times of up to several  $10^4$  yr.

### 3.2.7 Spins

To test the possibility of producing LGRBs according to the “collapsar” scenario (Woosley, 1993) from our MOB models, we compare in Fig. 3.8 angular-momentum profiles at the point of core helium

depletion for a few systems that fall below the PISN gap. A significant amount of mass ejected during an LGRB event could modify the final orbital periods of double BHs, although we find that this probably does not play a determining role in our rate estimates (as discussed further in Sect. 4).

As Fig. 3.8 shows, models at a metallicity of  $Z_{\odot}/10$  experience significant braking due to winds, and thus they are unlikely to produce LGRBs. In contrast, several systems at  $Z_{\odot}/50$  that result in helium stars below the PISN gap have specific angular-momentum profiles above the values for the last stable orbit, assuming all mass collapses into a critically rotating black hole. The results at  $Z_{\odot}/20$  are more ambiguous, and it is not clear whether the stars would produce an LGRB or not. For systems forming black holes above the PISN gap, wind braking is strong enough even for low metallicity to avoid the formation of LGRBs. This is confirmed when considering the Kerr parameters of our models in Fig. 3.9 in the different mass and metallicity regimes.

### 3.2.8 Models up to core collapse

To depict the effect of the PISN gap, we took three models with masses  $200 M_{\odot}$ ,  $90 M_{\odot}$  and  $35 M_{\odot}$  and metallicity  $Z_{\odot}/50$  after helium depletion and evolved these through the late evolutionary phases. Figure 3.10 shows the evolution of central density and temperature of each star, together with the region in which pair production results in an adiabatic index of  $\Gamma < 4/3$ .

The least massive of the three stars avoids the pair-unstable region altogether and experiences core collapse after silicon depletion. In the  $90 M_{\odot}$  model, the core collapses during oxygen burning, resulting in explosive burning that injects enough energy to halt the collapse and drive an explosion. At the highest mass, the oxygen core also collapses, but explosive burning is not sufficient to stop it, and in the end burning proceeds very fast up to silicon depletion, resulting in an iron core with an infall velocity  $> 1000 \text{ km s}^{-1}$ .

### 3.2.9 Explosive mass loss and momentum kicks

In all models below the pair-instability regime we expect the formation of black holes. If the whole star collapses without ejecting any mass or energy, the masses and periods in Fig. 3.4 would also represent the masses of the final black holes and the post-collapse orbital periods. On the other hand, as our helium stars tend to be rapidly rotating, some of them may experience a collapsar phase (Woosley, 1993), producing LGRBs, in which part of the collapsing star is ejected, and the binary orbit may receive a supernova kick. The effect of the mass loss would be to reduce the final black hole masses (and to reduce the strength of any eventual gravitational-wave signal) and widen the system (and increase the merger time), while the effect of a kick can be to either increase or decrease the orbital period and the merger time (see Appendix A for a more detailed discussion). While the details of the collapse phase are still very uncertain, which may have an effect on the BH+BH detection rates, our main conclusions are not dependent on them.

The final angular-momentum profiles of our models (see Sect. 3.2.7) suggest that only the lowest mass models ( $M_{\text{final}} \lesssim 40 M_{\odot}$ ) at the two lowest metallicities ( $Z = Z_{\odot}/20$ ,  $Z_{\odot}/50$ ) may retain enough angular momentum in the core to be good LGRB candidates. Nevertheless, because of the large amount of available angular momentum, we expect many of the BHs formed in this scenario to be rapidly rotating, with the spin parameter roughly scaling inversely with the final orbital period shown in Fig. 3.4 (i.e. the fastest spins are expected for the lowest mass BHs at the lowest metallicity). Finally, we note that a regime of pulsational PISNe (Chatzopoulos and Wheeler, 2012) lies below the disruptive PISN regime, where substantial mass loss is expected, but a BH is ultimately formed (Woosley, Blinnikov and Heger, 2007).

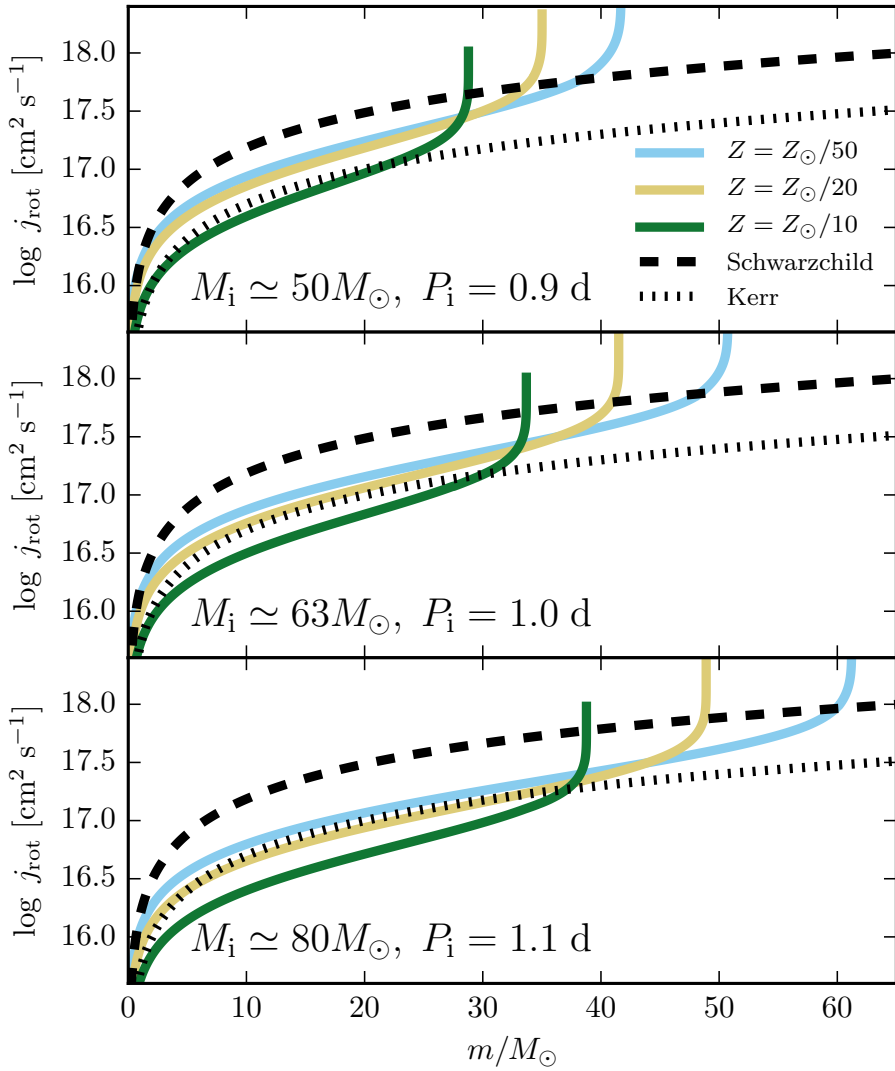


Figure 3.8: Angular-momentum profiles at core helium depletion for the primary stars of binaries from our grid that result in double helium star binaries. We show stars of three different initial masses in binaries with similar initial orbital periods at metallicities of  $Z = Z_\odot/50, Z_\odot/20$ , and  $Z_\odot/10$ . The curves for the specific angular momentum of the last stable orbit for a non-rotating (Schwarzschild) and critically rotating (Kerr) black hole are also included.

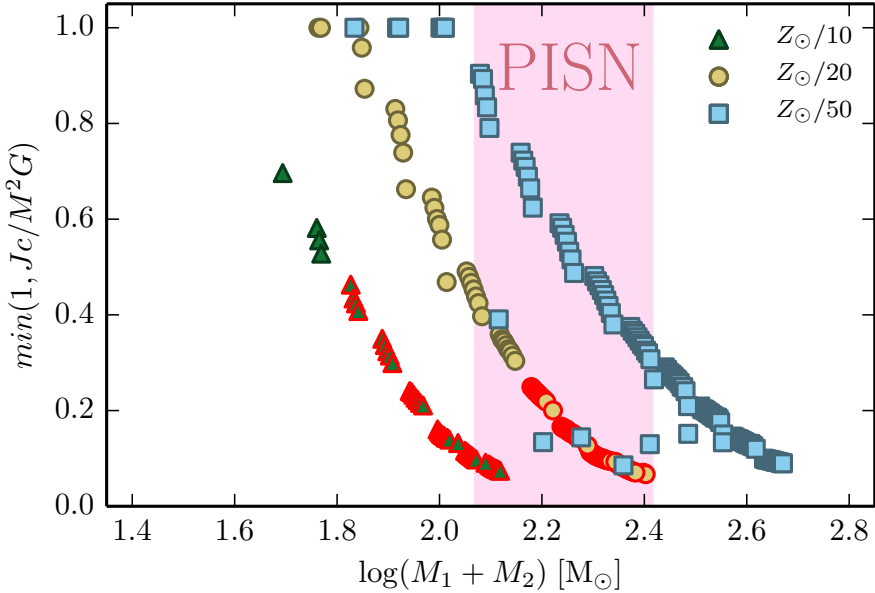


Figure 3.9: Kerr parameter as function of the final system mass for our models at  $Z = Z_{\odot}/50, Z_{\odot}/20$ , and  $Z_{\odot}/10$ , assuming a complete collapse of our helium stars to black holes. Binaries indicated by symbols with a red frame have merger times that exceed the Hubble time.

### 3.3 Merger rates

For the conventional scenario in which close double compact binaries are produced through common-envelope evolution (see Appendix B), except for a few cases (Voss and Tauris, 2003; Belczynski, Dominik et al., 2010; Dominik, Berti et al., 2015), the far majority of published population synthesis studies predict a much higher NS+NS merger rate per Milky Way equivalent galaxy (MWEG) than they do for the rate of BH+BH mergers. Based on a detailed comparison study of published models (Abadie, B. P. Abbott, R. Abbott, Abernathy et al., 2010), the NS+NS merger rate was estimated to be  $100 \text{ MWEG}^{-1} \text{ Myr}^{-1}$ , which is about 100 times higher than the rate predicted for BH+BH binaries. However, because there are more massive compact objects in BH+BH binaries than in NS+NS binaries, their emitted gravitational-wave amplitudes are significantly larger, so that the LIGO detection rates of both are approximately equal. The so-called realistic rates quoted by Abadie, B. P. Abbott, R. Abbott, Abernathy et al. (2010) are 40 and  $20 \text{ yr}^{-1}$  for NS and mostly low-mass BH mergers, respectively, but the uncertainty in these numbers is larger than three orders of magnitude.

#### 3.3.1 Chirp masses and MOB evolution

Two important assumptions need to be kept in mind with regard to these quoted rates. First, the BH+BH binaries are assumed to be composed of  $10 M_{\odot}$  BHs (even  $5 M_{\odot}$  BHs in all LIGO result papers published before 2010), corresponding to an intrinsic chirp mass,  $M_0$  of  $\sim 8.7 M_{\odot}$  (for equal mass binaries,  $M_0 = (1/4)^{3/5} M \simeq 0.435 M$ , where the total mass,  $M$ , is twice the BH mass,  $M_{\text{BH}}$ ). For low metallicities, our MOB scenario predicts the formation of BHs with masses of  $25 - 60 M_{\odot}$  and  $130 - 230 M_{\odot}$  (i.e. below and above the PISN mass range, respectively), resulting in very high intrinsic

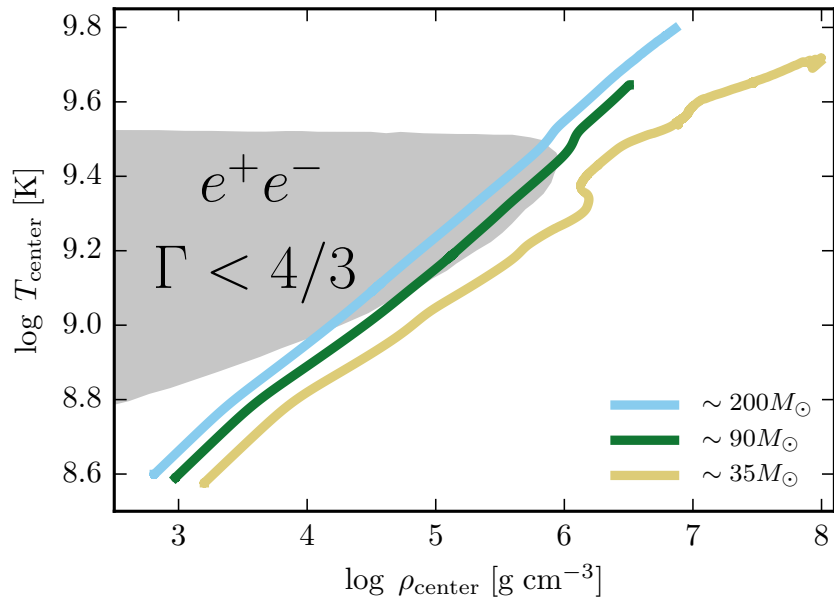


Figure 3.10: Evolution in the  $T_c - \rho_c$ -diagram for the three stellar models at  $Z = Z_\odot/50$  (with the masses at helium depletion as indicated) calculated to the final evolutionary stage. The shaded region shows the region that is unstable to pair creation. Both the  $35 M_\odot$  and the  $200 M_\odot$  stars collapse to form black holes, while the  $90 M_\odot$  is disrupted in a PISN.

chirp masses of about  $20 - 50 M_\odot$  and  $115 - 200 M_\odot$ , respectively (cf. Fig. 3.5). Mergers like this can be seen throughout a significant part of the Universe, since the distance luminosity,  $d_L \propto M_0^{5/6}$ . We note that the detected chirp masses will be redshifted to  $M_0(1+z)$ , where  $z$  is the BH+BH system redshift with respect to the detector on Earth (Finn, 1996).

Secondly, all previously published rates were based on common-envelope-evolution (cf. App. B), which creates uncertainties in the rates by more than two orders of magnitude as a result of our poor understanding of the common-envelope physics (Dominik, Belczynski et al., 2012). The new BH+BH formation scenario (MOB evolution) presented in this work does not involve any common-envelope phase. Instead, it is based on much less uncertain physics (as discussed in the previous section). Equally important, it leads to the formation of much more massive BHs than in previous studies.

Assuming, as a first approximation, that the detection rate,  $\mathcal{R}$ , scales with  $d_L^3 \propto M_0^{5/2}$ , we conclude that the expected LIGO detection rates for these massive BH+BH binaries could easily dominate the overall rates; they are therefore excellent candidates for the first LIGO source detection (see the more detailed discussion below). It should be noted that some previous studies (Belczynski, Dominik et al., 2010; Dominik, Berti et al., 2015; Rodriguez, Morscher et al., 2015) have alluded to a dominance of relatively massive BH+BH mergers in a low-metallicity environment (or, in particular, through dynamical channels in dense clusters), although without a specific detailed model for the binary case.

The expected LIGO detection rate of BH+BH binary mergers was estimated in the following manner,

$\mathcal{R} = r_{\text{MW}} \times N_{\text{gal}}$ , where  $r_{\text{MW}}$  is the expected merger rate in an MWEG, and

$$N_{\text{gal}} = \frac{4}{3} \pi \left( \frac{d_{\text{horizon}}}{\text{Mpc}} \right)^3 (2.26)^{-3} (0.0116) \quad (3.3)$$

is the number of MWEGs out to a horizon distance,  $d_{\text{horizon}}$  (Abadie, B. P. Abbott, R. Abbott, Abernathy et al., 2010). Here the factor 1/2.26 is included to average over all binary orientations and sky locations, i.e.  $d_{\text{horizon}} = 2.26 d_{\text{avg}}$  (Finn and Chernoff, 1993), and  $1.16 \times 10^{-2} \text{ Mpc}^{-3}$  is the extrapolated space density of MWEGs (Kopparapu et al., 2008). For relatively low-mass BH+BH mergers, assuming  $M_{\text{BH}} = 10 M_{\odot}$  and a corresponding average design distance luminosity of  $d_L \simeq 1000 \text{ Mpc}$  for advanced LIGO (aLIGO), the estimated values are (Abadie, B. P. Abbott, R. Abbott, Abernathy et al., 2010)  $r_{\text{MW}} = 0.4 \text{ Myr}^{-1} \text{ MWEG}^{-1}$  and  $\mathcal{R} = 20 \text{ yr}^{-1}$ . For a massive BH+BH merger with  $M_{\text{BH}} = 60 M_{\odot}$  (or  $130 M_{\odot}$ ), we obtain  $d_L \simeq 4.5 \text{ Gpc}$  (or  $d_L \simeq 8.5 \text{ Gpc}$ ), and thus  $d_{\text{horizon}} \simeq 10 \text{ Gpc}$  (or  $d_{\text{horizon}} \simeq 19 \text{ Gpc}$ ). The expected redshift is  $z = 1.4$  (or  $z = 2.3$ ) for standard cosmological parameters ( $H_0 = 69.6 \text{ km s}^{-1} \text{ Mpc}^{-1}$ ,  $\Omega_M = 0.286$ ,  $\Omega_{\text{vac}} = 0.714$ ).

### 3.3.2 Model assumptions for estimating aLIGO detection rates

To calculate the aLIGO detection rate of these massive BH+BH mergers, we first need to calculate the intrinsic merger rate in an MWEG. For a given metallicity, it is straightforward to calculate the rate for various events from our binary evolution grids. We used simple standard assumptions about the initial binary parameters: we assumed that (1) the orbital period distribution is flat in  $\log P$  and covers the range (0.5 d – 1 yr), (2) the primary mass distribution is described by a Salpeter power law ( $dN/d \log M \propto M_1^{-1.35}$ ), (3) the mass-ratio distribution is flat, (4) stars more massive than  $8 M_{\odot}$  produce a core-collapse SN, and (5) there is one binary system for every three core-collapse SNe (i.e. two out of three massive stars are formed in close binaries).

Guided by the results from our grids, we required that the initial mass ratio has to be higher than 0.8 to ensure chemically homogeneous evolution for both stars. With these assumptions we calculated the fraction of systems that produce BH+BH mergers relative to the core-collapse SN rate. These are shown in the first two rows in Table 3.1 for various metallicities for BH+BH mergers below and above the PISN gap. These numbers imply that for  $Z < Z_{\odot}/10$ , there is typically one BH+BH merger event for about 1000 core-collapse SNe. To relate these numbers to a rate for an MWEG, we need to multiply these fractions by the core-collapse rate for an MWEG. Adopting a typical rate of  $0.01 \text{ yr}^{-1}$ , this implies, for instance, that in an MWEG with  $Z = Z_{\odot}/50$ , the BH+BH merger rates are  $6.7 \text{ Myr}^{-1}$  and  $2.7 \text{ Myr}^{-1}$  below and above the PISN gap, respectively. We note that our model only predicts BH+BH mergers above the PISN gap at the lowest metallicity.

### 3.3.3 Accounting for the star-forming history and the galactic metallicity distribution throughout the Universe

The actual aLIGO detection rate depends on two main factors: (1) the detection volume within which a particular event can be detected, and (2) the cosmological distribution of the sources, which depends on the star formation history and the chemical evolution of the Universe. The detection volume can be estimated using Eq. 3.3, where  $d_{\text{horizon}}$  depends on the aLIGO sensitivity and the BH masses. However, Eq. 3.3 is only a good approximation for  $d_{\text{horizon}} \lesssim 1 \text{ Gpc}$  because it ignores cosmological expansion. To take this into account (in a very approximate way), we introduced a simple cut-off of  $N_{\text{gal}} = 10^{10}$  in Eq. 3.3. For reference, this implies that our simple model assumes that there are about three core-collapse

SNe per second in the Universe. Scaling the horizon distance of the BH+BH masses produced in our grids to the design sensitivity of aLIGO, we started by calculating the aLIGO detection rate assuming that all galaxies have a particular metallicity. These rates are shown in the last two rows of Table 3.1, in Cols. 2–5.

One of the main problems is that our rates are a strong function of metallicity and therefore depend on the evolution of metallicity with time and the spread of the metallicity distribution at a given redshift. For example, the mean metallicity of galaxies will only be lower than  $Z_\odot/50$  at redshifts higher than  $5 - 7$  (A. Fruchter; private communication). On the other hand, even in the local Universe some galaxies (mostly dwarf galaxies) have extremely low metallicities. A proper calculation of this is beyond the scope of this paper. However, we can derive lower and upper limits using a local and a global approximation of the metallicity distribution.

For the former, we followed Langer and C. A. Norman, 2006, who computed the formation rate of stars with a metallicity below a threshold metallicity  $Z^*$  in the local Universe. For their fiducial parameters, they found fractions compared to the local total star formation rate of 0.61, 0.01, 0.0025, and 0.0004 for the four metallicities used in our binary evolution models ( $Z_\odot/4$ ,  $Z_\odot/10$ ,  $Z_\odot/20$ , and  $Z_\odot/50$ , respectively). If the merger delay times were negligible (which they are not; see below), and the detection volume were restricted to the low-redshift Universe – which, from the point of view of the statistics mentioned above remains roughly true for redshifts up to  $2 \sim 3$  – the above factors would need to be applied to obtain local detection rates for the various metal-poor sources.

A global upper limit to the rates can be obtained by considering the metallicity distribution of all massive stars that have ever formed in the Universe. Using the global metallicity distribution provided by C. Kobayashi (based on the simulations presented in P. Taylor and Kobayashi 2015), we estimate the fraction of massive stars that have formed with metallicities of  $Z_\odot/10$ ,  $Z_\odot/20$ , and  $Z_\odot/50$  to be 0.086, 0.052, and 0.068, respectively (using appropriate linear binning).

### 3.3.4 Resulting predictions for aLIGO detection rates

Using these metallicity weightings, we can estimate ranges for the aLIGO detection rates (at the design sensitivity) of  $19 - 550 \text{ yr}^{-1}$  for BH+BH mergers below the PISN gap and of  $2.1 - 370 \text{ yr}^{-1}$  above the PISN gap, compare the last column in Table 3.1. Here, the first quoted number of the ranges corresponds to the local approximation, the second to the global approximation. Even for the ongoing first science run (O1) of aLIGO the prospects for detection are promising. Given that the sensitivity of aLIGO is currently about one-third of the design sensitivity, the expected detection rate is  $\sim 4\%$  of our calculated values (see last column of Table 3.1).

The lower mass BH+BH mergers are more likely to sample the low-redshift Universe, therefore the lower limit may be more applicable for the mergers below the PISN gap. On the other hand, because the most massive BH+BH mergers can be detected throughout most of the visible Universe, the upper limit may be more appropriate for the mergers above the PISN gap. We note that for these, the redshift factor  $1/(1+z)$  has not yet been taken into account, as we did not compute the redshift distribution of events. Even our lower limits suggest, however, that aLIGO should detect BH+BH mergers from the MOB scenario. The most massive mergers, which probe a large portion of the whole Universe, might well be the dominant source for aLIGO detections (Flanagan and Hughes, 1998; Abadie, B. P. Abbott, R. Abbott, Abernathy et al., 2010).

Another factor that helps detecting BH+BH mergers from low-metallicity populations is not taken into account in the above estimates: because of the possibly long merger delay times (see Fig. 3.7), even systems that were formed in the early Universe may merge at low redshift (cf. Mandel and de Mink 2016).

Table 3.1: Fraction of systems per SN that result in double BHs that would merge in less than 13.8 Gyr (upper two rows) and aLIGO detection rates (lower two rows), assuming that all galaxies have the corresponding metallicity (Cols. 2–5) or are distributed according to our applied integrated metallicity distributions (last column ‘Integrated Z’). Here, the first number of the quoted range corresponds to our local approximation, the second to the global approximation, which form lower and upper limits (see text). Numbers are given for merging BH+BH binaries both below and above the PISN gap. The uncertainties in aLIGO detections rates are mainly caused by mapping the galactic metallicity distribution throughout the Universe (Sect. 3.3.3).

Metallicity →	$Z_{\odot}/50$	$Z_{\odot}/20$	$Z_{\odot}/10$	$Z_{\odot}/4$	Integrated Z
$N_{\text{BHBH}}/N_{\text{SN}}$ below PISN gap	$6.7 \times 10^{-4}$	$1.3 \times 10^{-3}$	$3.4 \times 10^{-4}$	0	$(0.69 - 13) \times 10^{-5}$
$N_{\text{BHBH}}/N_{\text{SN}}$ above PISN gap	$2.7 \times 10^{-4}$	0	0	0	$(0.011 - 1.8) \times 10^{-5}$
aLIGO rate ( $\text{yr}^{-1}$ ) below PISN gap	3539	5151	501	0	19–550
aLIGO rate ( $\text{yr}^{-1}$ ) above PISN gap	5431	0	0	0	2.1–370

A remaining caveat of concern for our estimated detection rates is related to the relatively low gravitational-wave frequencies of the more massive BH+BH binaries. The emitted frequencies during in-spiral are expected to peak approximately at the innermost stable circular orbit (ISCO) before the plunge-in phase and the actual merging. However, even determining the ISCO for a merging binary system is non-trivial and depends, for example, on the spins of the BHs (Balmelli and Damour, 2015). This requires numerical or sophisticated (semi-)analytical calculations within general relativity and cannot simply be estimated using a test particle in a Kerr field. For the BH+BH mergers above the PISN gap, the emitted frequencies are most likely  $\leq 100$  Hz, and with redshift corrections, the frequencies to be detected are easily lower by a factor of two or more. A frequency this low is close to the (seismic noise) edge of the detection window of aLIGO. However, the waveform amplitudes of the more massive BH+BH binaries are larger (for a given distance) and are also enlarged further by a factor of  $(1 + z)$ . Finally, it may be possible that higher frequency signals from the ring down of the single rapidly spinning BH produced might be detectable, despite their expected smaller wave amplitudes.

An important question to address is whether the first generation of LIGO should have detected such massive BH+BH merger events. Given that the sensitivity of the first generation of LIGO was about ten times lower, the number of detections should have been 1000 times lower. Even for our upper limits, it is therefore not surprising that there have been no detections during the previous science runs of the first-generation LIGO detectors (Abadie, B. P. Abbott, R. Abbott, T. D. Abbott et al., 2012).

## 3.4 Concluding remarks

We emphasize that, unlike other channels, the MOB channel for the formation of merging BH binaries is quite robust, relying on reasonably well understood stellar evolution physics. The main uncertainty is the treatment of mixing in rapidly rotating stars, but even here we can derive some confidence from the fact that our models are able to reproduce observed local counterparts of various stages in the MOB scenario (see Fig. 3.2), such as HD 5980, IC10 X-1, and NGC 300 X-1. The MOB channel predicts the formation of very massive compact BH+BH binaries with a BH mass ratio close to 1 and a bimodal BH-mass distribution from BHs formed below and above the PISN regime.

The detection of GWs from BH+BH mergers with LIGO (and potentially other current or future GW

detectors) will not only start a revolution in observational astronomy and test general relativity in its highly dynamic strong-field regime, but will also have a great effect on our understanding of very massive stars throughout the Universe, including their fate as gamma-ray bursts or pair-instability supernovae.

**Acknowledgements:** PM and NL are grateful to Bill Paxton for his continuous help in extending the MESA code to contain all the physics required for this project over the last years. We are thankful to Selma de Mink and Norbert Wex for helpful discussions, and to Ed van den Heuvel for useful comments on an earlier version of this paper. We thank Chiaki Kobayashi for providing us with the global metallicity distribution of massive stars and Andy Fruchter for plots of the mean metallicity evolution with redshift. NL’s Alexander von Humboldt Professorship and PP’s Humboldt Research Award provided essential support for this research. The Geryon2 cluster housed at the Centro de Astro-Ingeniería UC was used for the calculations performed in this paper. The BASAL PFB-06 CATA, Anillo ACT-86, FONDEQUIP AIC-57, and QUIMAL 130008 provided funding for several improvements to the Geryon2 cluster.

## CHAPTER 4

---

# Ultra-luminous X-ray sources and neutron-star–black-hole mergers from close very massive binaries at low metallicity

---

Pablo Marchant, Norbert Langer, Philipp Podsiadlowski, Thomas M. Tauris, Selma de Mink, Ilya Mandel and Takashi J. Moriya  
Astronomy & Astrophysics, submitted

**ABSTRACT:** The detection of gravitational waves from the binary black hole (BH) merger GW150914 may enlighten our understanding of ultra-luminous X-ray sources (ULXs), as BHs of masses  $> 30M_{\odot}$  can reach luminosities  $> 4 \times 10^{39} \text{ erg s}^{-1}$  without exceeding their Eddington luminosities. It is then important to study variations of evolutionary channels towards merging BHs, as these might undergo accretion at some point and become ULXs. It was recently shown that very massive binaries with mass ratios close to unity and tight orbits can undergo efficient rotational mixing and evolve chemically homogeneously, resulting in a compact BH binary. We study the evolution of similar systems by computing  $\sim 120\,000$  detailed binary evolution models with the MESA code covering a wide range of masses, orbital periods, mass ratios and metallicities. We show that for close binaries with initial mass ratios  $q \equiv M_2/M_1 \simeq 0.1–0.4$ , primaries with masses above  $40M_{\odot}$  may evolve chemically homogeneously, remaining compact and forming a BH without experiencing Roche-lobe overflow. The secondary then expands and initiates mass transfer to the BH and thus, a ULX phase. At a given metallicity this channel is expected to produce the most massive accreting stellar BHs and the brightest ULXs. We predict that  $\sim 1$  out of  $10^4$  massive stars evolves this way, and that in the local universe  $0.13 \text{ ULXs per } M_{\odot} \text{ yr}^{-1}$  of star-formation rate are observable from this channel, with a strong preference for low-metallicity environments. An additional channel is still required to explain the less luminous ULXs and the full population of high-mass X-ray binaries. At metallicities higher than  $\log Z = -3$ , we find BH masses in ULXs from our channel to be limited to  $60M_{\odot}$  due to the occurrence of pair-instability supernovae for higher masses which leave no compact remnant, resulting in an X-ray luminosity cut-off for accreting BHs. At lower metallicities, we find that very massive stars in our binaries can avoid exploding as pair-instability supernovae and instead form BHs with masses above  $130M_{\odot}$ , producing a gap in the ULX luminosity distribution. After the ULX phase, neutron-star–BH binaries that merge in less than a Hubble time are produced, but with a low formation rate of  $< 0.2 \text{ Gpc}^{-3} \text{ yr}^{-1}$ . Future X-ray observatories are expected to be capable of testing these predictions, which, together with upcoming gravitational wave detections, will provide strict constraints on the origin of the most massive BHs that can be produced in stellar binary systems.

One of the most puzzling discoveries made by the Einstein observatory are the off-nucleus point X-ray sources with luminosities above  $10^{39}$  erg s $^{-1}$  (Long and van Speybroeck, 1983), which owing to their extreme luminosities were termed as ultra-luminous X-ray sources (ULXs). Compared to the typical properties of high-mass X-ray binaries (HMXBs), such high luminosities are difficult to explain in terms of accreting compact objects, as the Eddington limit for neutron stars ( $\sim 10^{38}$  erg s $^{-1}$ , hereafter NS) and stellar mass black holes ( $\sim 2 \times 10^{39}$  erg s $^{-1}$  for a  $10M_{\odot}$  black hole, hereafter BH), is well below the luminosities of some of the observed sources.

Two main ideas have been put forward to explain the nature of these sources, and both are still strongly debated. One possibility to explain these high luminosities is to consider the existence of a population of intermediate-mass BHs (IMBHs), with masses between  $\sim 10^2 - 10^5 M_{\odot}$ , possibly arising from the collapse of primordial stars (eg. Madau and Rees 2001) or in dense globular clusters (eg. Miller and Hamilton 2002). The second possibility is that the compact object is either a NS or a stellar mass BH, but can reach a brightness well beyond what the standard Eddington limit implies. For instance, beaming of the radiation emitted would imply that the actual full-sky luminosity of these sources is much lower, so that ULXs could consist of BHs with masses below  $10M_{\odot}$  accreting at or below the Eddington rate. This could be a purely geometrical effect (A. R. King et al., 2001), or the result of relativistic beaming (Körding, Falcke and Markoff, 2002), but measurements from ionization nebulae around some ULXs appear to confirm the isotropic estimate of their luminosities (Pakull and Mirioni, 2003). On the other hand, Begelman (2002) and Ruszkowski and Begelman (2003) proposed that the photon-bubble instability, which acts on radiation-dominated accretion disks and produces clumping, would cause photons to be radiated away through low density regions allowing for accretion rates up to 10 times the Eddington rate. The presence of a corona supported by strong magnetic fields could also help to counter the radiation pressure and allow super-Eddington accretion (Socrates and Davis, 2006).

A clear case of super-Eddington accretion is the recently observed NS-ULX (Bachetti et al., 2014), for which accretion rates above a hundred times the Eddington rate are required to explain its luminosity in excess of  $10^{40}$  erg s $^{-1}$ . The flux observed from this object has both a pulsed component with a period of 1.37 days, and a non-pulsed component, so beaming alone appears insufficient to explain its nature. Very recently, two more ULXs powered by NSs have been discovered (Israel, Belfiore et al., 2016; Israel, Papitto et al., 2016), and some argue that a significant fraction of ULXs could contain a NS accretor (A. King and Lasota, 2016). The very high luminosities of these accreting NSs do not necessarily imply that accreting BHs can also radiate well above their Eddington luminosities, since the accretion flows around NSs and BHs should differ substantially.

It should also be considered that, although Galactic BHs are limited to masses below  $\sim 20M_{\odot}$  due to strong wind mass loss (Fryer and Kalogera, 2001; Spera, Mapelli and Bressan, 2015; Sukhbold et al., 2016), in lower metallicity environments BH masses could reach up to  $45M_{\odot}$  (Heger and Woosley, 2002; Belczynski, Heger et al., 2016), with the mass being limited by the effects of pair-instability supernovae (PISNe) and pulsational-pair-instability supernovae (PPISNe). Such massive BHs can easily account for the luminosity of ULXs, requiring accretion rates only slightly above the Eddington limit to explain some of the brightest sources (Zampieri and Roberts, 2009). For massive enough progenitors, it is expected that PISNe can be avoided, resulting in BHs with masses above  $\sim 130M_{\odot}$  and possibly causing a gap in the BH mass distribution (Heger and Woosley, 2002). However, for single stars this requires extremely high zero-age main-sequence masses and low metallicity.

As the Chandra X-ray observatory and other facilities opened up the possibility of studying populations of point X-ray sources in galaxies down to much lower luminosities, Grimm, M. Gilfanov and Sunyaev (2003) showed that ULXs generally correspond to the tail of the HMXB population, and their number is strongly correlated with star-formation rate (SFR). Swartz et al. (2011) estimated a typical number of  $\sim 2$  ULXs per  $M_{\odot}$  yr $^{-1}$  of SFR for a local sample of galaxies, while Luangtip et al. (2015) observed

---

that there is a scarcity of ULXs in luminous infrared galaxies, with an estimated number of 0.2 ULXs per  $M_{\odot} \text{ yr}^{-1}$  of SFR. All of this points towards both a stellar origin for ULXs, and possibly a strong metallicity dependence. Using a sample of 64 galaxies at various metallicities, Mapelli, Ripamonti et al. (2010) found that the number of ULXs per  $M_{\odot} \text{ yr}^{-1}$  of SFR scales with metallicity as  $Z^{-0.55 \pm 0.23}$ .

There are two ULXs for which dynamical estimates of the masses are available from measurements of radial-velocity variations due to the orbital motion of the donor star, detected as a Wolf-Rayet (WR) star: M101 ULX-1, with a BH mass likely in the range  $20M_{\odot} - 30M_{\odot}$  (Liu et al., 2013), and P13, with a BH mass below  $15M_{\odot}$  (Motch et al., 2014). Both exclude the possibility of an IMBH as the compact object and set constraints on the properties of the donor. However, these dynamical mass estimates need to be considered with care, as is shown by the case of the HMXB IC10 X-1. Using measurements of radial-velocity variations, Silverman and Filippenko (2008) concluded that this system contains a BH with a mass in excess of  $20M_{\odot}$ , but Laycock, Maccarone and Christodoulou, 2015 showed that the radial-velocity variation detected does not follow the stellar motion, but rather comes from a shadowed region in the stellar wind. This means that the dynamical mass estimate is incorrect, making the mass of the compact object much more uncertain and even consistent with a NS accretor.

Although the evidence appears to rule out IMBHs as the central engines of most ULXs, there remain a handful of particularly bright sources (in excess of  $3 \times 10^{41} \text{ erg s}^{-1}$ ) which appear to form an independent population (Sutton, Roberts, Walton et al., 2012; Swartz et al., 2011). The term hyper-luminous-X-ray-source (HLX) has been coined for these objects, with ESO243-49 HLX-1 being the best current candidate for an IMBH (Farrell et al., 2009). However, some of these have been confirmed to be background AGN (Sutton, Roberts, Gladstone et al., 2015), reducing the number of known objects of this class.

The first observation from the twin LIGO detectors in Hanford and Livingston of gravitational waves (GWs) from the inspiral and merger of two  $\sim 30M_{\odot}$  BHs (GW150914, B. P. Abbott et al. 2016a), plays a particularly important role in our understanding of ULX progenitor systems. Any formation channel that can produce BHs above  $30M_{\odot}$  is likely to be related to the formation of ULXs, as the occurrence of Roche-lobe overflow (hereafter RLOF) would easily result in very high luminosities. There are three main channels that can explain the origin of GW150914, the classical field scenario involving common-envelope (CE) evolution (Belczynski, Holz et al., 2016; Kruckow et al., 2016), the dynamical scenario in globular and nuclear clusters (Rodriguez, Chatterjee and Rasio, 2016), and the chemically homogeneous evolution (CHE) channel for field binaries (Mandel and de Mink, 2016; Marchant et al., 2016; de Mink and Mandel, 2016) which we illustrate in Figure 4.1. BHs formed in this way can have very large spins, which makes them potential long-gamma-ray burst (hereafter LGRB) progenitors in the collapsar scenario of Woosley (1993). Also, owing to the large Wolf-Rayet masses that can be achieved through the CHE channel, it can potentially result in PISN/PPISNe. The occurrence of CHE in binaries was first proposed by de Mink, Cantiello et al. (2009), and has only recently been studied in more detail (Song et al., 2016; Mandel and de Mink, 2016; Marchant et al., 2016; de Mink and Mandel, 2016).

The commonly assumed model for ULX formation involves the occurrence of a CE phase in an initially very wide binary (S. A. Rappaport, Podsiadlowski and Pfahl, 2005). In these models, the envelope of the primary is stripped in a CE phase, which significantly reduces the orbital period. The primary then collapses to a BH, and when the secondary expands and initiates RLOF the system becomes an active X-ray source. Whether a standard HMXB or a ULX is produced, depends on the mass of the BH formed, providing a simple explanation for the continuous luminosity distribution function from HMXBs to ULXs, although accretion rates  $\sim 10$  times Eddington are still required to explain the brightest sources. This evolutionary path is closely related to the classical channel for merging binary BHs, in which the primary is stripped through stable mass transfer in a very wide orbit, and a CE phase happens when the secondary expands to become a giant. In addition, considering the possibility that stable mass transfer develops instead of a CE, Pavlovskii et al. (2016) showed that systems similar to the progenitor

of GW150914 could instead form a ULX with a red supergiant as a donor. In this sense, recognizing branches of binary BH formation channels resulting not only in GW emission, but also in electromagnetic waves, will play a fundamental role in constraining different formation scenarios of GW sources.

A different possibility is the formation of ULXs containing a BH through dynamical interactions in star clusters (Mapelli and Zampieri, 2014; MacLeod, Trenti and Ramirez-Ruiz, 2016), which could potentially produce more massive BHs at a given metallicity, as the progenitor of the BH can evolve as a single star and avoid envelope stripping in a binary.

In this paper we consider an alternative channel for the formation of ULXs, involving the evolution of very close, very massive binaries, where only the primary star undergoes efficient rotational mixing (as proposed by de Mink, Cantiello et al. 2009), avoiding binary interaction before the formation of a massive BH. The less massive component in such a system will evolve normally, eventually undergoing RLOF and initiating mass transfer. As the resulting BH will usually be more massive than the secondary, this results in a long-lived ULX phase, as mass transfer proceeds on a nuclear timescale. Such a channel of evolution is strongly related to the formation of merging double BHs, PISNe and LGRBs, and could be the source of the most luminous X-ray sources of stellar origin that can be formed under any given conditions. In Section 4.1 we describe the setup of our stellar evolution models, and present our model for ULX formation in Section 4.2. We then discuss the consequences of this channel for the luminosity distribution of ULXs in Section 4.3, and their orbital parameters in Section 4.4. In Section 4.5 we discuss the formation of NS-BH and BH-BH binaries after a ULX phase, and the possibility to form systems compact enough to merge in less than a Hubble time. We give our concluding remarks in Section 4.6.

## 4.1 Methods

We extend the models computed by Marchant et al. (2016) to lower initial mass ratios to study the possibility of the primary evolving chemically homogeneously and forming a BH, while the secondary evolves on a much longer timescale, avoiding early interaction. Our tool of choice for stellar modeling is version 8845 of the MESA code (Paxton, Bildsten et al., 2011; Paxton, Cantiello et al., 2013; Paxton, Marchant et al., 2015)<sup>1</sup>.

We use the Ledoux criterion for convection, which we model using mixing-length theory (Böhm-Vitense, 1958) with a mixing length parameter  $\alpha = 1.5$ . In regions that are stable according to the Ledoux criterion, but unstable according to the Schwarzschild criterion, we include semiconvective mixing as in Langer, Fricke and Sugimoto (1983) with an efficiency parameter  $\alpha_{sc} = 1$ . Opacities are computed using CO-enhanced tables from the OPAL project (Iglesias and F. J. Rogers, 1996) with solar scaled abundances from Grevesse, Noels and Sauval (1996). As we do not need to follow the detailed nucleosynthetic evolution of our models, we use the simple nuclear networks `basic.net`, `co_burn.net` and `approx21.net` that are provided with MESA and are switched during runtime as needed to account for the later burning phases.

Rotational mixing and angular momentum transport are treated as diffusive processes following Heger and Langer (2000), including the effects of Eddington-Sweet circulations, the Goldreich-Schubert-Fricke instability, and secular and dynamical shear, with an efficiency parameter  $f_c = 1/30$  (Chaboyer and Zahn, 1992), and a sensitivity to composition gradients parametrized by  $f_\mu = 0.1$  (Yoon, Langer and C. Norman, 2006). We also include transport of angular momentum due to the Spruit-Tayler dynamo (Spruit, 2002) following the implementation by Petrovic, Langer, Yoon et al. (2005). The effect of centrifugal forces is modeled as in Endal and Sofia (1976). Our models do not include the impact of tidal deformation

<sup>1</sup> The inlist files and sources to reproduce our models are provided at [https://github.com/orlox/mesa\\_input\\_data/tree/master/2016\\_ULX](https://github.com/orlox/mesa_input_data/tree/master/2016_ULX), together with most of the data used for this paper.

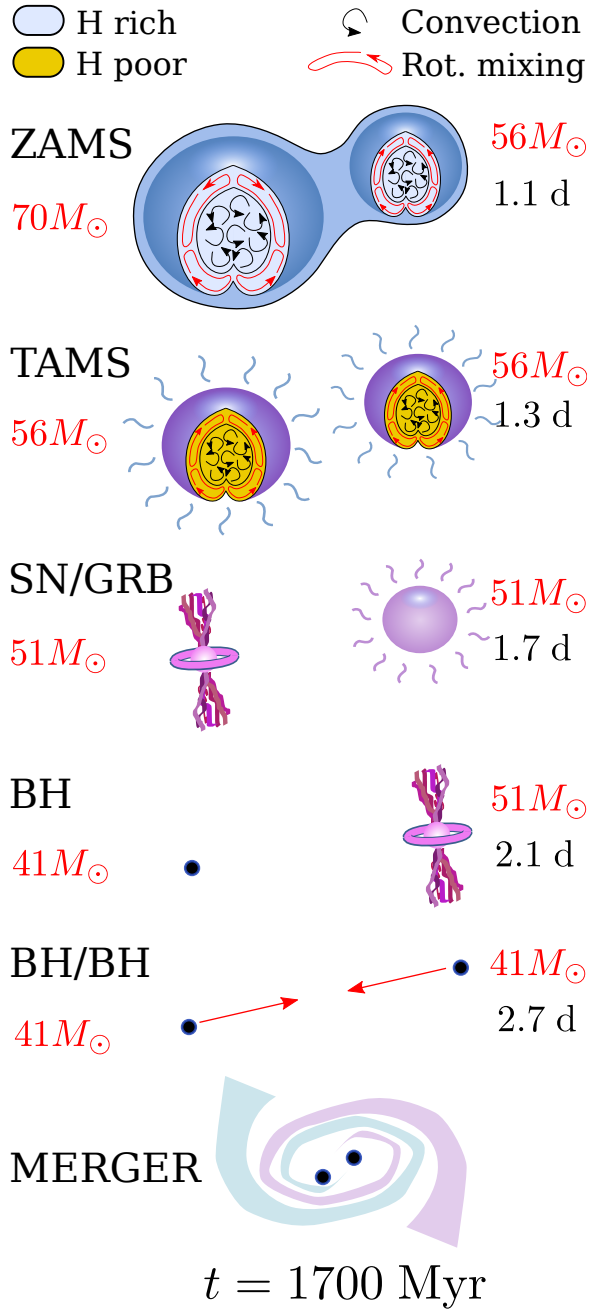


Figure 4.1: The CHE channel for the formation of double-BHs, including the occurrence of an overcontact phase as in Marchant et al. (2016). Numbers correspond to a system with  $Z = Z_{\odot}/50$ , initial masses  $M_1 = 70M_{\odot}$  and  $M_2 = 56M_{\odot}$ , and a very short initial period at the zero-age main sequence (ZAMS). This system evolves early on into a contact configuration, where mass is transferred back and forth until a mass ratio of unity is achieved. Efficient rotational mixing distributes the helium rich material from the core throughout the entire envelope, resulting in an almost pure helium star at the terminal-age main sequence (TAMS). Depending on the final masses of each component, the system may then proceed to form a compact BH binary that can merge within a Hubble time, or explode as a PISNe. The models from Marchant et al. (2016) had an error in the computation of spin-orbit coupling which resulted in slightly wider orbits. We have corrected for this, so the values differ slightly from those in Marchant et al. (2016). We have also verified that the conclusions of that work remain valid despite this issue.

on stellar structure, but account for tidal synchronization following Hurley, Tout and Pols (2002) and Detmers et al. (2008), which follow the model for dynamical tides of Zahn (1975) and Zahn (1977).

Stellar winds are implemented as in Brott, de Mink et al. (2011), with mass loss for hot hydrogen-rich stars modeled as in Vink, de Koter and Lamers (2001). Between a surface hydrogen composition of  $X = 0.7$  to  $0.4$  we interpolate between the Vink rate and a tenth of the mass loss rate for hydrogen-poor stars of Hamann, Koesterke and Wessolowski (1995). For temperatures below that of the bi-stability jump, the rate is taken as the maximum between the Vink rate and that of Nieuwenhuijzen and de Jager (1990), though in practice, the stars we model remain blue over most of their lifetimes, so this plays a negligible role. We scale the strength of stellar winds by a factor  $(Z/Z_{\odot})^{0.85}$ , extending the metallicity dependence predicted by Vink, de Koter and Lamers (2001) for O/B stars to hydrogen-poor Wolf-Rayet and cool stars. The value of the solar metallicity is taken as  $Z_{\odot} = 0.017$  (Grevesse, Noels and Sauval, 1996). In a binary system, we assume that winds carry the specific orbital angular momentum corresponding to each component.

We model about a 120 000 binary systems for metallicities in the range  $\log Z = -2$  to  $-6$  in steps of 0.5 dex, primary masses between  $\log M_1/M_{\odot} = 1.5 - 2.5$  ( $30M_{\odot} - 300M_{\odot}$ ) in steps of 0.05 dex, mass ratios  $q = M_2/M_1 = 0.05 - 0.6$  (which results in a range of secondary masses between  $1.5M_{\odot} - 180M_{\odot}$ ) in steps of 0.05 and initial orbital periods between 0.5 and 3 days, in steps of 0.05 days. At higher mass ratios we expect the formation of binary-BHs, as discussed in detail by Marchant et al. (2016). The initial helium mass fraction is determined by assuming that it linearly increases with metallicity from the primordial value  $Y = 0.2477$  (M. Peimbert, Luridiana and A. Peimbert, 2007) at  $Z = 0$  to  $Y = 0.28$  at  $Z = Z_{\odot}$ . Both components in the binary are assumed to be tidally locked at the ZAMS, although for the lowest mass ratios and shortest orbital periods the Darwin instability (Darwin, 1879) could make the formation of such systems impossible. To account for this, we consider the minimum orbital separation  $a_{\text{Darwin}} = \sqrt{3(I_1 + I_2)/\mu}$  below which a binary would become unstable, where  $I_1$  and  $I_2$  are the moments of inertia of both components and  $\mu$  is the reduced mass. Systems that have an initial orbital separation below  $a_{\text{Darwin}}$  are ignored in our analysis.

For these mass ratios and short orbital periods we expect systems to quickly evolve to an overcontact configuration and a merger if the primary experiences RLOF. CE ejection is unlikely in this case due to the short orbital period and the strongly bound envelope. If the primary undergoes CHE, but the secondary expands and initiates mass transfer before BH formation, the orbit is expected to widen as mass is transferred from the less massive to the more massive star. This slows down the rotation of the primary as it remains tidally locked. At the same time, the primary accretes hydrogen-rich material at its surface. These two effects lead to the interruption of CHE. Because of this, we terminate our simulations if there is mass transfer from any component before BH formation.

For the primary star, if central and surface helium mass fractions differ by more than 0.2, we consider the system not to be homogeneously evolving and terminate the simulation. If the primary star evolves to helium depletion, with a final mass outside the range  $60 - 130M_{\odot}$ , we assume it collapses directly to a BH, while inside that range we assume the star explodes as a PISN leaving no remnant. Note that this ignores possible mass loss due to PPISNe or LGRBs. In particular, PPISNe are expected to result in strong mass loss for helium stars with final masses above  $\sim 40M_{\odot}$ , and to limit the remnant mass to  $\sim 47M_{\odot}$  (Woosley, 2016). Taking into account this effect would produce a reduction of  $\sim 25\%$  in the maximum luminosity we predict from sources below the PISN gap. This is much smaller than the variations coming from uncertainties in the accretion rates.

After BH formation, if the secondary does not evolve chemically homogeneously, it will eventually expand and undergo RLOF. Low-mass helium stars are expected to undergo an additional phase of mass transfer after helium depletion, which is called Case ABB or BB depending on whether the first mass-transfer event occurred before or after core-hydrogen depletion (Delgado and Thomas, 1981; Dewi,

Pols et al., 2002). This can result in ultra-stripped CO-cores that might produce electron-capture and iron-core-collapse supernovae (SNe), often with small kicks (Tauris, Langer and Podsiadlowski, 2015). To study the possibility of forming merging BH-NS or BH-BH systems after interaction, we need to consider this additional phase of mass transfer, as due to the large mass ratios involved (the primary is expected to become a BH of more than  $20M_{\odot}$ ), it can result in extreme orbital widening. To take this into account, we consider the evolution of the secondary star until core carbon depletion, or until mass transfer reaches hydrogen depleted regions. In case the latter happens, the orbit should widen significantly making the system irrelevant as a source of GWs.

#### 4.1.1 The Eddington limit for accretion to a BH

A BH accreting matter through a disk at a rate  $\dot{M}_{\text{acc}}$  is expected to have a luminosity  $L_{\text{acc}} = \eta \dot{M}_{\text{acc}} c^2$ , where  $\eta \simeq 0.06 - 0.42$  is dependent on the position of the innermost-stable-circular orbit (ISCO) of the BH, which in turn varies with its spin. If this radiation is emitted isotropically, there is a limit at which the force exerted by radiation exceeds the gravitational pull of the BH, which is given by the Eddington luminosity,

$$L_{\text{Edd}} = \frac{4\pi GM_{\text{BH}}c}{\kappa} \quad (4.1)$$

$$= 1.47 \times 10^{39} \left( \frac{M_{\text{BH}}}{10M_{\odot}} \right) \left( \frac{1 + X_s}{1.7} \right)^{-1} \text{ erg s}^{-1}, \quad (4.2)$$

where  $X_s$  is the surface hydrogen mass fraction of the donor, and we have assumed electron scattering to be the main source of opacity. The mass-accretion rate at which this luminosity is reached, is given by

$$\dot{M}_{\text{Edd}} = 2.6 \times 10^{-7} \left( \frac{M_{\text{BH}}}{10M_{\odot}} \right) \left( \frac{1 + X_s}{1.7} \right)^{-1} \left( \frac{\eta}{0.1} \right)^{-1} M_{\odot} \text{ yr}^{-1}, \quad (4.3)$$

and we assume that the accretion rate  $\dot{M}_{\text{acc}}$  is limited to this value, i.e. if the mass-transfer rate from the donor is  $\dot{M}_{\text{mt}}$ , then  $\dot{M}_{\text{acc}} = \min(\dot{M}_{\text{Edd}}, \dot{M}_{\text{mt}})$ , with the non-accreted material being ejected from the system with the specific orbital angular momentum of the BH.

Although there are many indications that beamed emission can allow for much higher mass-transfer rates and luminosities, in particular the case of the NS ULX (Bachetti et al., 2014), we consider isotropic emission as a lower limit for the luminosities these objects can achieve. As it will be shown in Section 4.2, the high BH masses produced through CHE can easily account for ULX luminosities without the need of super-Eddington accretion, and can reach the highest luminosities observed by accreting at only 3 times the Eddington rate. As the energy released as radiation will not contribute to the BH mass, it increases as

$$\dot{M}_{\text{BH}} = (1 - \eta) \dot{M}_{\text{acc}}. \quad (4.4)$$

Following Podsiadlowski, S. Rappaport and Han (2003), we consider the evolution of the BH spin as it

accretes material, which for a BH with zero initial spin and mass  $M_{\text{BH},0}$ , results in (Bardeen, 1970)

$$\eta = 1 - \sqrt{1 - \left(\frac{M_{\text{BH}}}{3M_{\text{BH},0}}\right)^2}, \quad (4.5)$$

$$a = \sqrt{\frac{2}{3}} \frac{M_{\text{BH},0}}{M_{\text{BH}}} \left( 4 - \sqrt{18 \left(\frac{M_{\text{BH},0}}{M_{\text{BH}}}\right)^2 - 2} \right), \quad (4.6)$$

so long as  $M_{\text{BH}} < \sqrt{6}M_{\text{BH},0}$ . If the BH mass reaches  $\sqrt{6}M_{\text{BH},0}$ , we assume  $a = 1$  and  $\eta = 0.42$ , though in practice the absorption of radiation from the disc can produce a torque that limits the BH spin to  $\simeq 0.998$  (Thorne, 1974), with a correspondingly lower  $\eta$ . If the BH has a non-zero initial spin parameter  $a_0$ , then we can still make use of these expressions by computing an effective initial BH mass  $M_{\text{BH},0}^{\text{eff}}$ , corresponding to a BH with zero spin that would reach  $a = a_0$  after accreting material up to  $M_{\text{BH},0}$ . This effective mass can be easily computed from a simple relation between the radius of the ISCO  $r_{\text{ISCO}}$  and the mass of the BH as it accretes (Bardeen, 1970; Bardeen, Press and Teukolsky, 1972). If  $z = r_{\text{ISCO}}/M_{\text{BH}}$ , then in geometrized units we have

$$M_{\text{BH},0}^{\text{eff}} = \sqrt{\frac{z(a_0)}{6}} M_{\text{BH},0}, \quad (4.7)$$

which reduces to  $M_{\text{BH},0}^{\text{eff}} = M_{\text{BH},0}/\sqrt{6}$  for  $a_0 = 1$  and  $M_{\text{BH},0}^{\text{eff}} = M_{\text{BH},0}$  for  $a_0 = 0$ , as expected.

## 4.2 Formation of ULXs through CHE

Our proposed model for ULX formation involves binary systems at low mass ratios, where the more massive component undergoes CHE, while the secondary evolves normally. This is in contrast to the CHE binary BH formation channel which requires mass ratios closer to unity, for which both stars evolve chemically homogeneously. Because of this it is important to understand under which conditions one, both or neither of the components of a binary would experience efficient rotational mixing. To illustrate this, Figure 4.2 shows the required initial rotation rates (in terms of the ratio of the angular frequency to its critical value  $\Omega/\Omega_{\text{crit}}$ ) for which single stars with a given ZAMS mass would undergo CHE. The critical value of the angular frequency depends on the Eddington factor  $\Gamma$  at the surface of the star, and is given by (Langer, 1997)

$$\Omega_{\text{crit}} = \sqrt{\frac{GM}{R^3}(1-\Gamma)}, \quad \Gamma \equiv \frac{L}{L_{\text{Edd}}} = \frac{\kappa}{4\pi c G} \frac{L}{M} \quad (4.8)$$

Despite the reduction in stellar lifetimes with mass, rotational mixing is expected to play a larger role for the more massive stars, owing to the increasing importance of radiation pressure which reduces the stability of the stratification in the radiative envelope (Yoon, Langer and C. Norman, 2006), and to the larger mass of the convective cores, relative to the total mass (see, eg. Köhler et al., 2015). This makes the threshold  $\Omega/\Omega_{\text{crit}}$  for efficient mixing decrease with mass. In contrast,  $\Omega_{\text{crit}}$  at the ZAMS decreases with mass, so at a constant initial rotation period  $\Omega/\Omega_{\text{crit}}$  increases with mass, as is shown by the solid lines in Figure 4.2. If we consider a binary with tidally locked components, this means that for mass ratios close to unity both stars can be inside the region for CHE, while for lower mass ratios the less massive component would evolve normally.

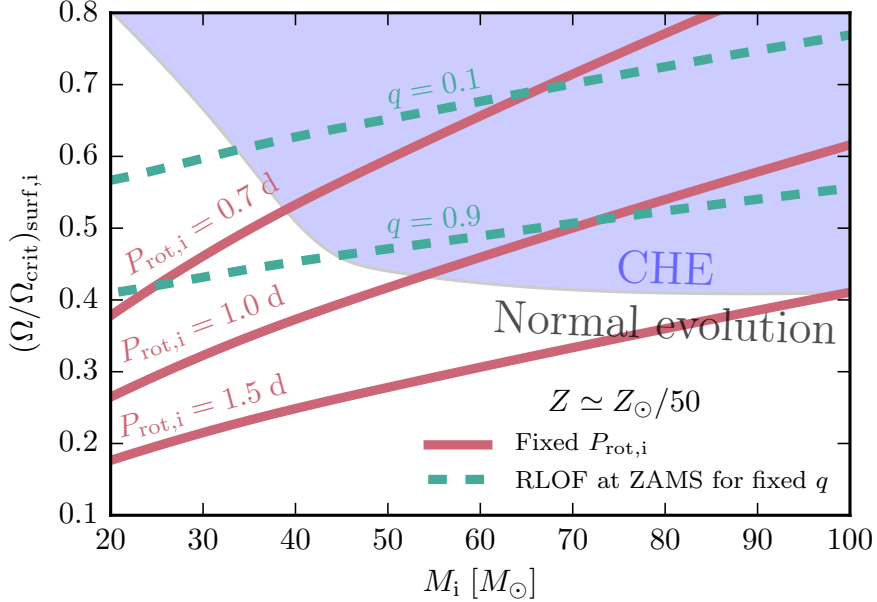


Figure 4.2: Initial conditions for the occurrence of CHE in single stars at a metallicity  $Z = 10^{-3.5} \simeq Z_\odot/50$ , in terms of mass at the ZAMS and initial ratio of angular frequency  $\Omega$  to its critical value  $\Omega_{\text{crit}}$  at the surface. The colored region indicates stars for which the surface helium abundance at TAMS exceeds 0.8, and is a sharp transition. Solid lines correspond to a fixed initial rotational period, while dashed lines indicate the value of  $\Omega/\Omega_{\text{crit}}$  if the star is the primary of a binary system at a fixed mass ratio  $q$  which exactly fills its Roche lobe at the ZAMS.

Another important point is that to form a ULX the binary has to avoid RLOF before the primary forms a BH. This again is in contrast to the binary-BH formation channel with CHE, where the detailed simulations of Marchant et al. (2016) showed that most systems need to be in contact to undergo efficient rotational mixing. Figure 4.2 also illustrates why binaries with lower mass ratios can experience CHE while avoiding contact (cf. Yoon, Langer and C. Norman, 2006; de Mink, Cantiello et al., 2009). Dashed lines indicate the value of  $\Omega/\Omega_{\text{crit}}$  the primary star would have for a fixed mass ratio, when the orbital period is the smallest possible for which there is no RLOF at the ZAMS. For lower mass ratios, binaries can have shorter orbital periods, allowing for a larger range of systems where the primaries fall into the CHE region. The requirement of having a system that avoids RLOF at the ZAMS also limits the minimum primary mass at which CHE evolution can happen in a binary. In all of our binary simulations, the least massive primary that evolves chemically homogeneously has an initial mass  $M_1 = 45M_\odot$ .

Although Figure 4.2 is useful to illustrate the requirements for CHE in a binary system, this boundary depends on how rotation rates change due to mass loss through the full main sequence evolution, and this is different for single and binary stars. In a tidally synchronized binary, changes in the rotational period depend on how mass loss alters the orbital period, and this is mass-ratio dependent. To assess whether a binary would undergo CHE we then need to model each individual system in detail. In what follows, we describe in more detail how a ULX is formed through CHE, what sets the lower and upper limits in mass ratio for the formation of ULXs, and discuss the effect of metallicity on this channel.

#### 4.2.1 Mass-ratio dependence

To exemplify the formation of a ULX via CHE, let us consider the evolution of systems with metallicity  $Z = 10^{-3.5} \approx Z_{\odot}/50$  and primary mass  $M_1 = 70M_{\odot}$  as the example shown in Figure 4.1, but for three different mass ratios  $q = 0.05, 0.2$  and  $0.6$ . For a mass ratio  $q = 0.05$  (a secondary mass of  $3.5M_{\odot}$ ) and an initial period of 0.8 days, the primary is close to filling its Roche-lobe at the ZAMS, with  $R/R_{\text{RL}} \approx 0.92$ . However, this binary would have an initial orbital separation of  $15R_{\odot}$ , while the minimum separation at which the system would avoid the Darwin instability is  $a_{\text{Darwin}} = 21R_{\odot}$ . Because of this we do not expect this system to be formed, as it would have resulted in a merger instead of a tidally synchronized binary which is our assumed initial state.

At larger initial mass ratios the initial configuration is not Darwin unstable, and we show in Figure 4.3 the evolution in the Hertzsprung-Russell diagram for two systems with mass ratios  $q = 0.2$  and  $0.6$ . For an initial mass ratio  $q = 0.6$  (a secondary mass of  $42M_{\odot}$ ) and an initial period of 1.2 days, after 1.6 Myrs the orbital separation is still 1.2 days, and the primary experiences a significant amount of mixing, with  $Y_c = 0.44$  and  $Y_s = 0.35$ . However, the secondary does not evolve homogeneously, and by this point it has expanded enough to undergo RLOF. Since the secondary is the less massive component, mass transfer will widen the orbit and transfer hydrogen-rich material on the surface of the primary. The steep change in mean molecular weight at the base of the accreted material prevents it from mixing inwards, so we terminate the simulation as we expect the system to break away from CHE.

To form a ULX, a system with a mass ratio high enough to avoid the Darwin instability, but small enough to avoid interaction before forming a BH is needed. This is the case for the system shown in Figure 4.4, depicting the evolution for an initial mass ratio  $q = 0.2$  and an initial period of 1.1 days. The primary in this system evolves chemically homogeneously, depleting central helium after 4.6 Myrs. At this point the orbital period has slightly increased to 1.7 days, but more importantly, the secondary has barely evolved, and its core hydrogen mass fraction is  $X_c = 0.62$ . At helium depletion the primary is still rapidly rotating, with a dimensionless spin angular momentum  $a_0 = 1.25$ , making a direct collapse into a  $55M_{\odot}$  BH impossible without shedding excess angular momentum, and thus possibly resulting in a LGRB following the collapsar scenario (Woosley, 1993). Moreover, for this mass, we would expect a PPISN to occur (Woosley, 2016). For simplicity, we ignore this and assume direct collapse to a critically rotating BH ( $a_0 = 1$ ), though the relationship of the black hole’s angular momentum to that of the progenitor star is uncertain. 12.6 Myrs after the formation of the system, and with  $X_c = 0.24$ , the secondary overflows its Roche-lobe and undergoes a phase of Case A mass transfer lasting 1.6 Myrs, and reducing its mass from  $14M_{\odot}$  to  $8.6M_{\odot}$ . The typical mass-transfer rate during this phase is  $\dot{M}_{\text{mt}} = 10^{-5.7} M_{\odot} \text{ yr}^{-1}$ , which is only a factor of five above the Eddington rate of the BH. The Eddington luminosity of the BH exceeds  $8 \times 10^{39} \text{ erg s}^{-1}$ , so during mass transfer the system would be an ultra-luminous source.

After the secondary depletes its central hydrogen, it expands to undergo a short-lived phase (lasting only 28000 yrs) of Case B mass transfer which reduces its mass to  $5.8M_{\odot}$ , with mass-transfer rates as high as  $\dot{M}_{\text{mt}} = 10^{-3.4} M_{\odot} \text{ yr}^{-1}$ . At detachment the orbital period is 20 days, and the star has a helium core of  $3.6M_{\odot}$ , with a significant hydrogen-rich envelope left. During core helium burning most of the envelope is turned into pure helium, resulting in a  $5.8M_{\odot}$  star with a  $5.1M_{\odot}$  helium core. After helium depletion, the remaining envelope expands and manages to initiate Case BB mass transfer, however carbon is rapidly depleted after only  $0.3M_{\odot}$  is transferred, though this is already enough to increase the orbital period to 23 days. Assuming the  $5.5M_{\odot}$  star explodes as a SN with a possibly strong kick oriented in a random direction, there is a small chance that the system remains bound and in a tight an eccentric orbit that would allow a BH-NS merger within a Hubble time (see Section 4.5).

In general, considering our complete set of simulations, we find that ULXs can be formed for initial mass ratios in the range  $q \approx 0.1–0.45$ . The lower limit on mass ratios is a product of the Darwin instability,

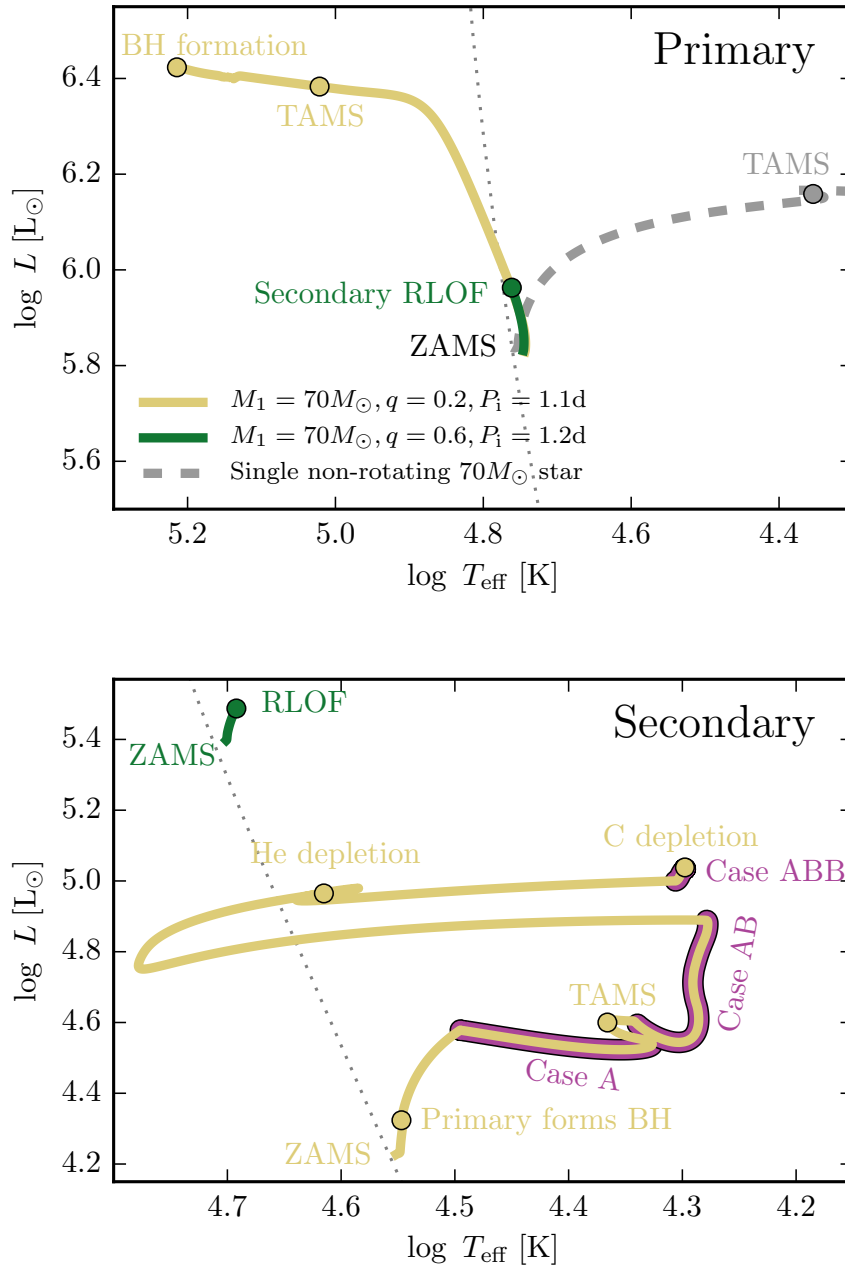


Figure 4.3: Evolution in the Hertzsprung-Russell diagram of the primary (top) and secondary (bottom) stars in binary systems with  $Z = 10^{-3.5} \approx Z_\odot/50$  consisting of a  $70M_\odot$  primary with mass ratios  $q = 0.2, 0.6$  and initial orbital periods that are close to producing RLOF at the ZAMS. The dotted line shows the location of the ZAMS for non-rotating stars, and the track of a non-rotating  $70M_\odot$  star is also shown for reference. The system with initial mass ratio  $q = 0.6$  has the primary evolving chemically homogeneously, but the secondary initiates mass transfer before a BH is formed. The system with initial  $q = 0.2$  manages to form a BH, and afterwards undergoes three distinct phases of mass transfer. See Section 4.2.1 for details.

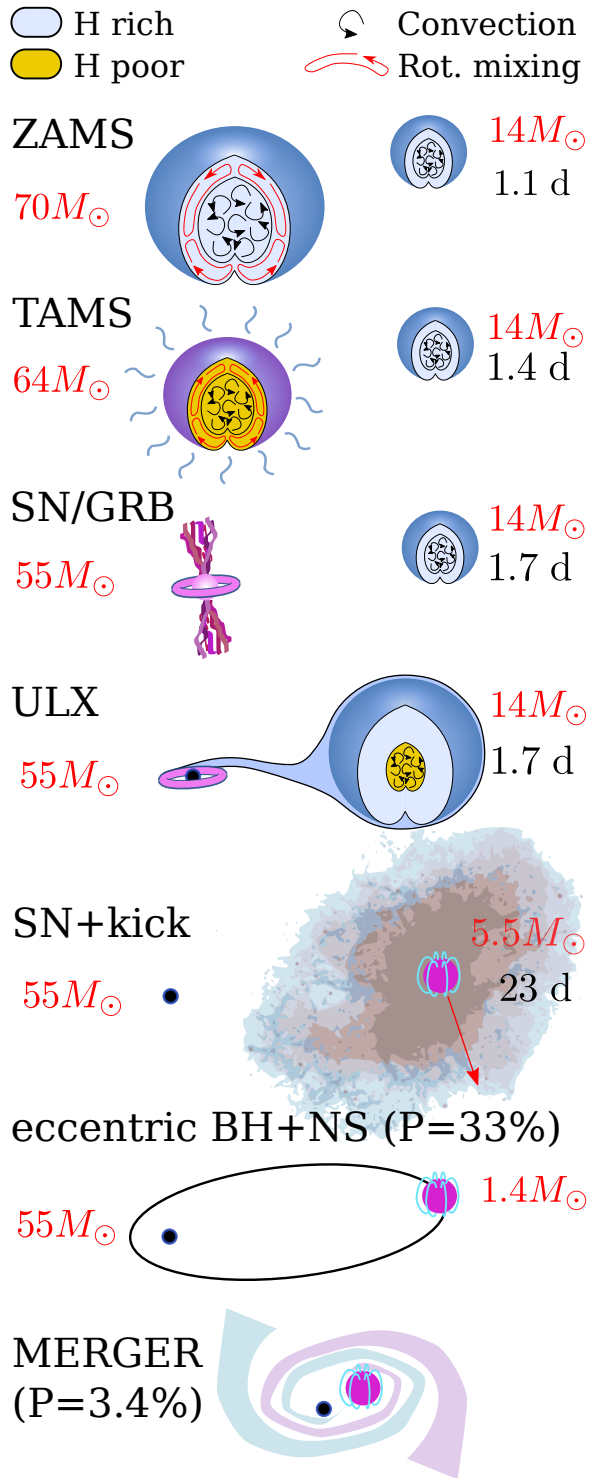


Figure 4.4: Schematic evolution of a ULX model arising from CHE of the more massive component in a compact binary with unequal masses and  $Z = 10^{-3.5} \approx Z_{\odot}/50$ . The phase of RLOF actually corresponds to three distinct mass-transfer phases. If at the moment of formation of the NS (or BH for the most massive secondaries) there is a kick in a favorable direction, a compact enough system can be formed such that a merger is possible in less than a Hubble time. For this system in particular, assuming a Maxwellian kick distribution with 1D root-mean-square  $\sigma = 265 \text{ km s}^{-1}$ , there is a 67% chance that the binary is disrupted, and a 3.4% chance that it results in a NS+BH merger in less than a Hubble time. For simplicity, mass loss at the moment of formation of the first BH is ignored.

while the upper limit results because secondaries initiate RLOF before BH formation, interrupting CHE. For reference, the detailed outcomes of all our models are shown in Appendix C.

### 4.2.2 The impact of metallicity on the properties of ULXs

Figure 4.5 shows the outcome of simulations with  $q = 0.2$  for some of the metallicities modeled. At a fixed mass ratio and metallicity, the initial primary masses and orbital periods for which the primary can evolve chemically homogeneously are very similar to those that can produce binary BHs from initial mass ratios closer to unity (Marchant et al., 2016), the main difference being that the period window for contact-less evolution is much larger. Although wind mass loss typically disfavors CHE as it brakes the star's rotation, for the most massive primaries it can help expose helium-enriched layers from their large convective cores, significantly widening the window for this channel at the highest masses (Köhler et al., 2015; Szécsi et al., 2015).

The properties of ULXs produced through CHE are strongly dependent on metallicity. Metal-poor stars are more compact, making it possible for binaries with the same component masses to have shorter initial orbital periods while still avoiding RLOF at the ZAMS, as can be seen in Figure 4.5. Although shorter initial orbital periods result in faster surface rotation velocities, this does not translate into more systems undergoing CHE, as the relevant quantity to consider mixing efficiency is not the absolute rotational velocity, but rather its ratio to the critical velocity, which also increases as stars become more compact at lower metallicity. The effect of metallicity-dependent mass loss is more complex. For the highest metallicity modeled,  $Z = 0.01$ , mass loss results in significant orbital widening, which together with tidal coupling significantly spins down the primary and results in very few systems evolving chemically homogeneously<sup>2</sup>. In contrast, for extremely low metallicities, reduced winds mean that the window for the channel does not widen too much at the highest masses.

For systems undergoing CHE, mass loss determines the occurrence of PISNe. At  $\log Z = -2.5$ , mass loss is strong enough that systems with initial masses of  $300M_{\odot}$  result in helium cores below  $60M_{\odot}$ , avoiding explosion as a PISNe and producing BHs. At a metallicity of  $\log Z = -3$ , the most massive primaries have final masses well above  $60M_{\odot}$ , which we would expect to explode as PISNe. At  $\log Z = -3.5$  mass loss has reduced to the point where we get primaries with final masses above  $130M_{\odot}$ , that could possibly avoid the PISNe fate and instead produce very massive BHs. This would translate into a gap in BH masses. At even lower metallicities, the region where PISNe occur moves further down in terms of initial primary mass, and as mass loss becomes negligible, the period window for CHE becomes narrower. This narrowing increases the minimum primary mass at which CHE occurs, such that at an extremely low metallicity of  $\log Z = -6$  only primaries above  $70M_{\odot}$  undergo CHE. As mass loss is very weak, these stars still fall into the mass range for PISNe, and there is no longer a gap in BH masses; all the resulting BHs come from systems above the mass limit for PISNe.

Mass loss of the primary star also affects the lifetime of a possible ULX phase. Figures 4.6 and 4.7 show the evolution of the orbital period and the mass-transfer phases for three of our ULX models with initial primary masses of  $70M_{\odot}$  and metallicities  $\log Z = -2.5, -3$  and  $-3.5$ . The highest metallicity model widens significantly due to mass loss before the BH forms, resulting in the secondary initiating RLOF only after core hydrogen depletion. This Case B mass-transfer phase is short-lived, making it unlikely to detect ULXs during this phase of evolution. In contrast, the two lower metallicity systems remain compact enough after BH formation to undergo long-lived phases of nuclear-timescale mass transfer, with the duration of these increasing at lower metallicities. The resulting luminosities for these

<sup>2</sup> Most of our models with  $Z = 0.01$  that evolve chemically homogeneously could not be modeled up to helium depletion due to numerical issues arising from envelope inflation. Still, only a small number of those models undergo this channel of evolution, and only for very high primary masses, so at these high metallicities the channel is negligible.

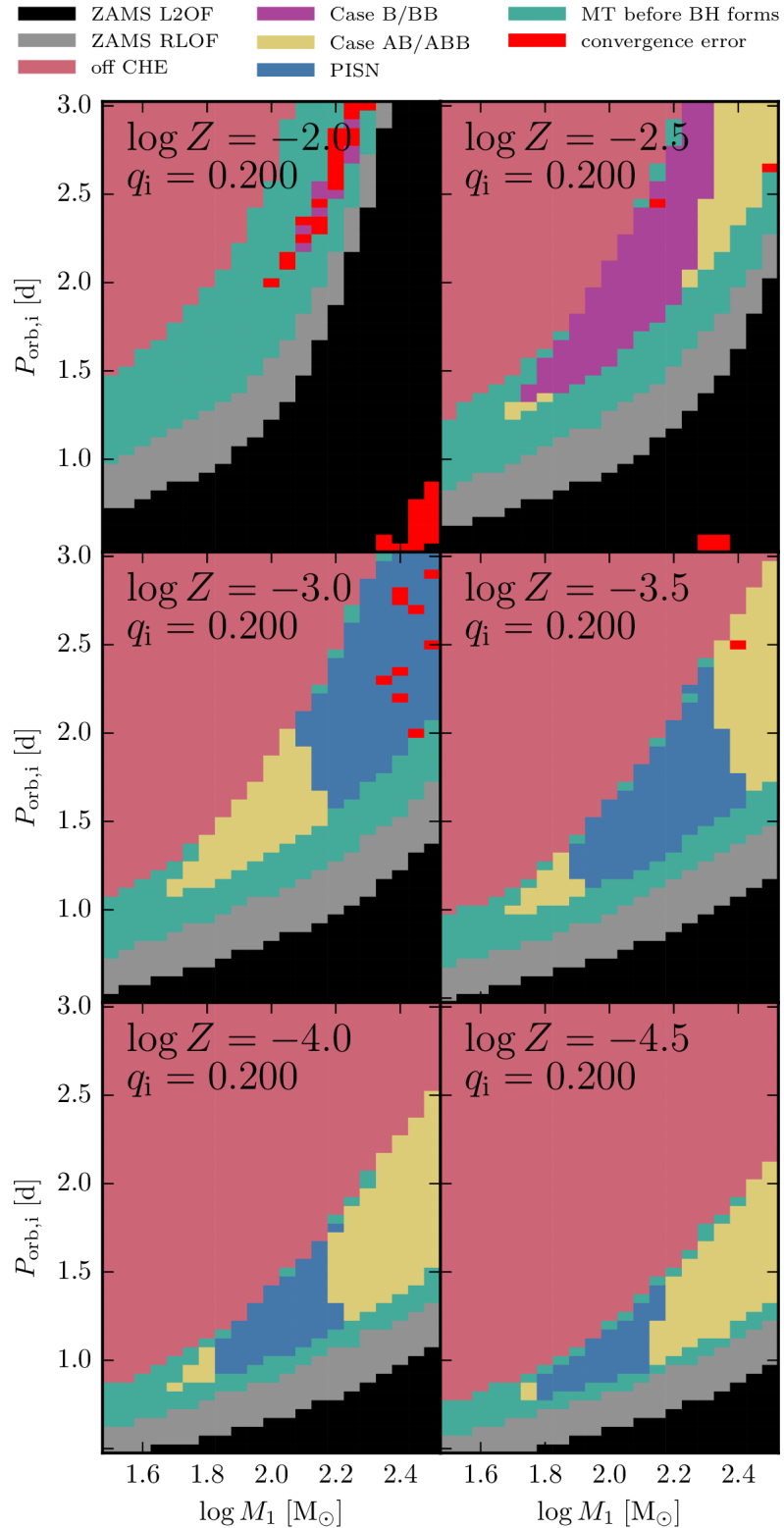


Figure 4.5: Outcome of simulations for different metallicities and a fixed mass ratio  $q$ . Systems marked as Case B/BB or Case AB/ABB have primaries that evolve chemically homogeneously and form BHs, to which the secondary then transfers mass resulting in a ULX. Systems marked in blue have primaries that evolve chemically homogeneously but have final masses resulting in PISNe. All other systems interact before the formation of a BH and would not form a ULX. See Appendix C for the outcome of all simulations, and a detailed description of all outcomes.

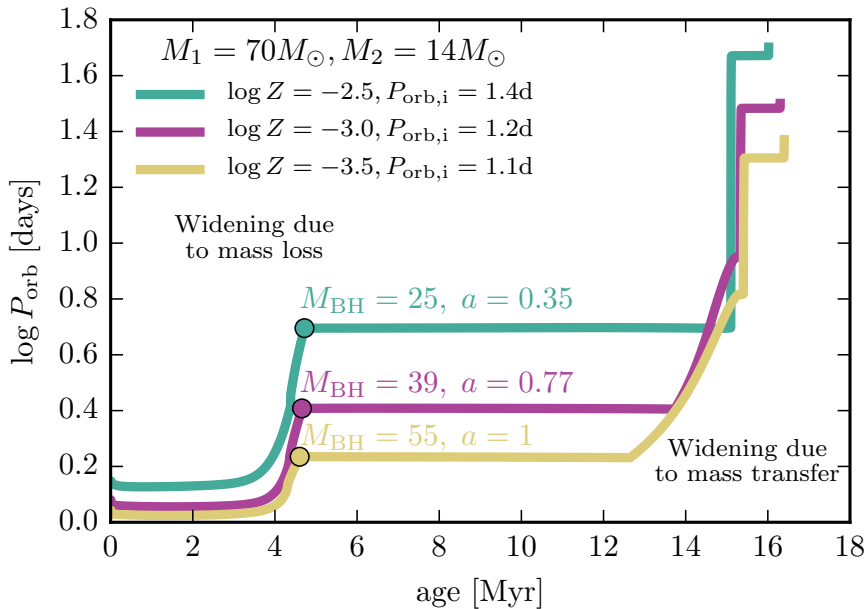


Figure 4.6: Orbital separation as a function of time for three different systems with the same initial component masses and different metallicities. The initial periods correspond to the shortest one in our simulations for which a system with those component masses and metallicity evolves chemically homogeneously and undergoes a ULX phase. Circles mark the moment of BH formation, and the initial mass and spin of the BH are shown.

Case A systems are well above  $10^{39}$  erg s $^{-1}$  even when strictly limited to the Eddington rate. During Case A, mass-transfer rates are not much higher than the Eddington rate, which means that even if the Eddington limit is ignored, luminosities can only increase by a factor of  $\sim 5$ . The situation is different during Case AB/B and ABB/BB mass transfer, where mass-transfer rates can go many orders of magnitude above  $\dot{M}_{\text{Edd}}$ , resulting in potential luminosities going above  $10^{42}$  erg s $^{-1}$ , which is the range for HLXs. However, achieving these luminosities requires a complete disregard of the Eddington limit, and even then, the short lifetimes involved would likely make these sources very rare. Note that, with mass accretion limited to the Eddington rate, the BHs modeled have only modest increases in their total masses and spins. The small increase in  $\dot{M}_{\text{Edd}}$  that can be observed during Case AB/B mass transfer in Figure 4.7 is only due to a decrease in the opacity of accreted material, as helium rich layers from the secondary are exposed.

### 4.3 Luminosity distribution function of ULXs

To estimate the expected properties of observed ULX samples at a fixed metallicity, we need to assume certain distribution functions describing the population of binaries at zero age. We follow the choices made by Marchant et al. (2016), which consider a Salpeter distribution for primary masses ( $dN/dM_1 \propto M_1^{-2.35}$ ), a flat distribution in  $\log P_{\text{orb}}$  ranging from 0.5 days to a year, a flat distribution in mass ratio from zero to unity, and a binary fraction  $f_b = 2/3$ . If we assume the threshold mass for SNe is  $8M_{\odot}$ , and that the SN rate is  $10^{-2}$  yr $^{-1}$  for a star-formation rate (SFR) of  $1M_{\odot}$  yr $^{-1}$ , we can then compute expected distributions of luminosities per  $M_{\odot}$  yr $^{-1}$  of SFR. This choice for the rate of SNe per  $M_{\odot}$  yr $^{-1}$  of SFR is consistent

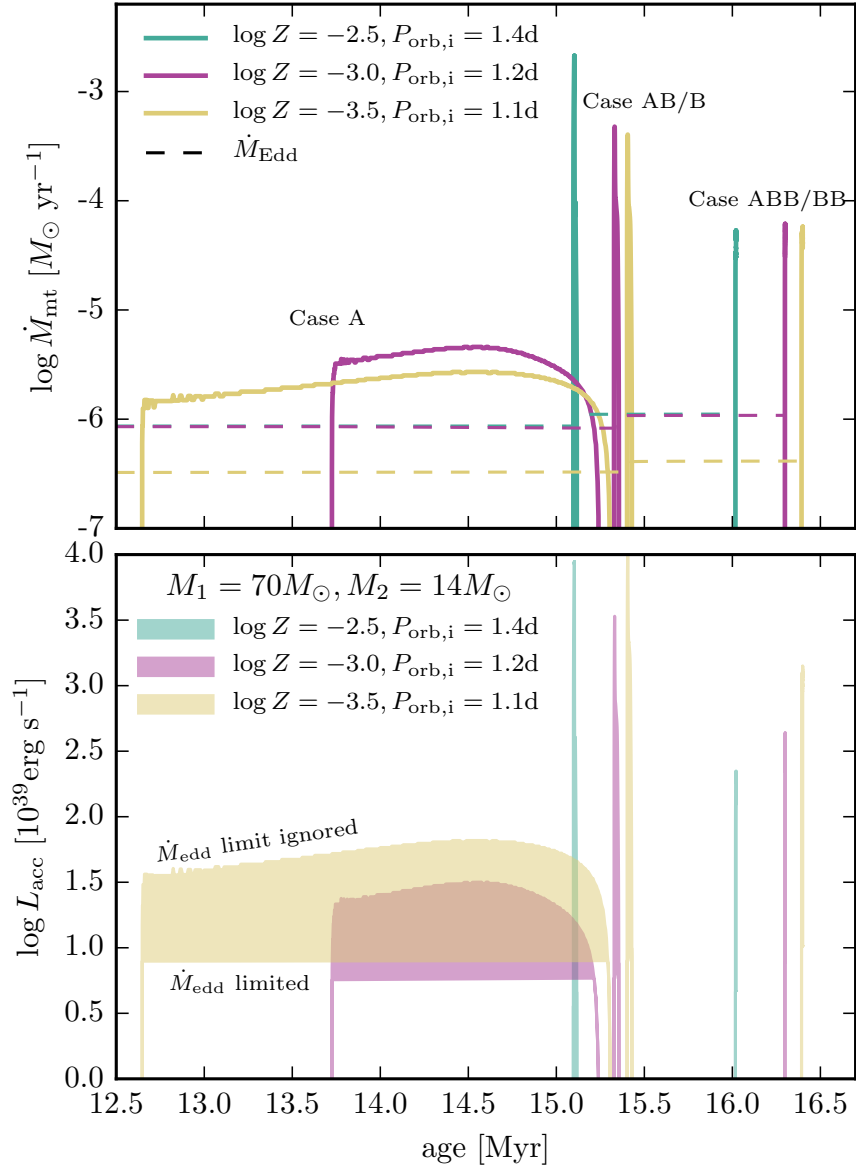


Figure 4.7: Mass-transfer rates and accretion luminosities during mass-transfer phases for the three systems shown in Figure 4.6. Accretion luminosities are shown as ranges going from the lower values given by strictly Eddington limited accretion rates, to the potential luminosities that could be achieved if the Eddington limit is ignored. Note that the Eddington accretion rates for the metallicities  $\log Z = -2.5$  and  $-3$  overlap. This is due to the lower BH spin at  $\log Z = -2.5$  compensating for the higher BH mass at  $\log Z = -3$ .

with Milky Way values (Diehl et al., 2006; Robitaille and Whitney, 2010). Note that the distributions we obtain depend linearly on this assumed ratio between the supernova rate and the SFR, which is uncertain to at least a factor of 2.

Our predicted luminosity distribution function and cumulative distribution function are shown in Figure 4.8. To consider possible uncertainties on the efficiency of mass transfer, we also include the distribution of luminosities if accretion rates of three times the Eddington rate would be possible. This is not done by running a full set of simulations with an adjusted Eddington limit, but rather by considering the potential luminosities of our models which are strictly limited to accrete at  $\dot{M}_{\text{Edd}}$ . For our models we consider the full bolometric accretion luminosity  $L_{\text{acc}}$ , although a fraction of this would not be emitted in the bands detectable by X-ray observatories.

To compare with observations, we also include the empirical distribution described by Grimm, M. Gilfanov and Sunyaev, 2003 for nearby (within 35 Mpc) late-type starburst galaxies, described by a power law with a slope of  $\sim -1.6$ , and a cutoff at a luminosity of  $2 \times 10^{40} \text{ erg s}^{-1}$ . Grimm, M. Gilfanov and Sunyaev (2003) and M. Gilfanov, Grimm and Sunyaev (2004) argue that the presence of such a cutoff is indicative of a maximum possible mass for stellar BHs. We also include the 117 ULXs described by Swartz et al. (2011), which represent complete samples of ULXs for local galaxies of diverse types within 14.5 Mpc. Swartz et al. (2011) consider two different methods to compute the luminosity of ULXs, one obtained from photon counts, and the other, for sources with  $> 130$  counts detected, from spectral modelling. Although the luminosities from Grimm, M. Gilfanov and Sunyaev (2003) correspond to the 2 – 10 keV band, while the photon counts from Swartz et al. (2011) are corrected to give the luminosities in the 0.3 – 10 keV range, the two samples agree well with each other. The galaxies considered by Grimm, M. Gilfanov and Sunyaev (2003) and Swartz et al. (2011) should be indicative of the formation of ULXs in the local environment of our Galaxy, and favor high metallicities. Moreover, as they do not properly sample dwarf galaxies, we expect an additional bias towards higher metallicities.

The CHE channel is expected to produce the most massive BHs possible for a given metallicity, as it transforms almost the whole star into a large helium core. Since large initial masses are required to have efficient rotational mixing, this results in the least massive BH possible at  $\log Z = -2.5$  to have a mass of  $20M_{\odot}$ , already falling into the ULX range when accreting at the Eddington rate. As Figure 4.8 shows, there is a much less luminous tail of objects that arises from brief moments at the beginning and end of mass-transfer phases, when transfer rates are below the Eddington limit. At a metallicity of  $\log Z = -3$  we reach a luminosity cutoff due to the lower limit for PISNe at about  $10^{40} \text{ erg s}^{-1}$ , which, barring possible mass loss from PPISNe, means that accretion rates that are only a factor of a few above Eddington are enough to explain the observed luminosity cutoff with our models. A population of lower mass BHs and NS accretors is still required to explain the lower end of the luminosity function of ULXs, extending to the HMXB regime. Such systems are likely to originate from CE evolution, meaning that the BH accretor results from an envelope stripped star (Podsiadlowski, S. Rappaport and Han, 2003), and thus should have lower masses than those possible through CHE. Although the inclusion of a different channel should in principle produce a break in the distribution function, a similar break that should be visible due to differences between NS and BH accretors is not observed (Grimm, M. Gilfanov and Sunyaev, 2003), and the distribution function for our highest metallicity models is not far off from that of the most luminous objects in the observed sample. It might be possible then that the population of NS and BH accretors resulting from CE evolution coexists with those produced by CHE, and results in a luminosity distribution function that can be described with a single slope.

At lower metallicities this should not be the case; Figure 4.8 shows that a gap in the luminosity function is expected. This is due to the formation of BHs above the limit for PISNe. The gap is not completely deserted, as systems at the beginning or end of mass-transfer phases to those very massive BHs accrete below the Eddington rate, resulting in a wide range of luminosities for a short period of time.

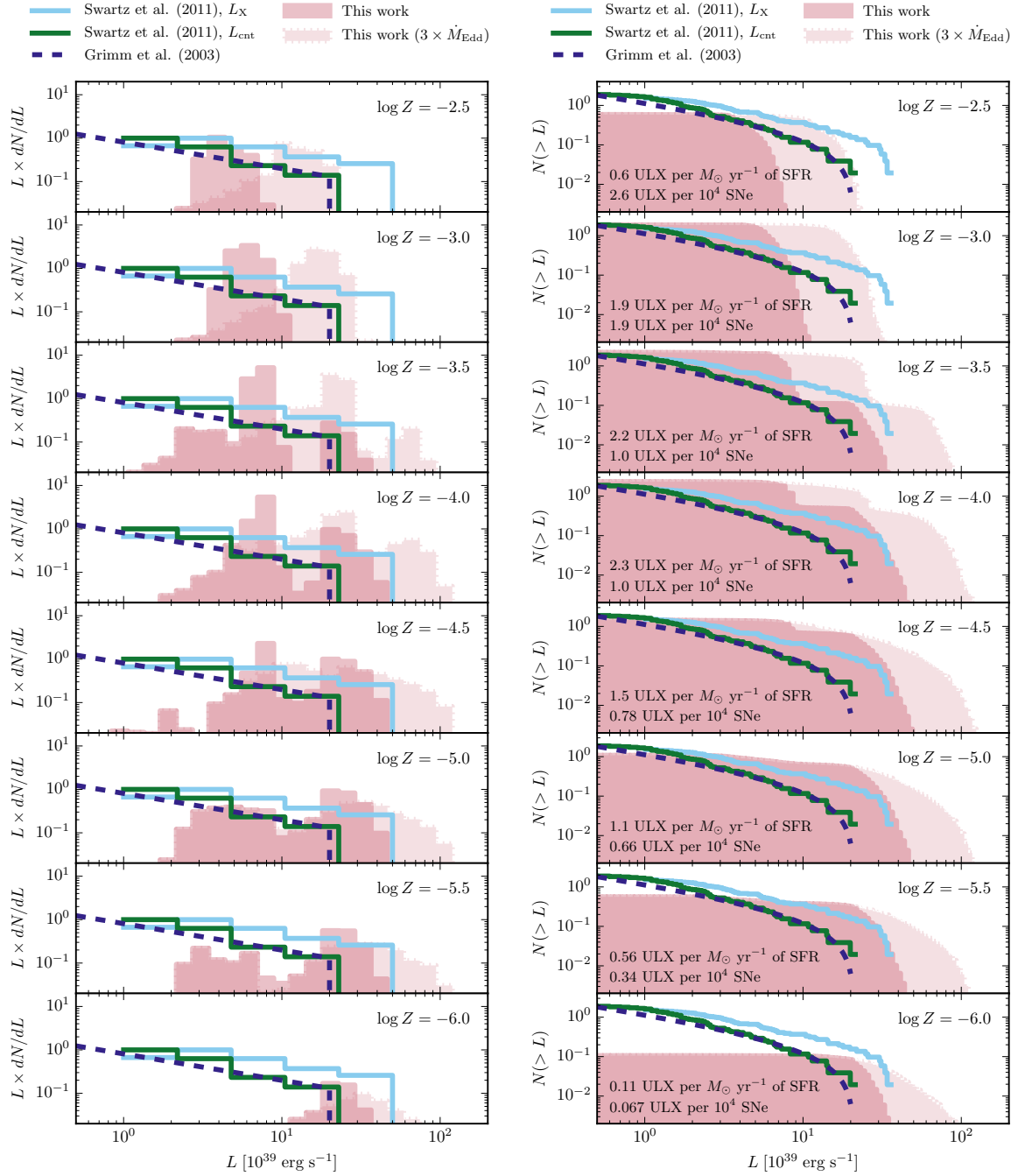


Figure 4.8: (left) Expected luminosity distribution function for ULXs formed through CHE, compared to the empirical distribution with a slope  $\alpha = -1.6$  derived by Grimm, M. Gilfanov and Sunyaev (2003) and the sample of 117 ULXs from nearby galaxies described by Swartz et al. (2011). For the sample of Swartz et al. (2011) we include the distributions considering their estimates on source luminosities from spectral modelling  $L_X$ , and that from number of counts  $L_{\text{cnt}}$ . All distributions are normalized to a star-formation rate of  $1 M_\odot \text{ yr}^{-1}$ . (right) Same figure but for the cumulative distribution function instead. Expected number of observable sources per  $M_\odot \text{ yr}^{-1}$  of SFR are also shown, as well as the expected formation rate of ULXs in terms of the SN rate. Although the number of ULXs produced per SN increases with metallicity, at lower metallicities phases with accretion are longer lived resulting in a peak in observable sources per  $M_\odot \text{ yr}^{-1}$  of SFR at  $\log Z = -4$ .

This gap in the distribution results in a clear feature in the cumulative distribution, as shown in Figure 4.8. Observations in the local universe would favor the observation of galaxies at the upper end of the metallicities modelled, but deeper observations sampling lower metallicity environments should show a significant digression from a population describable by a single power law.

In terms of observable sources, the CHE channel has a strong dependence with metallicity, with almost no sources being produced at metallicities  $Z \geq 0.01$ , and rising to a peak of 2.3 ULXs per  $M_{\odot} \text{ yr}^{-1}$  of SFR at a metallicity of  $\log Z = -4$ , though the rate is mostly flat in the range  $-4.5 < \log Z < -3$ . In a slightly counterintuitive way, at metallicities below  $\log Z = -2.5$  the number of ULXs formed per SNe monotonically decreases with metallicity, but it has to be taken into account, as described in Section 4.2.2, that due to orbital widening from wind mass loss, mass-transfer phases have shorter lifetimes at higher metallicities. This compensates for the smaller number of sources produced per SNe at lower metallicities, resulting in the local maximum of observable sources at  $\log Z = -4$ . Anyhow, with just a couple of systems formed every  $10^4$  SNe, it is clear that this evolution channel is only followed by a small fraction of massive stars. Although there are important uncertainties in our calculations, in particular in the choice of initial distribution functions at low metallicities, this systematic behaviour with metallicity should be a generic feature, despite uncertainties of at least a few in the rates we predict.

### 4.3.1 Luminosity distribution at redshift $z = 0$

It is tempting to relate the predicted rate of  $\sim 2$  ULXs per  $M_{\odot} \text{ yr}^{-1}$  of SFR with the equivalent observed number of sources by Swartz et al. (2011), but we need also consider the contribution from the tail of the normal HMXB population that reaches up to ULX luminosities. More importantly, both the Swartz et al. (2011) and Grimm, M. Gilfanov and Sunyaev (2003) sources sample the local universe. If we consider the metallicity distribution of Langer and C. A. Norman (2006) evaluated at a redshift  $z = 0$ , we would only expect  $\sim 1\%$  of the star-formation in the local universe to happen at a metallicity below  $\log Z = -3$ . We use this distribution to evaluate the local luminosity distribution function of ULXs formed through CHE, which we show in Figure 4.9. The metallicity weighting significantly reduces the number of expected sources to 0.13 ULXs per  $M_{\odot} \text{ yr}^{-1}$  of SFR, but if we consider mass accretion at three times the Eddington rate, the distribution we predict nicely matches that of the brightest sources of Grimm, M. Gilfanov and Sunyaev (2003) and of Swartz et al. (2011) estimated by photon counts. For the majority of ULXs which have lower luminosities, a different formation channel would be required. The luminosities estimated by Swartz et al. (2011) through spectral modeling should better represent the total luminosity of the source, which is what we consider for our models. However, if accretion rates ten times larger than Eddington are allowed to try to match these higher luminosities, Figure 4.9 shows that the gap produced by PISNe is lost. Instead, the presence of a gap in BH masses would result in a steeper drop of the luminosity distribution function, rather than a sharp cutoff. If the increased luminosity is due to a relatively constant beaming factor rather than accretion above the Eddington rate, then the luminosity gap would remain. In any case, the spectrum of BHs  $< 60M_{\odot}$  and  $> 130M_{\odot}$  radiating at the same luminosity should differ significantly.

Locally, ULXs with BH masses  $> 130M_{\odot}$  would only represent a small fraction of the total formed through CHE, around  $\sim 0.5\%$ . Moreover, since ULXs formed through this channel only represent the high-luminosity tail of the luminosity distribution function, they correspond to an even smaller fraction of the total. The upcoming *eROSITA* X-ray observatory will perform a full-sky survey, which at a sensitivity limit of around  $2 \times 10^{-14} \text{ erg s}^{-1} \text{ cm}^{-2}$  should detect sources with luminosities of  $10^{40} \text{ erg s}^{-1}$  up to a distance of 35 Mpc. Considering the distribution of known sources, around  $\sim 100$  ULXs should be detected (Prokopenko and M. R. Gilfanov, 2009), so that finding BHs above the PISN gap would appear unlikely. However, as shown in Figure 4.9, if BHs above the PISN gap can accrete at rates above a few

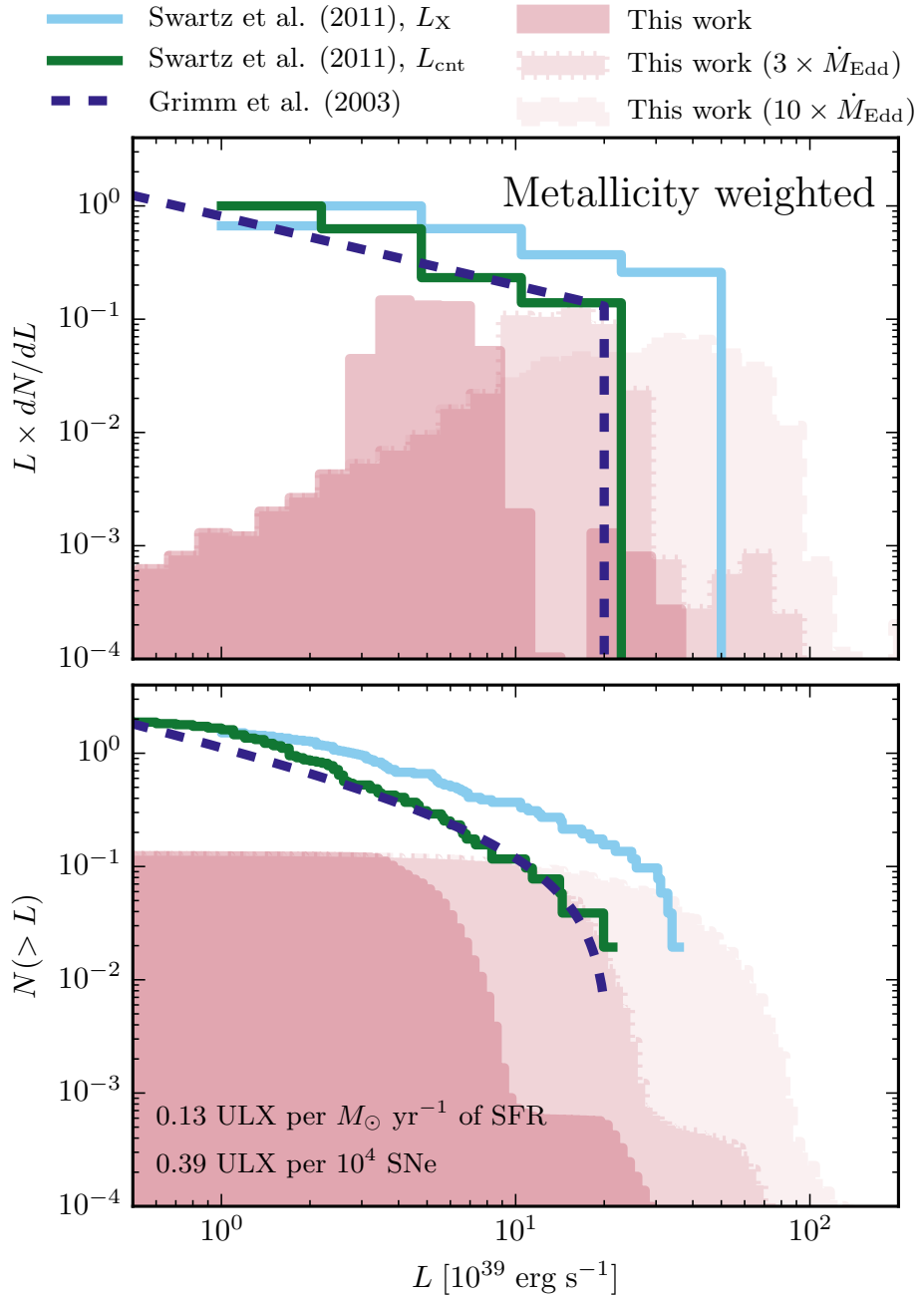


Figure 4.9: Same as Figure 4.8, but weighting our models according to the metallicity distribution of Langer and C. A. Norman (2006) at redshift  $z = 0$ .

times  $\dot{M}_{\text{Edd}}$  their luminosities would approach  $10^{41}$  erg s $^{-1}$ , with significantly larger detection volumes (for sources three times more luminous than the cutoff luminosity the detection volume would be  $\sim 5$  times larger). *eROSITA* could then potentially detect a few of these sources, likely in metal-poor dwarf galaxies. On a longer timescale, the *Athena* X-ray observatory will be capable of probing much deeper, and targeted observations to dwarf galaxies with very low metallicities and high SFRs could test the existence of these objects.

### 4.3.2 Galactic $L_{\text{X}}$ – SFR relation at low metallicities

As we predict the luminosity distribution of X-ray sources to change significantly at low metallicities, we also expect the relation between the total X-ray luminosity of a galaxy  $L_{\text{X}}$  and its SFR to be different than that in our local environment. Locally, the X-ray luminosity of a galaxy serves as a probe of its SFR (Grimm, M. Gilfanov and Sunyaev, 2003; M. Gilfanov, Grimm and Sunyaev, 2004), and the presence of a luminosity cutoff results in a linear  $L_{\text{X}}$  – SFR relationship for high enough SFR. M. Gilfanov, Grimm and Sunyaev (2004) argue that a population of IMBHs would result in a break from the linear relationship at very high SFR. As BHs formed above the limit for PISNe also form a distinct population of very massive BHs, they could as well result in differences in the dependence of  $L_{\text{X}}$  with SFR. Moreover, if the  $L_{\text{X}}$  – SFR relationship changes significantly at lower metallicities, that means it needs to be recalibrated to serve as a probe of star-formation.

To assess the  $L_{\text{X}}$  – SFR relationship, using our ULX models we construct multiple synthetic galaxies for different SFRs, for which we show the distribution of X-ray luminosities in Figure 4.10. For galaxies with low star-formation rates, that on average should have less than one ULX produced through CHE, low-number statistics plays an important role, and this effect can clearly be seen at SFRs less than  $1 M_{\odot} \text{ yr}^{-1}$ . Unlike the relationship observed by Grimm, M. Gilfanov and Sunyaev (2003), Figure 4.10 shows a very steep increase in luminosity at low SFRs, but this is just because our models do not include the contribution from HMXBs. Instead, the luminosities jump from zero to above  $10^{39}$  erg s $^{-1}$  for galaxies that happen to have a single ULX. Although we cannot properly assess the relationship at very low SFRs, the switch from a non-linear to a linear relationship depends on the sampling of the most luminous sources possible, and we expect ULXs formed through CHE to be the source of these. The SFR at which Grimm, M. Gilfanov and Sunyaev (2003) observe a break in the X-ray luminosity distribution of galaxies would then be equivalent to the SFR at which most galaxies would sample a few of the ULXs produced through CHE.

Figure 4.10 shows that the SFR at which the relationship becomes linear, as well as the expected luminosities at high SFR, has an important dependence on metallicity. This results both from the increased number of sources expected per  $M_{\odot} \text{ yr}^{-1}$  of SFR at lower metallicities, and the formation of BHs above the PISNe gap which can produce much higher luminosities. Table 4.1 shows the ratio of  $L_{\text{X}}$  to SFR that we expect in the linear regime at different metallicities. This value can vary up to an order of magnitude, which should be taken into account when using  $L_{\text{X}}$  as a measure of SFR. The presence of BHs above the PISNe gap does produce changes in the  $L_{\text{X}}$  – SFR relationship, but this happens in the low-SFR regime, likely making it hard to observe.

## 4.4 Orbital parameters of ULXs formed through CHE

An additional tool to discriminate between different formation scenarios is the detection of optical counterparts to ULXs, which can help identify the nature of the donor star. Different evolution channels can result in different distributions for component masses and orbital periods, which are poorly constrained

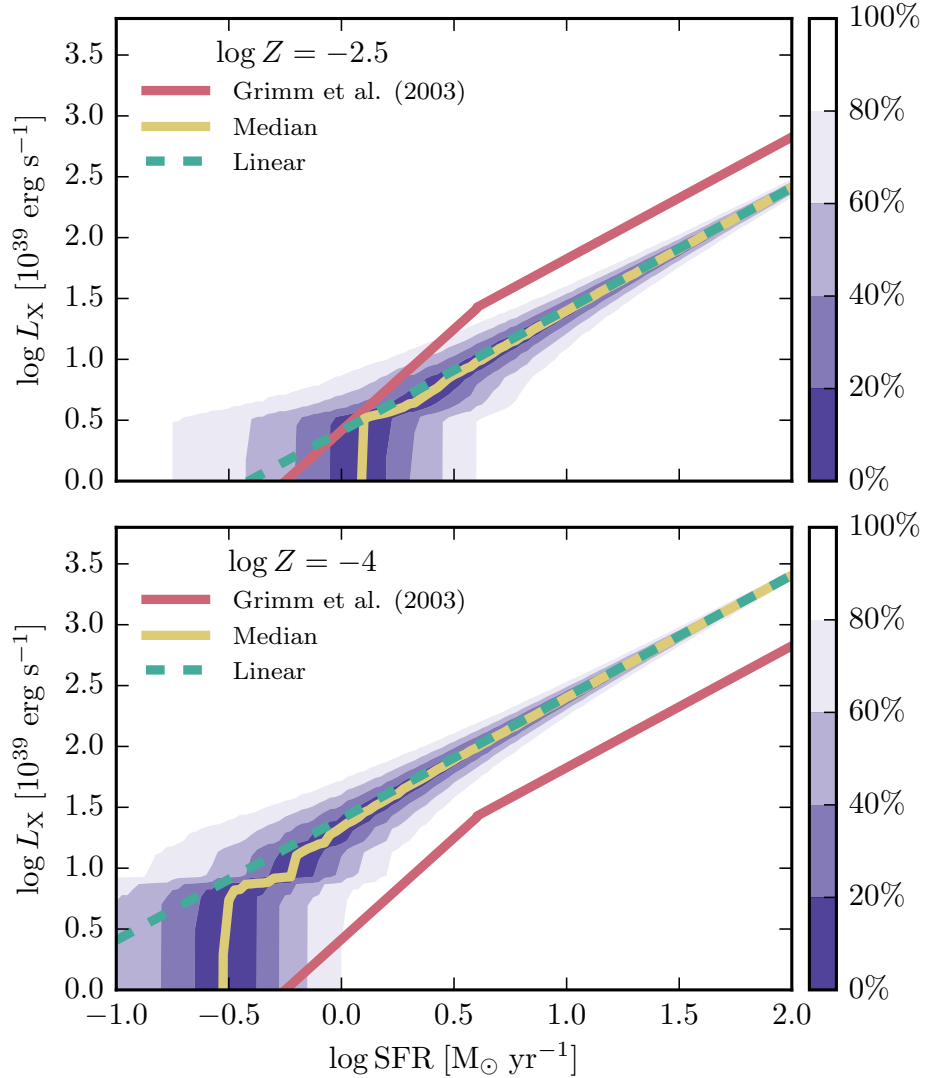


Figure 4.10: Galactic  $L_X$  – SFR relationship arising from ULXs produced through CHE at two different metallicities, compared to the predicted relationship from Grimm, M. Gilfanov and Sunyaev (2003) for the luminosity in the 2 – 10 keV band. Systems at  $\log Z = -4$  can also produce BHs above the pair instability gap, resulting in the slightly different structure at low SFR. For simplicity we assume all the luminosity from accretion is emitted as X-rays. For different values of the SFR modelled we constructed 10000 synthetic galaxies, and the color plot indicates the fraction of galaxies contained around the median (i.e., the 20% region is bounded by the fourth and sixth deciles).

$\log Z$	$n_{\text{ULX}}/\text{SFR} [M_{\odot}^{-1} \text{ yr}]$	$n_{\text{ULX}}/(10^4 \times \text{SNe})$	$L_{\text{X}}/\text{SFR} [10^{39} \text{ erg s}^{-1} M_{\odot}^{-1} \text{ yr}]$
-2.5	0.6 (0.6, 0)	2.6 (2.6, 0)	2.6
-3.0	1.9 (1.9, 0)	1.9 (1.9, 0)	11
-3.5	2.2 (2.1, 0.12)	0.98 (0.71, 0.26)	17
-4.0	2.3 (1.8, 0.51)	1.0 (0.44, 0.58)	26
-4.5	1.5 (0.77, 0.7)	0.78 (0.18, 0.61)	22
-5.0	1.1 (0.45, 0.64)	0.66 (0.13, 0.53)	17
-5.5	0.56 (0.18, 0.39)	0.34 (0.044, 0.29)	9.9
-6.0	0.11 (0, 0.11)	0.067 (0, 0.067)	2.3
local	0.13 (0.13, 0.00062)	0.39 (0.39, 0.0011)	

Table 4.1: General properties of ULXs formed through CHE at different metallicities. Shown here are the expected number of observable ULXs per  $M_{\odot} \text{ yr}^{-1}$  of SFR, the number of produced ULXs per SN, and the expected total X-ray luminosity of galaxies per  $M_{\odot} \text{ yr}^{-1}$  of SFR. In parenthesis we indicate separately the number of objects with BHs below the pair-instability gap ( $M_{\text{BH}} < 60M_{\odot}$ ) and above it ( $M_{\text{BH}} > 130M_{\odot}$ ). The last column is computed under the assumption that the bolometric luminosity from accreting sources is released as X-rays, and that accretion is strictly limited to the Eddington rate. Local rates are estimated using the metallicity distribution of Langer and C. A. Norman (2006) at redshift  $z = 0$ . A value for the locally weighted galactic  $L_{\text{X}}$  is ignored, as the local environment contains many galaxies at higher metallicities where the total luminosity would be dominated by HMXBs instead of the ULXs described in this work. Values given in terms of SFR are computed assuming a SN rate of  $0.01 \text{ yr}^{-1}$  per  $1M_{\odot} \text{ yr}^{-1}$  SFR.

if only X-ray data is available. The largest sample of counterparts to date is given by Gladstone et al. (2013), who study 33 ULXs observed with the Hubble Space Telescope. Out of this sample, no counterparts are found for 9 sources, while two are excluded as they are close to the galactic nucleus, leaving 22 sources in total (some with more than one possible counterpart detected). As the number of detections increases, and more measurements of radial velocity variations are available, strict constraints will be made on the progenitors of ULXs.

It is beyond the scope of this paper to study in detail the optical properties of our ULX models, which need modeling of the emission from the accretion disk, but we can check the distribution of donor and BH masses, together with orbital periods, as is done in Figure 4.11. The bulk (71%) of ULX models formed through CHE should contain main-sequence (MS) hydrogen rich ( $X_s > Y_s$ ) donors in the range  $\sim 8M_{\odot} - 30M_{\odot}$  with orbital periods below 20 days. More massive MS donors in the range  $30M_{\odot} - 70M_{\odot}$  are only a 16% of the total, with 3% being hydrogen poor ( $X_s < Y_s$ ). Although less numerous, these massive optical counterparts should be much easier to detect. Case AB/B systems correspond to only 6% of the total, have typical masses below  $10M_{\odot}$ , and typical periods above 10 days. As has already been mentioned, the predominance of Case A sources is owed to these systems undergoing mass transfer on a nuclear timescale, while mass transfer for post-MS donors operates on a much shorter thermal timescale.

A clear distinction with CE evolution is given by the mass ratio distribution. For the CE channel, the primary which will form the BH expands and initiates the CE phase, and for very low secondary masses, a merger is expected rather than envelope ejection (see, e.g. Kruckow et al., 2016). If the system survives the CE phase, after the BH is formed and the secondary initiates mass transfer, the mass ratio plays an important role in the lifetime of that phase (Podsiadlowski, S. Rappaport and Han, 2003). If the donor is more massive than the BH, mass transfer typically results in a reduction of the orbital separation leading to a short-lived thermal-timescale mass transfer, similar to the situation for intermediate-mass X-ray binaries (Tauris, van den Heuvel and Savonije, 2000). If instead the donor is less massive than the BH at

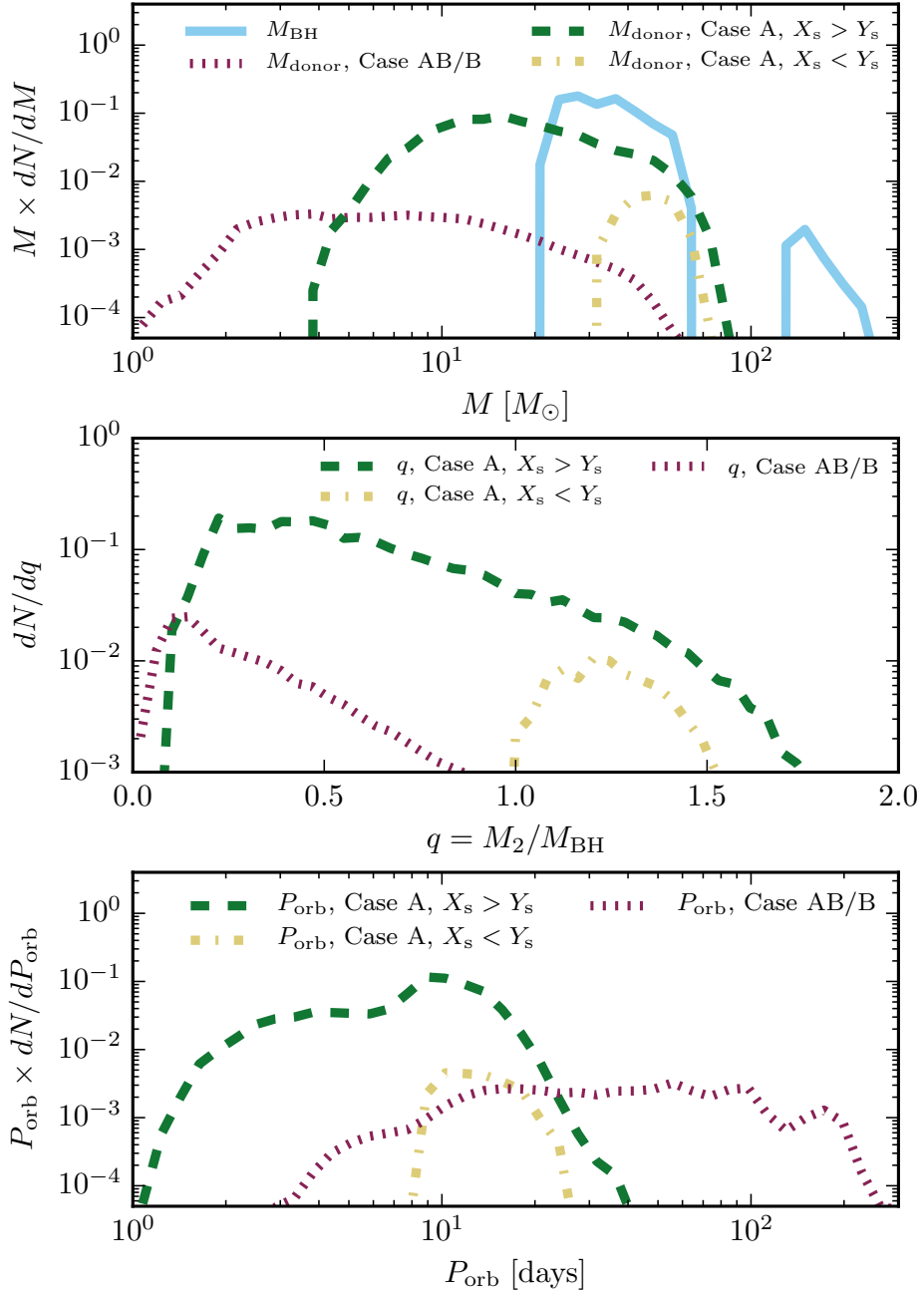


Figure 4.11: (top) Distribution of BH and donor masses in ULX systems, weighting our models to the metallicity distribution of Langer and C. A. Norman (2006) at redshift  $z = 0$ . (bottom) Distribution of orbital periods using the same metallicity distribution. Donor masses and orbital periods are separated between Case A and Case B systems, and furthermore, Case A systems are separated between donors that are hydrogen poor or hydrogen rich at their surfaces.

the onset of mass transfer, the orbital separation widens as a result of mass transfer, leading to a much longer-lived nuclear-timescale phase if the donor is a MS star. As a consequence, the distribution of mass ratios predicted from CE evolution favors mass ratios below, but not far, from unity (Madhusudhan, S. Rappaport et al., 2008).

The mass ratio distribution for ULXs produced through CHE at redshift  $z = 0$  is shown in the second panel of Figure 4.11. Although the initial mass ratio of these systems is smaller than  $q = 0.5$ , mass loss on the primary before BH formation can lead to mass ratios above unity during the ULX phase, but these are disfavored for the same reason discussed above for the CE channel. Nevertheless, the distribution clearly favors mass ratios significantly below unity, with  $\sim 50\%$  of the sources having  $q < 0.5$ . This preference for lower mass ratios is stronger at lower metallicites, as the primary undergoes a smaller amount of mass loss before forming a BH.

In the case of ULXs formed via dynamical capture in clusters, much higher BH than donor masses are also expected, but the orbital periods of these systems are well above 20 days (Mapelli and Zampieri, 2014), which differentiates them from the bulk of systems produced through CHE. The long orbital periods imply that such systems would have post-MS donors with short lifetimes as active sources, which reduces the likelihood of observing them.

The models of Madhusudhan, S. Rappaport et al. (2008) have an upper limit of  $25M_{\odot}$  for the BH mass, which makes it difficult to explain some of the brightest optical counterparts observed that would require  $\sim 50M_{\odot}$  donors, so they favor IMBHs as the compact object in these sources. This could be avoided if CE could produce higher mass BHs, but even at low metallicities it is difficult to reach BH masses well above  $30M_{\odot}$ , as envelope stripping significantly reduces the mass of the primary (Linden et al., 2010). ULXs formed through CHE can reach BH masses up to the lower end of the PISN gap ( $60M_{\odot}$ ), and even if PPISNe would reduce this to  $\sim 47M_{\odot}$  (Woosley, 2016), this easily allows for stable (and long-lived) RLOF from very massive donors. For BHs formed above the PISN gap donor masses can be much higher, but at least in the local universe ULXs with these very massive BHs should be uncommon (Section 4.3.1).

For reference purposes, the distribution of several properties of our ULX systems at different metallicities is provided in Appendix D.

## 4.5 NS-BH and BH-BH binaries after a ULX phase

After a ULX phase, the orbit widens significantly due to mass transfer, with final orbital periods well in excess of 10 days. Unless the secondary receives a strong kick in a favorable direction, reducing its orbital period and making the system very eccentric, a merger due to GW emission would not happen. As an example, a binary with a  $60M_{\odot}$  BH and a  $1.4M_{\odot}$  NS at a 10 day orbital period would take more than 1000 Gyrs to merge. Instead, the same system with an eccentricity  $e = 0.9$  would merge in only 3.5 Gyrs. This requires fine-tuning both the kick velocity and its direction, making it an unlikely outcome which we study in this section.

For the donor star, the ULX phase results in its hydrogen envelope being stripped, and its final mass plays a large role in determining whether it will evolve to become a NS or a BH, and whether the binary system is disrupted or not. For single stars there may not be a well defined threshold in the ZAMS mass below which NSs are formed, and above which the star collapses to a BH. Instead, detailed models predict so-called “islands of explodability”, where a range of initial masses results in NSs and SNe explosions, but with lower and upper boundaries where BHs would be formed instead (Sukhbold et al., 2016). Translating this into a criterion for final core-masses of envelope stripped stars is not straightforward, as the evolution of these differs from that of single stars (Brown, Heger et al., 2001) and is likely metallicity dependant. Nevertheless, to study the final fate of our systems, we assume a simple

threshold for final masses of envelope stripped stars, and to take into account possible uncertainties we vary this threshold between  $8M_{\odot}$  and  $12M_{\odot}$ . This range is chosen considering predictions from some massive star models for which with helium core masses up to  $10M_{\odot}$  are predicted to explode as a SNe and leave a NS (Sukhbold et al., 2016). For stars below the threshold we assume a  $1.4M_{\odot}$  NS is formed, while above it we consider the possibility of forming a BH with 10% of its mass being lost. This could be the case if instead of direct collapse a proto-neutron star is formed first, with a weak explosion that unbinds only a small fraction of the envelope, while the rest falls back (Fryer and Kalogera, 2001).

We consider the effect of a kick on the newly-formed compact object, following a Maxwellian distribution with a 1D root-mean-square (rms)  $\sigma = 265 \text{ km s}^{-1}$  for NSs (Hobbs et al., 2005), while for BHs we assume much weaker kicks with  $\sigma = 26.5 \text{ km s}^{-1}$ . The values chosen for the BHs are purely illustrative, as we will show briefly that we expect almost all systems where the secondary forms a BH to result in a wide orbit where GW radiation is unimportant<sup>3</sup>. In particular, the choice of  $\sigma = 26.5 \text{ km s}^{-1}$  mostly results in larger kicks than the commonly used momentum kick, where the BH kick velocity is assumed to follow the NS kick distribution, scaled by  $1.4M_{\odot}/M_{\text{BH}}$ . The Hobbs et al. (2005) distribution for NS kicks might also be observationally biased towards larger kick velocities, as the proper motions of HMXBs appear to favor smaller kicks (Coleiro and Chaty, 2013). The post-kick orbital period  $P_{\text{orb}}$  and eccentricity  $e$  are computed following Tauris, Fender et al. (1999) with no impulse velocity imparted to the BH formed by the primary.

Figure 4.12 shows the possible post-kick parameters when a NS is formed in a system of metallicity  $\log Z = -3.5$  with initial masses  $M_1 = 70M_{\odot}$ ,  $M_2 = 14M_{\odot}$  and an initial orbital period of 1.1 days (illustrated in Figure 4.4). At core carbon depletion of the secondary it consists of a  $55M_{\odot}$  BH and a  $5.5M_{\odot}$  star with an orbital period of 23 days. If there is no kick imparted on the NS, then the result is a NS-BH binary at a separation of  $P_{\text{orb}} \simeq 27$  days and a small eccentricity of  $e \simeq 0.07$ . Such a system would be too wide for GW radiation to have an important effect, with an expected merger time well in excess of 10000 Gyr. Still, detecting such a system while the NS is active as a pulsar would be very interesting, but considering a typical pulsar lifetime of 50 Myr, even if all ULXs would result in a NS-BH binary the expected number of observable sources would be low. As an upper bound, consider systems at a metallicity  $\log Z = -2.5$ , for which we expect 2.6 ULXs formed for every  $10^4$  SNe. For a galaxy with a SNe rate of  $0.01 \text{ yr}^{-1}$ , this would mean  $\sim 100$  NS-BH binaries with an active pulsar, which accounting for beaming, should result in less than  $\sim 30$  observable pulsars. These would be extragalactic sources, making them hard to observe in radio, and as is shown in Figure 4.12, we would expect an important fraction to be disrupted from SNe kicks. However, the Square Kilometer Array will be capable of detecting pulsars beyond the large Magellanic clouds, and the discovery of a NS-BH binary is one of its key science goals (Kramer, 2004).

If the NS receives a kick of  $\sim 200 - 500 \text{ km s}^{-1}$  in a direction opposite to the orbital velocity, then the orbit can become very eccentric, with a merger time from GW radiation below a Hubble time. At lower kick velocities, despite the direction of the kick, the system cannot be driven to a large eccentricity, while for larger kicks the system would likely be disrupted. The system would circularize before entering the LIGO band, but if it is observed earlier in the eLISA band, it could still retain a detectable eccentricity. As shown by Sesana, 2016, GW150914 would have been detectable by eLISA, and eccentricity measurements for sources at these high frequencies have been proposed as a way to distinguish between different formation scenarios for merging binary-BHs (Nishizawa et al., 2016; Breivik et al., 2016). This could also play a role in understanding the origin of NS-BH mergers.

<sup>3</sup> Note that CHE evolution can result in a large number of detectable binary-BH mergers, but this requires both stars to evolve chemically homogeneously, as was shown by Mandel and de Mink (2016), Marchant et al. (2016) and de Mink and Mandel (2016)

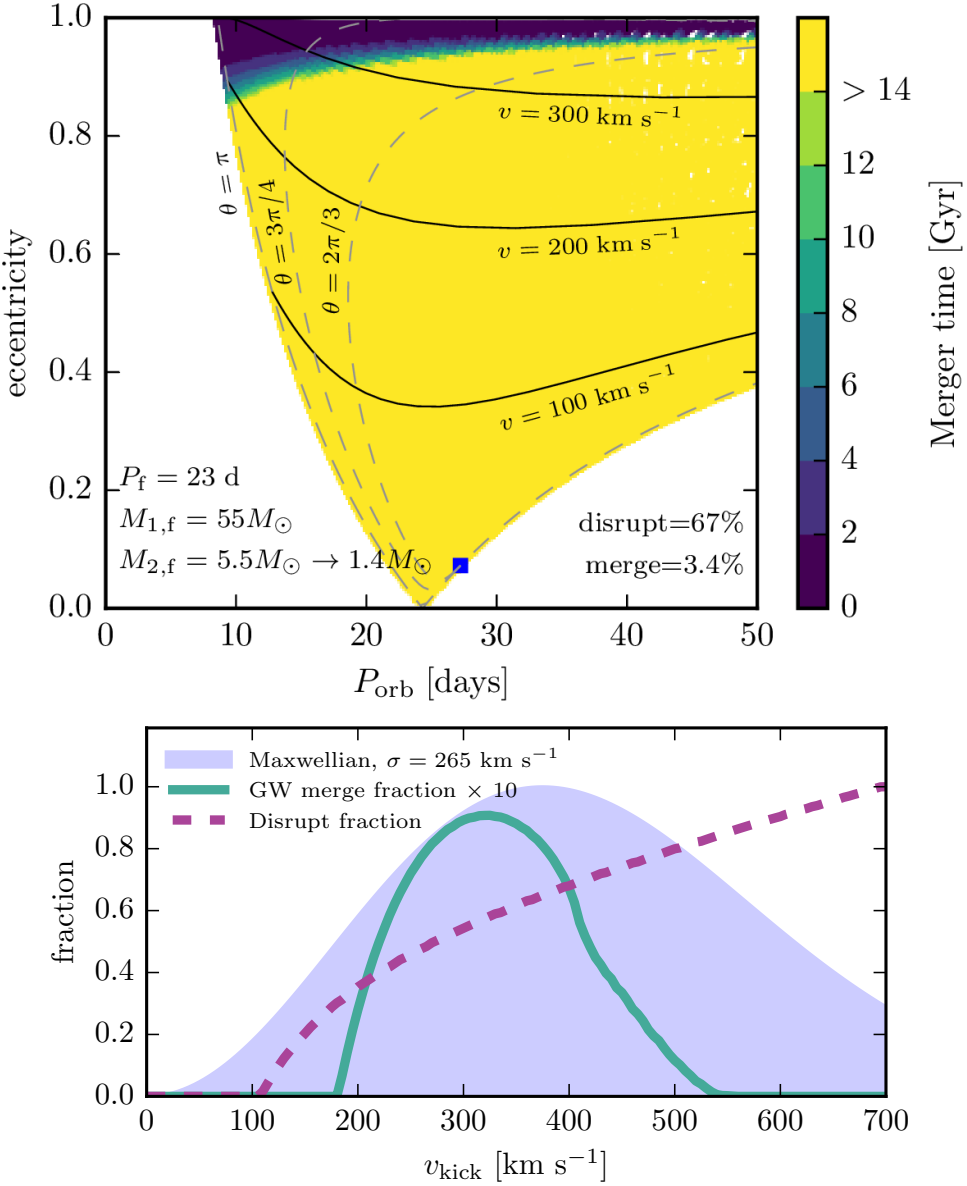


Figure 4.12: (Top) Possible post-kick orbital properties for a NS-BH binary formed from a low-metallicity system ( $\log Z = 10^{-3.5}$ ) that passed through a ULX phase. The period and masses shown correspond to the pre-SN orbital parameters, and the kick distribution is taken to be a Maxwellian with a 1D rms of  $\sigma = 265 \text{ km s}^{-1}$ , and isotropic in space. After the kick, there is a 67% chance that the binary is disrupted, and a 3.4% chance that the resulting system is compact and eccentric enough to merge in a Hubble time. Solid lines indicate final orbital parameters for fixed kick velocity  $v$  and variable angle  $\theta$  formed between the kick velocity and the orbital velocity, assuming the kick to be on the orbital plane. Dashed lines indicate the same, except for a fixed  $\theta$  and a variable  $v$ . The blue square at  $P_{\text{orb}} \approx 27 \text{ days}$  and  $e \approx 0.07$  corresponds to a symmetric SN (i.e. no kick). (Bottom) Fraction of systems that would be disrupted or that would merge in less than a Hubble time for an isotropic fixed kick velocity.

For the system shown in Figure 4.12, there is a 3.4% probability that it would merge in less than a Hubble time, and out of those 44% would have merger times under 1 Gyr. The resulting inspiral would have a mass ratio  $q = 39$ , and a BH with close to maximal spin. The spin and the mass ratio have opposite effects on the possibility of tidally disrupting the star and forming an accretion disk, with larger spins favoring tidal disruption. The simulations of Foucart (2012) show that at high mass ratios and low spins, the NS merges with the BH without being disrupted, producing no accretion disk, and no electromagnetic counterpart. For systems at a mass ratio  $q = 10$  (the largest considered by Foucart, 2012) spin parameters above  $a = 0.8$  are required to produce an accretion disk, but even close to critical rotation, the disk might not be massive enough to power a strong EM signal. Owing to this, for the much higher mass ratios involved in our simulations, we would not expect the production of counterparts to a GW signal even if the BH is close to critical rotation. In the absence of an electromagnetic counterpart, it would be difficult to assess purely from a GW detection if the system contains a NS or if it is a BH-BH binary, since there is a strong degeneracy between mass-ratios and spins in parameter estimation (see, e.g. Hannam et al., 2013).

A case where the secondary would form a BH is depicted in Figure 4.13. This system is the product of a binary with metallicity  $\log Z = -3.5$ , initial masses  $M_1 = 250M_\odot$  and  $M_2 = 63M_\odot$  with an orbital period of  $P_{\text{orb}} = 1.75$  days. The primary in this case forms a BH above the PISNe gap with a mass of  $133M_\odot$ , while the secondary reaches carbon depletion with a final mass of  $36M_\odot$ . Assuming a weak kick is imparted to the BH as described before, the chances of the system being disrupted are essentially zero, with 0.014% of systems merging in less than a Hubble time formed from kick velocities at the tail of the Maxwellian distribution.

#### 4.5.1 Rate estimates for NS-BH and BH-BH mergers

Considering our full sample of ULX models, the different possible outcomes as a function of metallicity are shown in Figure 4.14. These values take into account the same distribution functions for the initial conditions as used in Section 4.3, and also consider possible uncertainties on the mass limit for BH formation by assuming a threshold of either  $8M_\odot$  or  $12M_\odot$  for final masses above which BHs are formed. At all metallicities considered the majority of systems would result in either wide BH-BH binaries or NS-BH systems that are disrupted due to the kick to the NS. The fraction that would result in a bound NS-BH binary is  $\sim 10\%$ , further reducing the chances of detecting such a system with an active pulsar. A similar fraction of systems undergo Case ABB/BB mass transfer driven by shell helium burning before carbon ignition, resulting in layers of hydrogen depleted material being stripped from the secondary. These stars are expected to lose most of their helium envelopes, resulting in stripped CO cores and, owing to the small mass ratio, very wide binaries.

The most interesting possibility is the formation of NS-BH and BH-BH systems compact enough to merge from the emission of GWs in less than a Hubble time. For most of the metallicity range studied,  $\sim 2\%$  of the ULXs would become a NS-BH binary compact enough to merge in a Hubble time, while for BH-BH binaries it is only at metallicities below  $\log Z = -4$  that a non-negligible number of sources could produce a merger. As the BH-BH rate is only relevant at extremely low metallicities and is strongly dependent on the strength of BH kicks which is not well understood, the numbers we provide for BH-BH mergers should be considered speculative. Table 4.2 shows the expected formation rates per SN for NS-BH and BH-BH compact enough to result in a merger, including the values weighted with the metallicity distribution of Langer and C. A. Norman (2006) at redshift  $z = 0$  to represent the local production rate. The expected local formation rate is below one every million SNe for NS-BH mergers and below one every billion for BH-BH mergers, making this a very unlikely outcome of the evolution of massive stars.

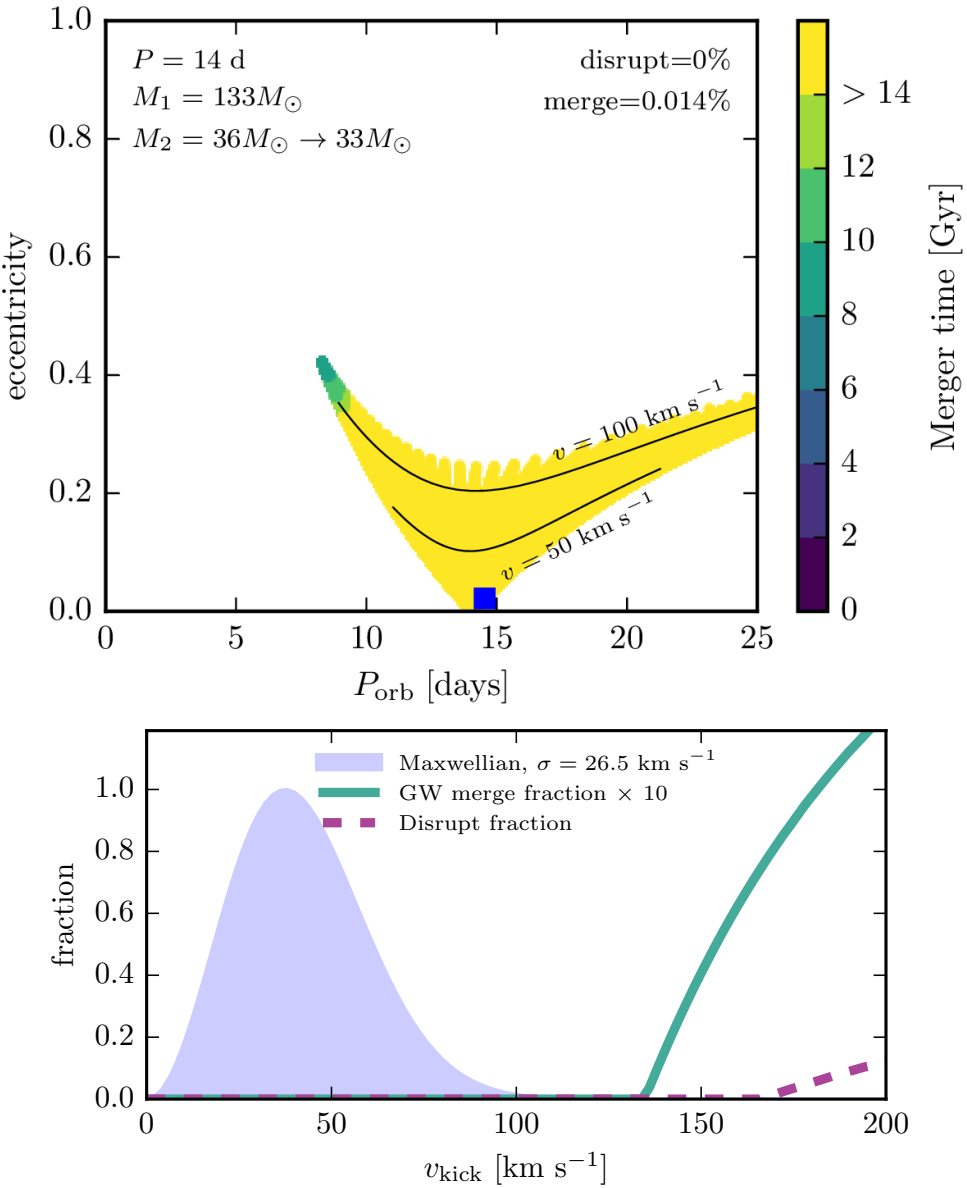


Figure 4.13: Same as Figure 4.12 but for a system where a BH would be expected to form from the secondary. We assume that 10% of the stellar mass is lost during BH formation, and that the BH receives a kick with a 1D rms of  $\sigma = 26.5 \text{ km s}^{-1}$ . Kick velocities up to  $v = 135 \text{ km s}^{-1}$  are considered on the top panel, which corresponds to 99.999% of the Maxwellian distribution.

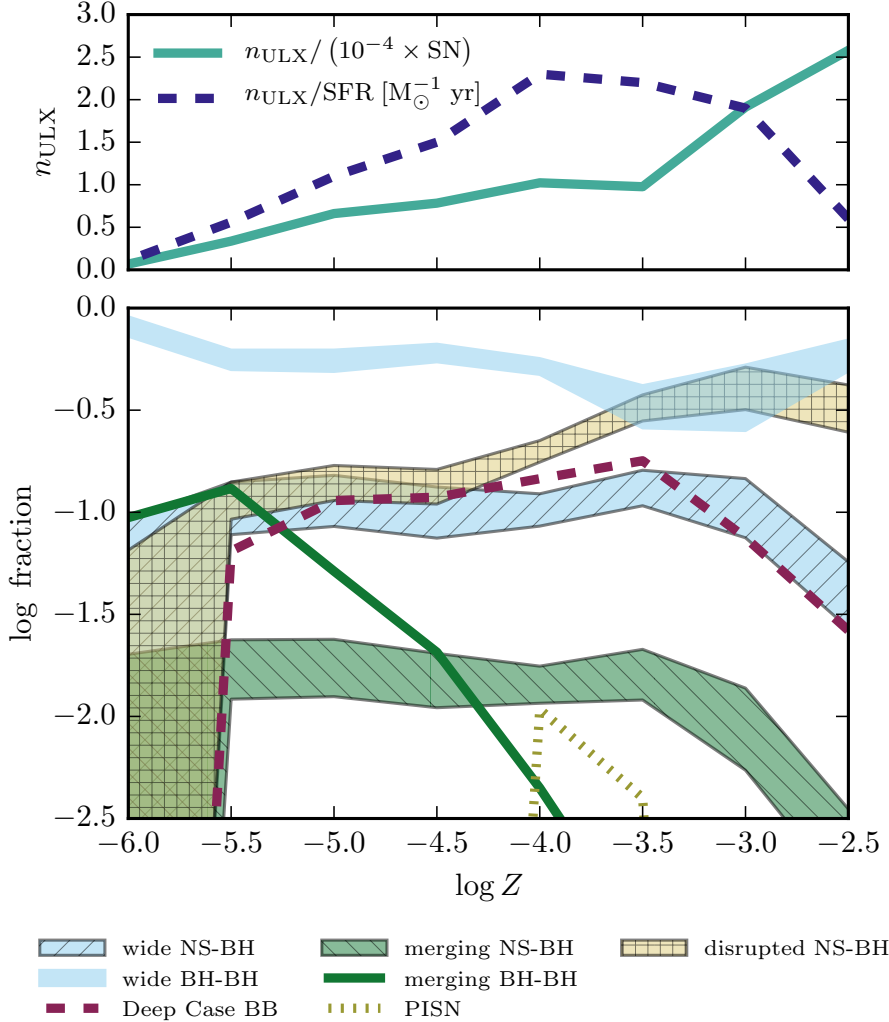


Figure 4.14: (Top) Production rate of ULXs in terms of the SN rate, and number of observable ULXs per  $M_{\odot} \text{ yr}^{-1}$  of SFR. (Bottom) Final outcomes after a ULX phase, represented as the fraction of the total of ULXs. Wide NS-BH and BH-BH systems correspond to binaries for which the merger time from GWs is longer than 13.8 Gyrs, while merging NS-BH and BH-BH systems are compact and/or eccentric enough to merge in less than that. Disrupted NS-BH systems correspond to binaries that were disrupted due to the kick imparted on the NS, while the number of disrupted BH-BH systems is negligible. Systems marked as Deep Case BB widen significantly due to mass transfer stripping hydrogen depleted layers of the donor, and we do not model them until core-carbon depletion. A small fraction of systems marked as PISN have secondaries massive enough to explode as PISNe, leaving only the BH produced by the primary. The values for NS-BH binaries, and for wide BH-BH binaries depend on the choice of threshold mass for BH formation.

$\log Z$	$n_{\text{NS-BH}}/(10^6 \times \text{SNe})$	$n_{\text{BH-BH}}/(10^6 \times \text{SNe})$
-2.5	0.33 – 0.91	0
-3.0	1.0 – 2.6	0
-3.5	1.2 – 2.1	0.076
-4.0	1.2 – 1.9	0.045
-4.5	0.87 – 1.6	0.16
-5.0	0.83 – 1.6	3.4
-5.5	0.41 – 0.80	4.4
-6.0	0 – 0.014	0.63
local	0.069–0.18	0.00029

Table 4.2: Rate of production per SNe of NS-BH and BH-BH systems formed after a ULX phase, which are compact enough to merge in less than a Hubble time. The NS-BH rate depends on the threshold mass at which a NS is formed, and the lower and upper bounds given correspond to assuming that for final core masses above  $8M_\odot$  and  $12M_\odot$  respectively BHs are formed instead of NSs.

To put this in the context of detectability by GW detectors, we can estimate a corresponding volumetric rate for the production of these objects. Taking a volumetric SNe rate of  $1 \times 10^5 \text{ Gpc}^{-3} \text{ yr}^{-1}$  (see, e.g. Madau and Dickinson 2014) and using our upper bound for the local production rate of NS-BH binaries that would result in a merger, gives a very low rate of  $0.018 \text{ Gpc}^{-3} \text{ yr}^{-1}$ , which owing to the large fraction of short delay times these systems would have, is closely tracked by the rate of actual mergers. Even assuming a metallicity of  $\log Z = -3.5$  at which we get the largest formation rate, this would still give a very low upper boundary  $< 0.2 \text{ Gpc}^{-3} \text{ yr}^{-1}$ . These values are comparable to the lower end of the estimates from CE models (Abadie, B. P. Abbott, R. Abbott, Abernathy et al., 2010). At its third science run the LIGO detectors are expected to probe down to rates of  $\sim 50 \text{ Gpc}^{-3} \text{ yr}^{-1}$  (B. P. Abbott et al., 2016b) for the merger of a  $1.4M_\odot$  NS with a  $10M_\odot$  BH, which is well above our estimated rate. It is then uncertain whether even third generation detectors like the Einstein telescope or the Big Bang Observatory would be sensitive to this channel.

## 4.6 Conclusions

In this work we have studied a new formation channel for ULXs. We find ULXs to form from massive very compact binaries with large mass ratios, where only the initially more massive star undergoes tidally induced chemically homogeneous evolution (CHE), and evolves into a massive BH without ever filling its Roche lobe. Thereafter, the less massive component expands and undergoes mass transfer to the more massive BH, often on the nuclear time scale (cf., Fig. 4). We explore this channel by computing large grids of detailed binary evolution models (see Appendix A), which allows us to fully characterize the ensuing ULX population (Appendix B). We summarize our main conclusions as follows:

1. At metallicities below  $Z = 0.01$ , in binaries with initial orbital periods of  $1 \dots 3 \text{ d}$  and mass ratios of  $q \simeq 0.1 – 0.4$ , primaries more massive than  $45M_\odot$  may undergo CHE to form BHs of  $20M_\odot$  or more. The secondary in these systems then expands and starts mass transfer to the BH. Assuming Eddington-limited accretion leads to mega-year long phases with X-ray luminosities in excess of  $10^{40} \text{ erg/s}$  for many cases. This evolutionary path is expected to result in the most massive accreting stellar BHs possible at a given metallicity.

2. The occurrence of PISNe, which leave no compact remnant, leads to a gap in BH masses in the range  $\sim 60M_{\odot} - 130M_{\odot}$ . At metallicities higher than  $\log Z = -3$  no BHs above the gap are expected, resulting in a cutoff in BH masses that might be observed as a cutoff in ULX luminosities. At lower metallicities, very massive stars are expected to form BHs above the PISN gap, potentially producing an observable gap in ULX luminosities (Fig. 8).
3. Locally, our new channel can account for the brightest observed ULXs, with  $\sim 0.2$  sources per  $M_{\odot} \text{ yr}^{-1}$  of SFR. Observations of nearby galaxies give a rate of  $2$  ULXs per  $M_{\odot} \text{ yr}^{-1}$  of SFR, so a different channel is required to explain the less luminous sources. The rate from our channel increases significantly in low metallicity environments, with a maximum of  $2.3$  sources per  $M_{\odot} \text{ yr}^{-1}$  of SFR expected at a metallicity of  $\log Z = -4$ .
4. The metallicity dependence of both the number and the luminosity of the ULXs predicted through our channel, implies that the ratio of the total X-ray luminosity of galaxies and the SFR drops significantly at extremely low metallicities.
5. The majority of our ULX binaries have orbital periods below  $20$  d and MS donors in the mass range  $8M_{\odot} \dots 30M_{\odot}$ , with a non-negligible number of donors up to  $70M_{\odot}$ , possibly explaining some bright optical counterparts to observed ULXs that are hard to explain with CE models. More than  $90\%$  of our sources contain MS donors, transferring mass at rates below ten times  $\dot{M}_{\text{Edd}}$ . ULXs formed through CHE are also expected to favor low mass ratios, with about  $\sim 50\%$  of nearby sources having  $q < 0.5$ .
6. After a ULX phase, depending on the mass of the donor, a NS-BH or BH-BH binary could be produced. There is a small but finite probability to produce NS-BH systems which are compact enough to merge in less than a Hubble time, with a formation rate of  $< 0.2 \text{ Gpc}^{-3} \text{ yr}^{-1}$ . The detection of such mergers in the near future is not likely, but they would be characterized by having large mass ratios, with BHs more massive than  $20M_{\odot}$ .

Together with the results of (Marchant et al., 2016), who investigated similar binary systems to this study only focussing on mass ratios closer to one, we find that the tightest low-metallicity massive binaries may produce a wealth of exciting phenomena (Fig. 4.15). Since the primaries above  $\sim 30M_{\odot}$  evolve chemically homogeneously (Fig. 2) due to tidal synchronisation, they do not expand and may produce BHs with a mass close to their initial mass. For mass ratios of  $q \gtrsim 0.8$ , the secondary may also follow CHE and form a second massive BH in the system, potentially leading to massive BH mergers, at lower mass ratios the secondaries follow ordinary evolution, leading to luminous ULXs. In both cases, the mass range of BH formation is interrupted by the pair instability regime, leading to pair instability supernovae for primary masses roughly in the range  $60M_{\odot} \dots 130M_{\odot}$ . Finally, as rapid rotation is required for CHE, the BHs may form with high Kerr parameters, which may give rise to LGRBs in the frame of the collapsar model.

Many of these outcomes can be assessed observationally in the coming years. We have argued that, at low metallicities, the distribution of X-ray luminosities of ULXs could present a pronounced gap, which upcoming missions such as *eROSITA* and *Athena* could possibly detect. A similar gap is expected in the distribution of chirp masses of merging double BHs (Marchant et al., 2016), which may be detectable by aLIGO at its design sensitivity. Current transient surveys such as the intermediate Palomar Transient Factory (Rau et al., 2009), the upcoming Zwicky Transient Facility (Bellm, 2014; R. M. Smith et al., 2014) and the Large-Synoptic-Survey telescope LSST (Tyson, 2002) may provide strong constraints on the existence and rates of PISNe. All these observations from very different instruments will provide strong tests of our models, and in particular of CHE in the closest massive binary systems.

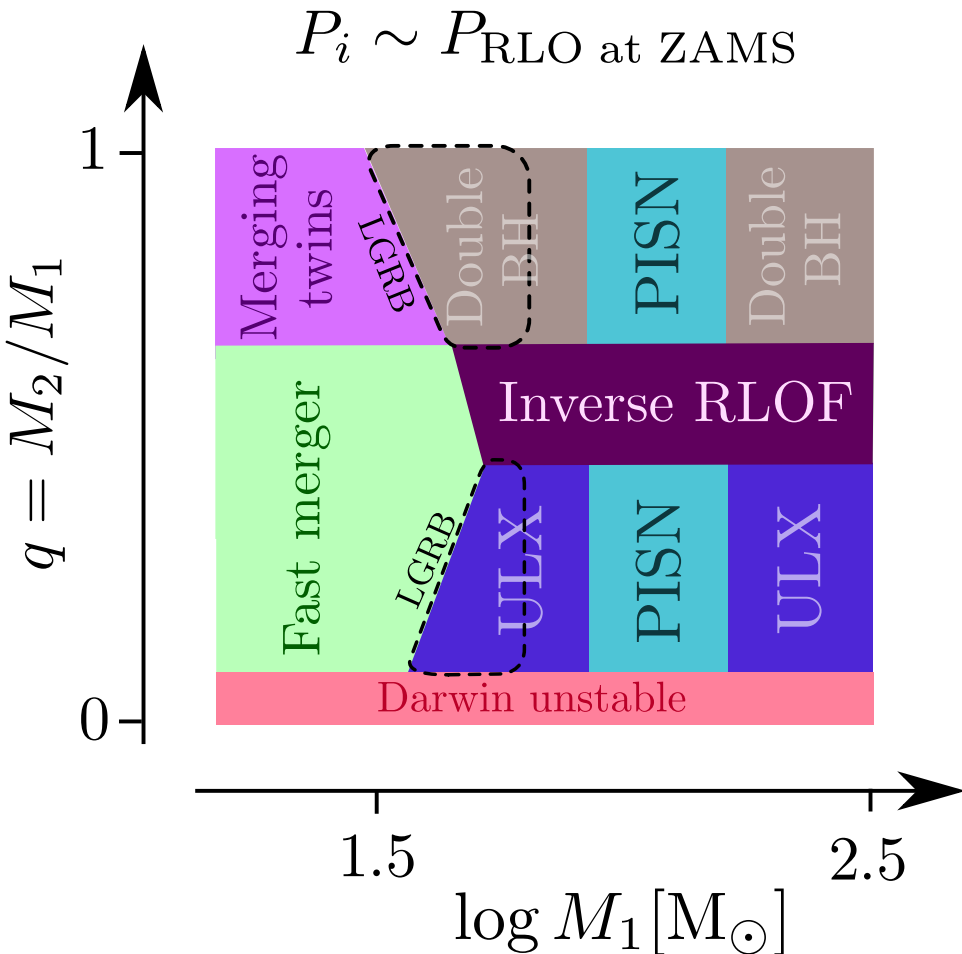


Figure 4.15: Schematic representation of the evolutionary end stages of massive low metallicity binaries with the smallest possible initial orbital periods. See text for discussion.

Acknowledgements: PM and NL are grateful to Bill Paxton for his continuous help in extending the MESA code to contain all the physics required for this project over the last years. PM would like to thank the Kavli Institute for theoretical physics of the university of California Santa Barbara, together with all the participants of the “Astrophysics from LIGO’s First Black Holes” workshop for helpful discussion. PhP is grateful for a Humboldt Research award at the university of Bonn. SdM acknowledges support by a Marie Skłodowska-Curie Action (H2020 MSCA-IF-2014, project id 661502). IM acknowledges partial support from the STFC. We would also like to thank Richard Saxton and Luca Zampieri for helpful discussion, and Martin Carrington for reporting an issue with spin-orbit coupling in MESA.



## CHAPTER 5

---

# Surface abundances and spins of massive stars in interacting binary systems

---

**Pablo Marchant**, Norbert Langer, Selma de Mink  
In preparation

**ABSTRACT:** In massive stars, rapid rotation can potentially induce large scale mixing in their envelopes, dramatically altering their path of evolution. A common prediction of models of massive stars including rotation is the rapid enrichment of their surfaces with material that has been processed through the CNO cycle deep inside the star, which significantly increases their surface nitrogen abundance. Although some observed stars confirm the trend of an increasing surface nitrogen with rotation, a large number of objects fall outside this expectation, with both unenriched rapid rotators and enriched slow rotators forming a significant part of the sample. Moreover, nitrogen enrichment needs not to be an intrinsic feature, as mass transfer in a binary system can also result in the accretion of CNO processed material and spin-up. In this work we perform detailed numerical simulations of single and binary stars in the LMC using the MESA code, including the effects of rotation. Our grid of simulations is appropriate to study the evolution of stars in the range  $15M_{\odot} - 25M_{\odot}$ . We show that even under assumptions that minimize the impact of binary stars in observations (low mass-transfer efficiency and inefficient rejuvenation), a sample of apparent single stars is predicted to contain a large number of spun-up accretors from binary systems with various levels of nitrogen enrichment. This result makes it difficult to argue in favor of rotational mixing using only observations of rapidly rotating stars with significant nitrogen enrichment. The determination of precise nitrogen abundances or detections of binary companions for fast rotators seems necessary to break this degeneracy.

Recent observations have shown that binary interaction dominates the evolution of massive stars (Kobulnicky and Fryer, 2007; Sana et al., 2012; Kobulnicky, Kiminki et al., 2014; Almeida, Sana, W. Taylor et al., 2016), with more than half of observable objects consisting of close binary systems that will undergo Roche-lobe overflow (RLOF). Given the large impact massive stars have on the universe at large scales, both through chemical enrichment (Burbidge et al., 1957) and mechanical feedback (McKee and Ostriker, 1977) from supernovae, together with the emission of large quantities of ionizing photons (Haiman and Loeb, 1997), a detailed understanding of the evolution of binary systems becomes fundamental. Rotation has also been recognized as an important feature in the evolution of massive stars, possibly inducing strong mixing throughout their radiative envelopes such that they can undergo chemically homogeneous evolution (hereafter CHE, Maeder, 1987). At low metallicities, this channel of evolution can have dramatic consequences for the post main-sequence evolution of a star, leading to the formation of very massive helium stars that could end their lifetimes as long-duration gamma-ray bursts (Yoon and Langer, 2005; Woosley and Heger, 2006; Yoon, Langer and C. Norman, 2006) or pair-instability supernovae (Yoon, Dierks and Langer, 2012). Moreover, in very compact massive binaries tidal locking may induce rapid rotation and CHE (de Mink, Cantiello et al., 2009; Song et al., 2016), providing a channel for the formation of massive merging black holes (Mandel and de Mink, 2016; Marchant et al., 2016; de Mink and Mandel, 2016).

Although rotational mixing is predicted to have a large impact on massive stars, direct evidence of this effect is elusive. One of the expected products of rotational mixing in massive stars, even if not strong enough to result in CHE, is an increase in their surface nitrogen abundance owing to the mixing of CNO processed material (Maeder and Meynet, 2000; Maeder, 2000; Heger, Langer and Woosley, 2000). Models of massive single stars including rotation indicate that their surface rotational velocity should closely correlate with their nitrogen abundance, but a large number of observed objects fall outside of this prediction (Hunter et al., 2008; Morel, Hubrig and Briquet, 2008; Brott, C. J. Evans et al., 2011; Grin et al., 2016). This includes slowly rotating stars with a high enrichment in their nitrogen abundances, as well as rapidly rotating unenriched stars. As binary interaction can result in the accretion of CNO processed material as well as spin-up (Langer, Cantiello et al., 2008), a careful consideration of both single and binary stars is required to disentangle both effects. This may become feasible as large observational programmes such as the VLT-FLAMES (Hunter et al., 2008) and the VLT-FLAMES Tarantula Survey (VFTS, C. J. Evans, W. D. Taylor et al., 2011) provides us with large samples of massive stars.

The computation of detailed sets of single stellar evolution models has been a constant industry since the 50s (A. R. Sandage and Schwarzschild, 1952; Hofmeister, Kippenhahn and Weigert, 1964a; Iben, 1967), with recent studies producing extensive grids covering the parameter space of initial masses, metallicities and rotational velocities (Bertelli et al., 2009; Brott, de Mink et al., 2011; Ekström et al., 2012; Chieffi and Limongi, 2013; Martins and Palacios, 2013). However, most simulations of massive binary stars computed with detailed stellar evolution codes study either a small fraction of the initial parameter space (Wellstein and Langer, 1999; Wellstein, Langer and Braun, 2001; Petrovic, Langer and Hucht, 2005), or account only for compact systems interacting during the main sequence (i.e. Case A evolution, C. A. Nelson and Eggleton, 2001; de Mink, Pols and Hilditch, 2007). The recent models computed with the BPASS code cover a wide range of the binary parameter space, but use simplifying assumptions for the evolution of the secondaries and consider only rigid rotation (Eldridge and Stanway, 2009; Stanway, Eldridge and Becker, 2016).

A powerful tool to study the large parameter space of binary systems, coupled with the many uncertainties in single and binary stellar evolution, has been the development of rapid population synthesis codes, which use the output of single stellar evolution models together with simplifying assumptions to account for binary interaction (Hurley, Tout and Pols, 2002; De Donder and Vanbeveren, 2004; Izzard et al., 2006;

Belczynski, Kalogera et al., 2008). With such an approach, de Mink, Langer et al. (2013) demonstrated that accreting stars in binaries can potentially account for most of the observed rapidly rotating massive stars, which conflicts with the interpretation of rapidly rotating stars showing an enrichment in nitrogen as the product of single stellar evolution and rotational mixing. Moreover, de Mink, Sana et al. (2014) showed that the common approach of removing stars with observable radial velocity variations from a sample to reduce the impact of binary effects is counterproductive. This is because most of the objects detectable as binaries are actually pre-interaction systems, and excluding them would result in a sample with a comparable number of stars that were born single and products of binary evolution. Even though rapid population synthesis is a powerful tool to explore uncertainties in input physics, it cannot account self-consistently for the mixing processes resulting in nitrogen and helium enrichment in stars.

In this work we present detailed models of massive single and binary systems including differential rotation, tidal synchronization, and mass and angular momentum transfer, which are calibrated to the composition of the LMC and consider the evolution of both components. The outline of this work is as follows: In Section 5.1 we describe our methods to model both single and binary stars. Before discussing the results of grids of simulations, we briefly derive estimates on the relevance of different binary products in Section 5.2, which provides a straightforward way to study the impact of different physical assumptions. In Section 5.3 we describe our grids of binary and single star models, describing how accreting stars can become enriched in nitrogen both with efficient and inefficient accretion. Finally, we briefly discuss our results in Section 5.5.

## 5.1 Methods

To perform our calculations we use the MESA code<sup>1</sup> (Paxton, Bildsten et al., 2011; Paxton, Cantiello et al., 2013; Paxton, Marchant et al., 2015), which is a detailed 1D stellar evolution code that can model both single and binary stars. The initial chemical composition of our models is set according to the LMC composition used in the stellar models of Brott, de Mink et al. (2011), for which we created custom made opacity tables from the OPAL project (Iglesias and F. J. Rogers, 1996). The nuclear networks used for our models are the simple `basic.net`, `co_burn.net` and `approx21.net`, which are switched dynamically during runtime to account for later burning stages. The `basic.net` nuclear network which covers hydrogen and helium burning has the isotopes  $^1\text{H}$ ,  $^3\text{He}$ ,  $^{12}\text{C}$ ,  $^{14}\text{N}$ ,  $^{16}\text{O}$ ,  $^{20}\text{Ne}$  and  $^{24}\text{Mg}$ . It includes reactions for the pp-I, pp-II and pp-III chains, as well as the CN and CNO-I cycles for hydrogen burning, using equilibrium assumptions for isotopes not included in the network. Helium burning includes the triple-alpha process as well as alpha captures on  $^{12}\text{C}$ ,  $^{14}\text{N}$ ,  $^{16}\text{O}$ ,  $^{20}\text{Ne}$ . For the range of masses studied in this paper, we have tested that abundances of CNO elements predicted by models using this simple network match those from models with much larger grids. Convection is modeled using the mixing-length theory (Böhm-Vitense, 1958) with a mixing-length parameter  $\alpha = 1.5$ , and the boundary for convection is determined using the Ledoux criterion. For convective hydrogen burning cores, we consider step overshooting that extends the convective region by  $0.335H_P$ , where  $H_P$  is the pressure scale height at the convective core boundary. This overshooting value was derived by Brott, de Mink et al. (2011) to account for the drop in rotational velocities from stars as they leave the main sequence. We consider the effect of weak semiconvective mixing following (Langer, Fricke and Sugimoto, 1983) with an efficiency parameter  $\alpha_{sc} = 0.01$ , while thermohaline mixing is modeled as in Kippenhahn, Ruschenplatt and Thomas, 1980 with an efficiency parameter of  $\alpha_{th} = 1$ . Note however that observations of low-mass red giants suggest that the efficiency of thermohaline mixing is more than two

<sup>1</sup> In lists to reproduce the results of this work can be downloaded from [https://github.com/orlox/mesa\\_input\\_data/tree/master/2016\\_binary\\_models](https://github.com/orlox/mesa_input_data/tree/master/2016_binary_models)

times larger (Charbonnel and Zahn, 2007; Cantiello and Langer, 2010).

Stellar wind mass loss is implemented following Brott, de Mink et al. (2011), with winds for main-sequence hydrogen rich stars computed following the recipe by Vink, de Koter and Lamers (2001). For temperatures below that of the bi-stability jump, we take the maximum of the rate of Vink, de Koter and Lamers (2001) and Nieuwenhuijzen and de Jager (1990). For surface hydrogen abundances  $0.4 < X < 0.7$ , we interpolate between the mass loss rate of Vink, de Koter and Lamers (2001) and that of Hamann, Koesterke and Wessolowski (1995) to account for the stronger winds of Wolf-Rayet stars. For all phases of evolution, we assume that mass loss rates scale as  $(Z/Z_{\odot})^{0.85}$ , extending the metallicity dependence derived by Vink, de Koter and Lamers (2001) for hot main-sequence stars to later phases of evolution. We include the enhancement of wind mass loss following Langer (1998), and whenever the ratio between the rotational frequency of the star and its critical value would exceed  $\Omega/\Omega_{\text{crit}} = 0.99$ , we implicitly adjust mass loss such that the actual ratio is just below that limit (see Paxton, Marchant et al. 2015 for details).

We model rotational mixing as a diffusive process, including the effects of dynamical and secular shear instabilities, the Goldreich-Schubert-Fricke instability, and Eddington-Sweet circulations, as described in Heger, Langer and Woosley (2000). We also including the transport of angular momentum due to magnetic fields from the Tayler-Spruit dynamo (Spruit, 2002; Heger, Woosley and Spruit, 2005), following the implementation of Petrovic, Langer, Yoon et al. (2005). We consider the stabilizing effect of mean molecular weight gradients using a parameter  $f_{\mu}$  as defined by Heger, Langer and Woosley (2000), with a value of  $f_{\mu} = 0.1$  as in Yoon, Langer and C. Norman (2006). For the efficiency of rotational mixing, we take  $f_c = 1/30$ , as proposed by Chaboyer and Zahn (1992). We do not adopt the value  $f_c = 0.228$  calibrated by Brott, de Mink et al. (2011) for reasons described in Section 5.1.1. Tidal effects in binary systems are modeled using the model for radiative envelopes described in Hurley, Tout and Pols (2002), following the implementation of Detmers et al. (2008). This model is based on the dynamical model for tides of Zahn (1975) and Zahn (1977).

Mass transfer is modelled using the `roche_lobe` scheme of mass transfer of MESA, which implicitly adjusts mass loss such that the donor star is restricted to its Roche lobe radius. The accretion of angular momentum follows de Mink, Langer et al. (2013), which differentiates between disk and ballistic accretion (see Paxton, Marchant et al. 2015 for details). We assume wind mass loss is strongly enhanced as a star approaches its critical rotation rate, which allows us to determine the mass transfer efficiency self consistently (see Section 5.1.3). We also consider contact models as in Marchant et al. (2016), and this model is described in more detail in Section 5.1.4. In binary systems, we assume both components are synchronized to the orbital period at their zero-age main sequence (ZAMS). When the primary reaches core carbon depletion, we assume the occurrence of a supernova, leaving the secondary as a single star.

### 5.1.1 Comparison to the models of Brott, de Mink et al. (2011)

In order to reproduce observations of CNO enhancement, Brott, de Mink et al. (2011) use non-solar scaled abundances that are representative of the Galaxy, the LMC and the SMC. However, this makes the use of standard opacity tables computed using solar-scaled metal abundances inappropriate. To compensate for this issue, they use OPAL opacity tables (Iglesias and F. J. Rogers, 1996) computed with solar-scaled abundances, but take an effective metallicity  $(\text{Fe}_{\text{surf}}/\text{Fe}_{\odot}) \times Z_{\odot}$  when computing opacities, with  $Z_{\odot} = 0.017$  (Grevesse, Noels and Sauval, 1996). For our models we use the LMC composition of Brott, de Mink et al. (2011), but avoid the issue with opacities by using custom-made OPAL tables. Figure 5.1 shows a comparison between a  $20M_{\odot}$  non-rotating MESA model using both custom OPAL tables and solar-scaled tables with an iron-scaled metallicity, together with the equivalent track from Brott, de Mink et al. (2011). It can be seen that the method of Brott, de Mink et al. (2011) gives results

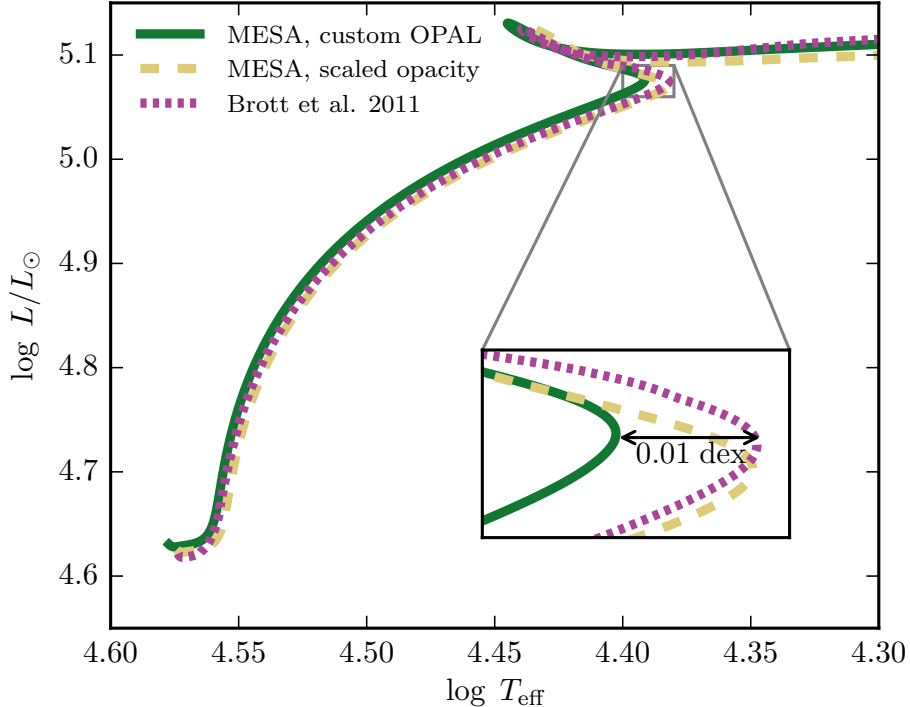


Figure 5.1: Non-rotating  $20M_{\odot}$  model from Brott, de Mink et al. (2011) compared to MESA models using custom OPAL tables or standard solar-scaled OPAL tables, where opacity is computed with the same method of Brott, de Mink et al. (2011).

very close to that of using custom OPAL tables. The difference between the MESA models and that of Brott, de Mink et al. (2011) is very small, having a maximum of just 0.01 dex at the red end of the main sequence.

Although the luminosities of our models match those of Brott, de Mink et al. (2011), and the amount of hydrogen burnt during the main sequence also matches up to  $\sim 1 - 2\%$ , the main sequence lifetime of the MESA models is consistently larger by about 16%, as depicted by Figure 5.2. For the MESA models we verified that the integrated luminosity from hydrogen burning including the energy lost through neutrinos matches the expected energy output from the burnt hydrogen. Even with differences in the energy generation rates used, the models of Brott, de Mink et al. (2011) would require more than 15% of the energy produced by hydrogen burning to be lost as neutrinos in order to be consistent. We conclude that the models of Brott, de Mink et al. (2011) have a numerical error which produces consistently lower main sequence ages. This issue has already been noted by Martins and Palacios (2013).

Different stellar lifetimes also modify predictions from rotational mixing, so we do not use the value of  $f_c = 0.0228$  used by Brott, de Mink et al. (2011) for the calibration of the efficiency of rotational mixing, but rather use the value  $f_c = 1/30$  which was determined from theoretical considerations by Chaboyer and Zahn (1992). Although we have a larger value of  $f_c$ , and our stars have a longer main sequence lifetime, our models mix slightly less CNO processed material to the surface, as shown in Figure 5.3.

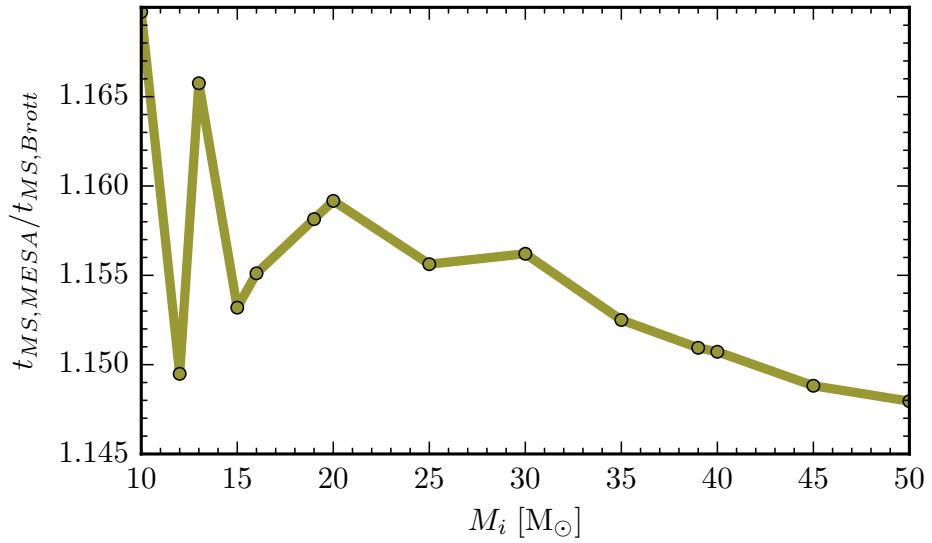


Figure 5.2: Discrepancy on main sequence ages between MESA models and those of Brott, de Mink et al. (2011), using equivalent physical assumptions.

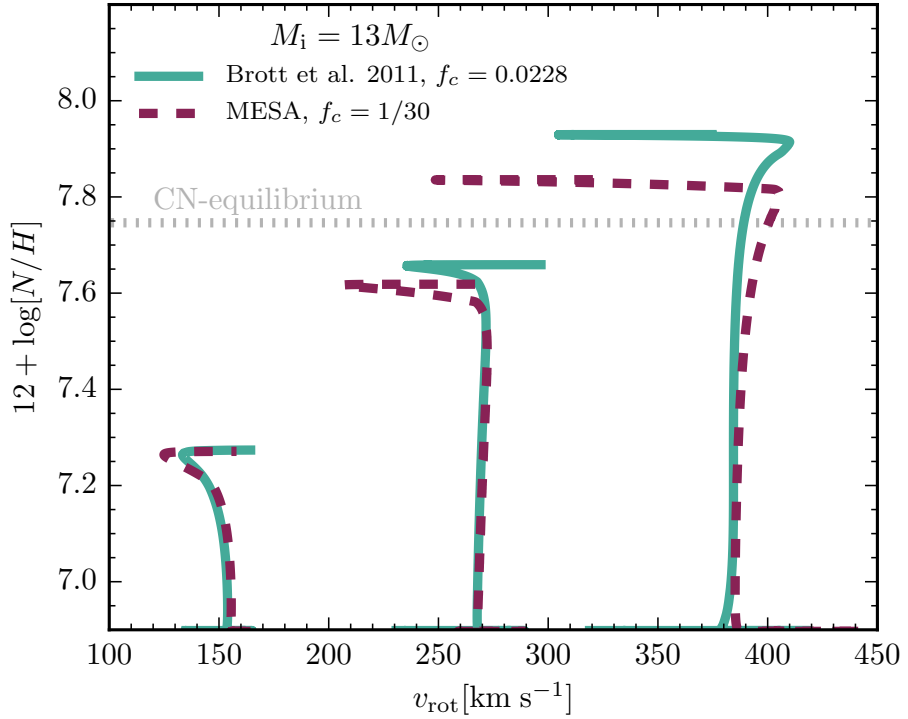


Figure 5.3: Comparison of the effect of rotational mixing during the main sequence on a  $13M_\odot$  star between our models and those of Brott, de Mink et al. (2011). Dotted line indicates the abundance of nitrogen for CN-equilibrium, while CNO-equilibrium corresponds to an abundance of 8.5.

### 5.1.2 Overshooting limitation

During the main sequence lifetime of massive stars their superadiabatic cores reduce in size, so the boundary of the convective core, including extra mixing from overshooting, is also expected to recede. Mass transfer in a binary system can change this significantly, as the boundary of the superadiabatic region in the accreting star will move outwards in mass potentially leading to rejuvenation (Hellings, 1983; Hellings, 1984; Braun and Langer, 1995; Dray and Tout, 2007). But whether or not the convective core will manage to mix through the mean molecular weight gradient ( $\mu$  gradient for short) that has already developed is not quite certain. This presents a problem when using the standard definition of overshooting as an extension of the Ledoux-unstable regions by a fixed fraction of  $H_P$ , since it is insensitive to the presence of an important composition gradient. Modelling binary systems with overshooting implemented in this way then always leads to instantaneous rejuvenation.

To account for the stabilizing effect of  $\mu$  gradients we limit the extent of the overshooting region up to a mass coordinate where the composition term in the Ledoux criteria is above a given threshold, i.e., there will be no overshooting in regions that satisfy the condition

$$\frac{\varphi}{\delta} \nabla_\mu > f, \quad (5.1)$$

where  $f$  is the arbitrary threshold and

$$\varphi = \left( \frac{\partial \ln \rho}{\partial \ln \mu} \right)_{P,T}, \quad \varphi = \left( \frac{\partial \ln \rho}{\partial \ln T} \right)_{\mu,P}, \quad \nabla_\mu = \frac{d \ln \mu}{d \ln P}. \quad (5.2)$$

Although the value for  $f$  is arbitrary, the left hand side of Eq. (5.1) normally experiences a large change between the very well mixed convective regions and those with a composition gradient, and thus the particular choice of  $f$  does not carry a significant impact on our models. We use  $f = 0.1$ , and some test cases with  $f = 0.2$  and  $f = 0.05$  show that this choice makes little difference on the end results.

In binary systems, our assumption of limited overshooting reduces the core size of post-interaction accretors in binary systems. This is depicted in Figures 5.4 and 5.5, where we show the evolution of a binary system with an initial period of three days and initial component masses  $M_1 = 20M_\odot$  and  $M_2 = 17M_\odot$ . We model the same system using both efficient ( $\alpha_{sc}=1$ ) and inefficient ( $\alpha_{sc} = 0.01$ ) semiconvective mixing, and as can be seen, it is semiconvection that regulates the growth of the convective core and rejuvenation. For comparison, we also show the evolution of a  $22M_\odot$  star, which corresponds to the mass the secondary reaches after accretion. In both binary systems modeled the final helium core mass of the accretor is significantly smaller than that of the  $22M_\odot$  single star, which significantly alters their post main-sequence evolution. Our choice of inefficient semiconvection for our grid of models minimizes rejuvenation after mass transfer, and as we argue in Section 5.2 this minimizes the number of observable post-interaction systems. This allows us to provide lower estimates on the importance of post-interaction systems in observed samples of massive stars.

### 5.1.3 Rotationally enhanced winds and mass transfer efficiency

Stars undergoing efficient mass accretion can be easily spun up to critical rotation by accreting, with Packet (1981) demonstrating that through disk accretion a star needs only to accrete a few percent of its mass for this to happen. At this point, unless angular momentum is lost from the star accretion of further material is not possible. To model this situation we use the implicit wind scheme of MESA, which artificially increases wind mass loss if  $\Omega/\Omega_{crit}$  is above 0.99. In our models, very close binaries for which tidal effects are important can prevent rapid spin-up, allowing for efficient mass transfer. In

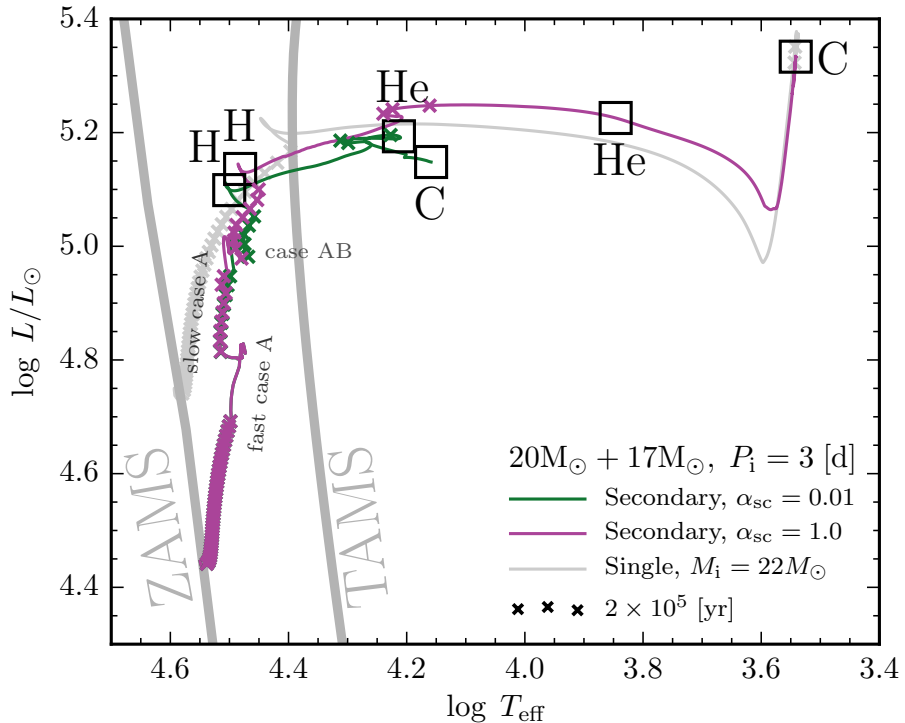


Figure 5.4: HR diagram for the secondaries in a  $20M_{\odot} + 18M_{\odot}$  system at an initial period of  $\log P_i$  [d] = 3 days, with both inefficient ( $\alpha_{sc} = 0.01$ ) and efficient ( $\alpha_{sc} = 1.0$ ) semiconvection. The evolution of a single star with initial mass  $M_i = 25M_{\odot}$  is also shown. TAMS stands for terminal-age main sequence. Squares and the corresponding symbols indicate depletion of different nuclear fuels at the core.

contrast our case B systems have accretion efficiencies under 10%. In reality, tidal effects might act on the outer regions of accretion disks, allowing angular momentum to be transported back onto the orbit and accretion to proceed with high efficiency (Popham and Narayan, 1991). The efficiency of mass transfer remains a largely unsolved problem in binary evolution, but taking a limit which minimizes efficiency allows us to set a lower limit on the impact of binary products in observable samples of massive stars, as we argue in Section 5.2.

Figure 5.6 shows two example systems depicting mass transfer efficiency for different initial periods. Note that this method provides a self-consistent determination of the mass transfer efficiency, which is not equivalent to completely halting mass transfer efficiency when critical rotation is reached. In fact, the case B system shown in Figure 5.6 keeps accreting through the complete mass transfer phase, although at a very low efficiency, and in the case A system shown, the accretor switches from accretion to mass loss during case AB, as it thermally contracts once the mass accretion rate is reduced. Since accretion is non-zero for case B systems, small amounts of helium rich material will be accreted into the surface of the secondaries. The amount of accreted material is too low to produce any important enrichment by itself, but it induces thermohaline mixing throughout the entire envelope of the star, which causes it to self-enrich with CNO processed material, dredged up from its deeper layers, as shown in Figure 5.7.

Our assumptions can lead to extremely inefficient mass transfer with very large mass loss rates from the system, and whether or not the obtained values are physically reasonable needs to be assessed. As an

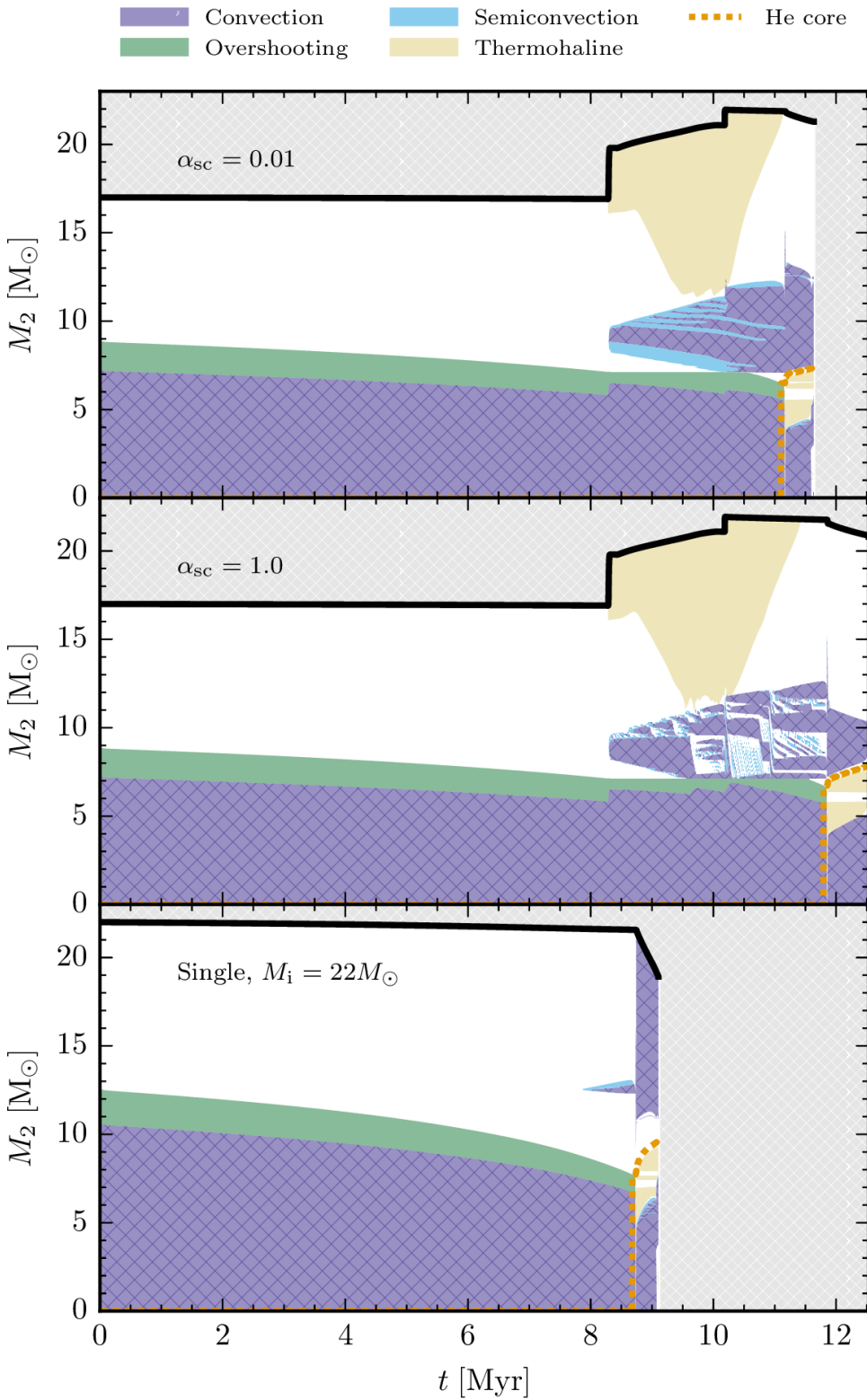


Figure 5.5: Kippenhahn diagram for the accreting star in a  $20M_\odot + 18M_\odot$  binary with an initial period of  $P_i = 3$  days, and different choices for the efficiency of semiconvection. The evolution of a single star with an initial mass of  $M_i = 25M_\odot$  is also shown. All plots end at core-carbon depletion.

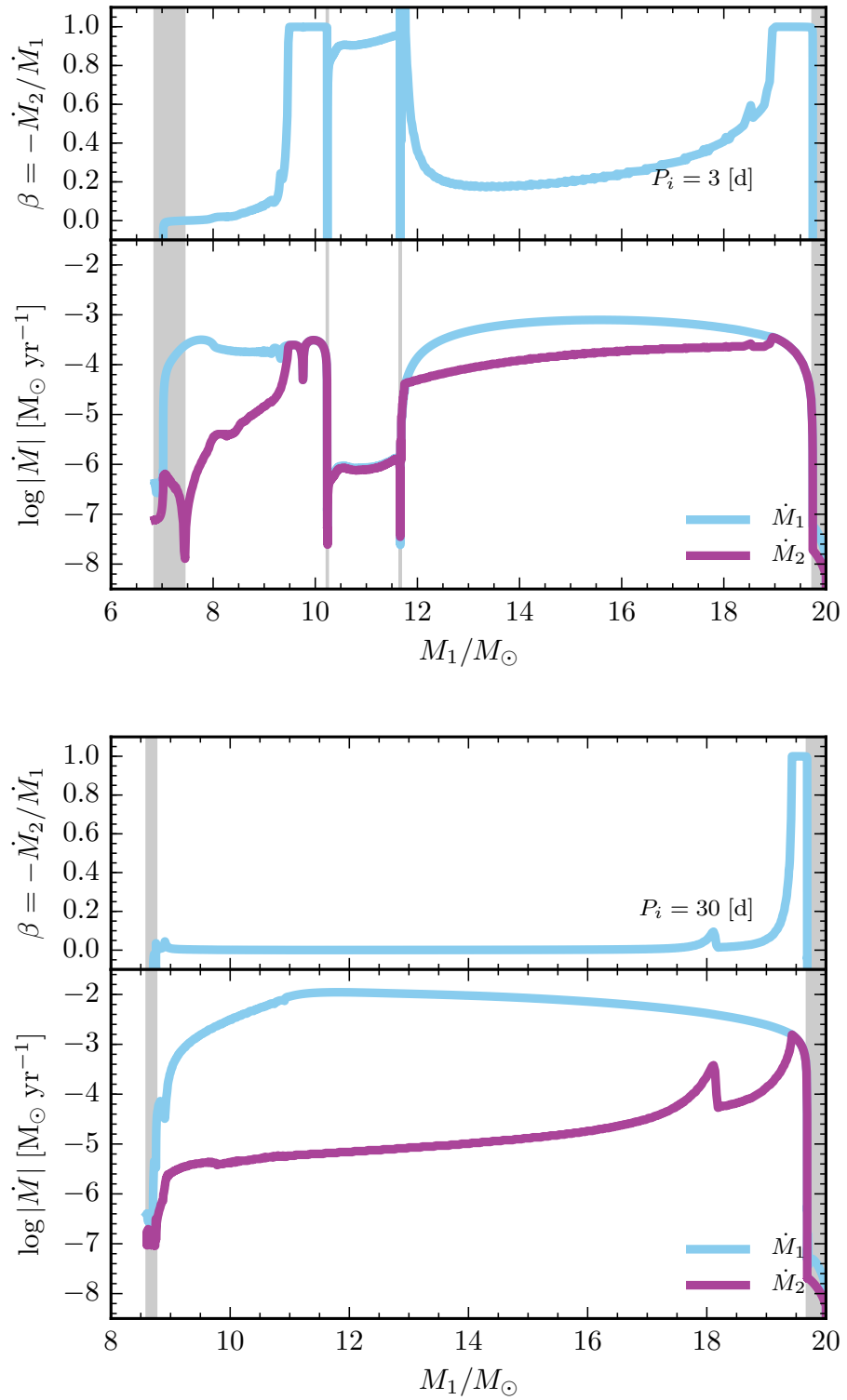


Figure 5.6: Mass transfer efficiencies for a  $20M_\odot + 19M_\odot$  system at different initial periods. The system with  $P_i = 3$  days experiences case A and case AB mass transfer, while the system with  $P_i = 30$  days undergoes a single phase of case B mass transfer. Gray shaded regions indicate phases where  $\beta < 0$ .

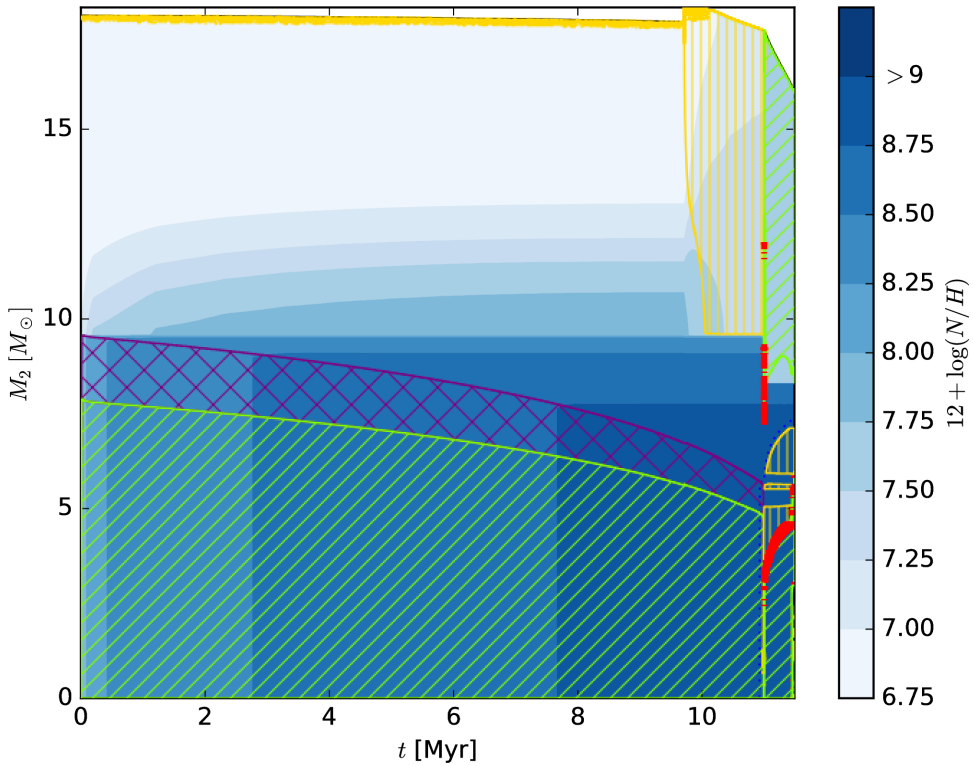


Figure 5.7: Kippenhahn diagram showing the abundance of nitrogen in the interior of the secondary in a binary system with component masses  $M_1 = 20M_\odot$  and  $M_2 = 18M_\odot$  at an initial period of 30 days. Regions are shaded depending on the different mixing processes acting, with green indicating convection, purple overshooting, red semiconvection, and yellow thermohaline mixing. Although mass transfer is very inefficient, small amounts of helium rich material are accreted, which can mix deep inside the star due to thermohaline mixing.

upper limit to the mass loss rate possible from a radiation driven wind, we can consider all material lost as being accelerated from a Keplerian disc right at the surface of the accretor. Ignoring the donor, the energy required per unit mass to drive this material to infinity is  $GM_2/2R_2$ , and if all energy radiated from the stars is used to drive the wind, the resulting mass loss is

$$\log \frac{\dot{M}}{M_\odot \text{ yr}^{-1}} = -7.19 + \log \frac{L_1 + L_2}{L_\odot} - \log \frac{M_2}{M_\odot} + \log \frac{R_2}{R_\odot}. \quad (5.3)$$

A less restrictive limit can be considered if we assume material to be accelerated from the edge of a disk with a radius equal to the Roche lobe radius of the accretor. The corresponding mass loss rate is then simply given by Equation (5.3) with  $R_2$  replaced by the Roche lobe radius of the accretor. In our models, whenever this less restrictive limit is reached, we assume material cannot be ejected or accreted to the secondary, resulting in a common envelope and a merger.

#### 5.1.4 Contact systems

Close binaries undergoing fast mass transfer often evolve into contact, as the accreting star bloats significantly due to its thermal timescale usually being much larger than that of the donor (Neo et al., 1977; Braun and Langer, 1995; Wellstein, Langer and Braun, 2001). Further evolution breaks significantly

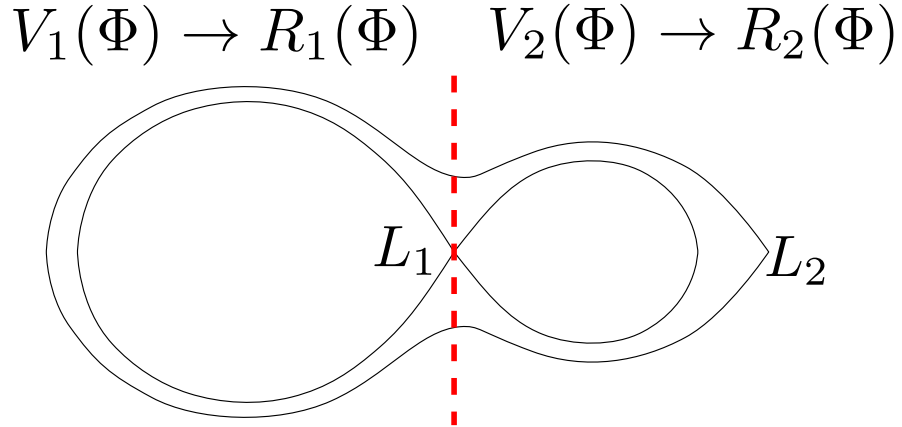


Figure 5.8: Division of an over-contact system into two distinct volumes by a plane crossing the inner Lagrangian point. To each of these a volume equivalent radius can be assigned.

from one dimension, but is of fundamental importance to understand if contact derives into a merger, or rather a semi-detached system after a period of over-contact. Evolution during the over-contact phase also differs from a classical common envelope, as co-rotation can in principle be maintained as long as material does not overflow the L2 point. This means that a spiral-in due to viscous drag can be avoided, resulting on a stable system evolving on a nuclear timescale. This is the case for VFTS 352, an over-contact system composed of two  $30M_{\odot}$  stars (Almeida, Sana, de Mink et al., 2015).

As a simple approximation to the modeling of over-contact systems with a 1D code, we follow the approach of Marchant et al. (2016), which we explain in more detail here. We consider the photosphere of such an over-contact binary to lie on a Roche equipotential, and divide it into two distinct volumes for each star,  $V_1(\Phi)$  and  $V_2(\Phi)$ , separated by a plane crossing through  $L_1$ , as shown in Figure 5.8. We then associate a volume equivalent radius to each of these,  $R_1(\Phi)$  and  $R_2(\Phi)$ , with the radii corresponding to the potential at  $L_1$  being the Roche lobe radius  $R_{RL}$  of each. When both stars overflow their Roche lobes, the amount of overflow of one component is a function of the mass ratio, and the overflow of its companion, i.e.

$$\frac{R_2(\Phi) - R_{RL,2}}{R_{RL,2}} = F\left(q, \frac{R_1(\Phi) - R_{RL,1}}{R_{RL,1}}\right), \quad (5.4)$$

where the function  $F(q, x)$  must satisfy that  $F(q, 0) = 0$  and  $F(1, x) = x$ . By numerically integrating  $V_1(\Phi)$  and  $V_2(\Phi)$  for different  $q$  ratios and potential values between those at  $L_1$  and  $L_2$  (see Figure 5.9) we find the fit  $F(q, x) = q^{-0.52}x$ , with the Roche lobe radius computed as in Eggleton (1983). During an over-contact phase, mass transfer is then adjusted in such a way that the amount of overflow from each component satisfies this relationship.

Once both stars overflow past the outer Lagrangian point, we expect the system to rapidly merge, either due to mass loss from  $L_2$  carrying a high specific angular momentum, or due to a spiral-in due to the loss of co-rotation. Figure 5.10 shows that the amount of overflow of the least massive star in a system that

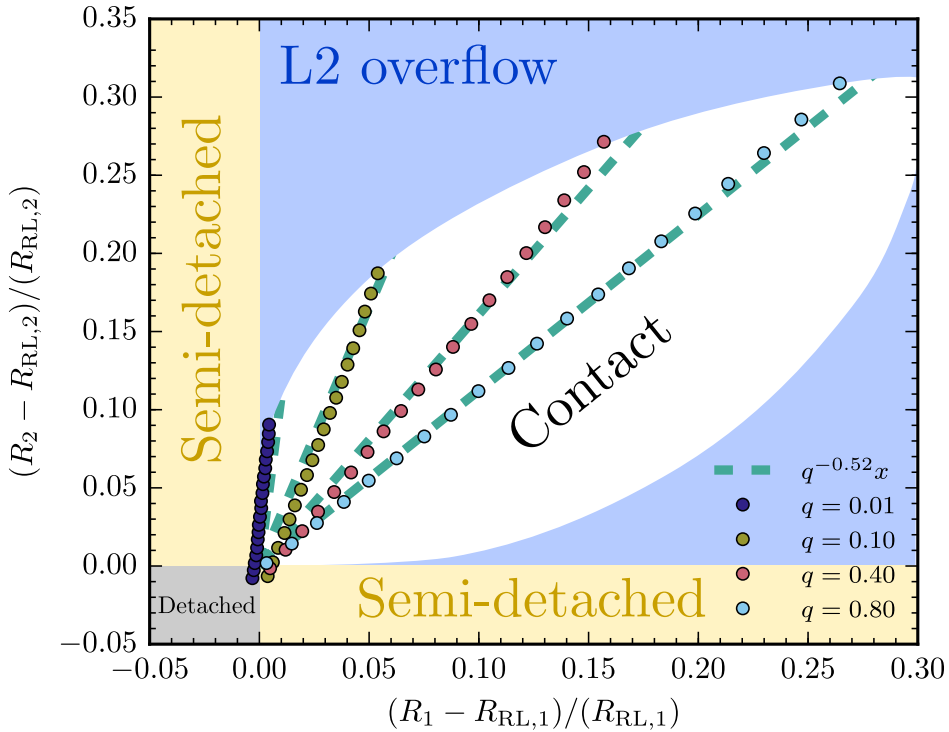


Figure 5.9: Relationship between the amount of overflow of each component for different mass ratios, assuming the surface of each star to lie on the same Roche equipotential. The mass ratio is defined as  $q = M_2/M_1$ , and for each value the outermost point corresponds to the equipotential that contains  $L_2$ , while the innermost one corresponds to the one that contains  $L_1$ . The values at  $L_1$  do not map to  $(0, 0)$  as we use the fit of Eggleton (1983) to the Roche lobe radius, which has a small (< 1%) error.

reaches  $L_2$  satisfies approximately the relationship

$$\frac{R_{L2,2} - R_{RL,2}}{R_{RL,2}} = 0.299 \operatorname{atan}(1.84q^{0.397}) \quad (5.5)$$

with an error of only a few percent in the range of interest for  $q$ . Between the moment of contact and reaching  $L_2$ , both stars can expand significantly, leaving much more space for a compact binary to survive through one of these phases. In the limit  $q = 0$  the  $L_1$  and  $L_2$  points lay on opposite sides of the Hill sphere of the secondary, and thus  $R_{L2,2} = R_{RL,2}$ .

Note that for the moment we ignore the important effects of energy and element transfer through the shared envelope.

## 5.2 Estimating the impact of binaries

Before discussing the results of a large number of simulations in terms of predicted properties of stellar populations, it is instructive to construct estimates on how the impact of binaries depends on uncertain physics. This allows us to quantify the impact of varying physical assumptions without the need to recompute a full set of stellar models. The main information required for these estimates are the scalings

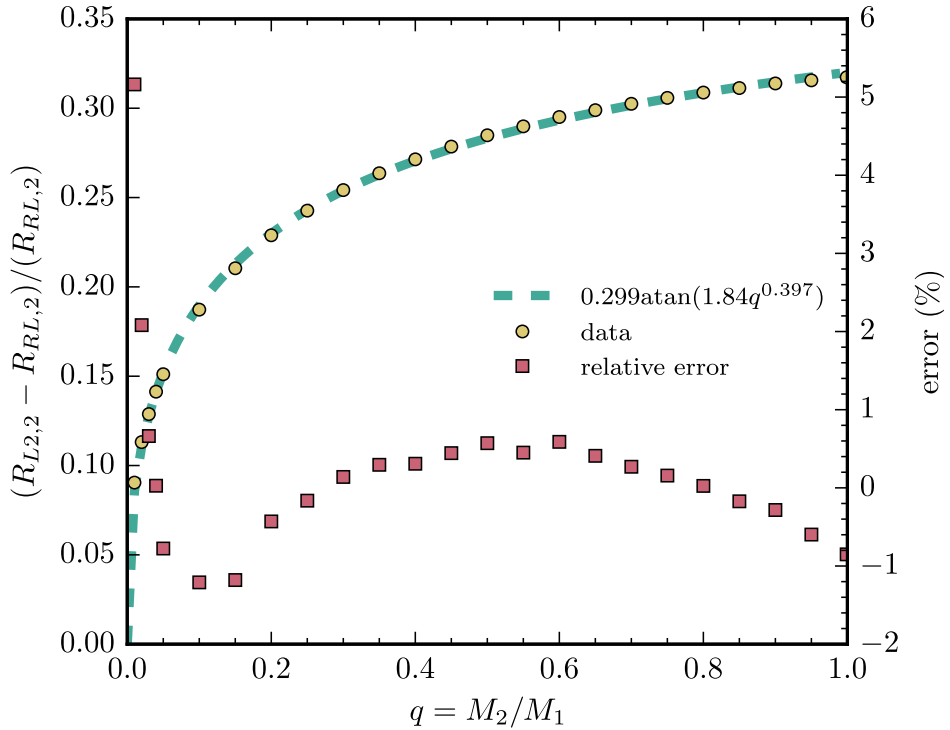


Figure 5.10: Amount of overflow of the least massive star in an over-contact system that reaches the outer Lagrangian point.

with mass of the initial mass function (IMF), the mass luminosity relationship, and main sequence lifetimes,

$$f(M) \propto M^\gamma, \quad L(M) \propto M^\alpha, \quad t_{\text{MS}} \propto M^\beta, \quad (5.6)$$

where the power for the main-sequence lifetime should be close to  $\beta = 1 - \alpha$ . Standard homology relationships show that the power of the mass luminosity relationship should be  $\alpha \sim 5$  for low mass stars burning material through the PP-cycle, while for massive stars with radiative envelopes and CNO burning at their cores, a flatter dependence is expected, with  $\alpha \sim 3$ . For very massive stars approaching the Eddington limit, this dependence becomes almost linear (Langer, Sanyal et al., 2015). Considering stars above a given luminosity threshold  $L_{\text{lim}}$ , which approximately corresponds to stars with a mass above a value  $M_{\text{lim}}$ , we can estimate what fractions of pre-interaction binaries, post-interaction systems and mergers should be observable in this sample. This is similar to the estimates computed by de Mink, Sana et al. (2014) using population synthesis calculations to estimate the fractions of different objects above a luminosity threshold  $L_{\text{lim}} = 10^4 L_\odot$ . For all our estimates, we assume a flat distribution in the initial mass ratio  $q = M_2/M_1$ .

### 5.2.1 Pre-interaction binaries

In pre-interaction binaries the combined luminosity of both components can make the system brighter than the specified luminosity threshold even if the individual masses are below  $M_{\text{lim}}$ . The minimum

primary mass  $M_{1,\text{lim}}$  for which this can happen is given by

$$M_{\text{lim}}^\alpha = 2M_{1,\text{lim}}^\alpha \rightarrow M_{1,\text{lim}} = 2^{-1/\alpha} M_{\text{lim}}. \quad (5.7)$$

For a primary mass  $M_1$  between  $M_{1,\text{lim}}$  and  $M_{\text{lim}}$ , there is a minimum mass ratio  $q_{\text{lim}}$  for which the total luminosity of the binary is just that of a single star of mass  $M_{\text{lim}}$ ,

$$M_{\text{lim}}^\alpha = M_1^\alpha + q_{\text{lim}}^\alpha M_1^\alpha \rightarrow q_{\text{lim}} = \left( \left( \frac{M_{\text{lim}}}{M_1} \right)^\alpha - 1 \right)^{1/\alpha}. \quad (5.8)$$

If the binary fraction is  $f_{\text{bin}}$ , and we also assume the lifetime of pre-interaction binaries is a fraction  $a$  of the main sequence lifetime of a single star with the mass of the primary, then we can estimate the ratio of observable pre-interaction binaries to single stars above the luminosity threshold as

$$F = \frac{af_{\text{bin}}}{1-f_{\text{bin}}} \frac{\int_{M_{\text{lim}}}^{\infty} f(M_1) t_{\text{MS}}(M_1) dM_1 + \int_{M_{1,\text{lim}}}^{M_{\text{lim}}} (1-q_{\text{lim}}) f(M_1) t_{\text{MS}}(M_1) dM_1}{\int_{M_{\text{lim}}}^{\infty} f(M) t_{\text{MS}}(M) dM}. \quad (5.9)$$

Assuming  $\alpha, \beta$  and  $\gamma$  are independent of mass, we can show this value is independent of  $M_{\text{lim}}$ ,

$$\frac{F}{a} = \frac{f_{\text{bin}}}{1-f_{\text{bin}}} \left[ 1 - (\gamma + \beta + 1) \int_{2^{-1/\alpha}}^1 \left( 1 - (x^{-\alpha} - 1)^{1/\alpha} \right) x^{\gamma+\beta} dx \right] \quad (5.10)$$

This can be numerically integrated for different  $\alpha, \beta$  and  $\gamma$ , with Figure 5.11 showing the result for a Salpeter IMF ( $\gamma = -2.35$ ) and a binary fraction  $f_{\text{bin}} = 0.7$  as in de Mink, Sana et al. (2014), which is based in the observations of Sana et al. (2012). For typical values  $\alpha = 3, \beta = 1 - \alpha = -2$ , we get  $F/a = 3$ , which assuming a typical lifetime of pre-interacting systems equal to 75% of the main-sequence lifetime results in a fraction of pre-interaction to single stars of  $F = 2.25$ , very close to the value of  $F = 2.27$  obtained by de Mink, Sana et al. (2014). Although Equation 5.10 is independent of  $M_{\text{lim}}$ , at higher luminosities the mass luminosity relationship is flatter, so Figure 5.11 implies that the relative contribution of pre-interaction binaries in a sample increases with mass.

## 5.2.2 Mergers

Let us assume all binaries with a mass ratio below a critical value  $q_{\text{crit}}$  merge, and call the fraction of total mass lost during merger  $\mu_{\text{loss}}$ . Smooth-particle-hydrodynamic simulations of mergers resulting from head-on collisions of stars point towards low values of order  $\mu_{\text{loss}} < 0.1$  (Gaburov, Lombardi and S. Portegies Zwart, 2008; Glebbeek et al., 2013). In this case, as before, there is a minimum primary mass  $M_{1,\text{lim}}$  for which a merger can reach the cutoff luminosity corresponding to  $M_{\text{lim}}$ , which is

$$M_{1,\text{lim}} = \frac{M_{\text{lim}}}{(1+q_{\text{crit}})(1-\mu_{\text{loss}})}. \quad (5.11)$$

There is as well a maximum mass  $M_{1,\text{up}}$  above which all mergers will have a mass above  $M_{1,\text{lim}}$ ,

$$M_{1,\text{up}} = \frac{M_{\text{lim}}}{1-\mu_{\text{loss}}}. \quad (5.12)$$

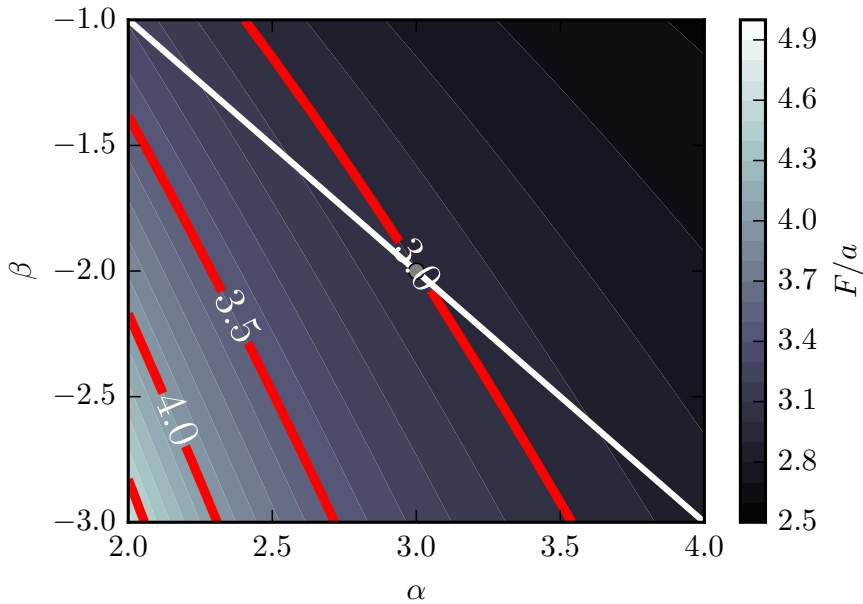


Figure 5.11: Value of the fraction  $F$  of pre-interaction binaries to single stars, for different values of  $\alpha$  and  $\beta$  assuming a salpeter IMF  $\gamma = -2.35$  and a binary fraction  $f_{\text{bin}} = 0.7$ . White line corresponds to  $\beta = 1 - \alpha$ , and the marked dot corresponds to  $\alpha = 3, \beta = -2$ .

Between  $M_{1,\text{lim}}$  and  $M_{1,\text{up}}$ , the minimum mass ratio to go above the threshold can be computed as

$$M_{\text{lim}} = (1 + q_{\text{lim}})(1 - \mu_{\text{loss}})M_1 \rightarrow q_{\text{lim}} = \frac{M_{\text{lim}}}{(1 - \mu_{\text{loss}})M_1} - 1. \quad (5.13)$$

Assuming the merged star lives for a fraction  $a$  of the main sequence lifetime corresponding to a single star with its mass, the ratio of observable single stars to mergers can be estimated as

$$F = \frac{af_{\text{bin}}}{1 - f_{\text{bin}}} \left( \int_{M_{1,\text{up}}}^{\infty} \int_0^{q_{\text{crit}}} f(M_1) t_{\text{MS}}((1 + q)(1 - \mu_{\text{loss}})M_1) dq dM_1 + \int_{M_{1,\text{lim}}}^{M_{1,\text{up}}} \int_{q_{\text{lim}}}^{q_{\text{crit}}} f(M_1) t_{\text{MS}}((1 + q)(1 - \mu_{\text{loss}})M_1) dq dM_1 \right) / \int_{M_{\text{lim}}}^{\infty} f(M) t_{\text{MS}}(M) dM, \quad (5.14)$$

which after integration results in an expression that is independent of both  $\alpha$  and  $\beta$ ,

$$\frac{F}{a} = \frac{f_{\text{bin}}}{1 - f_{\text{bin}}} \frac{1 - (1 + q_{\text{crit}})^{-\gamma}}{\gamma} (1 - \mu_{\text{loss}})^{-\gamma-1}. \quad (5.15)$$

Assuming that half of the mergers would correspond to case B systems and that mergers only live for 75% of the main-sequence lifetime corresponding to their mass, we take  $a = 0.5 \times 0.75$ . Evaluating Equation (5.15) for  $q_{\text{crit}} = 0.5$  and  $\mu_{\text{loss}} = 0.1$  results then in  $F = 0.51$ , not far from the value  $F = 0.36$  computed by (de Mink, Sana et al., 2014). Figure 5.12 shows the results for different values of  $\mu_{\text{loss}}$  and  $q_{\text{crit}}$ , and indicate that an increase in mass loss during mergers reduces their relative number compared to

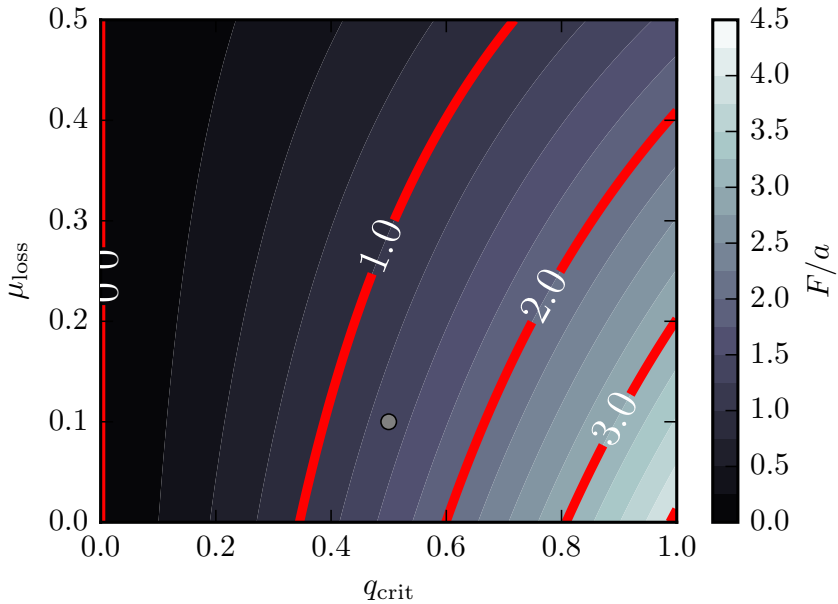


Figure 5.12: Value of  $F/a$  for mergers for different values of  $\mu_{\text{loss}}$  and  $\gamma$  (the value is independent of  $\alpha$  and  $\beta$ ) and a binary fraction  $f_{\text{bin}} = 0.7$ . The marked dot corresponds to  $\beta = -2$ ,  $\mu_{\text{loss}} = 1$ .

single stars.

### 5.2.3 Post-interaction

To account for post-interaction systems, we can assume that secondaries accrete a fraction  $\eta$  of the mass of the primary, such that its post-interaction mass is  $(\eta + q)M_1$ . If mass transfer typically results in exposed helium cores with a third of the mass of the primary, then  $\eta = 1/3$  can be understood as a 50% efficiency in mass accretion. We also need to consider the critical mass ratio  $q_{\text{crit}}$  below which mass transfer would result in a merger. For post-interaction systems we ignore the luminosity of the primary, as the secondary is likely to dominate radiation in the optical. The minimum donor primary mass required for the secondary to fall above our luminosity cut for  $M_{\text{lim}}$  is

$$M_{1,\text{lim}} = \frac{M_{\text{lim}}}{\eta + 1}, \quad (5.16)$$

and there is as well an upper mass limit  $M_{1,\text{up}}$  above which all post-interaction systems will be above the threshold,

$$M_{1,\text{up}} = \frac{M_{\text{lim}}}{\eta + q_{\text{crit}}}. \quad (5.17)$$

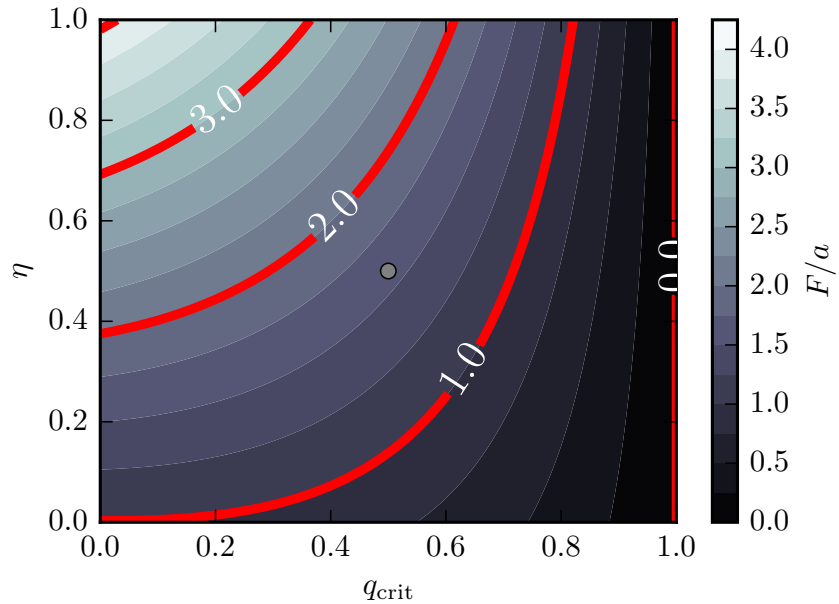


Figure 5.13: Value of  $F/a$  for post-interaction systems for different values of  $q_{\text{crit}}$  and  $\eta$ , assuming  $\gamma = -2.35$  (the value is independent of  $\alpha$  and  $\beta$ ) and a binary fraction  $f_{\text{bin}} = 0.7$ . The marked dot corresponds to  $\eta = 0.5$ ,  $q_{\text{crit}} = 0.5$ .

For  $M_{1,\text{lim}} < M_1 < M_{1,\text{up}}$ , there is a minimum mass ratio  $q_{\text{lim}}(M_1)$  for post-interaction systems to fall above the threshold,

$$(\eta + q_{\text{lim}})M_1 = M_{\text{lim}} \rightarrow q_{\text{lim}} = \frac{M_{\text{lim}}}{M_1} - \eta. \quad (5.18)$$

Using this we can estimate the ratio of post-interaction to single stars just as with the case of mergers

$$F = \frac{af_{\text{bin}}}{1 - f_{\text{bin}}} \left( \int_{M_{1,\text{up}}}^{\infty} \int_{q_{\text{crit}}}^1 f(M_1) t_{\text{MS}}((\eta + q)M_1) dq dM_1 + \int_{M_{1,\text{lim}}}^{M_{1,\text{up}}} \int_{q_{\text{lim}}}^1 f(M_1) t_{\text{MS}}((\eta + q)M_1) dq dM_1 \right) / \int_{M_{\text{lim}}}^{\infty} f(M) t_{\text{MS}}(M) dM. \quad (5.19)$$

Integrating this result gives again a value that is independent of  $\alpha$  and  $\beta$ ,

$$\frac{F}{a} = \frac{f_{\text{bin}}}{1 - f_{\text{bin}}} \frac{1}{\gamma} \left[ (\eta + q_{\text{crit}})^{-\gamma} - (\eta + 1)^{-\gamma} \right]. \quad (5.20)$$

For simplicity, we assume this estimate for post-interaction systems accounts as well for semi-detached binaries. Figure 5.13 shows the value of  $F/a$  for all possible values  $\eta$  and  $q_{\text{crit}}$  can have. Assuming  $\eta = 0.5$  (which would correspond to a 75% efficiency if the donor transfers two thirds of its mass) and  $q_{\text{crit}} = 0.5$ , results in  $F/a = 1.58$ . If post-interaction systems have typical lifetimes equal to 75% of their main sequence lifetime, this results in  $F = 1.2$ , which, again, is comparable to the value of de Mink, Sana

et al. (2014) who obtain  $F = 0.91$  when accounting for both post-interaction and semi-detached systems.

#### 5.2.4 Comparing the effect of different assumptions

Using the formulae just derived, we can quantify the impact of individual changes in the different physical assumptions, as well as account for the combined effect of different uncertainties. This is shown in Figure 5.14, where the change in the relative fractions of objects considered is shown for a wide range of parameters, assuming a fixed binary fraction  $f_{\text{bin}} = 0.7$ . It can be seen that independent of our assumptions, the fraction of single stars to binary products always remains close to unity. Even when taking the combined effect of all assumptions that reduce the fraction of binary products to single stars, we still find that the number of post-interaction products is comparable to that of single stars. As has been pointed out, inefficient accretion and a lack of rejuvenation minimize the contribution of post-interaction systems, making the physical assumptions chosen for our binary models (inefficient semiconvective mixing and accretion becoming inefficient once a star reaches critical rotation) allow us to estimate a lower limit on the impact of binary stars.

### 5.3 Evolutionary properties of the binary models

For our binary models, we consider primary masses in the range  $\log M_{1,i}/M_{\odot} = 1.0 - 1.6$  ( $M_{1,i} \simeq 10M_{\odot} - 40M_{\odot}$ ), in bins of 0.05 dex. We model systems with initial periods in the range  $\log P_i [\text{d}] = 0.15 - 2.5$  ( $P_i \simeq 1.4 - 3000$  days) in bins of 0.025 dex and mass ratios  $q = 0.975 - 0.025$  in bins of size  $\Delta q = 0.025$ . We assume tidal synchronization at the ZAMS. This is not a good assumption for the wider systems, but including the additional parameter space of initial rotation makes the parameter space too large to study with detailed models. Figure 5.15 shows the outcome of simulations with a donor mass  $\log M_{1,i} = 1.3 \simeq 20M_{\odot}$ . The meaning of the different labels in the figures is as follows:

- Both dep. C: Both stars evolved up to carbon depletion. Note that due to convergence problems, we only model stars with helium core masses in excess of  $M = 14M_{\odot}$  up to helium depletion instead. This only affects the more massive donors in the grid. After one component depletes carbon, we model the remainder of the evolution of its companion as a single star, ignoring the possibility of forming a binary with a compact object.
- L2 overflow: During a contact phase L2 overflow happens, and the binary is expected to merge.
- Post MS + Inv. MT: Inverse mass transfer happens in a binary with a post main-sequence component. These systems are expected to merge and form a post main-sequence star.
- Upper  $\dot{M}$  limit: The limit on mass loss rates given by Equation (5.3) with  $R_{\text{RL},2}$  instead of  $R_2$  is reached. In this case the luminosity of the system is insufficient to expel the transferred material, which cannot be accreted unto the critically rotating secondary. We expect such systems to develop a common envelope and merge.
- MT with  $q_i < 0.25$ : Mass transfer is initiated in a system with an initial mass ratio below  $q_i < 0.25$ . We assume such systems will result in a merger.
- Convergence error: Owing to numerical problems the simulation could not be completed. This normally happens during late phases of mass transfer, or whenever unstable mass transfer develops. In the latter case, systems could undergo common envelope evolution with successful envelope

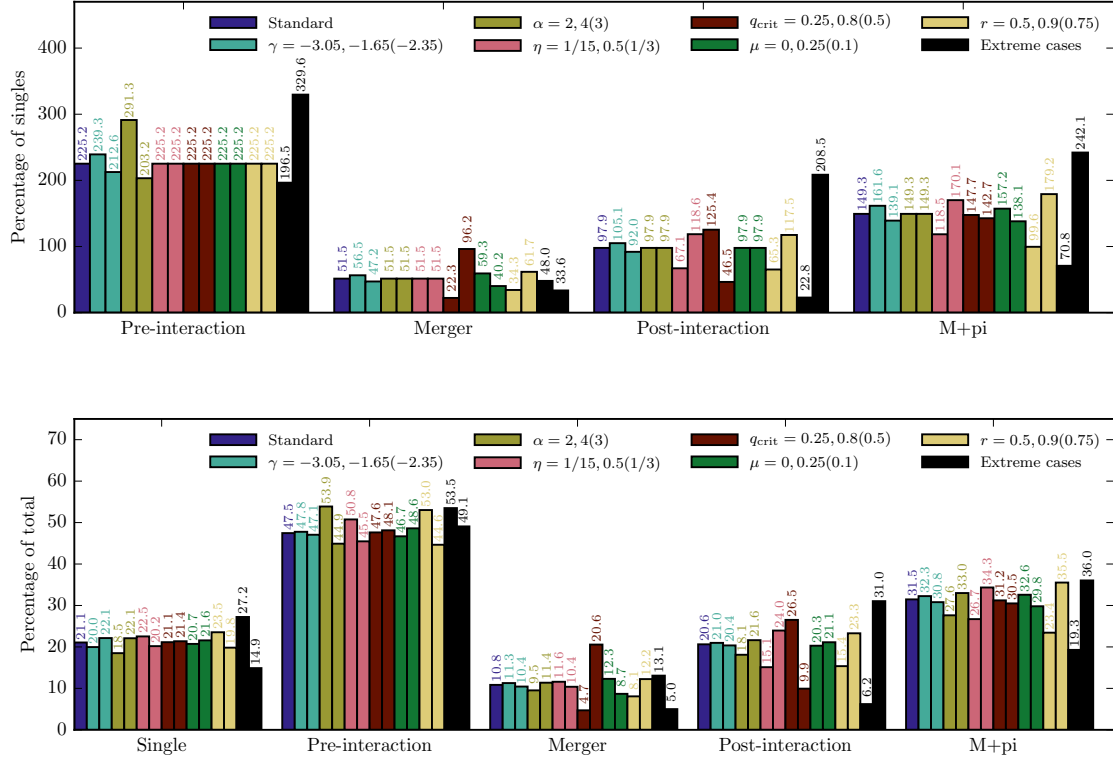


Figure 5.14: (top) Back of the envelope estimates for the contribution of single stars, mergers and both pre and post interaction binaries to an observable sample above a given threshold luminosity. Values are given in terms of the ratio to single stars. For simplicity we assume semi-detached systems are accounted in our estimate of post-interaction stars. The initial binary fraction is assumed to be  $f_{\text{bin}} = 0.7$ , pre-interaction systems are assumed to have average lifetimes corresponding to 75% of the main sequence lifetime of their primaries, while for mergers and post-interaction systems we assume their lifetimes are a factor  $r = 75\%$  of the main sequence lifetime corresponding to their final masses. For mergers, we assume 50% of them include a post main-sequence star and would not form core hydrogen burning objects. Different assumptions are made for the free parameters included, with values in parenthesis indicating the values chosen for the “standard” column. The “Extreme cases” columns combine the extreme values that respectively minimize and maximize the contribution of binaries. (bottom) Same as above, but showing the fraction of the total represented by each category.

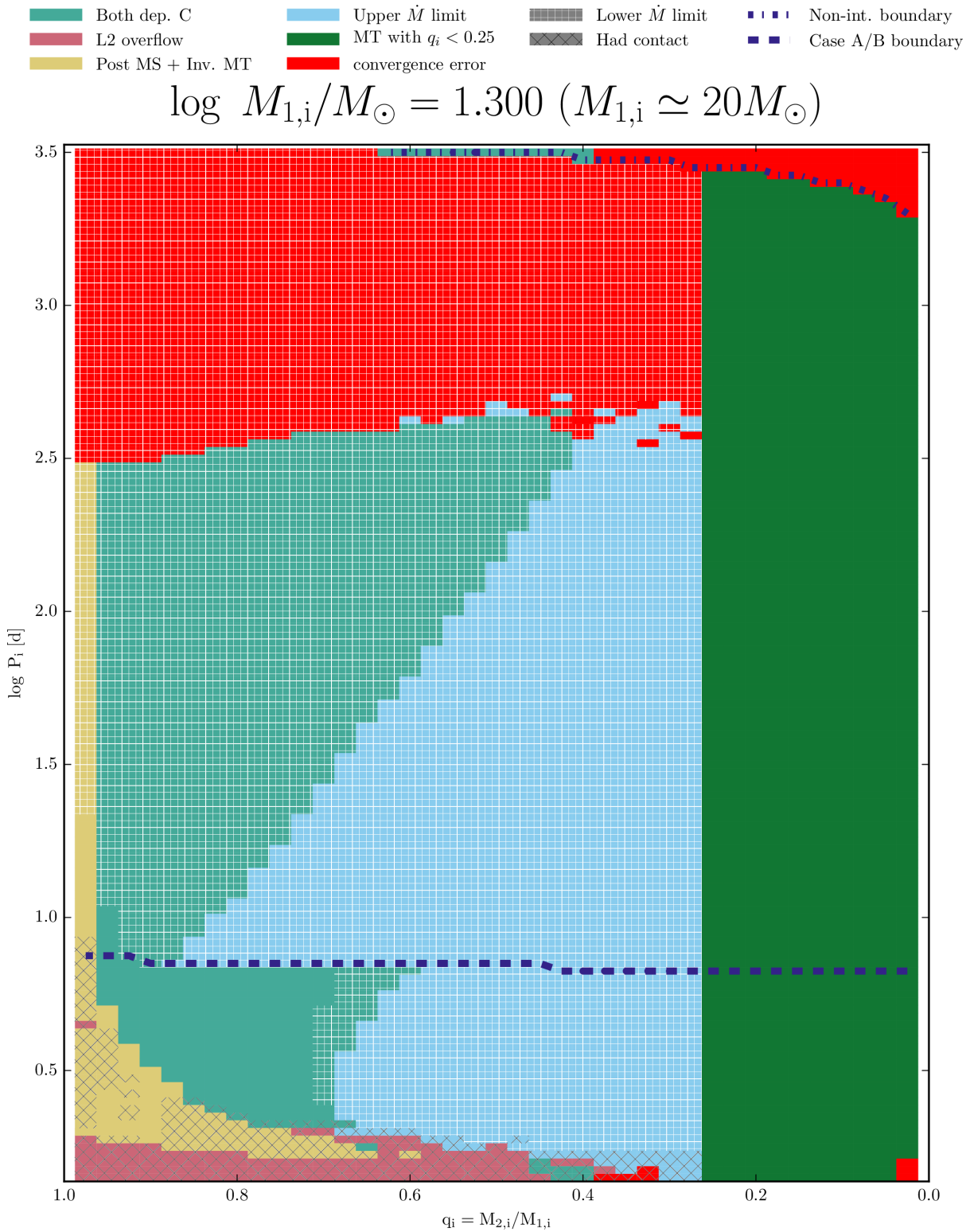


Figure 5.15: Grid of binary models for  $\log M_{1,i}/M_{\odot} = 1.30$  ( $M_{1,i} \simeq 20M_{\odot}$ ). See text for a detailed description of the different outcomes. At long initial orbital periods, interacting systems run into convergence issues due to the occurrence of unstable mass transfer.

ejection instead of a merger. We do not model this effect, but rather assume the outcome would be a merger.

- Lower  $\dot{M}$  limit: The limit on mass loss rates given by Equation (5.3) is reached. Models are evolved despite this happening, but it should be taken as a warning that radiation could be insufficient to drive such a strong mass loss from the system.
- Had contact: System underwent a contact phase. This does not necessarily imply that a merger happens.
- Non-int. boundary: Systems with periods above this boundary do not undergo RLOF.
- Case A/B boundary: Boundary between systems undergoing Case A and Case B mass transfer.

Model grids for all primary masses are included in Appendix E.

For three different primary masses we show the properties of binary models at detachment in Figure 5.16. In general, the highest mass transfer efficiencies are achieved in systems with higher initial primary masses undergoing case A mass transfer. Case AB and Case B mass transfer is very inefficient, with most case B systems modeled accreting less than 5% of the transferred material. For case A systems, accretion efficiency decreases with initial orbital period. This matches the prediction of de Mink, Pols and Hilditch (2007), who compare observed semi-detached systems to case A binary models with fixed mass transfer efficiencies. Modeled systems with high mass transfer efficiencies can also reproduce the massive eclipsing binary LMC-SC1-105, a semi-detached system composed of a  $30.9 \pm 1 M_{\odot}$  and a  $13 \pm 0.7 M_{\odot}$  star with an orbital period of 4.25 days (Bonanos, 2009).

## 5.4 Rotation and nitrogen enhancement

### 5.4.1 Single stars

Our single star models cover the range of masses  $\log M_i = 0.7 - 1.8$  ( $M_i \simeq 5 M_{\odot} - 60 M_{\odot}$ ) in intervals of 0.02 dex, and initial equatorial rotational velocities between 0 and  $600 \text{ km s}^{-1}$ . Systems are modeled until core carbon depletion, although for the more massive stars that lose their envelopes due to strong mass loss as red supergiants numerical problems limit our models to a point between helium ignition and helium depletion. In this work we focus on the main-sequence evolution of massive stars, so this does not affect our conclusions. Figure 5.17 shows the outcome of our stellar models in terms of nitrogen and helium enrichment during the main sequence. For slow rotators this is consistent with the results of Brott, de Mink et al. (2011), but in terms of helium enrichment we only find it happens in stars with masses above  $\sim 40 M_{\odot}$ , while the models of Brott, de Mink et al. (2011) show important amounts of enrichment already for  $20 M_{\odot}$  rapidly rotating stars.

### 5.4.2 Binary stars

In binaries that go through mass transfer and become detached post-interaction systems, nitrogen enrichment in the accreting stars is mainly determined by the accretion efficiency. Figure 5.18 shows how the surface nitrogen abundance and rotational velocities of the accretors in a Case A and a Case B system evolve. These are the same systems depicted in Figure 5.6, both of which don't have a particularly large accretion efficiency. The Case A system shown accretes  $\sim 40\%$  of the transferred material, with most of case AB mass transfer having a low accretion efficiency. The Case AB system shown is extremely inefficient with just a  $\sim 3.5\%$  of transferred material being accreted.

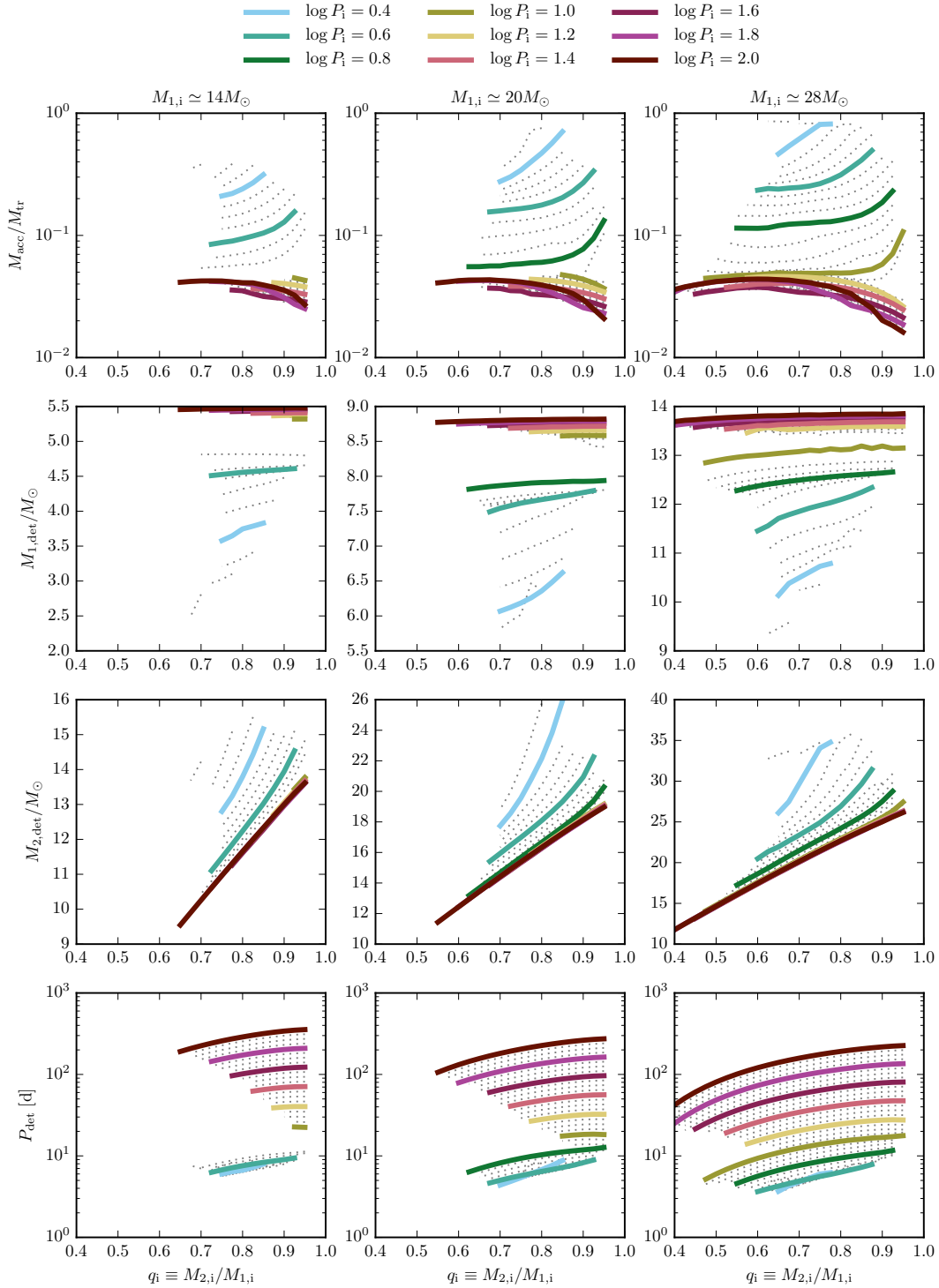


Figure 5.16: Properties of binary systems at detachment as a function of initial primary mass, orbital period and mass ratio. Individual lines correspond to a fixed initial orbital period, with dotted lines in intervals of 0.05 dex in  $\log P_i$  and colored lines in intervals of 0.2 dex in  $\log P_i$ . Results are shown for three different primary masses,  $\log M_{1,i} = 1.150$  ( $M_{1,i} \simeq 14M_\odot$ ) on the left column,  $\log M_{1,i} = 1.300$  ( $M_{1,i} \simeq 20M_\odot$ ) on the middle column and  $\log M_{1,i} = 1.450$  ( $M_{1,i} \simeq 28M_\odot$ ) on the right column. Top row indicates the mass transfer efficiency, middle rows show the mass of primaries and secondaries at the moment of detachment, while the bottom panel depicts the orbital period at detachment.

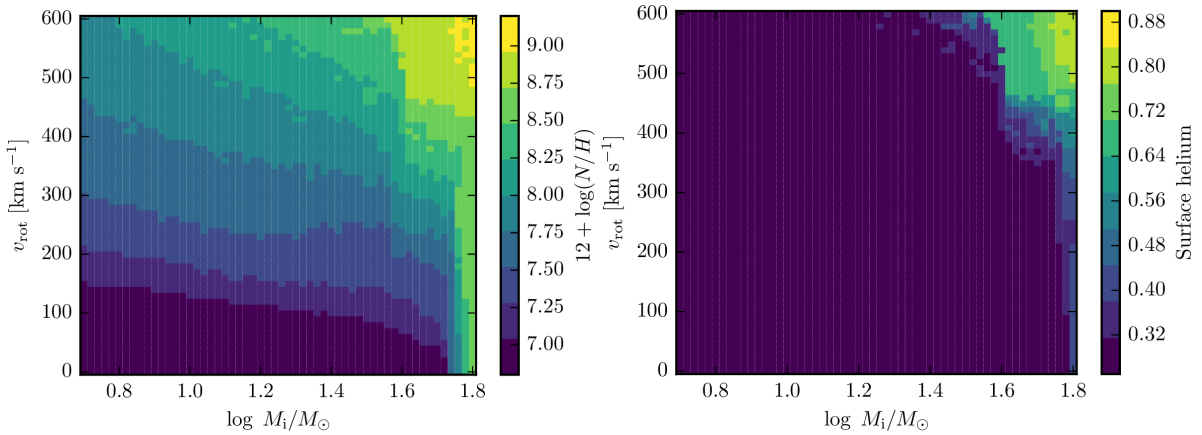


Figure 5.17: Surface nitrogen abundance and helium mass fraction at TAMS of single star models including rotation.

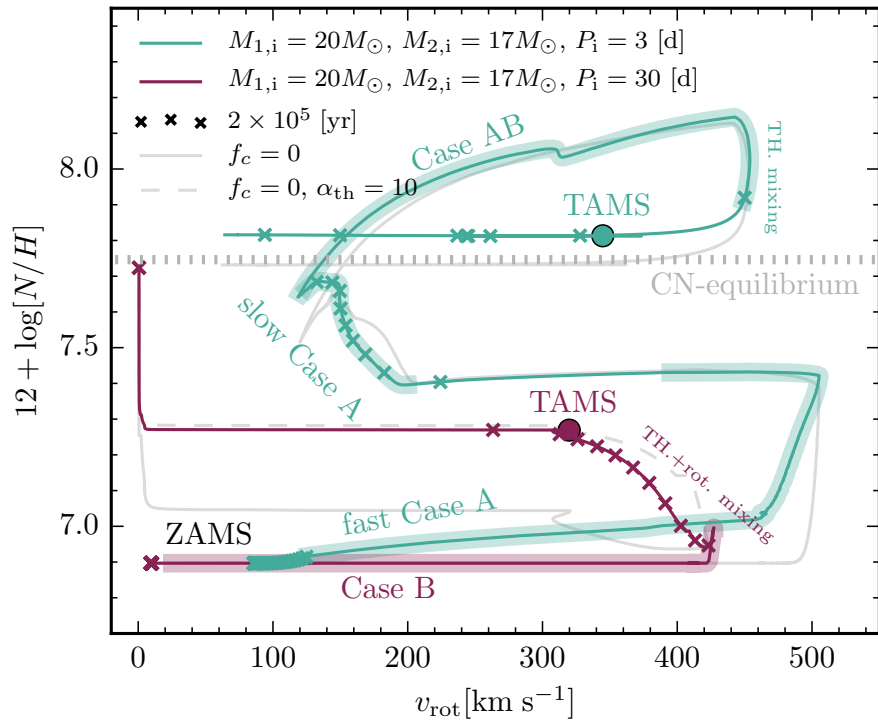


Figure 5.18: Nitrogen abundance and equatorial rotational velocity in the accreting stars of a Case A and a Case B binary. Thicker lines indicate the presence of mass transfer, and grey lines show the outcome of the same simulations, but with the efficiency of rotational mixing set to zero ( $f_c = 0$ ). For the Case B system modeled, we also include the results of a simulation with no rotational mixing, but with the efficiency of thermohaline mixing boosted by a factor of 10.

In the Case A system of Figure 5.18, most of the enrichment happens during Case A mass transfer, reaching close to CN-equilibrium values. Nitrogen abundance during Case AB rises significantly, but most of the enriched material that is accreted is rapidly mixed inwards and diluted due to thermohaline mixing. Also shown in Figure 5.18 is the evolution of this system in the absence of rotationally induced mixing (though we still include all angular momentum transport processes). Rotational mixing makes a very small difference in the final nitrogen abundance of this case A system, and together with its rotational velocity post-interaction, is very similar to the expectations from a rapidly rotating single star with rotational mixing.

For the case B system shown, The very small amount of accreted material means that after mass transfer the nitrogen abundance barely increases. However, two different processes take place that increase its surface nitrogen abundance during the remainder of its main sequence lifetime. The first and most obvious one is rotational mixing, but the mean molecular weight gradient left by the receding convective core limits the amount of mixing possible. The other process, which was already shown in Figure 5.7, is thermohaline mixing. Although mass transfer is very inefficient, a small amount of helium rich material is still accreted. This produces a mean molecular weight inversion which drives thermohaline mixing all the way down to helium rich layers. For the same model without rotational mixing, thermohaline mixing on its own can increase nitrogen abundances in  $\sim 0.15$  dex. Although this is small compared to observational errors (in particular for rapid rotators), it introduces an additional complexity, as the efficiency of thermohaline mixing is poorly well constrained. For the same model without rotational mixing, but with  $\alpha_{\text{th}} = 10$ , the same level of nitrogen enrichment as the model with rotational mixing can be reached.

### 5.4.3 Expected properties of apparent single stars

To model a population of binaries and single stars, we need to assume distributions for the initial parameters at zero age. Following Sana et al. (2012), we assume a flat distribution in mass ratios  $q \equiv M_2/M_1$  from zero to one, a distribution of initial periods  $f(\log P) \propto (\log P)^{-0.55}$ , and a binary fraction  $f_{\text{bin}} = 0.7$ . We assume a Salpeter mass distribution for primaries as well as for single stars, with  $dN/dM \propto M^\gamma$  with  $\gamma = -2.35$ . For the initial rotational velocities of single stars, we use the distribution of Ramírez-Agudelo et al. (2015) for single stars. Rapid rotators in this distribution could very well be the products of binary interaction (de Mink, Langer et al., 2013), so we expect this choice to overestimate the number of single stars that are rapid rotators at birth. To consider a region where our grid of models represents the full sample, we only count stars contained in a region of the HR diagram bounded by the location of the ZAMS and the TAMS for a  $15M_\odot$  and a  $25M_\odot$  star, and extended from the TAMS to lower temperatures ( $\log T_{\text{eff}} = 3.8$ ) to account as well for the possibility of long-lived blue supergiant phases.

Under these assumptions, the corresponding distributions of single stars and binaries in the HR diagram, and the distribution of rotational velocities and nitrogen abundances is shown in Figure 5.19 for apparent single stars. We do not model merged stars, so these are not included. Post-interaction systems in this mass range are seen not to contribute to the group of enriched and slowly rotating stars, which observations of B (Hunter et al., 2008) and O (Grin et al., 2016) type objects show to be overpopulated compared to the predictions of single stellar models. This region could potentially be populated by post-interaction systems if tidal interaction is strong enough, as shown by the models of Langer, Cantiello et al. (2008), but our grids of models do not display this effect. Models with inefficient accretion can properly account for rapidly rotating stars with low nitrogen abundances, though rotational and thermohaline mixing still increase the surface abundances by  $\sim 0.3 - 0.4$  dex.

Although in Figure 5.19 the ratio of binaries to true single stars is just of 18%, if we restrict the sample to those stars with projected rotational velocities in excess of  $200 \text{ km s}^{-1}$ , this ratio goes up to

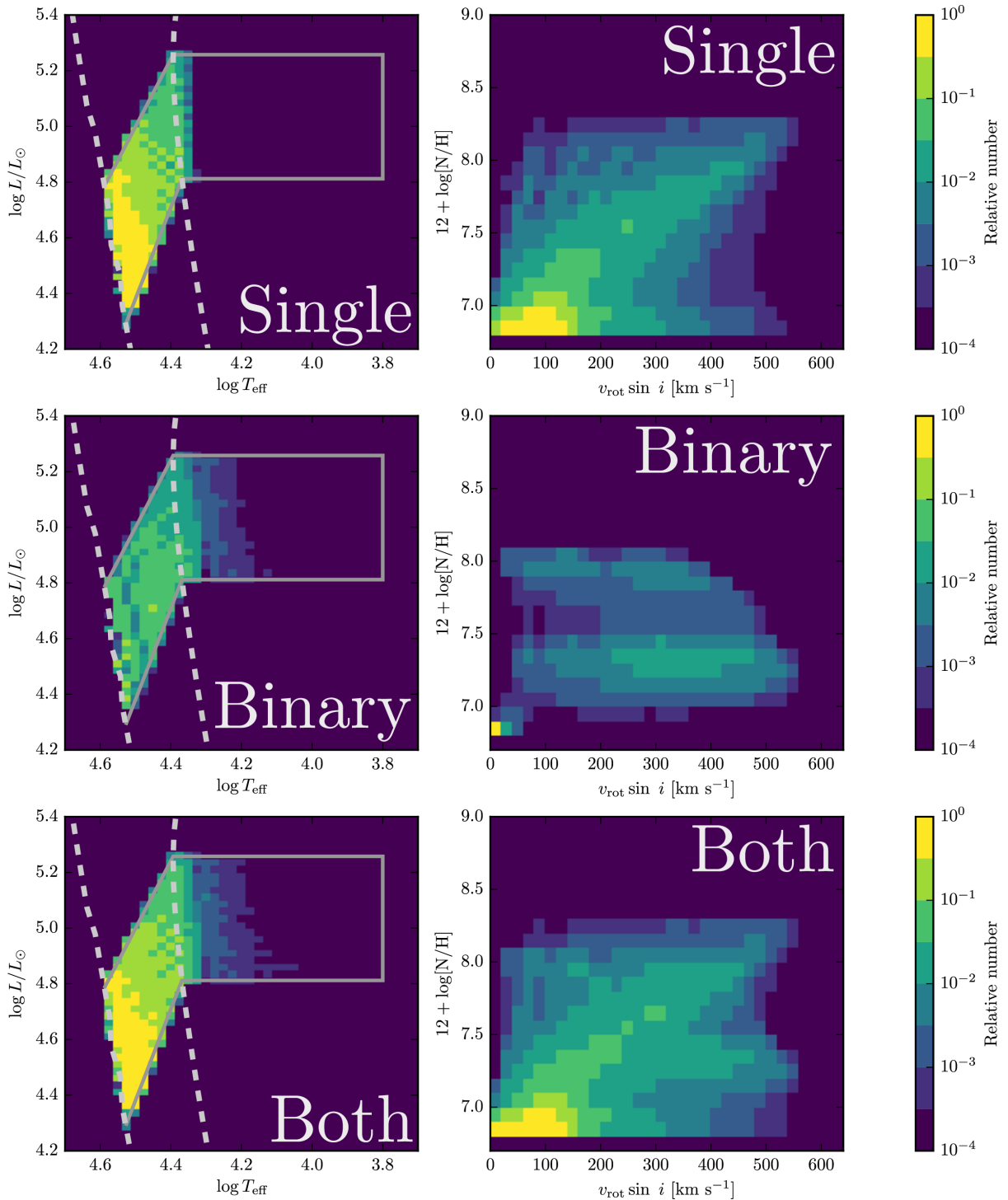


Figure 5.19: Single and binary apparent single stars (i.e. with radial velocity variations  $K < 10 \text{ km s}^{-1}$ ). Each row shows the distribution of objects in the HR diagram, together with their expected distributions of projected rotational velocities against nitrogen abundance, with the top row showing single stars, the middle row showing binaries, and the bottom row showing the combination of both. We limit our sample to the white box marked in the HR-diagram, which covers the main sequence evolution of single stars in the range of initial masses  $15M_{\odot} - 25M_{\odot}$ . Dashed lines indicate the ZAMS and the TAMS. The color plot represents the relative fraction of objects in each bin, normalized to the largest value in the combined sample of single+binary stars (bottom row). The ratio of post-interaction to single stars is just 18%, but if we only consider stars with projected rotational velocities above  $200 \text{ km s}^{-1}$ , the fraction of binaries to single stars is 57%. Note that stellar mergers are not included in this figure.

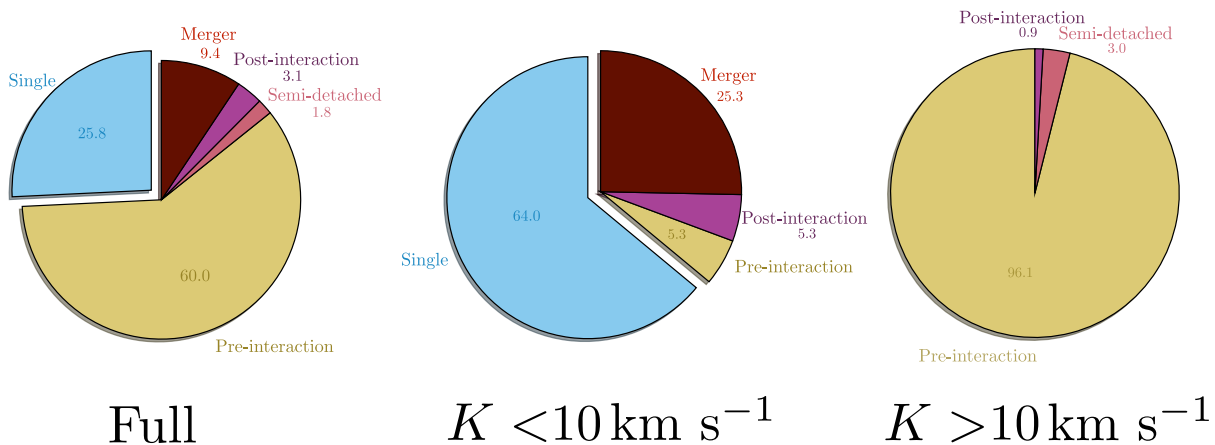


Figure 5.20: Fractions of each type of object contributing to the population of the limited region in the HR diagram depicted in Figure 5.19. Leftmost diagram contains the full sample, while the other two correspond to the case of objects with non detectable radial velocity variations ( $K < 10 \text{ km s}^{-1}$ ) and detectable radial velocity variations ( $K > 10 \text{ km s}^{-1}$ ). We do not model merger systems, so for simplicity we assume the values from de Mink, Sana et al. (2014), in terms of the ratio of mergers to single stars.

57%. Considering that the assumed distribution of initial rotational velocities should overestimate the number of single stars that are rapid rotators at birth, and that our choice of physical assumptions is meant to minimize the impact of post-interaction binaries in an observed sample of stars, the detection of rapid rotators with high amounts of nitrogen enrichment does not provide a strong argument in favor of rotational mixing.

## 5.5 Summary and Conclusions

Despite the drastic consequences rotational mixing can have in the evolution of massive stars, clear tests of its efficiency remain elusive. A generic prediction of stellar evolution models with efficient rotational mixing is the enrichment of their surfaces with nitrogen, but this can also happen due to efficient accretion. In this work we have showed that under extreme assumptions that minimize the contribution of post-interaction products in observations, spun-up accretors still represent a significant fraction of the total of apparent single rapidly rotating stars, which are the basis of the evidence in favor of rotational mixing.

Figure 5.20 reproduces the experiment done by de Mink, Sana et al. (2014), who considered the effect of removing stars from a sample for which radial velocity variations can be detected. Note that to account for the number of mergers, we simply assume the same fraction of mergers to single stars for each category from de Mink, Sana et al. (2014). We essentially recover their main result, that indicates that the best method to isolate single stars is to consider those with detectable radial velocity variations, as in this case the sample is dominated by pre-interaction binaries that should have mostly evolved as single stars. Moreover, although due to our assumptions the number of binary products is significantly smaller than the values of de Mink, Sana et al. (2014) (and just slightly lower than our extreme estimate in Section 5.2), in a sample of apparent single stars we still expect them to play a big role in the group of rapidly rotating objects.

Post-interaction systems can exhibit various degrees of enrichment depending on the efficiency of mass transfer. At low mass transfer efficiencies, accreting stars are spun up, but only accrete very small quantities of nitrogen enriched material. However, this still induces rotational and thermohaline mixing,

which can bring up their nitrogen abundance by more than 0.4 dex. Precise measurements of nitrogen abundances in rapidly rotating stars can then provide a clue to the efficiency of both rotational and thermohaline mixing. Most calculations of nitrogen abundances have issues on getting accurate results for high rotation rates, as spectral lines become broader and merge with each other. For instance, for stars with  $v_e \sin i > 170 \text{ km s}^{-1}$ , Grin et al. (2016) could only find upper limits on the abundances of O stars with rotations rates for all but one star. Observations with a much higher S/N are then required.

Although our models reproduce the trend of decreasing mass transfer efficiencies with increasing initial orbital periods described by de Mink, Pols and Hilditch (2007), all case B systems modeled have efficiencies well below 20%, with similarly low efficiencies for case AB mass transfer. This makes it difficult to account for Be X-ray binaries such as  $\gamma$  Cas, which consists of a  $\sim 16M_\odot$  Be star with a  $\sim 1M_\odot$  companion in a 204 day orbit of low eccentricity  $e \lesssim 0.03$  (Postnov, Oskinova and Torrejón, 2017). To reach such mass ratio high mass transfer efficiency is required, which in our models is only obtained for short period systems that detach at periods  $\lesssim 10$  days (see Figure 5.16). This is in clear contrast with the observed period for  $\gamma$  Cas. A similar system is  $\phi$  Per, a  $\sim 9M_\odot + 1M_\odot$  Be-sdO binary with a period of 127 days. A proper understanding of what sets mass transfer efficiency is still lacking, and systems like these Be binaries will potentially point towards an answer.

# CHAPTER 6

---

## Outlook

---

Despite the enormous progress made in the early and mid-20th century in the theory of stellar evolution, many uncertainties still remain. This is particularly the case for the evolution of massive stars, which is further complicated by the realization of the fundamental importance of binary interaction in their evolution (Kobulnicky and Fryer, 2007; Sana et al., 2012; Kobulnicky, Kiminki et al., 2014). Owing to the large impact massive stars have on the universe at much larger scales, understanding their evolution is paramount to our understanding of the universe. A general thread through this thesis has been on the potential impact of efficient rotational mixing in stellar evolution, an effect which is predicted to be behind some of the most luminous events in the universe, including long-duration gamma ray bursts (Woosley, 1993), super-luminous supernovae (Woosley, Blinnikov and Heger, 2007) and merging compact objects (Mandel and de Mink, 2016; Marchant et al., 2016). Such energetic phenomena provide a window of observation to stellar evolution in environments significantly different to that of our Galactic neighborhood. In particular through the effect of chemically homogeneous evolution, we have discussed in detail how future gravitational wave detections and X-ray observations can provide evidence for rotational mixing in stellar evolution.

The advanced aLIGO detectors have only recently restarted operations, and based on the results of their first science run, multiple additional detections of merging binary black holes are expected (The LIGO Scientific Collaboration et al., 2016b). The eventual detection of merging binary neutron stars, or neutron-star-black-hole binaries opens up as well the possibility of a simultaneous detection of gravitational waves and electromagnetic radiation, providing an extremely rich laboratory to study the properties of matter under extreme conditions (Baiotti and Rezzolla, 2016). As detections of merging black holes accumulate, their study will transition in less than a decade from case studies for a handful of observations to a full consideration of their demographics. This will place significant pressure on theorists to devise methods to differentiate the contributions from different channels, and is certain to bring unexpected surprises. The formation channel for merging binary black holes discussed in Chapter 3 provides simple predictions for the properties of merging binary black holes, with mass ratios very close to unity, high spins, and a gap in the distribution of black hole masses arising from pair-instability supernovae. In practice however, measurements have an important degeneracy between mass ratios and spins (Hannam et al., 2013), so a large number of events will be required to place strong constraints on these processes. The next generation of gravitational wave detectors, as well as the first space based detectors, will provide important additional information, but are more than a decade away from being a reality.

The detection of gravitational waves also has potential implications for the nature of ultra-luminous X-ray sources, since black holes with masses in excess of  $30M_{\odot}$  can reach extremely high luminosities

through accretion, even when strictly limited to their Eddington rates. As we showed in Chapter 4, chemically homogeneous evolution acting only on the primary of a binary system leads to the formation of X-ray binaries with massive stellar-origin black holes. Just as is the case for merging double black holes formed through chemically homogeneous evolution, pair-instability supernovae are predicted to produce a gap in the black hole mass distribution. If accretion is strictly limited to the Eddington rate, this mass gap translates into a gap in luminosities of ultra-luminous sources. The upcoming *e*ROSITA X-ray observatory (Merloni et al., 2012) is expected to perform a full sky survey, and could discover some of these sources. Still the question remains on what fraction of ultra-luminous sources are powered by neutron stars or black holes (A. King and Lasota, 2016).

Ideally, the effects of rotational mixing would be observable directly in rapidly rotating massive stars, but as was discussed in Chapter 5 mass transfer in binary systems can have very similar consequences, resulting both in spin-up and enrichment from CNO processed material. Given the important number of uncertainties in binary stellar evolution, proper comparisons between data and models will require the simulation of detailed model grids of single and binary stars, with varying degrees of mass transfer efficiencies, tidal strengths and semiconvective efficiencies among other factors. Such simulations will need to be coupled to proper statistical comparisons of observed data, following the example of Schneider et al. (2014) who employ Bayesian statistics to derive the properties of observed stars given a set of models for single stars. One particular group of objects for which large uncertainties remain are mergers. Detailed smoothed-particle hydrodynamic simulations of mergers have been computed for massive stars (Gaburov, Lombardi and S. Portegies Zwart, 2008; Glebbeek et al., 2013), but these model head-on collisions rather than the softer spiral-in that would be expected for field binaries. As magnetic fields might arise due to strong differential rotation (Ferrario et al., 2009; Wickramasinghe, Tout and Ferrario, 2014), fully three dimensional magnetohydrodynamic simulations of mergers with realistic initial conditions for field binaries can provide valuable information, and serve as input for 1D stellar evolution codes to study their long-term evolution.

In the coming years new observational facilities will provide us with increasingly better constraints on the evolution of massive stars. Just in recent years transient surveys such as the Palomar Transient Factory (Rau et al., 2009), Pan-STARRS (Kaiser et al., 2002) and the Dark Energy Survey (Dark Energy Survey Collaboration et al., 2016) among many others have discovered several new types of transient events. Surveys like these have allowed the recognition of multiple progenitors to supernovae, which suggest a lack of supernovae explosions for stars with initial masses above  $18M_{\odot}$  (Smartt, 2015), as well as candidates for failed supernovae, where a red supergiant star suddenly disappears without the occurrence of a supernova (Gerke, Kochanek and Stanek, 2015; Adams et al., 2016). The detection of several supernovae by these transient surveys, coupled with measurements of metallicities for their host galaxies, can also serve to constrain stellar evolution models, as both mass loss and binary interaction can significantly modify the evolution of supernova progenitors (Podsiadlowski, Joss and Hsu, 1992; N. Smith, Li et al., 2011; Meynet et al., 2015). The relatively new class of luminous red novae is likely the product of a merger (Kulkarni et al., 2007), providing additional insight into some of the least understood aspects of binary evolution. This wealth of information is only expected to increase, as surveys such as the Zwicky Transient Facility (Bellm, 2014) and the Large Synoptic Survey Telescope (Oluseyi et al., 2012). Meanwhile, the Gaia space telescope will soon provide an unprecedented view on the distribution of stars in the Galaxy and the Large and Small Magellanic Clouds, while the James Webb Space Telescope and the European-Extremely Large Telescope are expected to observe the first stars within the next decade.

This enormous amount of information from multiple sources will provide valuable insight, as well as strong constraints to our theoretical models, certainly making the field of stellar evolution a very entertaining one to be a part of.

## APPENDIX A

---

### Dynamical implications of black hole kicks

---

After a tight binary system with two BHs is formed, the continuous radiation of gravitational waves will cause loss of orbital energy and a resulting shrinkage of the orbit (Einstein, 1918). The timescale until the two binary components finally merge depends on the BH masses, the orbital period, and the eccentricity of the system (Peters, 1964). The initial parameters of BH+BH binaries depend not only on the stellar evolution of the progenitor stars, but also on the physics of the BH formation process itself.

The formation of BHs may be accompanied by a momentum kick, similar in nature to those imparted onto newborn NSs (Janka, 2012), in particular if the core of the progenitor does not collapse directly to a BH but in a two-step process (Brandt, Podsiadlowski and Sigurdsson, 1995). However, while the magnitude of such kicks for NSs is fairly well constrained from pulsar observations (Hobbs et al., 2005), the magnitude of kicks imparted onto a BH during its formation is rather uncertain. So far, the measured masses of observed stellar-mass BHs are all relatively low:  $4 - 16 M_{\odot}$  for all the Galactic sources (McClintock, Narayan and Steiner, 2014), about  $16 M_{\odot}$  for M33 X-7 (Orosz et al., 2007) and  $24 - 33 M_{\odot}$  for IC 10 X1 (A. H. Prestwich et al., 2007). Their inferred BH kicks from observations and theoretical arguments span from basically no kicks (Nelemans, Tauris and van den Heuvel, 1999) to BH kicks of several 100 km/s (Janka, 2013) based on hydrodynamical kicks associated with asymmetric mass ejection and subsequent BH acceleration.

For massive stellar mass BHs, the situation is different since their progenitor stars more likely collapse directly to form a BH without a SN explosion, leading to BHs with very low kick velocities. Thus, a bimodality of the BH kick velocity distribution seems possible (Janka, 2013). Another, and possibly related, problem is the amount of mass loss during BH formation (ejected baryonic mass and rest mass energy carried away by neutrinos), which also affects the orbital period and the eccentricity of the post-collapse system.

To quantify the combined effects of mass loss and kicks, we assume in the following example that a  $50 M_{\odot}$  Wolf-Rayet (WR) star collapses to form a BH with a gravitational mass of  $40 M_{\odot}$ . In other words, we assume that  $10 M_{\odot}$  of mass is lost by a combination of baryonic mass loss and/or losses through neutrinos from outside the event horizon. A large amount of baryonic mass loss may be expected if the progenitor core rotates rapidly and the collapse is associated with an LGRB and an LGRB supernova.

We first consider the no-kick case for a circular pre-collapse system with two  $50 M_{\odot}$  stars and an orbital period of 2.0 days. If there is no mass loss and no kick imparted to the newborn BH, the orbital parameters of the binary system remain unchanged and the system would merge in 550 Myr. The result of an instantaneous mass loss of  $10 M_{\odot}$  during the BH formation produces a post-collapse system with an orbital period of 2.52 days and an eccentricity of 0.11 (and stellar masses of  $40 M_{\odot}$  and  $50 M_{\odot}$ ), which will merge in 1180 Myr. If BH formation is accompanied by an additional momentum kick, however, the

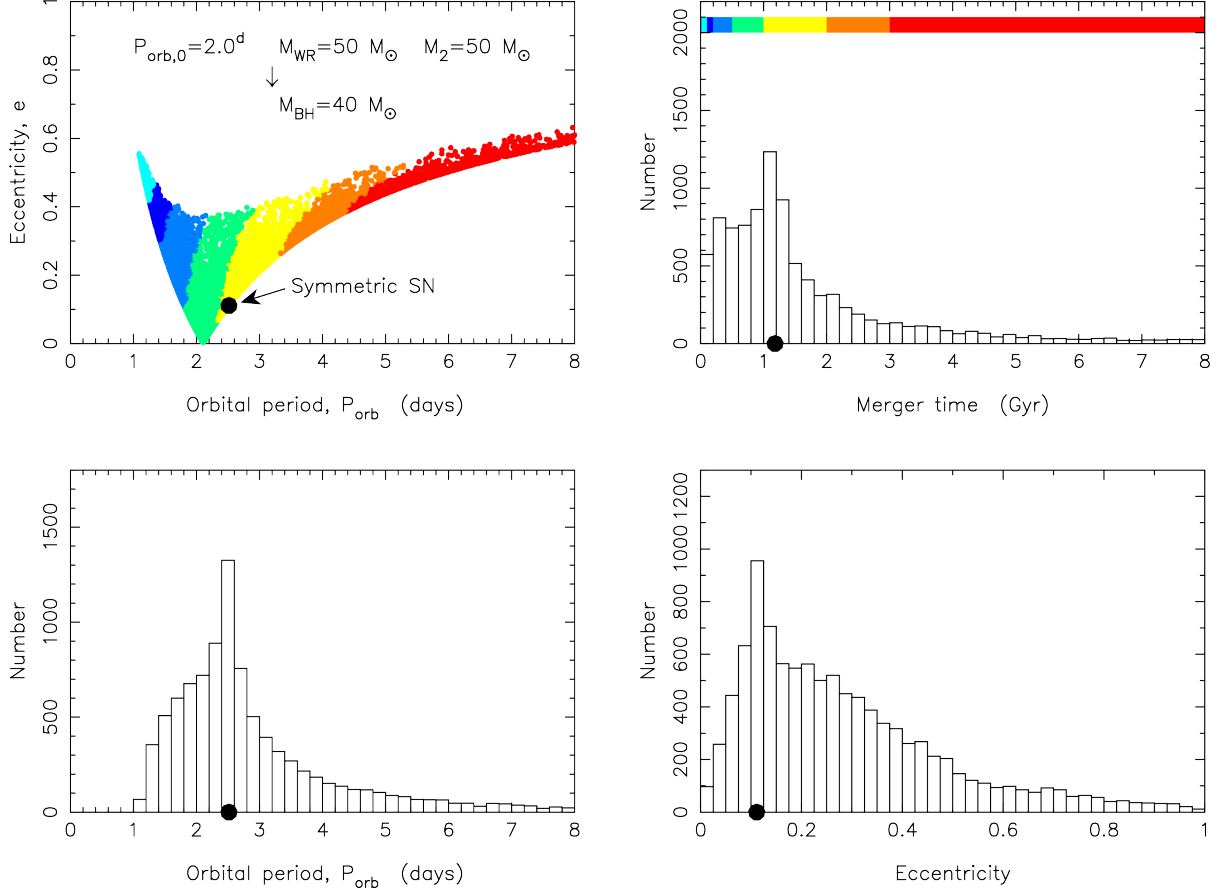


Figure A.1: Simulations of the dynamical effects of 10 000 asymmetric SNe on BH binary systems. The initial pre-SN system contains two  $50 M_{\odot}$  stars in a binary with an orbital period of 2.0 days. During the formation of a BH, it is assumed that  $10 M_{\odot}$  is lost instantaneously and a kick velocity is imparted with a magnitude between  $0 - 300 \text{ km s}^{-1}$ , drawn from a flat distribution and an isotropic (random) distribution of kick directions. The upper left panel shows the resulting post-SN systems in the orbital period–eccentricity plane. The colours indicate the merger time of the post-SN system as a result of gravitational-wave radiation (see the distribution in the upper right panel). The lower panels show the distributions in orbital period and eccentricity of the post-SN binaries. The case of a purely symmetric SN (no kick) is indicated with a black dot in all panels.

---

outcome can change significantly.

In Figure A.1 we plot the dynamical consequences for a surviving binary system, using the same initial parameters as before, in which a BH is produced with an asymmetric kick velocity and instantaneous mass loss, following the recipe of Hills, 1983. In a BH+BH binary, two kicks may be imparted, but here we restrict our example to just one kick to better illustrate the principal dynamical effects – the analysis can easily be generalized to two kicks without changing the main conclusions. We performed 10 000 trials, assuming a flat distribution of the BH kick magnitudes between  $0 - 300 \text{ km s}^{-1}$  and an isotropic (random) distribution of directions. If a randomly orientated kick of a fixed magnitude of  $300 \text{ km s}^{-1}$  ( $600 \text{ km s}^{-1}$ ) were applied in all cases, it would result in the disruption of about 7.3 per cent (43 per cent) of the cases. Using a flat distribution between  $0 - 300 \text{ km s}^{-1}$ , only 0.4 per cent of all systems are disrupted. Thus even for a wide range of assumed BH kick values, the survival rate of BH+BH binaries only changes by less than a factor of two.

More important for our investigation here is the merger timescale that is due to gravitational-wave radiation. Figure A.1 shows that the effect of a kick can either widen or shorten the post-collapse orbit. However, the merger timescale for a binary with given component masses is a function of both orbital period and eccentricity. Given that systems which widen more during BH formation (as a consequence of instantaneous effective mass loss and a kick) are also the systems attaining the higher eccentricities, the net effect of a kick on the resulting merger time is surprising small. For BH formation without a kick, the merger timescale of the resulting binary is 1180 Myr. Using a flat kick distribution between  $0 - 300 \text{ km s}^{-1}$  results in roughly half (47 per cent) of the surviving systems to merge on a shorter timescale, and the other half to merge on a longer timescale (and only 2.5 per cent exceeding a Hubble time).

Applying a strong kick of  $600 \text{ km s}^{-1}$  actually causes a larger fraction of surviving systems to merge (67 per cent) on a shorter timescale ( $< 1180 \text{ Myr}$ ) than in the symmetric case without a kick. Therefore, we can safely conclude that although BH kicks may, in general, widen a number of systems, the resulting merger timescale distribution will not change one of the main findings of this paper, namely that the LIGO detection rate is likely to be dominated by quite massive BH+BH mergers.



## APPENDIX B

---

# Comparison to the standard BH+BH formation scenario

---

The standard formation scenario of BH+BH binaries involves a number of highly uncertain aspects of binary interactions (Fig. B.1, Tauris and van den Heuvel 2006). The main uncertainties include, in particular, the treatment of common-envelope evolution (Ivanova et al., 2013) and the efficiency of accretion and spin-up from mass transfer. These lead to uncertainties in the expected merger rates of several orders of magnitude (Abadie, B. P. Abbott, R. Abbott, Abernathy et al., 2010). In contrast, the MOB scenario presented here mostly relies on reasonably well understood physics of the evolution of massive stars, although there are still significant uncertainties, for instance, in the treatment of stellar winds (Langer, 2012), rotational mixing (Maeder and Meynet, 2012), and the BH formation itself (Heger, Fryer et al., 2003; Ugliano et al., 2012; Pejcha and T. A. Thompson, 2015).

To produce a tight BH binary that will merge within a Hubble time, we could consider a very close massive binary system with an initial orbital period of a few days. The problem with such a model is that these systems would mostly be expected to merge early during their evolution when the more massive star evolves off the main sequence, expands, and starts to transfer mass to its companion star. Although other models have been proposed that evolve without a common-envelope phase, for example to explain the formation of IC 10 X-1 (de Mink, Cantiello et al., 2009) and M33 X-7 (Valsecchi et al., 2010), they often require some degree of fine-tuning to work and did not follow the evolution to the end to produce a binary with two BHs.

To avoid this problem, it has been common practice to model the formation of BH+BH systems starting from relatively wide systems and let the systems evolve through a common-envelope phase following the high-mass X-ray binary (HMXB) phase after the formation of the first BH (see Fig. B.1). There are currently no self-consistent hydrodynamical simulations for modelling the spiral-in of BHs inside a massive envelope; in particular, it is unclear whether the BH will experience hypercritical accretion, and under which conditions the systems will merge completely; all of this leads to large uncertainties in the number of post-common-envelope systems and their separations (Ivanova et al., 2013).

Another problem that is often ignored is that the fate of a massive star in a binary depends on when it loses its hydrogen-rich envelope. As first pointed out by Brown (Brown, Lee and Bethe, 1999) and confirmed in later calculations (Brown, Heger et al., 2001) (see also Petermann, Langer & Podsiadlowski; in preparation), if a massive star loses its hydrogen-rich envelope before or early during helium core burning, it ends its evolution with a much smaller iron core and is more likely to produce an NS than a BH. This means that the formation of a BH in a close binary may require that its progenitor loses its envelope only after helium core burning. To produce not just one, but two BHs, this may require extreme

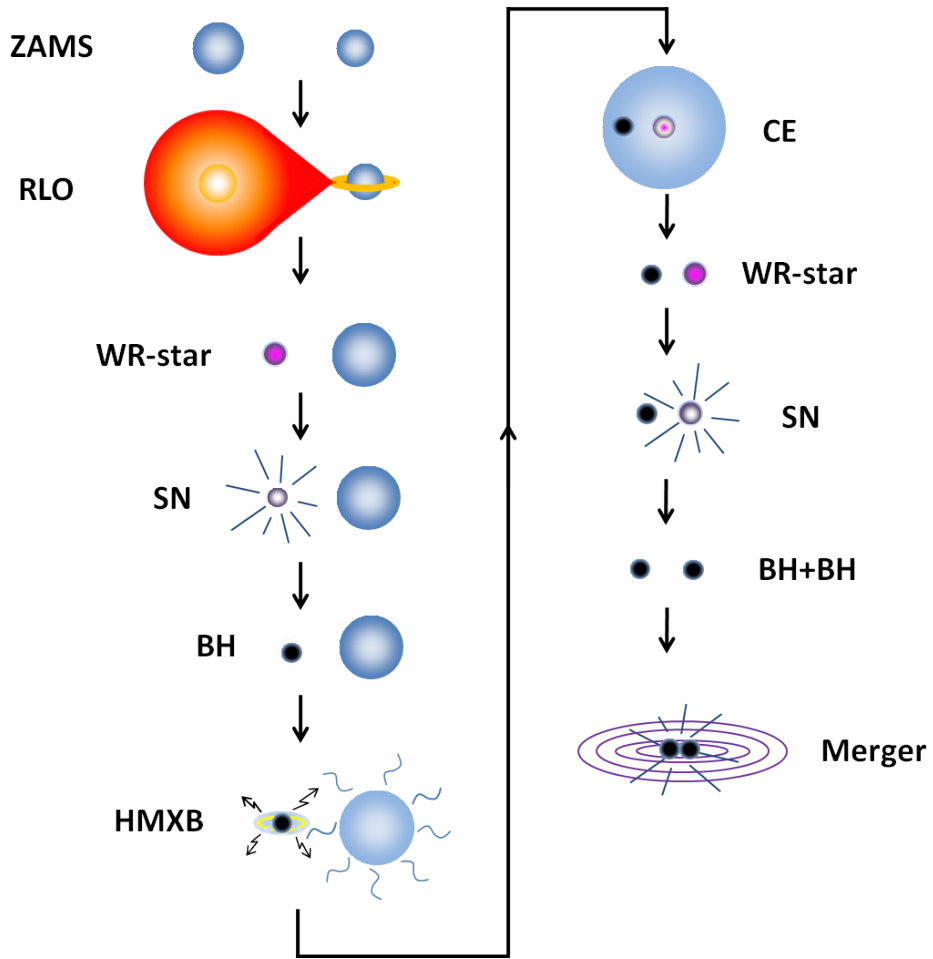


Figure B.1: Illustration of the binary stellar evolution leading to a BH+BH binary according to the standard scenario. Acronyms used in the figure. ZAMS: zero-age main sequence; RLO: Roche-lobe overflow (mass transfer); WR-star: Wolf-Rayet star; SN: supernova; BH: black hole; HMXB: high-mass X-ray binary; CE: common envelope.

fine-tuning and may even be impossible in the standard scenario in Fig. B.1. The problem may be avoided in the so-called double-core scenario (Brown, 1995; Dewi, Podsiadlowski and Sena, 2006), where the BH progenitors both evolve beyond helium core burning before experiencing a common-envelope phase in which the cores of both stars spiral in, producing a close binary of two helium stars that subsequently collapse to form BHs. However, this scenario requires significant fine-tuning since the initial masses of the two stars have to be very close to each other ( $q_i > 0.96$ ), and it may be impossible to produce quite massive BHs because very massive stars tend to avoid mass transfer after helium core burning (although this may be possible at sufficiently low metallicity ( $Z \lesssim 0.1 Z_\odot$ )).

Given that all measured stellar-mass BHs in the Milky Way have masses in the range of  $4 - 16 M_\odot$ , most population-synthesis models used for estimating LIGO detection rates were previously restricted to initial progenitor stellar masses of up to about  $100 M_\odot$ . The discovery of very massive stars (Crowther, Schnurr et al., 2010; Hainich et al., 2014) in the R136 region of the Large Magellanic Cloud with masses of up to  $300 M_\odot$ , however, suggests that BH+BH binaries may form with significantly more massive components, thus enabling LIGO to detect the merger of such massive BH+BH binaries, with chirp

---

masses easily exceeding  $30 M_{\odot}$ , out to long distances (see discussion in Sect. 3.3).

It has previously been argued (Belczynski, Buonanno et al., 2014; Rodriguez, Morscher et al., 2015) that massive BH+BH binaries to be potentially detected by LIGO can only form through dynamical channels in dense stellar environments. We here demonstrated that close binaries in the Galactic disk with very massive stars undergoing chemically homogeneous evolution (and which therefore do not expand after leaving the main sequence) can form massive BH+BH binaries that merge within a Hubble time at sufficiently low metallicity. An important consequence of our scenario is that massive BHs of a given mass can be produced from stars with a lower ZAMS mass – especially at low metallicity – than in the standard BH+BH formation scenario.

So far, no stellar-mass BH+BH binaries have been discovered anywhere, and there is only one known potential progenitor system in the Milky Way, Cyg X-3. The nature of the compact component in this system is still uncertain. Belczynski, Bulik et al., 2013 have argued that it contains a  $2 - 4.5 M_{\odot}$  BH and a  $7.5 - 14.2 M_{\odot}$  WR-star, which would make it a potential progenitor for a BH+BH system. However, the final destiny of this system is unclear, and it might also become a BH-NS binary or even NS+NS binary (if the first-formed compact object is a neutron star). It is also possible that the system is disrupted as a result of the explosion of the WR-star.



## APPENDIX C

---

### Grids of binary models leading to ULXs

---

A summary of the outcomes of our simulations is presented in Figures C.1-C.9. The meaning of the different labels in those figures is as follows:

- ZAMS L2OF: The initial orbital separation is so short that the system overflows the L2 Lagrangian point at ZAMS. Such a system should rapidly merge.
- ZAMS RLOF: System is undergoing RLOF at ZAMS. As shown in Marchant et al. (2016), these overcontact systems might survive interaction without merging, resulting in a binary with equal mass components. However, for low mass ratios we mostly expect the systems to evolve into deep contact and merge, and even for systems that avoid that, they would not follow the channel for ULX formation described in this work.
- off CHE: Primary reached a point where the difference between central and surface helium abundance is larger than 0.2. We consider such systems are not evolving chemically homogeneous, and terminate these simulations.
- Case B/BB: The primary evolves chemically homogeneous and forms a BH. The secondary then initiates mass transfer and a possible ULX phase after depleting its central hydrogen. These systems are only expected to have a brief ULX phase. Some of these systems undergo an additional phase of case BB mass transfer after core helium depletion.
- Case AB/ABB: Similar to the previous one, only that mass transfer is initiated while the secondary is on the MS so it operates on a much longer nuclear timescale.
- PISN: The final mass of the primary at helium depletion is in the range  $60 < M_{1,f} < 130$ , so we expect to result in a SN leaving the secondary as a single star.
- no MT (double BH): Both stars evolve chemically homogeneous, avoiding mass transfer and resulting in a compact binary BH. This is the path of evolution discussed in Marchant et al. (2016). For the mass ratios studied, only a handful of these systems are found.
- MT before BH forms: Mass transfer, either from the primary or the secondary, happens before BH formation. We expect such systems to either merge (in case the primary is the donor) or widen and interrupt CHE because of accretion of hydrogen-rich material (if the secondary is the donor), which would not result in the formation of a ULX.
- convergence error: Due to numerical problems the simulation was not completed.

- Darwin unstable: At its initial state the system has an orbital separation smaller than  $a_{\text{Darwin}}$ , and thus is Darwin unstable. It would not be possible to form a synchronized binary with this orbital separation, as it would result in a merger instead. The moment of inertia is dependent in the initial rotation rate, which results in some irregularities in the boundary between stable and unstable models.

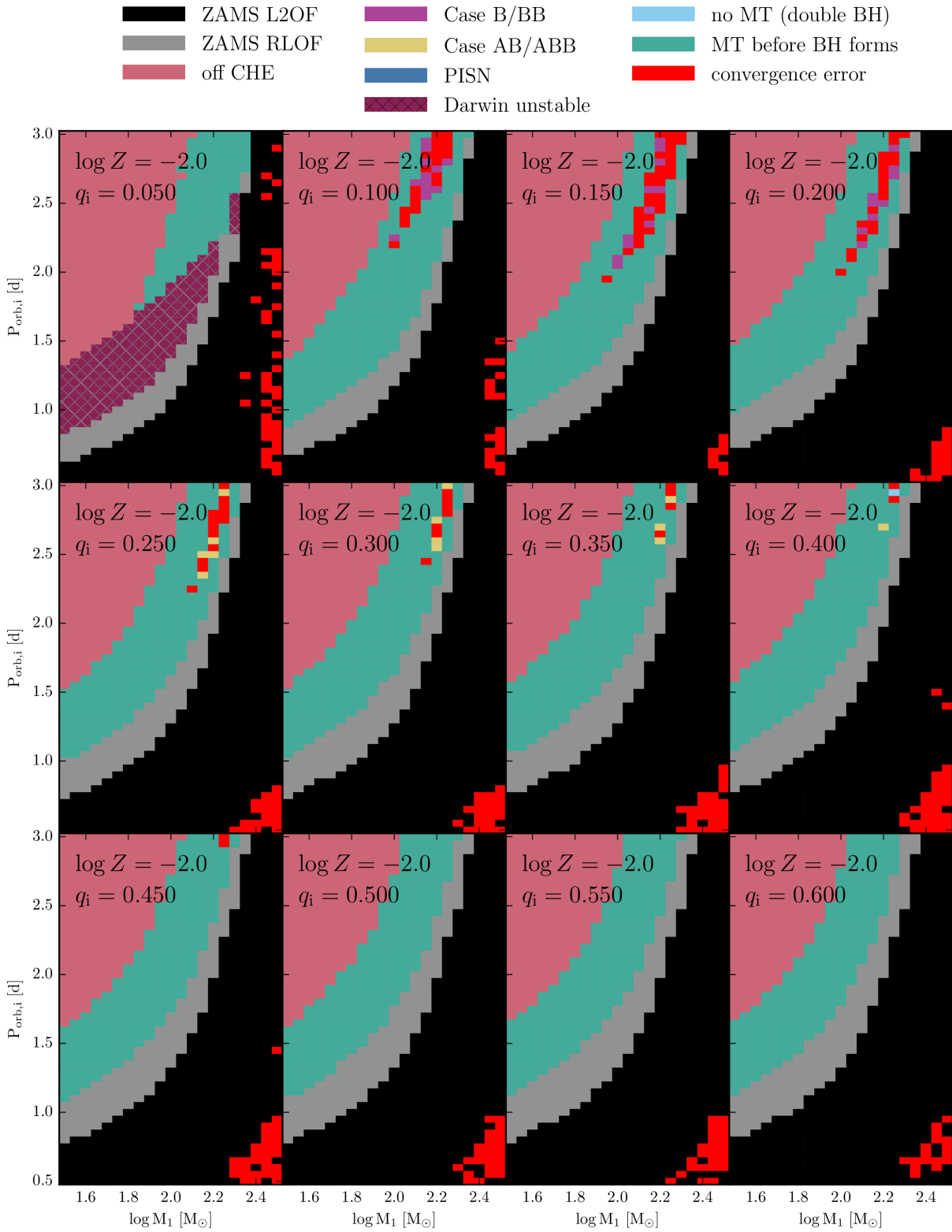


Figure C.1: Grid of models for  $\log Z = -2.0$ . See text in Appendix C for an explanation.

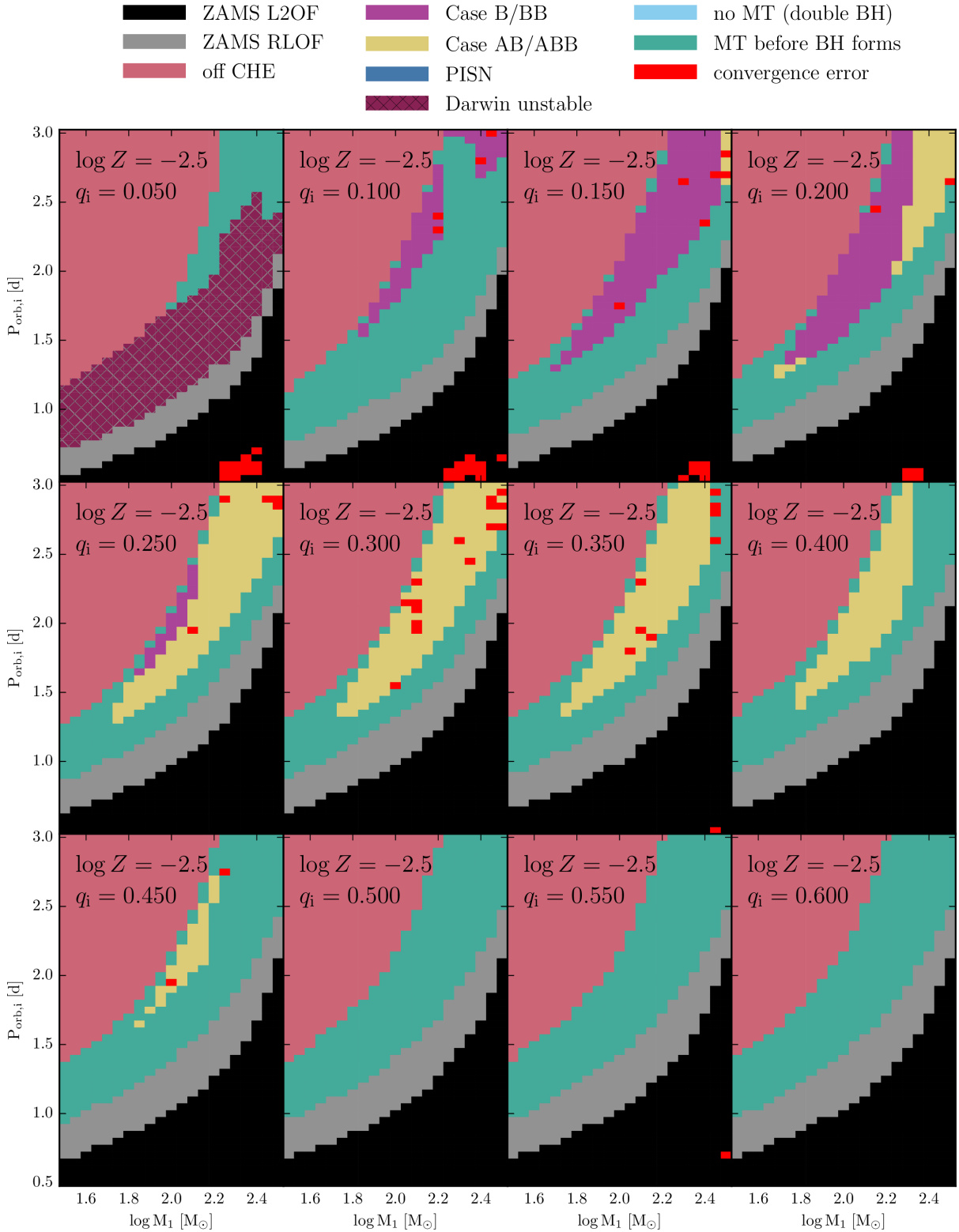


Figure C.2: Grid of models for  $\log Z = -2.5$ . See text in Appendix C for an explanation.

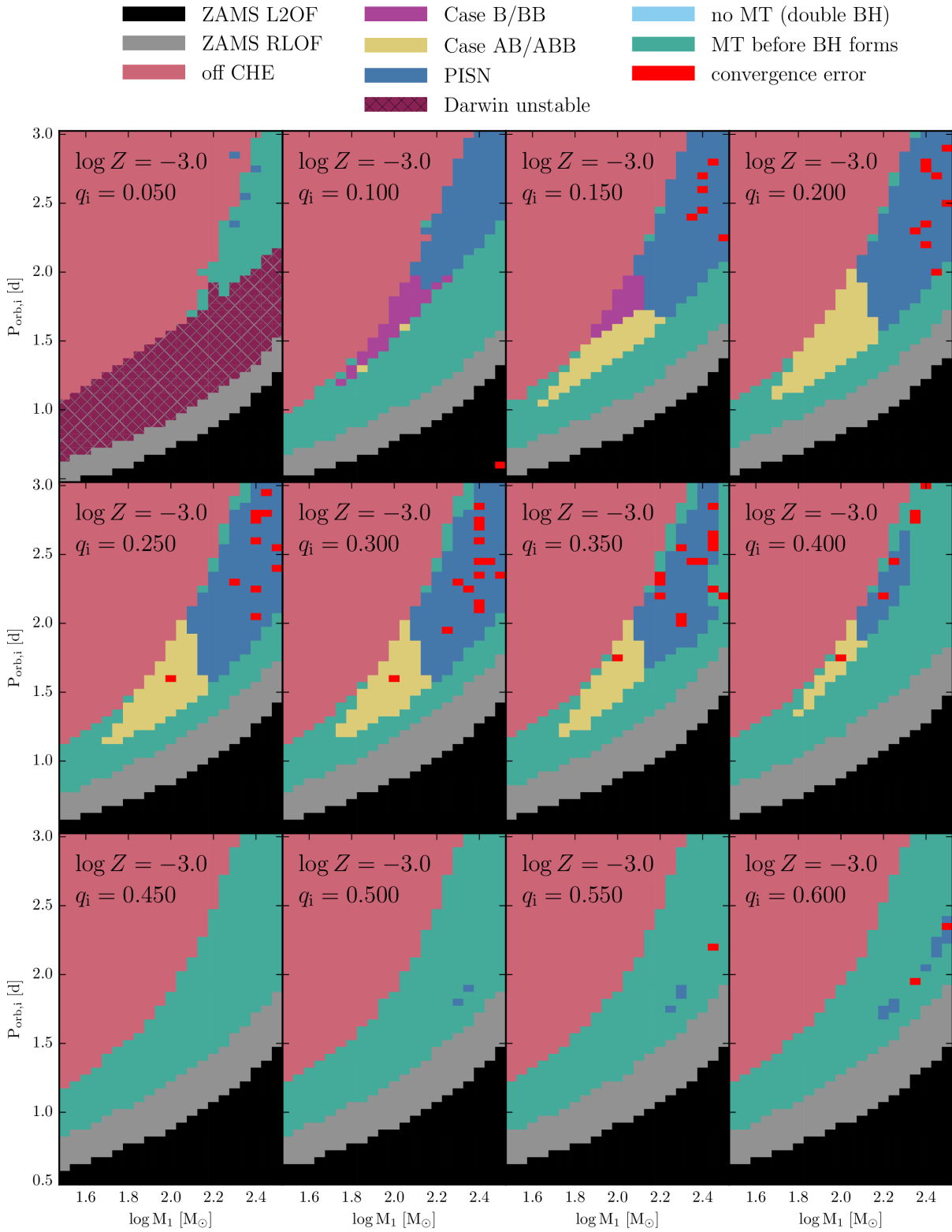


Figure C.3: Grid of models for  $\log Z = -3.0$ . See text in Appendix C for an explanation.

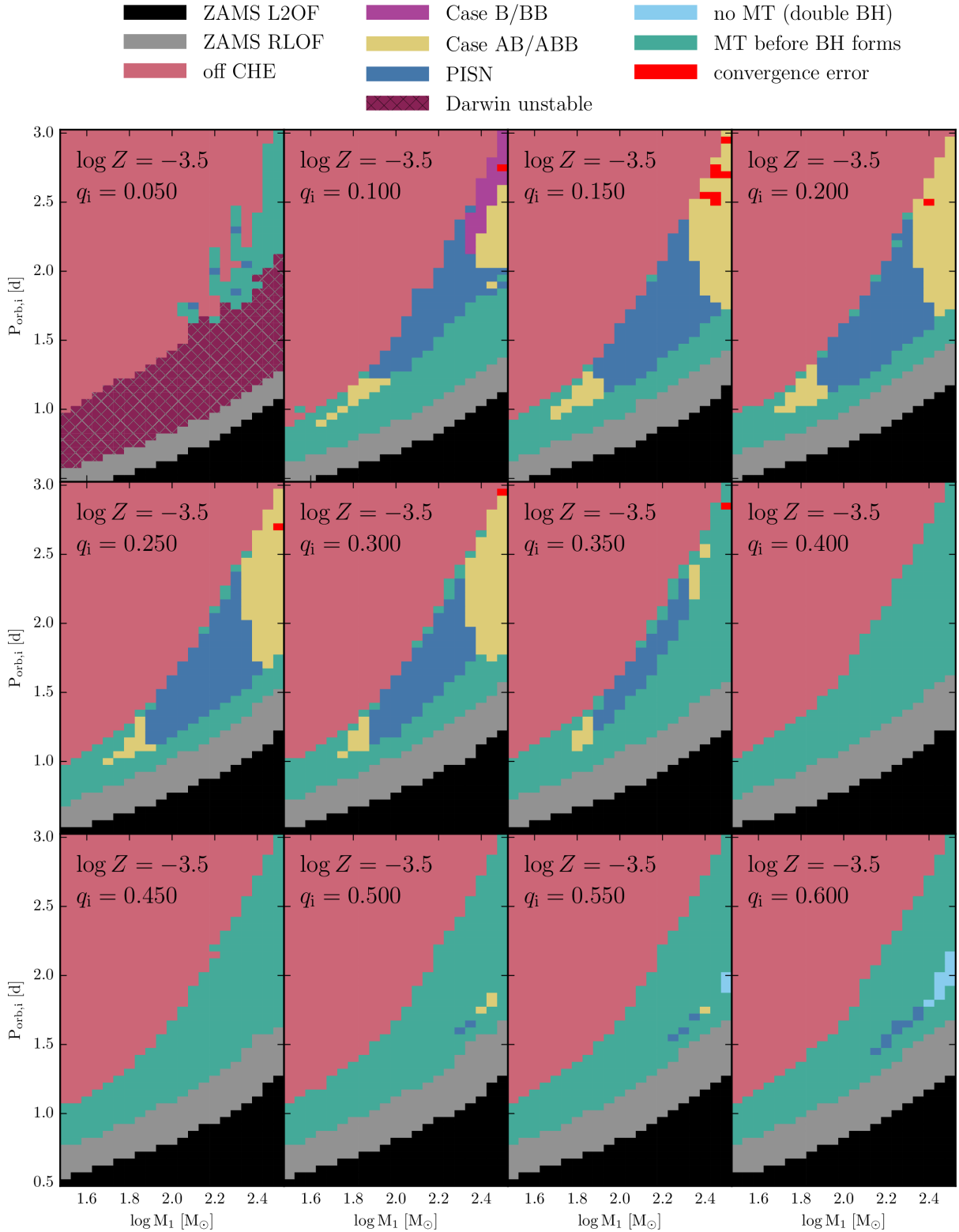


Figure C.4: Grid of models for  $\log Z = -3.5$ . See text in Appendix C for an explanation.

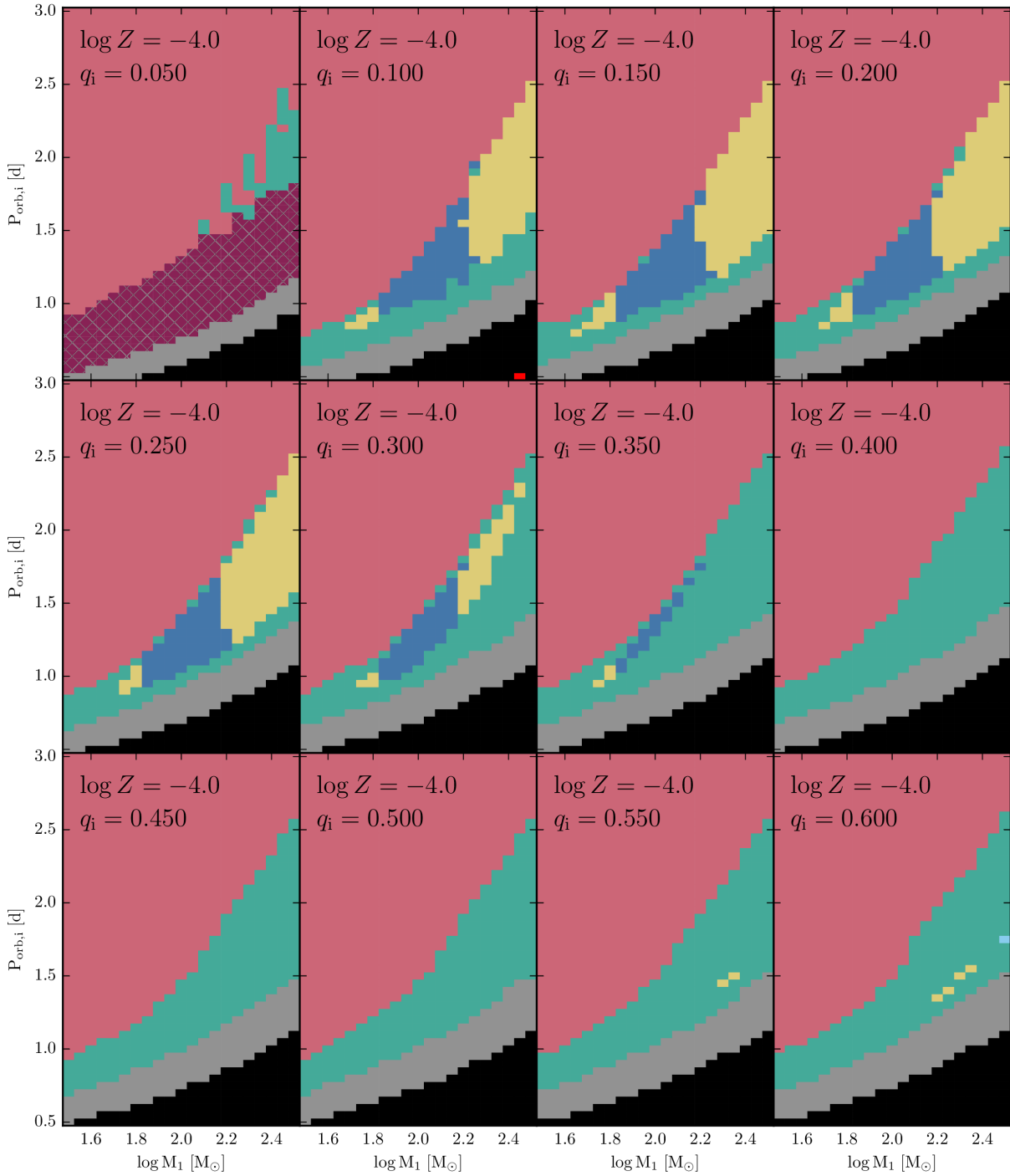
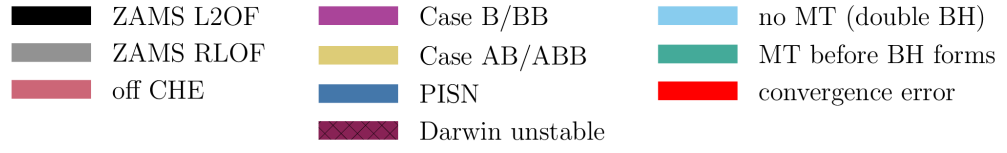


Figure C.5: Grid of models for  $\log Z = -4.0$ . See text in Appendix C for an explanation.

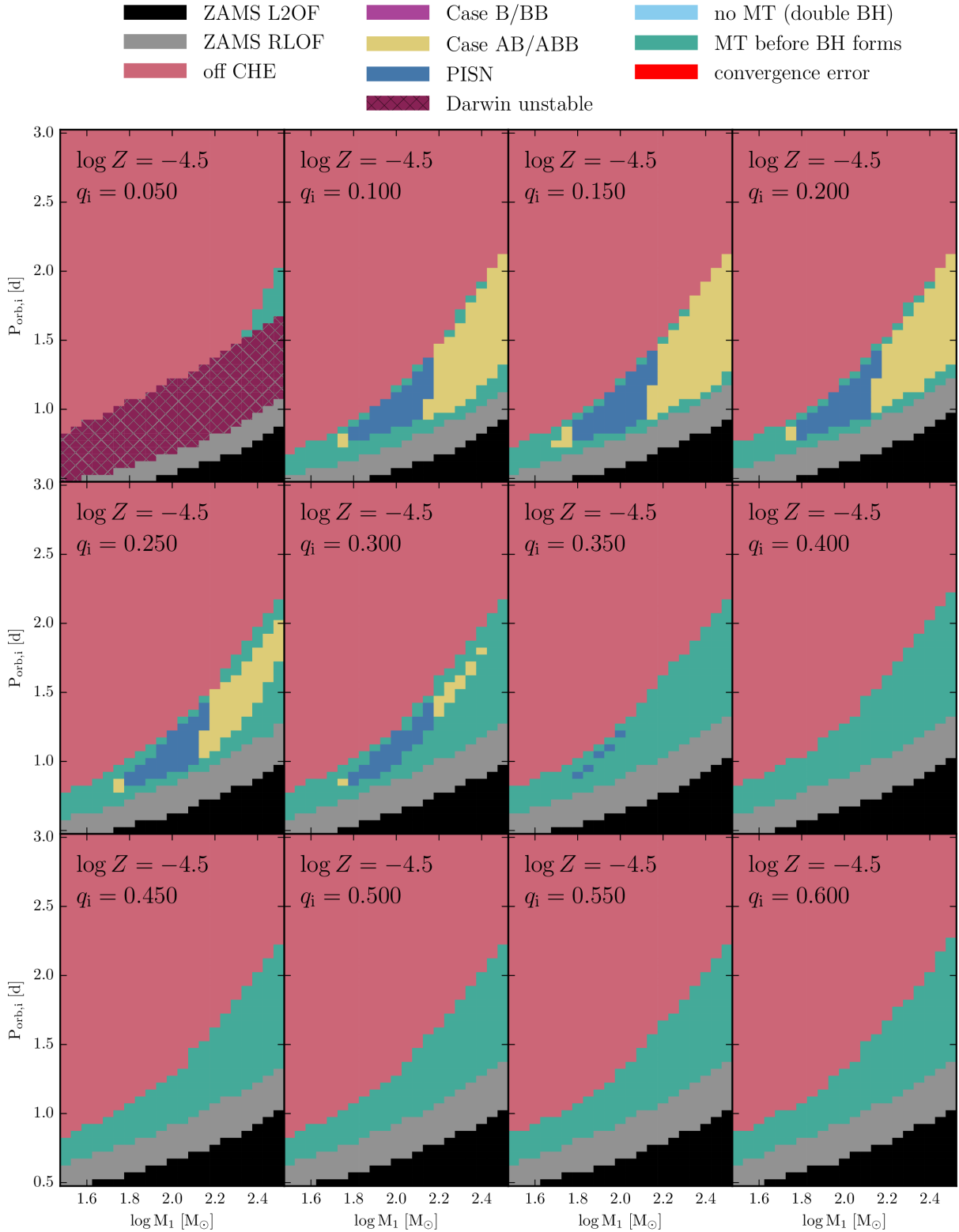


Figure C.6: Grid of models for  $\log Z = -4.5$ . See text in Appendix C for an explanation.

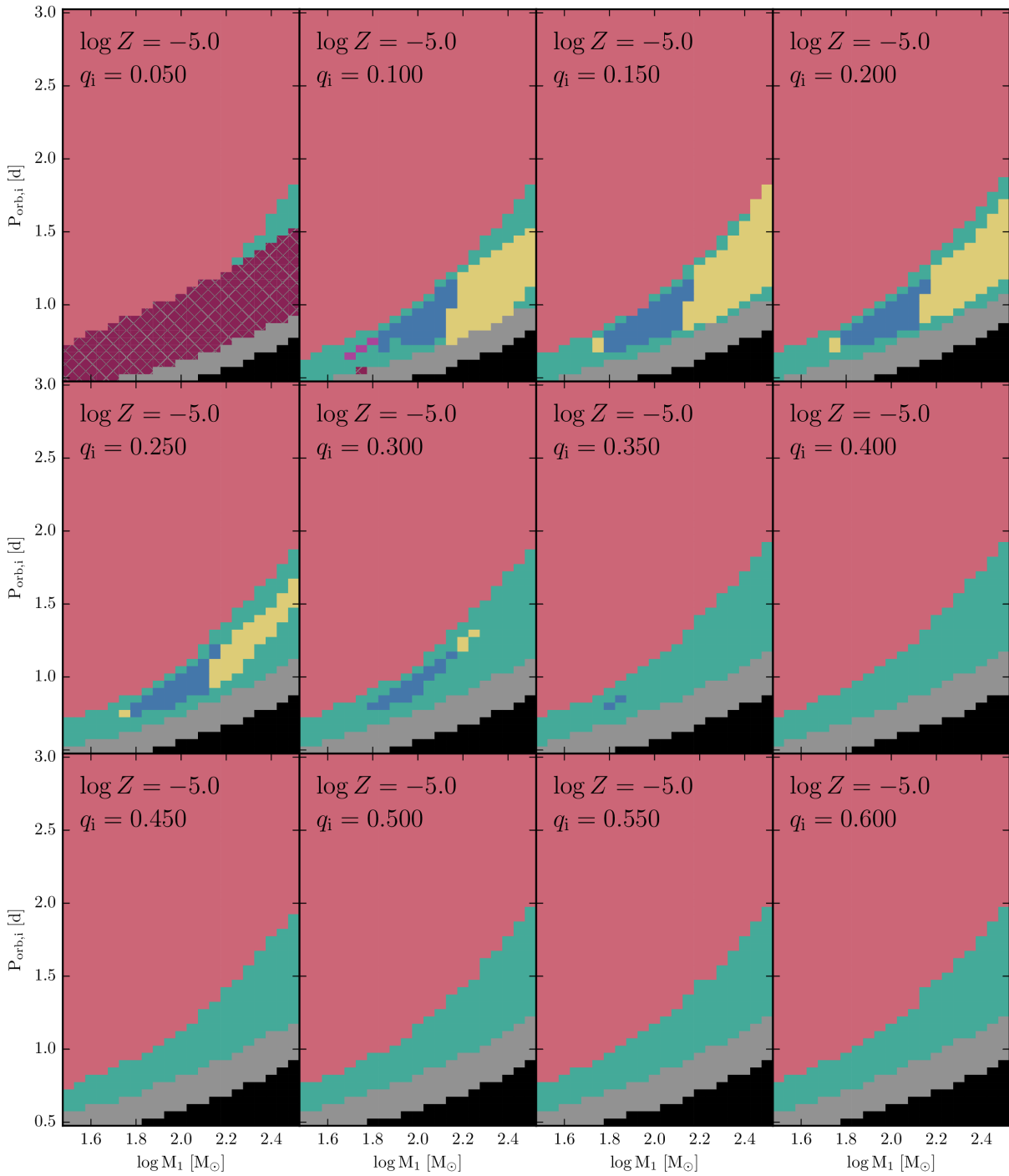
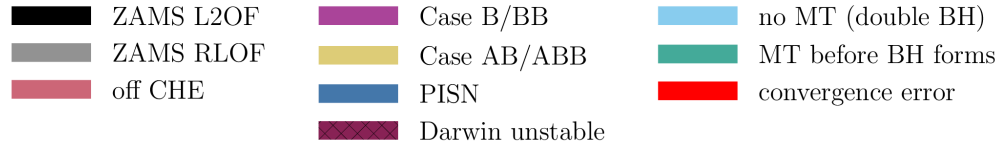


Figure C.7: Grid of models for  $\log Z = -5.0$ . See text in Appendix C for an explanation.

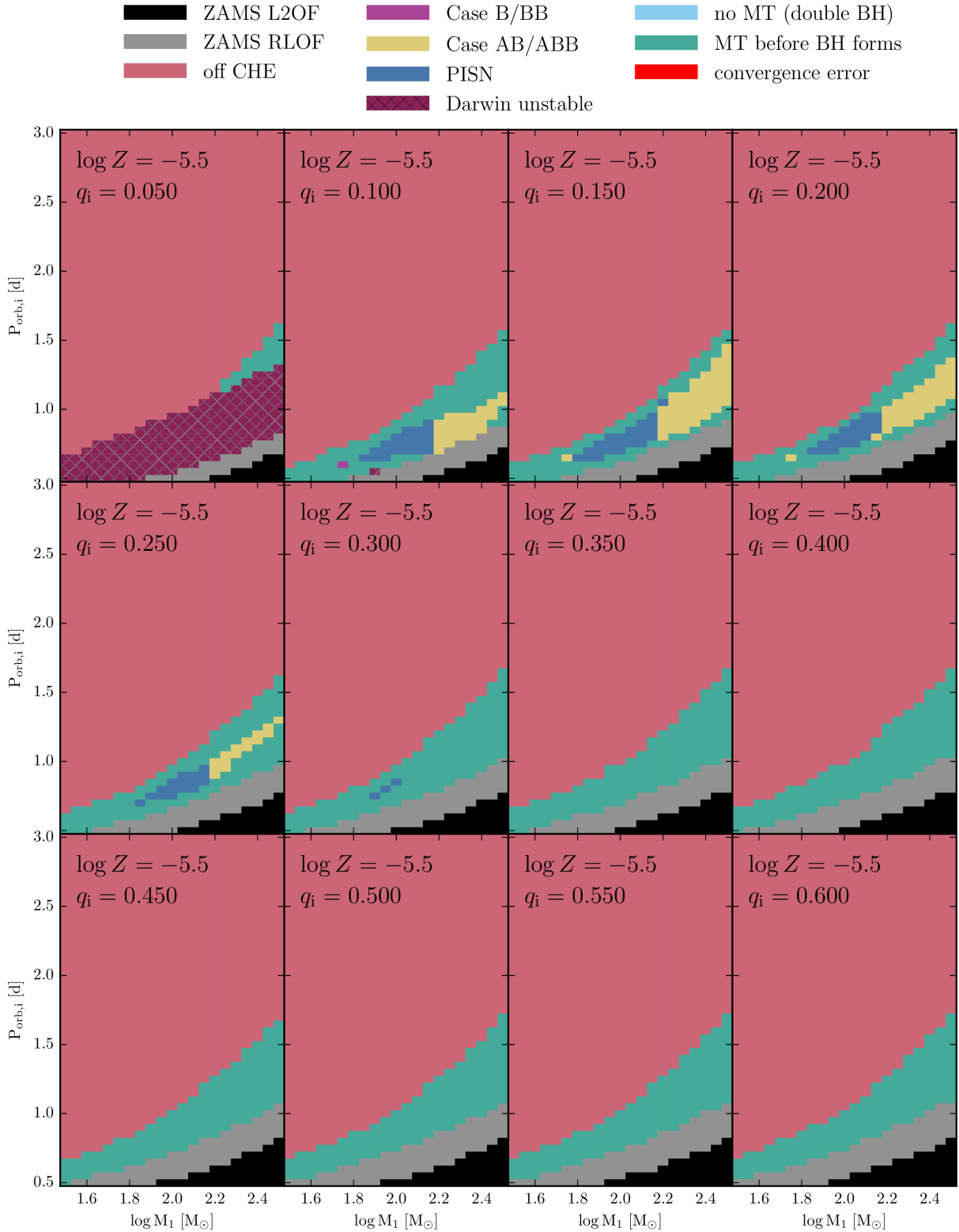


Figure C.8: Grid of models for  $\log Z = -5.5$ . See text in Appendix C for an explanation.

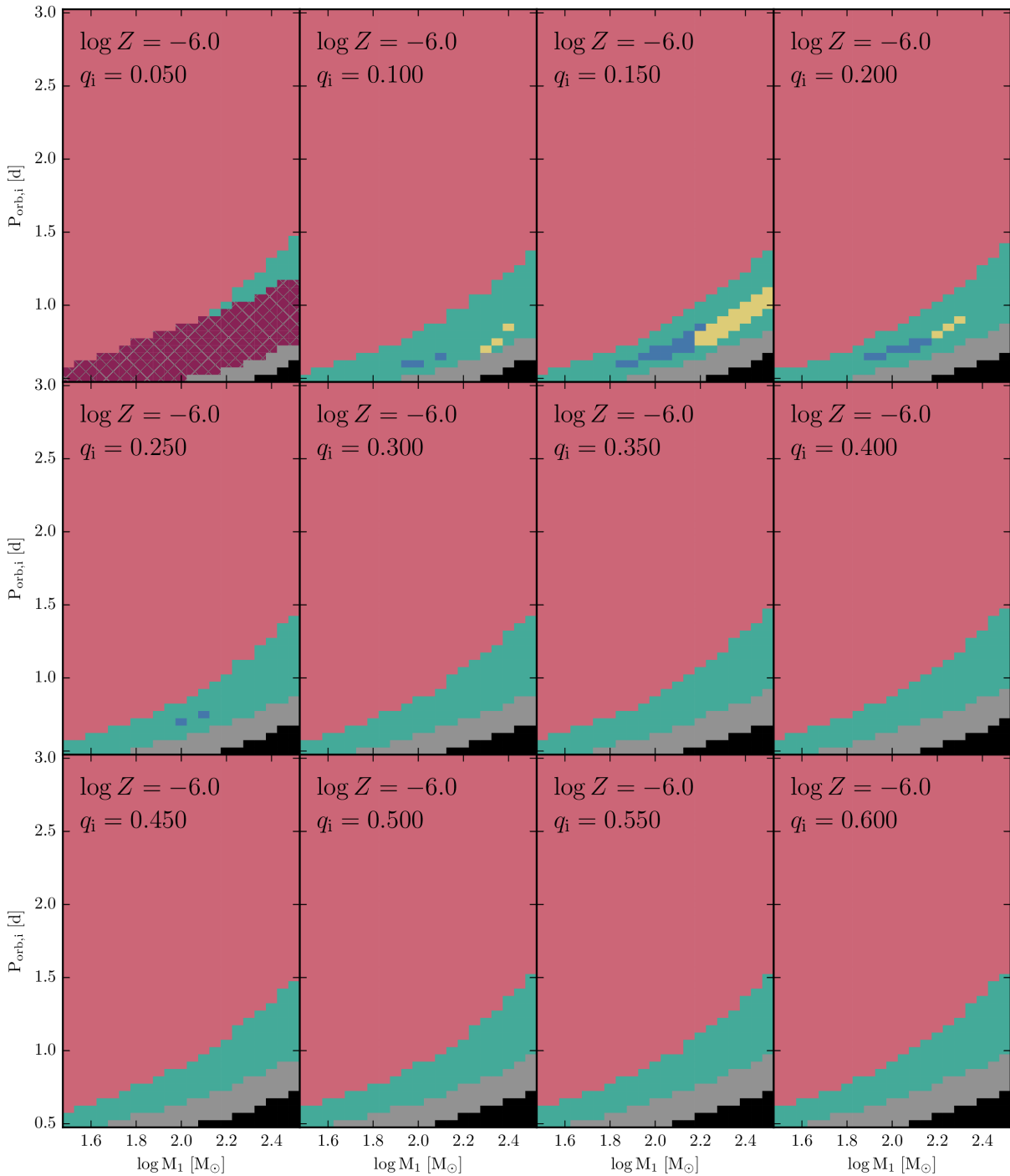
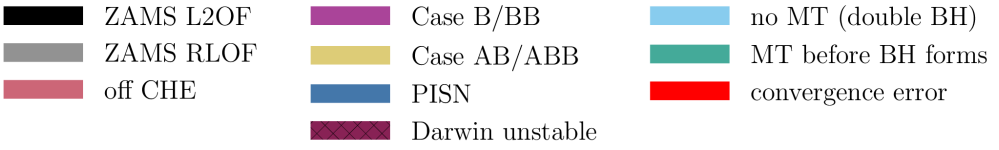


Figure C.9: Grid of models for  $\log Z = -6.0$ . See text in Appendix C for an explanation.



## APPENDIX D

---

### Properties of ULXs

---

Figures D.1-D.4 show several properties of our ULX models, including BH masses, accretion luminosities assuming mass transfer is limited to the Eddington rate, BH spins, the ratio between mass transfer and the Eddington rate  $\dot{M}_{\text{mt}}/\dot{M}_{\text{Edd}}$ , donor masses, and orbital periods. Color plots indicate in logarithmic scale 2D density distributions of all quantities against BH masses, while histograms are in a linear scale. For all metallicities, we use the distributions described in Section 4.3 for the mass of the primary, the mass ratio, and the orbital separation of the binary.

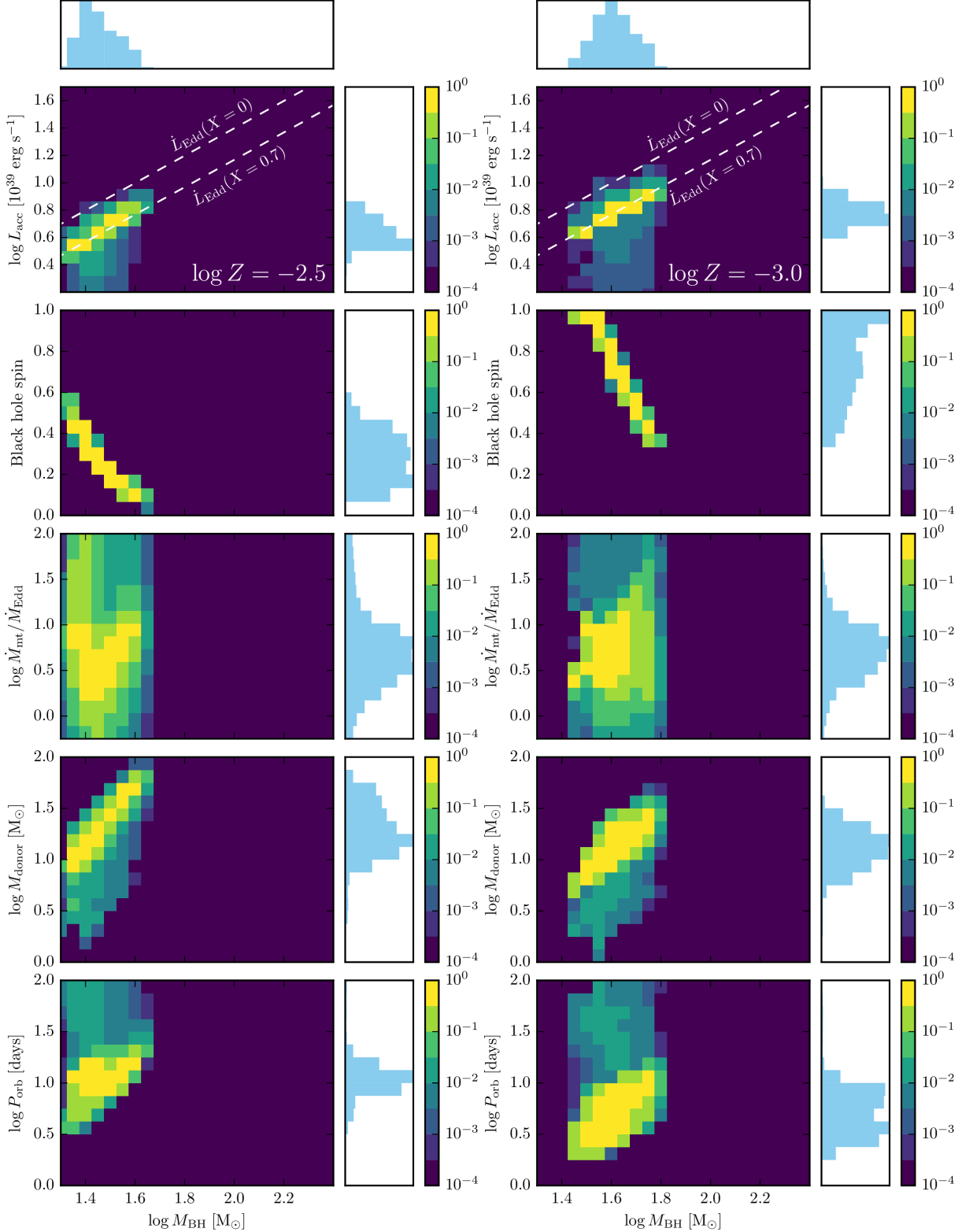


Figure D.1: General properties of ULXs for  $\log Z = -2.5, -3.0$ . See text in Appendix D for an explanation.

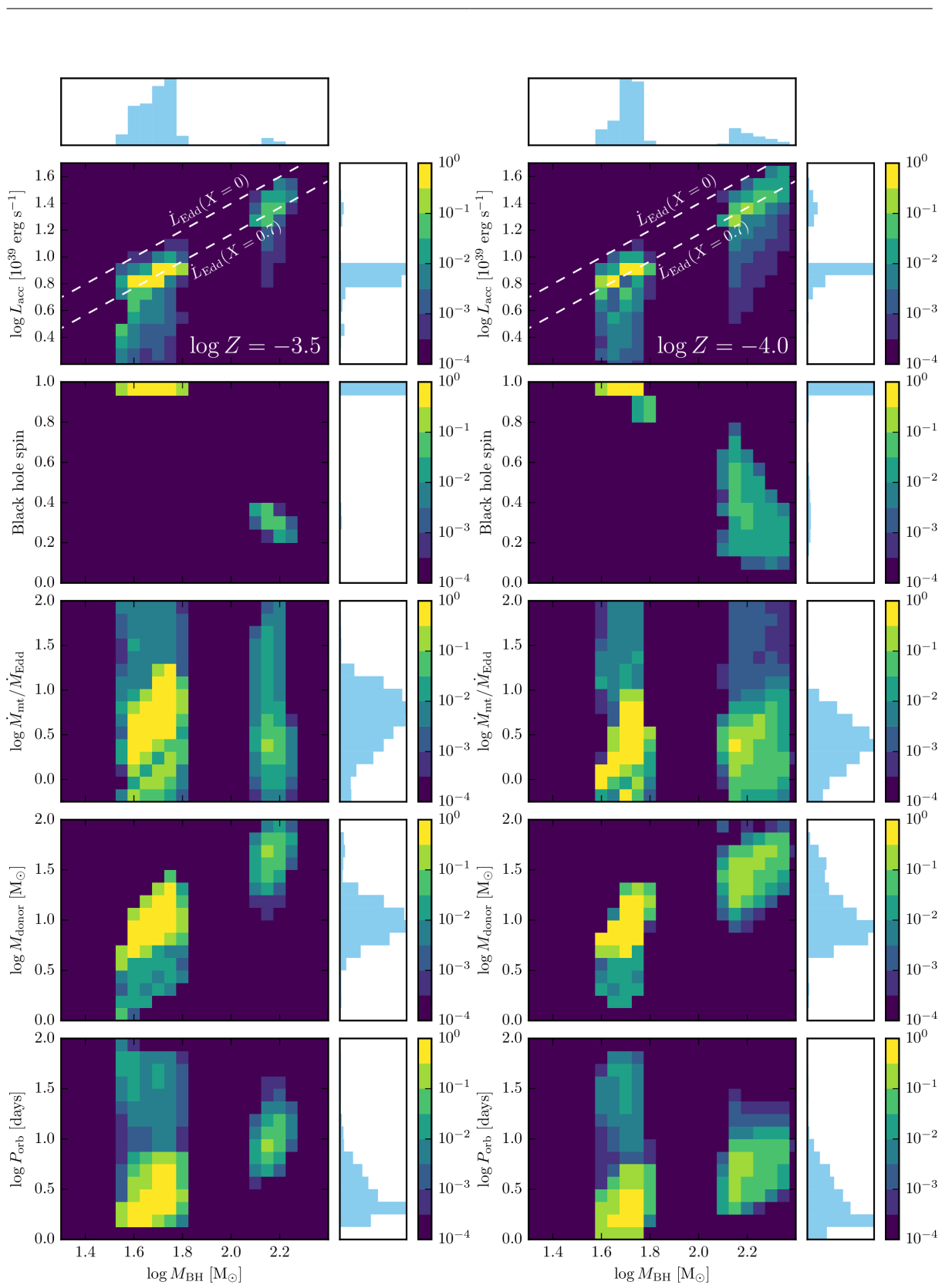


Figure D.2: General properties of ULXs for  $\log Z = -3.5, -4.0$ . See text in Appendix D for an explanation.

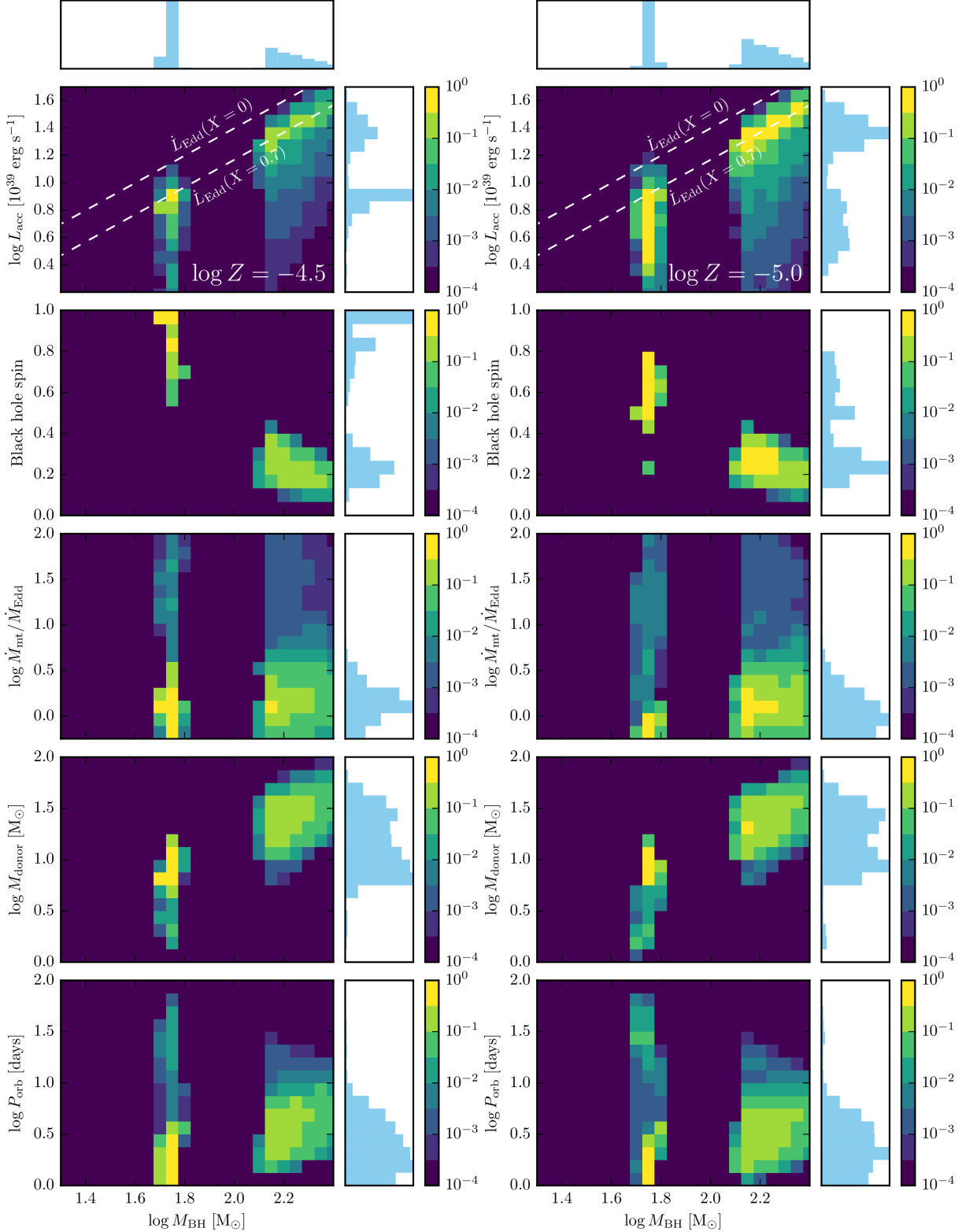


Figure D.3: General properties of ULXs for  $\log Z = -4.5, -5.0$ . See text in Appendix D for an explanation.

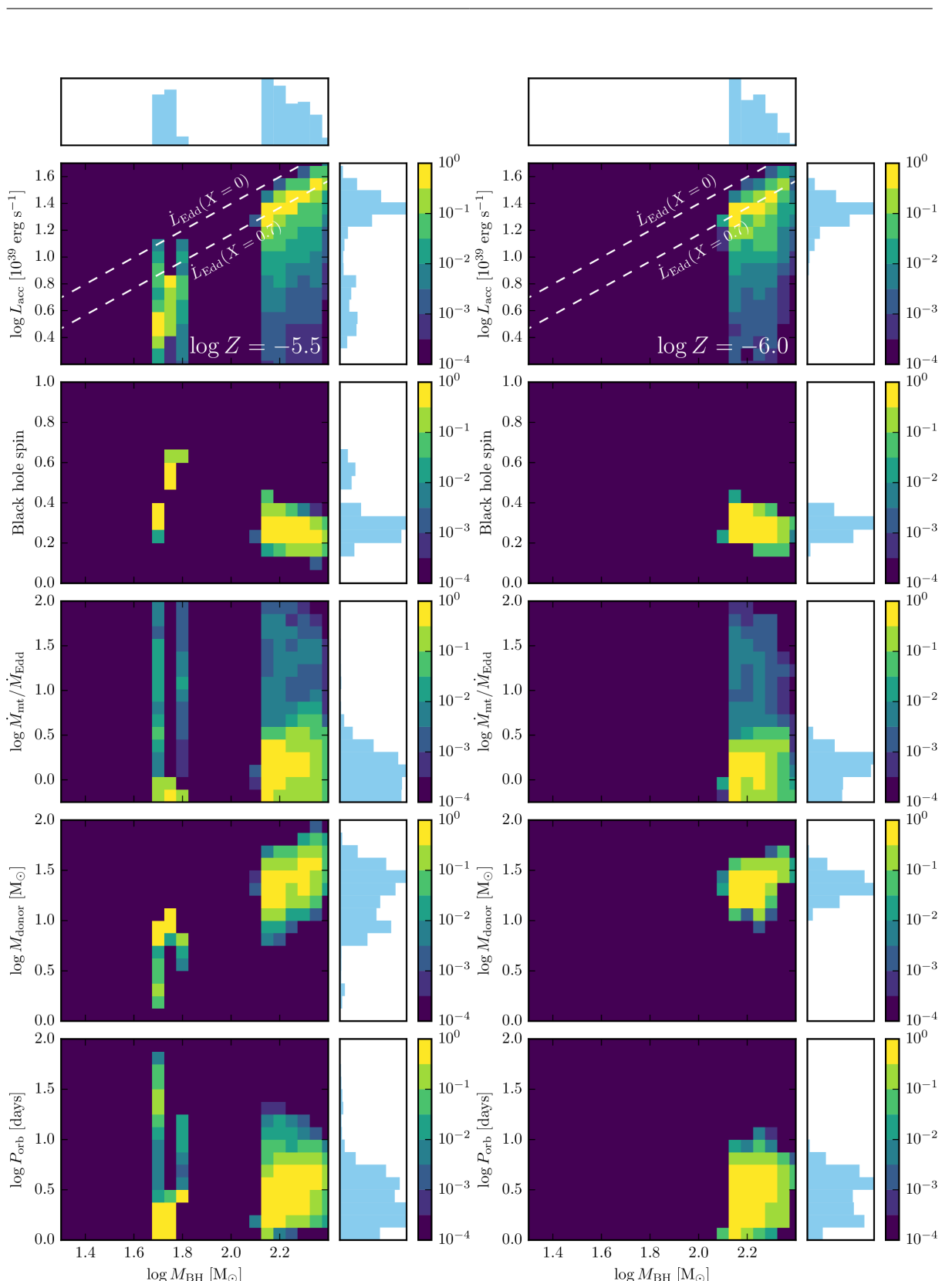


Figure D.4: General properties of ULXs for  $\log Z = -5.5, -6.0$ . See text in Appendix D for an explanation.



## APPENDIX E

---

### Grids of LMC binary models

---

A summary of the outcomes of our simulations of LMC binaries is presented in Figures E.1-E.12. The model grid for  $\log M_{1,i} = 1.3$  is shown in Figure 5.15 in the main body of the paper. For practical reasons we repeat here the description of the possible outcomes:

- Both dep. C: Both stars evolved up to carbon depletion. Note that due to convergence problems, we only model stars with helium core masses in excess of  $M = 14M_\odot$  up to helium depletion instead. This only affects the more massive donors in the grid.
- L2 overflow: During a contact phase L2 overflow happens, and the binary is expected to merge.
- Post MS + Inv. MT: Inverse mass transfer happens in a binary with a post main-sequence component. These systems are expected to merge and form a post main-sequence star.
- Upper  $\dot{M}$  limit: The limit on mass loss rates given by Equation (5.3) with  $R_{RL,2}$  instead of  $R_2$  is reached. In this case the luminosity of the system is insufficient to expel the transferred material, which cannot be accreted unto the critically rotating secondary. We expect such systems to develop a common envelope and merge.
- MT with  $q_i < 0.25$ : Mass transfer is initiated in a system with an initial mass ratio below  $q_i < 0.25$ . We assume such systems will result in a merger.
- Convergence error: Owing to numerical problems the simulation could not be completed. This normally happens during late phases of mass transfer, or whenever unstable mass transfer develops. In the latter case, systems could undergo common envelope evolution with successful envelope ejection instead of a merger. We do not model this effect, but rather assume the outcome would be a merger.
- Upper  $\dot{M}$  limit: The limit on mass loss rates given by Equation (5.3) is reached. Models are evolved despite this happening, but it should be taken as a warning that radiation could be insufficient to drive such a strong mass loss from the system.
- Had contact: System underwent a contact phase. This does not necessarily imply that a merger happens.
- Non-int. boundary: Systems with periods above this boundary do not undergo RLOF.
- Case A/B boundary: Boundary between systems undergoing Case A and Case B mass transfer.

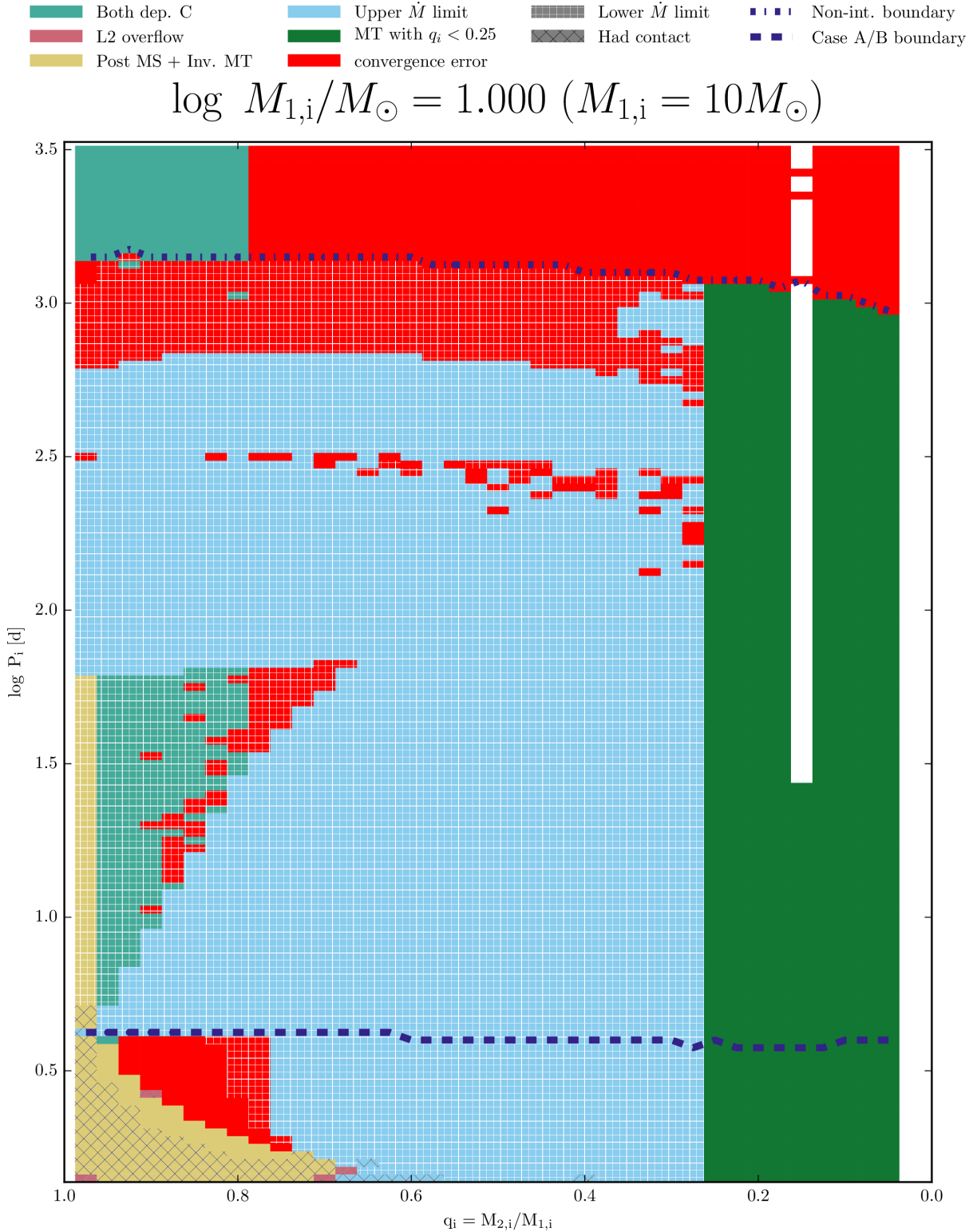
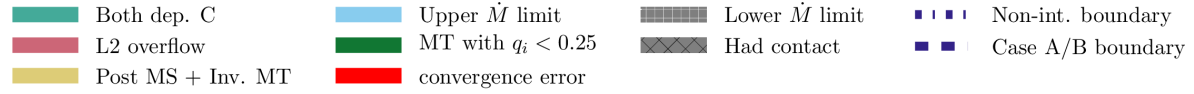


Figure E.1: Grid of binary models for  $\log M_{1,i}/M_{\odot} = 1.00$ . See text in Appendix E for an explanation.



$$\log M_{1,i}/M_\odot = 1.050 \quad (M_{1,i} \simeq 11.2M_\odot)$$

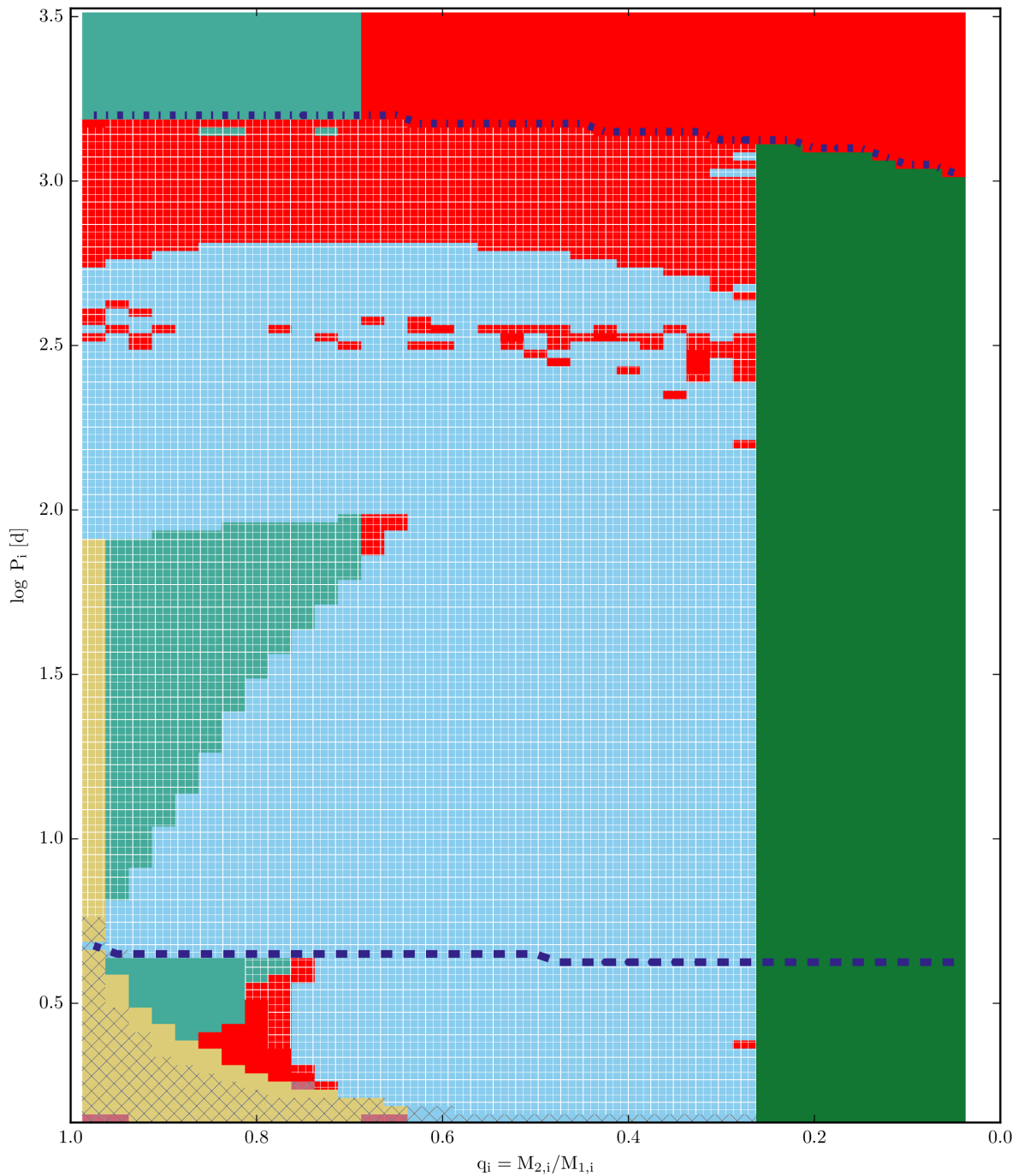


Figure E.2: Grid of binary models for  $\log M_{1,i}/M_\odot = 1.05$ . See text in Appendix E for an explanation.

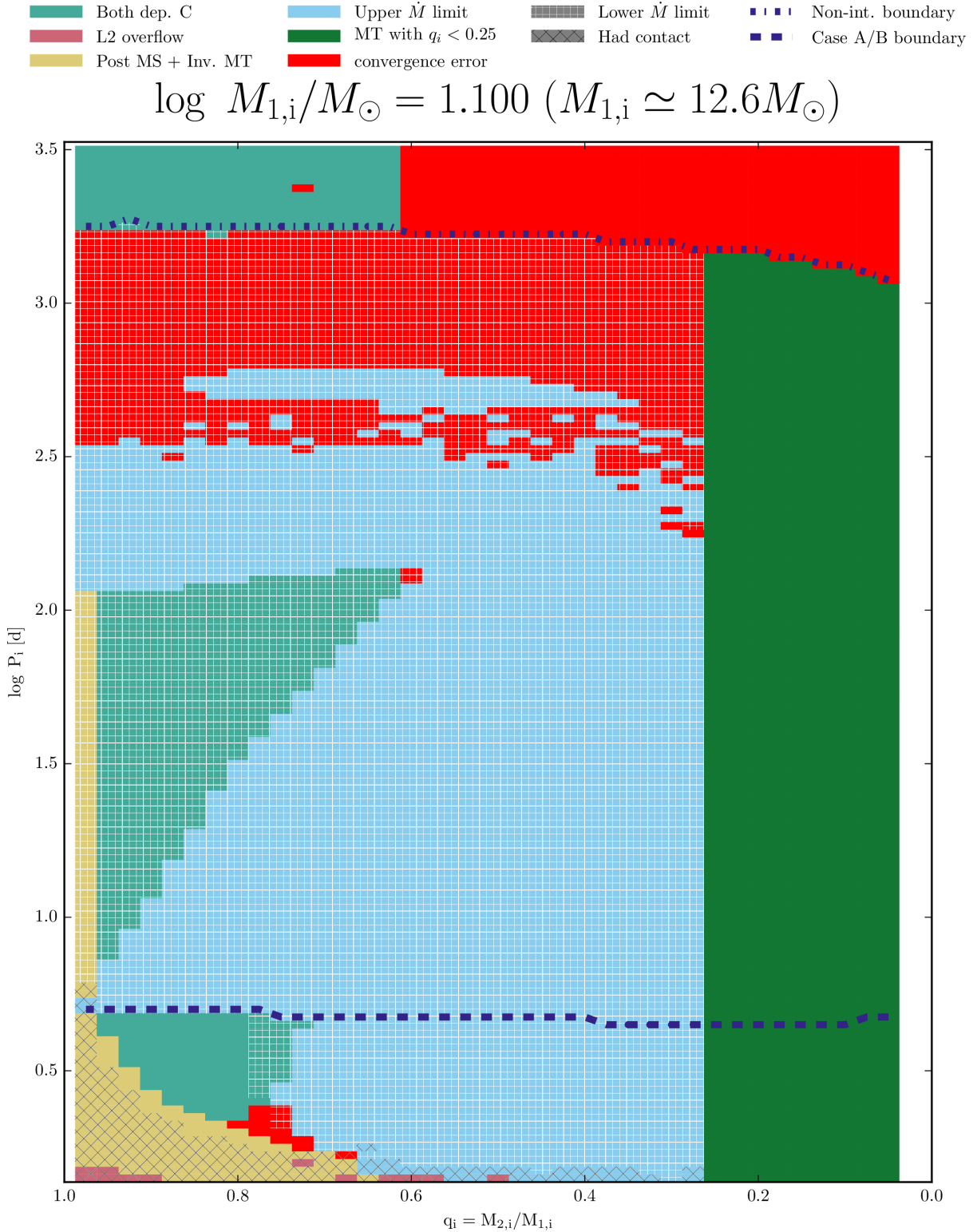
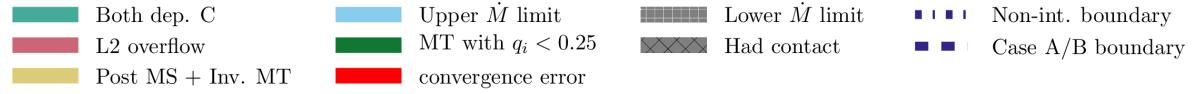


Figure E.3: Grid of binary models for  $\log M_{1,\text{i}}/M_\odot = 1.10$ . See text in Appendix E for an explanation.



$$\log M_{1,i}/M_\odot = 1.150 \quad (M_{1,i} \simeq 14.1 M_\odot)$$

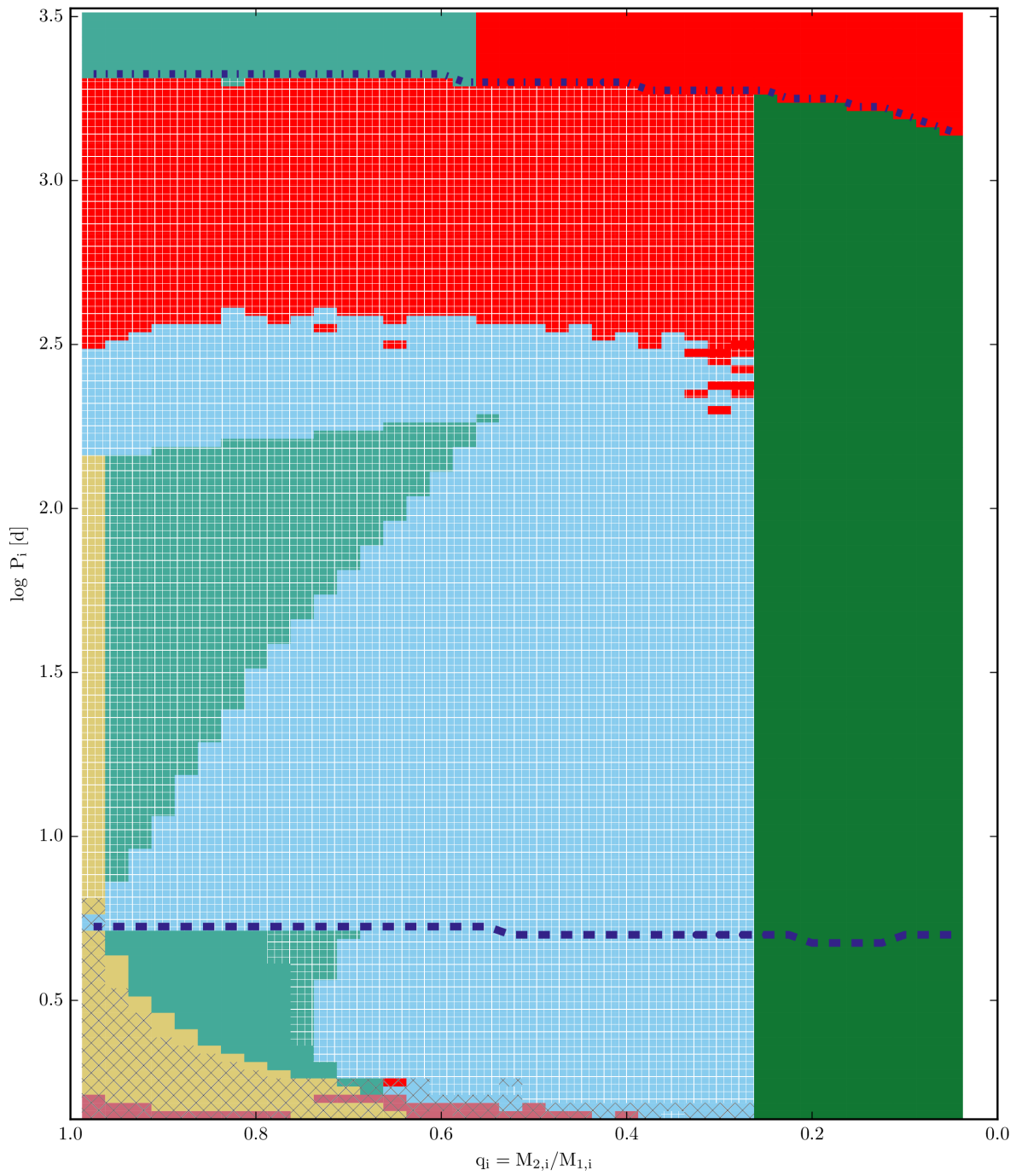


Figure E.4: Grid of binary models for  $\log M_{1,i}/M_\odot = 1.15$ . See text in Appendix E for an explanation.

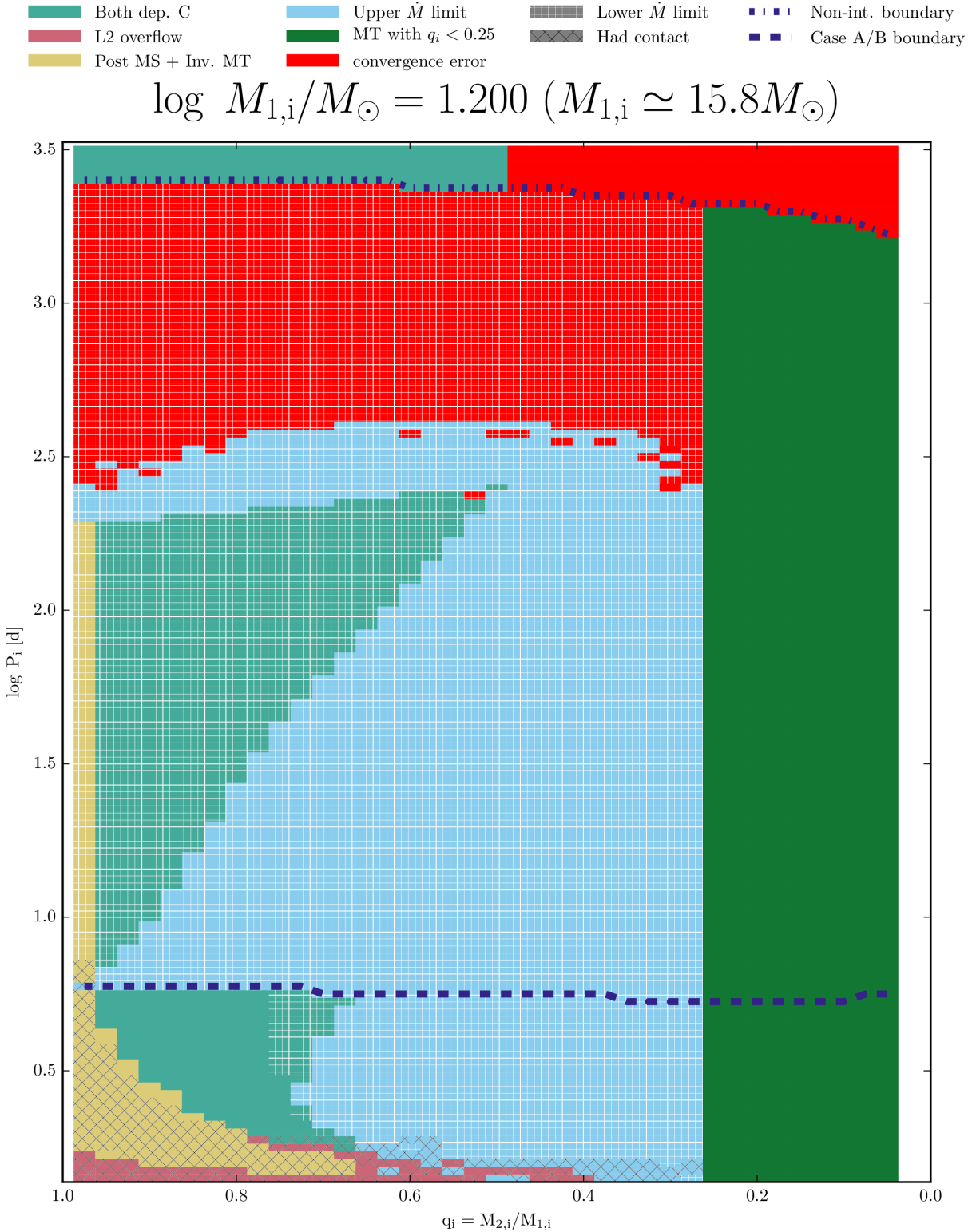


Figure E.5: Grid of binary models for  $\log M_{1,i}/M_\odot = 1.20$ . See text in Appendix E for an explanation.



$$\log M_{1,i}/M_\odot = 1.250 \quad (M_{1,i} \simeq 17.8M_\odot)$$

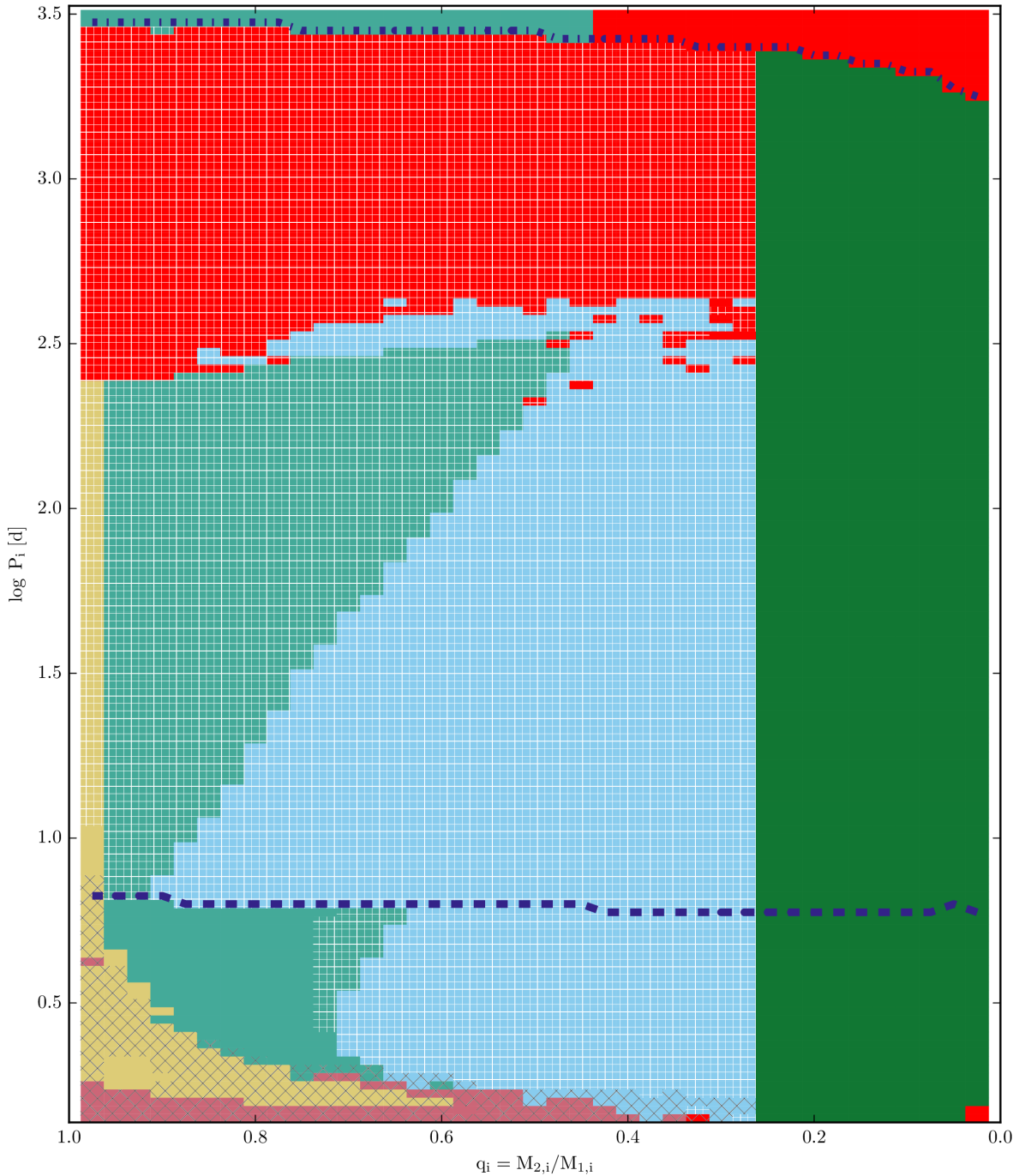


Figure E.6: Grid of binary models for  $\log M_{1,i} M_\odot = 1.25$ . See text in Appendix E for an explanation.

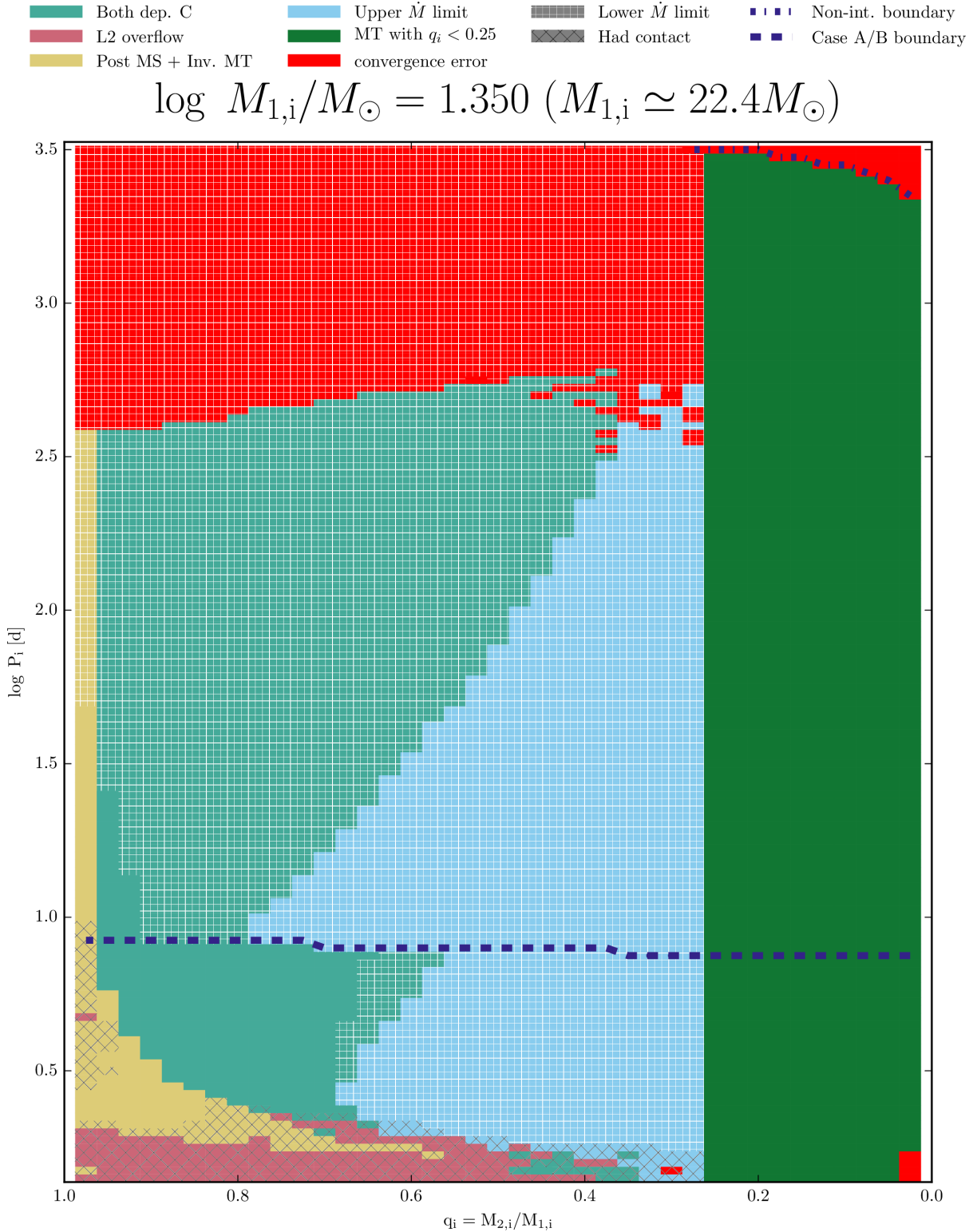


Figure E.7: Grid of binary models for  $\log M_{1,i}/M_{\odot} = 1.35$ . See text in Appendix E for an explanation.



$$\log M_{1,i}/M_\odot = 1.400 \quad (M_{1,i} \simeq 25.1 M_\odot)$$

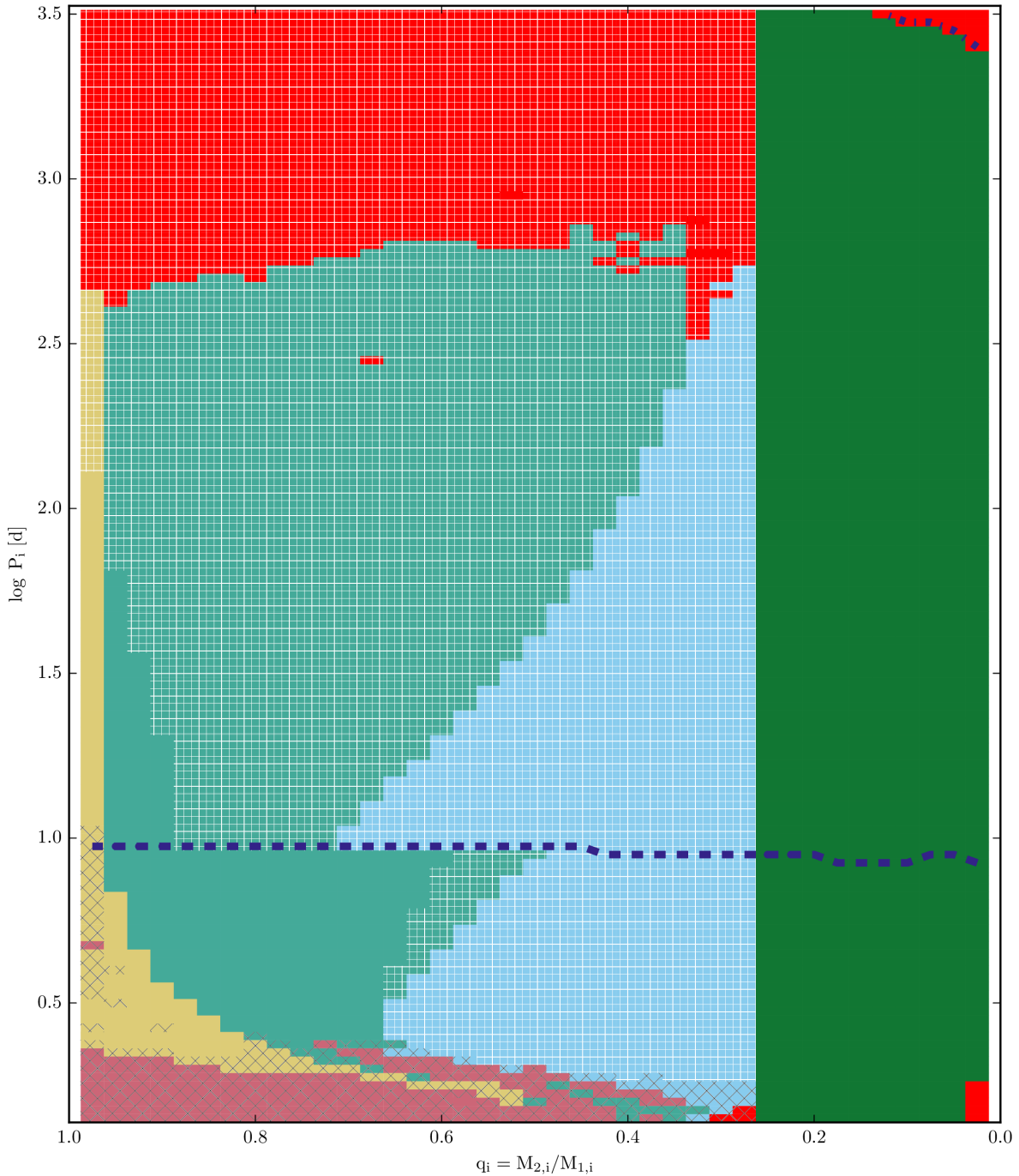


Figure E.8: Grid of binary models for  $\log M_{1,i}/M_\odot = 1.40$ . See text in Appendix E for an explanation.

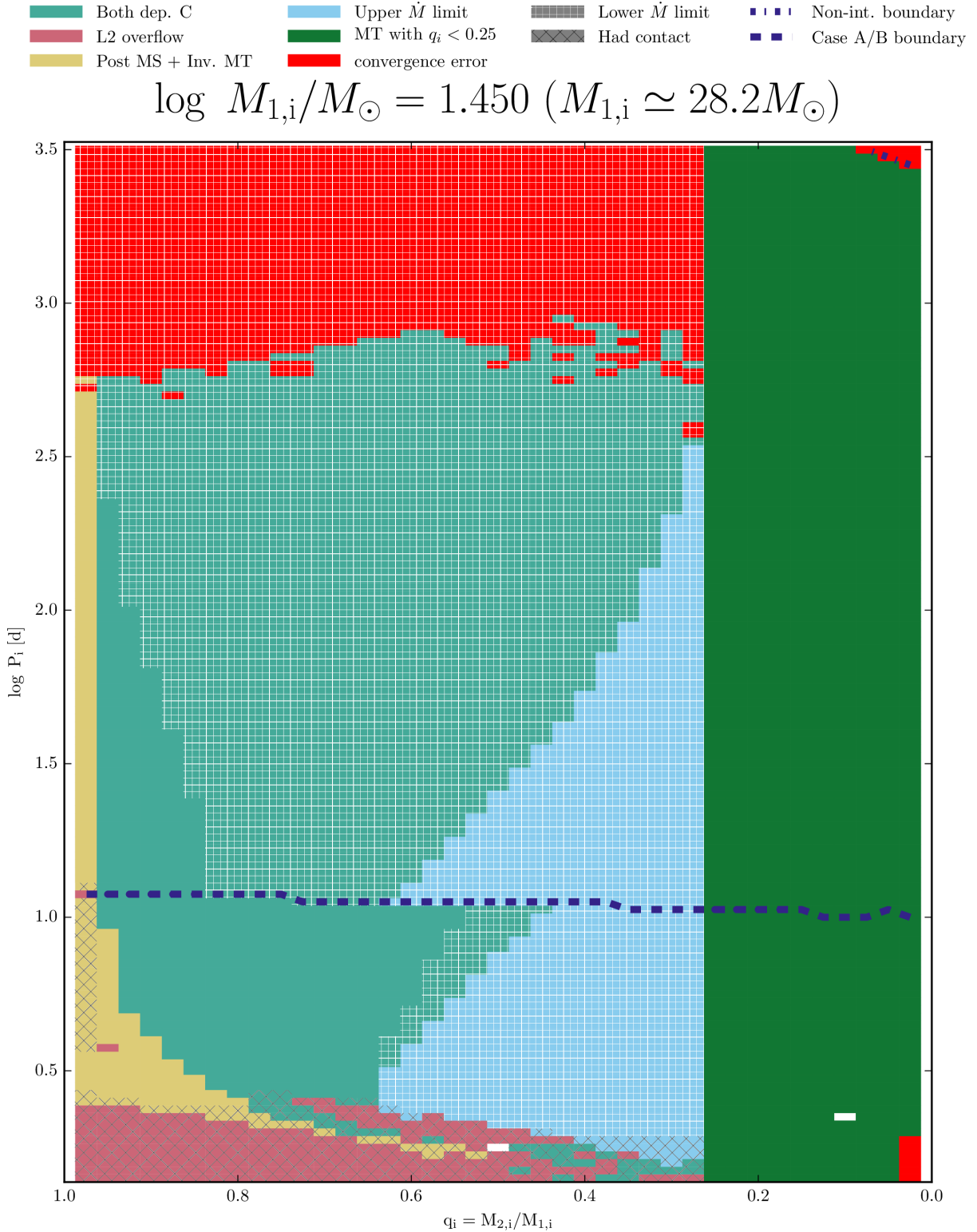


Figure E.9: Grid of binary models for  $\log M_{1,i}/M_{\odot} = 1.45$ . See text in Appendix E for an explanation.



$$\log M_{1,i}/M_\odot = 1.500 \quad (M_{1,i} \simeq 31.6 M_\odot)$$

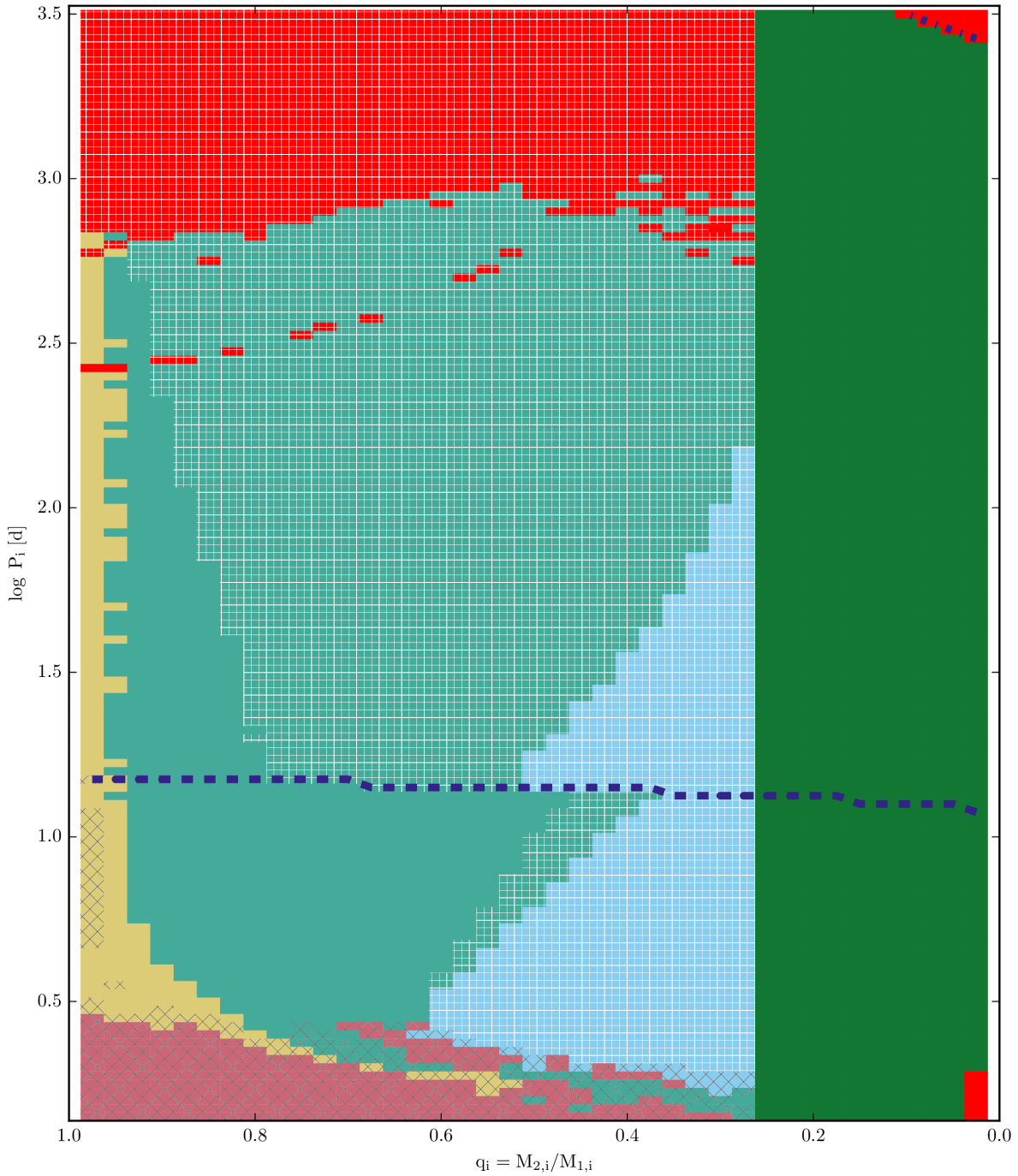


Figure E.10: Grid of binary models for  $\log M_{1,i}/M_\odot = 1.50$ . See text in Appendix E for an explanation.

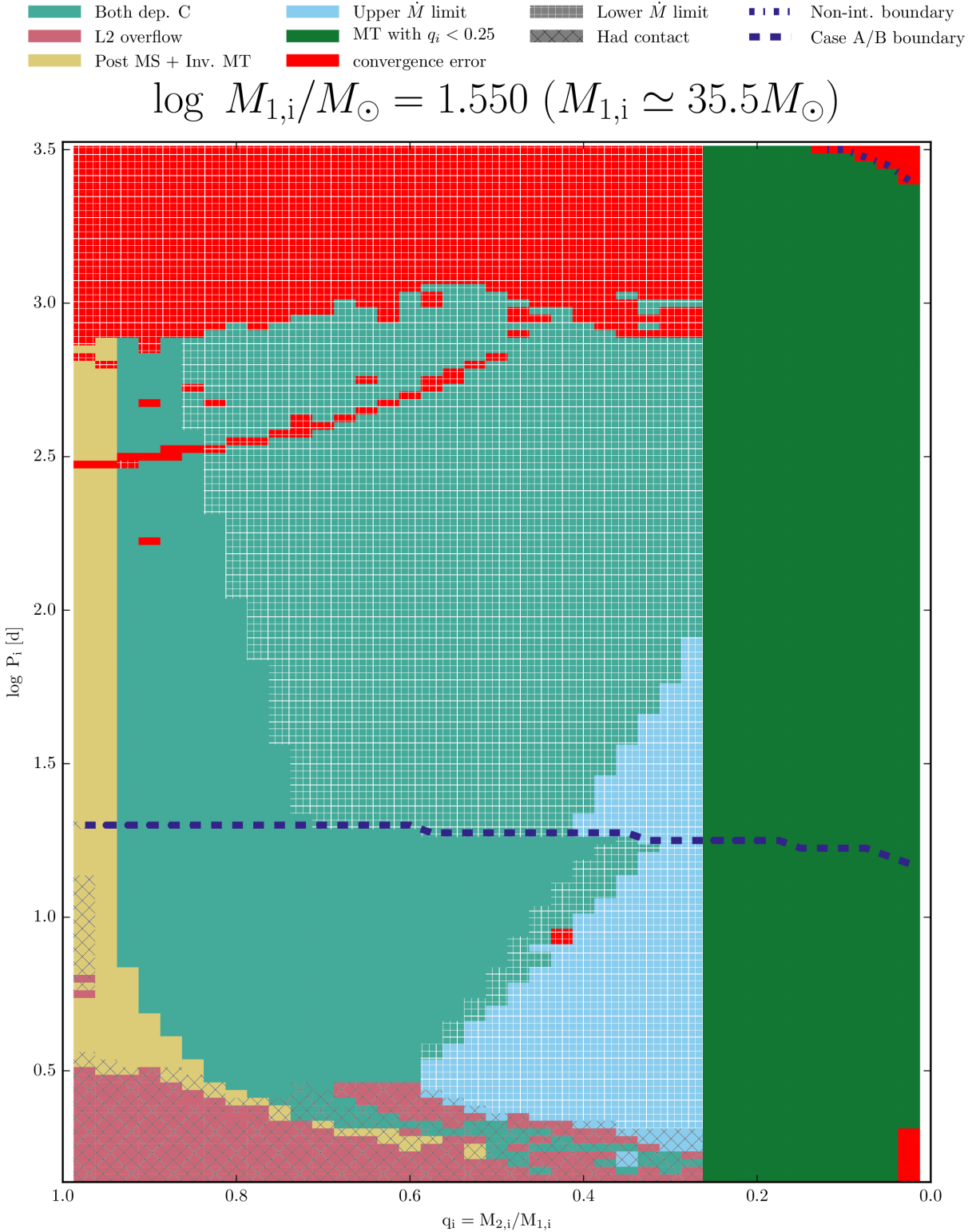


Figure E.11: Grid of binary models for  $\log M_{1,i}/M_{\odot} = 1.55$ . See text in Appendix E for an explanation.



$$\log M_{1,i}/M_\odot = 1.600 \quad (M_{1,i} \simeq 39.8M_\odot)$$

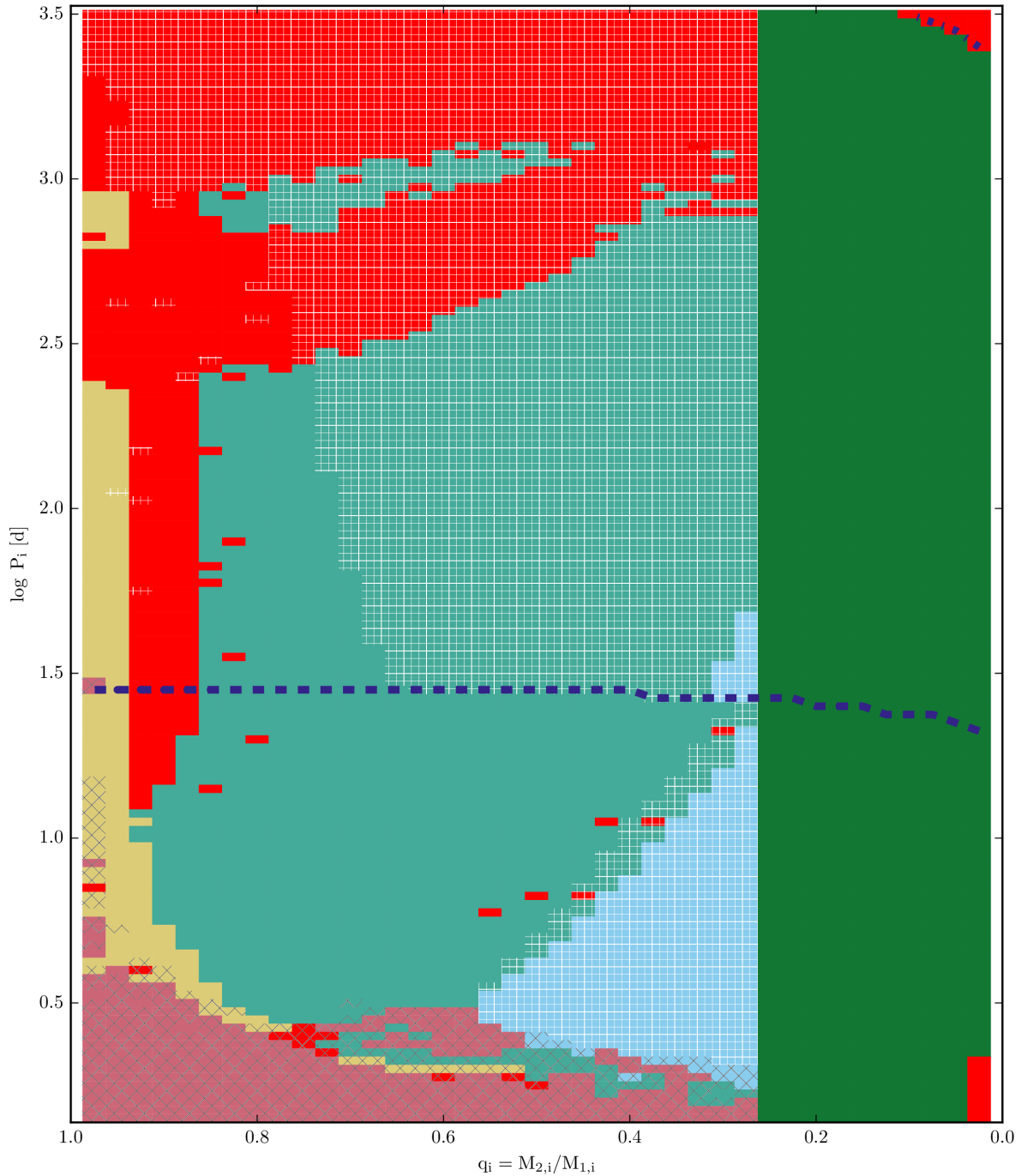


Figure E.12: Grid of binary models for  $\log M_{1,i}/M_\odot = 1.60$ . See text in Appendix E for an explanation.



# Acknowledgements

---

And so, it is done! This took much longer than I expected/wanted/needed, but I have to say I am very happy with the result. I have really learned a lot, and feel like this is just the beginning, with very exciting things to come! Through these years I've met a lot of great people and will miss this city and the creatures that inhabit it.

I deeply thank Norbert Langer for providing me with this opportunity. Through these years you have mostly trusted me to work independently, and I hope you consider that trust has paid well. I expect to keep working together and learning from you. To Andreas Reisenegger, you are a great Professor, and I am proud to have been your student. To Bill Paxton, I know you said you never wanted grad students, but I think I partially filled that role at times. Your assistance these last years was invaluable.

I thank my former officemates Alina and Fabian, who slowly dripped away from here and left me with this office to myself. I am sure I will see your faces often in the feature, (in the near future, especially yours Alina). To those coworkers that carry you down some stairs after breaking your foot in a completely idiotic way, the ones rescuing your house from becoming a biohazard, and to those that were always up for a friday beer. And to many others who provided insightful discussion and collaborations, such as Selma de Mink, Philipp Podsiadlowski, Thomas Tauris, Takashi Moriya, Matteo Cantiello and multiple others, including the broad community of MESA users.

And the rest goes in spanish. Gracias a mis papás por apoyarme desde siempre y ayudarme a sacar lo mejor de mí. Gracias a mi hermana, mi compañera de viajes por Europa y eterna fuente de estupideces del internet (gracias también a nuestro cocodrilo). A mi hermano y toda su familia, junto con mis hermosos sobrinos (los que ya llegaron y los que vendrán) que crecen a saltos gigantes cada ves que los veo. Gracias a mis tíos y a mi abuela, a quienes espero ver mucho mas a menudo en los años que vienen. Y gracias también a todos aquellos que por aquellas casualidades lean esto y sientan que me faltó mencionarlos. Estar tan lejos de todos es difícil...

A las “basuras” de Bonn, David, Javier, Arturo y Luchito, a la Yane y a muchos mas, a aquellos espacios queridos como el bar la victoria y el difunto blowup. Lugares y personas que no han visto mucho mi cara en estos últimos meses dedicados a la escritura y que voy a extrañar cuando me toque partir de aca.

Y para terminar, le doy las gracias a mi querida Sara por soportarme todos estos meses. Acabaste conociendome en una etapa muy ocupada de mi vida, pero por alguna razón te quedaste a mi lado. Te quiero mucho moñita, vamos a ver juntos por que parte del mundo acabamos :).



# Bibliography

---

- Abadie, J., B. P. Abbott, R. Abbott, T. D. Abbott et al. (2012), *Search for gravitational waves from intermediate mass binary black holes*, *Physical Review D* **85**, 102004 102004, arXiv: [1201.5999 \[gr-qc\]](#) (cit. on p. 65).
- Abadie, J., B. P. Abbott, R. Abbott, M. Abernathy et al. (2010), *TOPICAL REVIEW: Predictions for the rates of compact binary coalescences observable by ground-based gravitational-wave detectors*, *Classical and Quantum Gravity* **27**, 173001 173001, arXiv: [1003.2480 \[astro-ph.HE\]](#) (cit. on pp. 48, 61, 63, 64, 97, 135).
- Abbott, B. P. et al. (2016a), *Observation of Gravitational Waves from a Binary Black Hole Merger*, *Physical Review Letters* **116**, 061102 061102, arXiv: [1602.03837 \[gr-qc\]](#) (cit. on pp. 22, 23, 69).
- (2016b), *Upper limits on the rates of binary neutron star and neutron-star-black-hole mergers from Advanced LIGO's first observing run*, ArXiv e-prints, arXiv: [1607.07456 \[astro-ph.HE\]](#) (cit. on p. 97).
- Adams, S. M. et al. (2016), *The search for failed supernovae with the Large Binocular Telescope: confirmation of a disappearing star*, ArXiv e-prints, arXiv: [1609.01283 \[astro-ph.SR\]](#) (cit. on p. 130).
- Aitken, R. G. (1935), *The binary stars* (cit. on p. 17).
- (1942), *Edmund Halley and Stellar Proper Motions*, Leaflet of the Astronomical Society of the Pacific **4** 103 (cit. on p. 2).
- Almeida, L. A., H. Sana, S. E. de Mink et al. (2015), *Discovery of the Massive Overcontact Binary VFTS352: Evidence for Enhanced Internal Mixing*, *ApJ* **812**, 102 102, arXiv: [1509.08940 \[astro-ph.SR\]](#) (cit. on pp. 10, 19, 51, 58, 112).
- Almeida, L. A., H. Sana, W. Taylor et al. (2016), *The Tarantula Massive Binary Monitoring: I. Observational campaign and OB-type spectroscopic binaries*, ArXiv e-prints, arXiv: [1610.03500 \[astro-ph.SR\]](#) (cit. on pp. 15, 18, 102).
- Amaro-Seoane, P. et al. (2012), *Low-frequency gravitational-wave science with eLISA/NGO*, *Classical and Quantum Gravity* **29**, 124016 124016, arXiv: [1202.0839 \[gr-qc\]](#) (cit. on p. 23).
- Asplund, M. et al. (2009), *The Chemical Composition of the Sun*, *ARA&A* **47** 481, arXiv: [0909.0948 \[astro-ph.SR\]](#) (cit. on p. 10).
- Auvergne, M. et al. (2009), *The CoRoT satellite in flight: description and performance*, *A&A* **506** 411, arXiv: [0901.2206 \[astro-ph.SR\]](#) (cit. on p. 30).
- Baade, W. and F. Zwicky (1934a), *Cosmic Rays from Super-novae*, *Proceedings of the National Academy of Science* **20** 259 (cit. on p. 9).
- (1934b), *On Super-novae*, *Proceedings of the National Academy of Science* **20** 254 (cit. on p. 9).
- Bachetti, M. et al. (2014), *An ultraluminous X-ray source powered by an accreting neutron star*, *Nature* **514** 202, arXiv: [1410.3590 \[astro-ph.HE\]](#) (cit. on pp. 68, 73).
- Badnell, N. R. et al. (2005), *Updated opacities from the Opacity Project*, *MNRAS* **360** 458, eprint: [astro-ph/0410744](#) (cit. on p. 12).

- Baglin, A. et al. (2009), “CoRoT: Description of the Mission and Early Results”, *IAU Symposium*, ed. by F. Pont, D. Sasselov and M. J. Holman, vol. 253, IAU Symposium 71 (cit. on p. 30).
- Baiotti, L. and L. Rezzolla (2016), *Binary neutron-star mergers: a review of Einstein’s richest laboratory*, ArXiv e-prints, arXiv: [1607.03540 \[gr-qc\]](#) (cit. on p. 129).
- Balmelli, S. and T. Damour (2015), *A new effective-one-body Hamiltonian with next-to-leading order spin-spin coupling*, ArXiv e-prints, arXiv: [1509.08135 \[gr-qc\]](#) (cit. on p. 65).
- Bardeen, J. M. (1970), *Kerr Metric Black Holes*, *Nature* **226** 64 (cit. on p. 74).
- Bardeen, J. M., W. H. Press and S. A. Teukolsky (1972), *Rotating Black Holes: Locally Nonrotating Frames, Energy Extraction, and Scalar Synchrotron Radiation*, *ApJ* **178** 347 (cit. on p. 74).
- Barnard, R., J. S. Clark and U. C. Kolb (2008), *NGC 300 X-1 and IC 10 X-1: a new breed of black hole binary?*, *A&A* **488** 697, arXiv: [0807.0606](#) (cit. on p. 58).
- Beck, P. G., K. Hambleton et al. (2014), *Pulsating red giant stars in eccentric binary systems discovered from Kepler space-based photometry. A sample study and the analysis of KIC 5006817*, *A&A* **564**, A36 A36, arXiv: [1312.4500 \[astro-ph.SR\]](#) (cit. on p. 14).
- Beck, P. G., J. Montalban et al. (2012), *Fast core rotation in red-giant stars as revealed by gravity-dominated mixed modes*, *Nature* **481** 55, arXiv: [1112.2825 \[astro-ph.SR\]](#) (cit. on p. 14).
- Bedding, T. R. et al. (2010), *Solar-like Oscillations in Low-luminosity Red Giants: First Results from Kepler*, *ApJ* **713** L176, arXiv: [1001.0229 \[astro-ph.SR\]](#) (cit. on p. 30).
- Begelman, M. C. (2002), *Super-Eddington Fluxes from Thin Accretion Disks?*, *ApJ* **568** L97, eprint: [astro-ph/0203030](#) (cit. on p. 68).
- Belczynski, K., T. Bulik et al. (2013), *Cyg X-3: A Galactic Double Black Hole or Black-hole-Neutron-star Progenitor*, *ApJ* **764**, 96 96, arXiv: [1209.2658 \[astro-ph.HE\]](#) (cit. on p. 137).
- Belczynski, K., A. Buonanno et al. (2014), *The Formation and Gravitational-wave Detection of Massive Stellar Black Hole Binaries*, *ApJ* **789**, 120 120, arXiv: [1403.0677 \[astro-ph.HE\]](#) (cit. on p. 137).
- Belczynski, K., M. Dominik et al. (2010), *The Effect of Metallicity on the Detection Prospects for Gravitational Waves*, *ApJ* **715** L138, arXiv: [1004.0386 \[astro-ph.HE\]](#) (cit. on pp. 61, 62).
- Belczynski, K., A. Heger et al. (2016), *The Effect of Pair-Instability Mass Loss on Black Hole Mergers*, ArXiv e-prints, arXiv: [1607.03116 \[astro-ph.HE\]](#) (cit. on p. 68).
- Belczynski, K., D. E. Holz et al. (2016), *The first gravitational-wave source from the isolated evolution of two stars in the 40-100 solar mass range*, *Nature* **534** 512, arXiv: [1602.04531 \[astro-ph.HE\]](#) (cit. on pp. 27, 69).
- Belczynski, K., V. Kalogera et al. (2008), *Compact Object Modeling with the StarTrack Population Synthesis Code*, *ApJS* **174**, 223-260 223, eprint: [astro-ph/0511811](#) (cit. on p. 103).
- Bellm, E. (2014), “The Zwicky Transient Facility”, *The Third Hot-wiring the Transient Universe Workshop*, ed. by P. R. Wozniak et al. 27, arXiv: [1410.8185 \[astro-ph.IM\]](#) (cit. on pp. 98, 130).
- Bennett, P. D. (2010), “Chromospheres and Winds of Red Supergiants: An Empirical Look at Outer Atmospheric Structure”, *Hot and Cool: Bridging Gaps in Massive Star Evolution*, ed. by C. Leitherer et al., vol. 425, Astronomical Society of the Pacific Conference Series 181, arXiv: [1004.1853 \[astro-ph.SR\]](#) (cit. on p. 11).
- Bertelli, G. et al. (2009), *A&A* **508** 355, arXiv: [0911.2419 \[astro-ph.SR\]](#) (cit. on p. 102).
- Bessel, F. W. (1838), *On the parallax of 61 Cygni*, *MNRAS* **4** 152 (cit. on p. 2).
- Bestenlehner, J. M. et al. (2014), *The VLT-FLAMES Tarantula Survey. XVII. Physical and wind properties of massive stars at the top of the main sequence*, *A&A* **570**, A38 A38, arXiv: [1407.1837 \[astro-ph.SR\]](#) (cit. on p. 13).
- Böhm-Vitense, E. (1958), *Über die Wasserstoffkonvektionszone in Sternen verschiedener Effektivtemperaturen und Leuchtkräfte. Mit 5 Textabbildungen*, Zeitschrift für Astrophysik **46** 108 (cit. on pp. 13, 49, 70, 103).

- 
- Bolton, C. T. (1972), *Identification of Cygnus X-1 with HDE 226868*, *Nature* **235** 271 (cit. on p. 17).
- Bonaca, A. et al. (2012), *Calibrating Convective Properties of Solar-like Stars in the Kepler Field of View*, *ApJ* **755**, L12 L12, arXiv: 1207.2765 [astro-ph.SR] (cit. on p. 13).
- Bonanos, A. Z. (2009), *Toward an Accurate Determination of Parameters for Very Massive Stars: The Eclipsing Binary LMC-SC1-105*, *ApJ* **691** 407, arXiv: 0807.3742 (cit. on p. 122).
- Bond, J. R., W. D. Arnett and B. J. Carr (1984), *The evolution and fate of Very Massive Objects*, *ApJ* **280** 825 (cit. on p. 16).
- Borucki, W. J. et al. (2010), *Kepler Planet-Detection Mission: Introduction and First Results*, *Science* **327** 977 (cit. on p. 30).
- Brandt, W. N., P. Podsiadlowski and S. Sigurdsson (1995), *On the high space velocity of X-ray Nova SCO 1994: implications for the formation of its black hole*, *MNRAS* **277** L35 (cit. on p. 131).
- Braun, H. and N. Langer (1995), *Effects of accretion onto massive main sequence stars.*, *A&A* **297** 483 (cit. on pp. 107, 111).
- Breivik, K. et al. (2016), *Distinguishing between Formation Channels for Binary Black Holes with LISA*, *ApJ* **830**, L18 L18, arXiv: 1606.09558 (cit. on pp. 27, 92).
- Brott, I., S. E. de Mink et al. (2011), *Rotating massive main-sequence stars. I. Grids of evolutionary models and isochrones*, *A&A* **530**, A115 A115, arXiv: 1102.0530 [astro-ph.SR] (cit. on pp. 13, 48, 49, 56, 72, 102–106, 122).
- Brott, I., C. J. Evans et al. (2011), *Rotating massive main-sequence stars. II. Simulating a population of LMC early B-type stars as a test of rotational mixing*, *A&A* **530**, A116 A116, arXiv: 1102.0766 [astro-ph.SR] (cit. on pp. 15, 102).
- Brown, G. E. (1995), *Neutron star accretion and binary pulsar formation*, *ApJ* **440** 270 (cit. on p. 136).
- Brown, G. E., A. Heger et al. (2001), *Formation of high mass X-ray black hole binaries*, *New A* **6** 457, eprint: astro-ph/0102379 (cit. on pp. 91, 135).
- Brown, G. E., C.-H. Lee and H. A. Bethe (1999), *The formation of high-mass black holes in low-mass X-ray binaries*, *New A* **4** 313, eprint: astro-ph/9807221 (cit. on p. 135).
- Bulik, T., K. Belczynski and A. Prestwich (2011), *IC10 X-1/NGC300 X-1: The Very Immediate Progenitors of BH-BH Binaries*, *ApJ* **730**, 140 140, arXiv: 0803.3516 (cit. on p. 58).
- Burbidge, E. M. et al. (1957), *Synthesis of the Elements in Stars*, *Reviews of Modern Physics* **29** 547 (cit. on pp. 9, 102).
- Burgay, M. et al. (2003), *An increased estimate of the merger rate of double neutron stars from observations of a highly relativistic system*, *Nature* **426** 531, eprint: astro-ph/0312071 (cit. on p. 48).
- Burnham, S. W. (1906), *A General Catalogue of Double Stars within 121° of the North Pole* (cit. on p. 16).
- Cannon, A. J. and E. C. Pickering (1901), *Spectra of bright southern stars photographed with the 13-inch Boyden telescope as part of the Henry Draper Memorial*, *Annals of Harvard College Observatory* **28** 129 (cit. on p. 3).
- Cantiello, M. and N. Langer (2010), *Thermohaline mixing in evolved low-mass stars*, *A&A* **521**, A9 A9, arXiv: 1006.1354 [astro-ph.SR] (cit. on pp. 14, 36, 104).
- Cantiello, M., N. Langer et al. (2009), *Sub-surface convection zones in hot massive stars and their observable consequences*, *A&A* **499** 279, arXiv: 0903.2049 [astro-ph.SR] (cit. on p. 13).
- Cantiello, M., S.-C. Yoon et al. (2007), *Binary star progenitors of long gamma-ray bursts*, *A&A* **465** L29, eprint: astro-ph/0702540 (cit. on pp. 14, 30, 43).
- Casares, J., P. A. Charles and T. Naylor (1992), *A 6.5-day periodicity in the recurrent nova V404 Cygni implying the presence of a black hole*, *Nature* **355** 614 (cit. on p. 18).
- Castor, J. I., D. C. Abbott and R. I. Klein (1975), *Radiation-driven winds in Of stars*, *ApJ* **195** 157 (cit. on p. 11).

- Chaboyer, B. and J.-P. Zahn (1992), *Effect of horizontal turbulent diffusion on transport by meridional circulation*, A&A **253** 173 (cit. on pp. 70, 104, 105).
- Chandrasekhar, S. (1931), *The Maximum Mass of Ideal White Dwarfs*, ApJ **74** 81 (cit. on p. 8).
- Chaplin, W. J. and A. Miglio (2013), *Asteroseismology of Solar-Type and Red-Giant Stars*, ARA&A **51** 353, arXiv: [1303.1957 \[astro-ph.SR\]](#) (cit. on p. 30).
- Charbonneau, D. et al. (2007), *When Extrasolar Planets Transit Their Parent Stars*, Protostars and Planets V 701, eprint: [astro-ph/0603376](#) (cit. on p. 18).
- Charbonnel, C. and J.-P. Zahn (2007), *Thermohaline mixing: a physical mechanism governing the photospheric composition of low-mass giants*, A&A **467** L15, eprint: [astro-ph/0703302](#) (cit. on pp. 14, 104).
- Chatzopoulos, E. and J. C. Wheeler (2012), *Effects of Rotation on the Minimum Mass of Primordial Progenitors of Pair-instability Supernovae*, ApJ **748**, 42 42, arXiv: [1201.1328 \[astro-ph.HE\]](#) (cit. on pp. 55, 59).
- Chieffi, A. and M. Limongi (2013), ApJ **764**, 21 21 (cit. on p. 102).
- Christensen-Dalsgaard, J. and M. J. Thompson (2011), “Stellar hydrodynamics caught in the act: Asteroseismology with CoRoT and Kepler”, IAU Symposium, ed. by N. H. Brummell et al., vol. 271, IAU Symposium 32, arXiv: [1104.5191 \[astro-ph.SR\]](#) (cit. on p. 30).
- Clark, D. H. and F. R. Stephenson (1982), “The Historical Supernovae”, NATO Advanced Science Institutes (ASI) Series C, ed. by M. J. Rees and R. J. Stoneham, vol. 90, NATO Advanced Science Institutes (ASI) Series C 355 (cit. on p. 2).
- Coleiro, A. and S. Chaty (2013), *Distribution of High-mass X-Ray Binaries in the Milky Way*, ApJ **764**, 185 185, arXiv: [1212.5460 \[astro-ph.HE\]](#) (cit. on p. 92).
- Coleman Miller, M. and E. J. M. Colbert (2004), *Intermediate-Mass Black Holes*, International Journal of Modern Physics D **13** 1, eprint: [astro-ph/0308402](#) (cit. on p. 19).
- Couch, S. M., E. Chatzopoulos et al. (2015), *The Three-dimensional Evolution to Core Collapse of a Massive Star*, ApJ **808**, L21 L21, arXiv: [1503.02199 \[astro-ph.HE\]](#) (cit. on p. 13).
- Couch, S. M. and C. D. Ott (2015), *The Role of Turbulence in Neutrino-driven Core-collapse Supernova Explosions*, ApJ **799**, 5 5, arXiv: [1408.1399 \[astro-ph.HE\]](#) (cit. on p. 13).
- Creevey, O. L. et al. (2015), *Benchmark stars for Gaia Fundamental properties of the Population II star HD 140283 from interferometric, spectroscopic, and photometric data*, A&A **575**, A26 A26, arXiv: [1410.4780 \[astro-ph.SR\]](#) (cit. on p. 30).
- Crowther, P. A., S. M. Caballero-Nieves et al. (2016), *The R136 star cluster dissected with Hubble Space Telescope/STIS. I. Far-ultraviolet spectroscopic census and the origin of He II  $\lambda$ 1640 in young star clusters*, MNRAS **458** 624, arXiv: [1603.04994 \[astro-ph.SR\]](#) (cit. on p. 10).
- Crowther, P. A., O. Schnurr et al. (2010), *The R136 star cluster hosts several stars whose individual masses greatly exceed the accepted 150M<sub>solar</sub> stellar mass limit*, MNRAS **408** 731, arXiv: [1007.3284 \[astro-ph.SR\]](#) (cit. on pp. 10, 58, 136).
- Dark Energy Survey Collaboration et al. (2016), *The Dark Energy Survey: more than dark energy - an overview*, MNRAS **460** 1270, arXiv: [1601.00329](#) (cit. on pp. 16, 130).
- Darwin, G. H. (1879), *The Determination of the Secular Effects of Tidal Friction by a Graphical Method*, Proc. R. Soc. Lond. **29** 168 (cit. on p. 72).
- De Beck, E. et al. (2010), *Probing the mass-loss history of AGB and red supergiant stars from CO rotational line profiles. II. CO line survey of evolved stars: derivation of mass-loss rate formulae*, A&A **523**, A18 A18, arXiv: [1008.1083 \[astro-ph.SR\]](#) (cit. on p. 11).
- De Donder, E. and D. Vanbeveren (2004), *The influence of binaries on galactic chemical evolution*, New A Rev. **48** 861, eprint: [astro-ph/0410024](#) (cit. on p. 102).

- 
- de Jager, C., H. Nieuwenhuijen and K. A. van der Hucht (1988), *Mass loss rates in the Hertzsprung-Russell diagram*, A&AS **72** 259 (cit. on p. 11).
- de Mink, S. E., M. Cantiello et al. (2009), *Rotational mixing in massive binaries. Detached short-period systems*, A&A **497** 243, arXiv: [0902.1751 \[astro-ph.SR\]](#) (cit. on pp. 48, 69, 70, 75, 102, 135).
- de Mink, S. E., N. Langer et al. (2013), *The rotation rates of massive stars: the role of binary interaction through tides, mass transfer and mergers*, ApJ **764** (cit. on pp. 30, 36, 103, 104, 125).
- de Mink, S. E. and I. Mandel (2016), *The chemically homogeneous evolutionary channel for binary black hole mergers: rates and properties of gravitational-wave events detectable by advanced LIGO*, MNRAS **460** 3545, arXiv: [1603.02291 \[astro-ph.HE\]](#) (cit. on pp. 27, 69, 92, 102).
- de Mink, S. E., O. R. Pols and R. W. Hilditch (2007), *Efficiency of mass transfer in massive close binaries. Tests from double-lined eclipsing binaries in the SMC*, A&A **467** 1181, eprint: [astro-ph/0703480](#) (cit. on pp. 21, 102, 122, 128).
- de Mink, S. E., H. Sana et al. (2014), *The Incidence of Stellar Mergers and Mass Gainers among Massive Stars*, ApJ **782** (cit. on pp. 19, 22, 103, 114–116, 118, 127).
- De Ridder, J. et al. (2009), *Non-radial oscillation modes with long lifetimes in giant stars*, Nature **459** 398 (cit. on p. 30).
- Deheuvels, S. et al. (2012), *Seismic Evidence for a Rapidly Rotating Core in a Lower-giant-branch Star Observed with Kepler*, ApJ **756**, 19–19, arXiv: [1206.3312 \[astro-ph.SR\]](#) (cit. on p. 14).
- Delgado, A. J. and H.-C. Thomas (1981), *Mass transfer in a binary system - The evolution of the mass-giving helium star*, A&A **96** 142 (cit. on p. 72).
- Detmers, R. G. et al. (2008), *Gamma-ray bursts from tidally spun-up Wolf-Rayet stars?*, A&A **484** 831, arXiv: [0804.0014](#) (cit. on pp. 36, 49, 72, 104).
- Dewi, J. D. M., P. Podsiadlowski and A. Sena (2006), *Double-core evolution and the formation of neutron star binaries with compact companions*, MNRAS **368** 1742, eprint: [astro-ph/0602510](#) (cit. on p. 136).
- Dewi, J. D. M., O. R. Pols et al. (2002), *The evolution of naked helium stars with a neutron star companion in close binary systems*, MNRAS **331** 1027, eprint: [astro-ph/0201239](#) (cit. on p. 72).
- Diehl, R. et al. (2006), *Radioactive  $^{26}\text{Al}$  from massive stars in the Galaxy*, Nature **439** 45, eprint: [astro-ph/0601015](#) (cit. on p. 83).
- Dominik, M., K. Belczynski et al. (2012), *Double Compact Objects. I. The Significance of the Common Envelope on Merger Rates*, ApJ **759**, 52–52, arXiv: [1202.4901 \[astro-ph.HE\]](#) (cit. on pp. 22, 62).
- Dominik, M., E. Berti et al. (2015), *Double Compact Objects III: Gravitational-wave Detection Rates*, ApJ **806**, 263–263, arXiv: [1405.7016 \[astro-ph.HE\]](#) (cit. on pp. 61, 62).
- Donati, J.-F. and J. D. Landstreet (2009), *Magnetic Fields of Nondegenerate Stars*, ARA&A **47** 333 (cit. on p. 33).
- Dray, L. M. and C. A. Tout (2007), *On rejuvenation in massive binary systems*, MNRAS **376** 61, eprint: [astro-ph/0612539](#) (cit. on p. 107).
- Eddington, A. S. (1916), *On the radiative equilibrium of the stars*, MNRAS **77** 16 (cit. on p. 5).  
– (1920), *The Internal Constitution of the Stars*, Nature **106** 14 (cit. on p. 5).  
– (1924), *On the relation between the masses and luminosities of the stars*, MNRAS **84** 308 (cit. on p. 8).  
– (1926), *The Internal Constitution of the Stars* (cit. on p. 12).
- Eddington Sir, A. S. (1935), *On "relativistic degeneracy,"* MNRAS **95** 194 (cit. on p. 9).
- Eggenberger, P., G. Meynet and A. Maeder (2002), *The blue to red supergiant ratio in young clusters at various metallicities*, A&A **386** 576, eprint: [astro-ph/0202478](#) (cit. on p. 10).
- Eggleton, P. P. (1983), *Approximations to the radii of Roche lobes*, ApJ **268** 368 (cit. on pp. 33, 50, 112, 113).
- Eggleton, P. P. (1971), *The evolution of low mass stars*, MNRAS **151** 351 (cit. on p. 37).

- Einstein, A. (1916), *Näherungsweise Integration der Feldgleichungen der Gravitation*, Sitzungsberichte der Königlich Preußischen Akademie der Wissenschaften (Berlin), Seite 688-696. (cit. on p. 22).
- (1918), *Über Gravitationswellen*, Sitzungsberichte der Königlich Preußischen Akademie der Wissenschaften (Berlin), Seite 154-167. (cit. on p. 131).
- Ekström, S. et al. (2012), *A&A 537, A146 A146*, arXiv: [1110.5049 \[astro-ph.SR\]](#) (cit. on p. 102).
- Eldridge, J. J. and E. R. Stanway (2009), *Spectral population synthesis including massive binaries*, *MNRAS 400 1019*, arXiv: [0908.1386](#) (cit. on p. 102).
- Emden, R. (1907), *Gaskugeln*, B. Teubner. (cit. on p. 4).
- Endal, A. S. and S. Sofia (1976), *The evolution of rotating stars. I - Method and exploratory calculations for a 7-solar-mass star*, *ApJ 210 184* (cit. on p. 70).
- Evans, C. J., D. J. Lennon et al. (2006), *The VLT-FLAMES survey of massive stars: observations centered on the Magellanic Cloud clusters NGC 330, NGC 346, NGC 2004, and the N11 region*, *A&A 456 623*, eprint: [astro-ph/0606405](#) (cit. on p. 10).
- Evans, C. J., W. D. Taylor et al. (2011), *The VLT-FLAMES Tarantula Survey. I. Introduction and observational overview*, *A&A 530, A108 A108*, arXiv: [1103.5386 \[astro-ph.SR\]](#) (cit. on pp. 10, 19, 102).
- Evans, C. et al. (2008), *The VLT-FLAMES Survey of Massive Stars*, *The Messenger 131* 25, arXiv: [0803.2820](#) (cit. on p. 10).
- Fabbiano, G. (2006), *Populations of X-Ray Sources in Galaxies*, *ARA&A 44* 323, eprint: [astro-ph/0511481](#) (cit. on p. 19).
- Farrell, S. A. et al. (2009), *An intermediate-mass black hole of over 500 solar masses in the galaxy ESO243-49*, *Nature 460* 73, arXiv: [1001.0567 \[astro-ph.HE\]](#) (cit. on p. 69).
- Ferrario, L. et al. (2009), *The origin of magnetism on the upper main sequence*, *MNRAS 400* L71 (cit. on pp. 22, 130).
- Finn, L. S. (1996), *Binary inspiral, gravitational radiation, and cosmology*, *Physical Review D 53* 2878, eprint: [gr-qc/9601048](#) (cit. on p. 62).
- Finn, L. S. and D. F. Chernoff (1993), *Observing binary inspiral in gravitational radiation: One interferometer*, *Physical Review D 47* 2198, eprint: [gr-qc/9301003](#) (cit. on p. 63).
- Fitzpatrick, E. L. and C. D. Garmany (1990), *The H-R diagram of the Large Magellanic Cloud and implications for stellar evolution*, *ApJ 363* 119 (cit. on p. 10).
- Flanagan, É. É. and S. A. Hughes (1998), *Measuring gravitational waves from binary black hole coalescences. I. Signal to noise for inspiral, merger, and ringdown*, *Phys. Rev. D 57* 4535, eprint: [gr-qc/9701039](#) (cit. on p. 64).
- Fossati, L. et al. (2015), *B fields in OB stars (BOB): Low-resolution FORS2 spectropolarimetry of the first sample of 50 massive stars*, *A&A 582, A45 A45*, arXiv: [1508.00750 \[astro-ph.SR\]](#) (cit. on p. 22).
- Foucart, F. (2012), *Black-hole-neutron-star mergers: Disk mass predictions*, *Phys. Rev. D 86*, 124007 124007, arXiv: [1207.6304 \[astro-ph.HE\]](#) (cit. on p. 94).
- Fraley, G. S. (1968), *Supernovae Explosions Induced by Pair-Production Instability*, *Ap&SS 2* 96 (cit. on p. 16).
- Fraunhofer, J. (1817), *Bestimmung des Brechungs- und des Farbenzerstreuungs-Vermögens verschiedener Glasarten, in Bezug auf die Vervollkommenung achromatischer Fernröhre*, *Annalen der Physik 56* 264 (cit. on p. 2).
- (1823), *Kurzer Bericht von den Resultaten neuerer Versuche über die Gesetze des Lichtes, und die Theorie derselben*, *Annalen der Physik 74* 337 (cit. on p. 3).
- Fryer, C. L. and V. Kalogera (2001), *Theoretical Black Hole Mass Distributions*, *ApJ 554* 548, eprint: [astro-ph/9911312](#) (cit. on pp. 68, 92).

- 
- Fuller, J. et al. (2014), *Angular Momentum Transport via Internal Gravity Waves in Evolving Stars*, *ApJ* **796**, 17–17, arXiv: [1409.6835 \[astro-ph.SR\]](#) (cit. on p. 15).
- Gaburov, E., J. C. Lombardi and S. Portegies Zwart (2008), *Mixing in massive stellar mergers*, *MNRAS* **383** L5, arXiv: [0707.3021](#) (cit. on pp. 22, 115, 130).
- Gal-Yam, A. (2012), *Luminous Supernovae*, *Science* **337** 927, arXiv: [1208.3217](#) (cit. on p. 16).
- Gal-Yam, A. et al. (2009), *Supernova 2007bi as a pair-instability explosion*, *Nature* **462** 624, arXiv: [1001.1156](#) (cit. on p. 16).
- Gänsicke, B. T. et al. (2009), *SDSS unveils a population of intrinsically faint cataclysmic variables at the minimum orbital period*, *MNRAS* **397** 2170 (cit. on p. 39).
- Gerke, J. R., C. S. Kochanek and K. Z. Stanek (2015), *The search for failed supernovae with the Large Binocular Telescope: first candidates*, *MNRAS* **450** 3289, arXiv: [1411.1761 \[astro-ph.SR\]](#) (cit. on p. 130).
- Giacconi, R. et al. (1962), *Evidence for x Rays From Sources Outside the Solar System*, *Physical Review Letters* **9** 439 (cit. on p. 17).
- Gilfanov, M., H.-J. Grimm and R. Sunyaev (2004), *HMXB, ULX and star formation*, *Nuclear Physics B Proceedings Supplements* **132** 369, eprint: [astro-ph/0309725](#) (cit. on pp. 83, 87).
- Gladstone, J. C. et al. (2013), *Optical Counterparts of the Nearest Ultraluminous X-Ray Sources*, *ApJS* **206**, 14–14, arXiv: [1303.1213 \[astro-ph.HE\]](#) (cit. on p. 89).
- Glebbeek, E. et al. (2013), *Structure and evolution of high-mass stellar mergers*, *MNRAS* **434** 3497, arXiv: [1307.2445 \[astro-ph.SR\]](#) (cit. on pp. 22, 115, 130).
- Goodricke, J. (1783), *A Series of Observations on, and a Discovery of, the Period of the Variation of the Light of the Bright Star in the Head of Medusa, Called Algol. In a Letter from John Goodricke, Esq. to the Rev. Anthony Shepherd, D. D. F. R. S. and Plumian Professor at Cambridge*, Philosophical Transactions of the Royal Society of London Series I **73** 474 (cit. on p. 17).
- Gräfener, G. and W.-R. Hamann (2008), *Mass loss from late-type WN stars and its Z-dependence. Very massive stars approaching the Eddington limit*, *A&A* **482** 945, arXiv: [0803.0866](#) (cit. on p. 13).
- Gräfener, G., S. P. Owocki and J. S. Vink (2012), *Stellar envelope inflation near the Eddington limit. Implications for the radii of Wolf-Rayet stars and luminous blue variables*, *A&A* **538**, A40–A40, arXiv: [1112.1910 \[astro-ph.SR\]](#) (cit. on p. 13).
- Gräfener, G., J. S. Vink et al. (2011), *The Eddington factor as the key to understand the winds of the most massive stars. Evidence for a Γ-dependence of Wolf-Rayet type mass loss*, *A&A* **535**, A56–A56, arXiv: [1106.5361 \[astro-ph.SR\]](#) (cit. on p. 13).
- Grevesse, N., A. Noels and A. J. Sauval (1996), “Standard Abundances”, *Cosmic Abundances*, ed. by S. S. Holt and G. Sonneborn, vol. 99, Astronomical Society of the Pacific Conference Series 117 (cit. on pp. 49, 50, 70, 72, 104).
- Grigahcène, A. et al. (2010), *Kepler observations: Light shed on the hybrid γ Doradus - δ Scuti pulsation phenomenon*, *Astronomische Nachrichten* **331** 989 (cit. on p. 30).
- Grimm, H.-J., M. Gilfanov and R. Sunyaev (2003), *High-mass X-ray binaries as a star formation rate indicator in distant galaxies*, *MNRAS* **339** 793, eprint: [astro-ph/0205371](#) (cit. on pp. 19, 68, 83–85, 87, 88).
- Grin, N. J. et al. (2016), *The VLT-FLAMES Tarantula Survey XXV. Surface nitrogen abundances of O-type giants and supergiants*, ArXiv e-prints, arXiv: [1609.00197 \[astro-ph.SR\]](#) (cit. on pp. 15, 102, 125, 128).
- Gursky, H. et al. (1966), *A Measurement of the Location of the X-Ray Source SCO X-1*, *ApJ* **146** 310 (cit. on p. 17).
- Haiman, Z. and A. Loeb (1997), *Signatures of Stellar Reionization of the Universe*, *ApJ* **483** 21, eprint: [astro-ph/9611028](#) (cit. on pp. 9, 102).

## Bibliography

---

- Hainich, R. et al. (2014), *The Wolf-Rayet stars in the Large Magellanic Cloud. A comprehensive analysis of the WN class*, *A&A* **565**, A27 A27, arXiv: 1401.5474 [astro-ph.SR] (cit. on p. 136).
- Hamann, W.-R., L. Koesterke and U. Wessolowski (1995), *Spectral analyses of the Galactic Wolf-Rayet stars: hydrogen-helium abundances and improved stellar parameters for the WN class*, *A&A* **299** 151 (cit. on pp. 49, 72, 104).
- Han, Z. et al. (2003), *The origin of subdwarf B stars - II*, *MNRAS* **341** 669, eprint: astro-ph/0301380 (cit. on p. 48).
- Hannam, M. et al. (2013), *When can Gravitational-wave Observations Distinguish between Black Holes and Neutron Stars?*, *ApJ* **766**, L14 L14, arXiv: 1301.5616 [gr-qc] (cit. on pp. 27, 94, 129).
- Harrison, B. K. et al. (1965), *Gravitation Theory and Gravitational Collapse* (cit. on p. 9).
- Heger, A., C. L. Fryer et al. (2003), *How Massive Single Stars End Their Life*, *ApJ* **591** 288, eprint: astro-ph/0212469 (cit. on p. 135).
- Heger, A. and N. Langer (2000), *Presupernova Evolution of Rotating Massive Stars. II. Evolution of the Surface Properties*, *ApJ* **544** 1016, eprint: astro-ph/0005110 (cit. on p. 70).
- Heger, A., N. Langer and S. E. Woosley (2000), *Presupernova Evolution of Rotating Massive Stars. I. Numerical Method and Evolution of the Internal Stellar Structure*, *ApJ* **528** 368, eprint: astro-ph/9904132 (cit. on pp. 14, 30, 48, 49, 102, 104).
- Heger, A. and S. E. Woosley (2002), *The Nucleosynthetic Signature of Population III*, *ApJ* **567** 532, eprint: astro-ph/0107037 (cit. on pp. 16, 55, 68).
- Heger, A., S. E. Woosley and H. C. Spruit (2005), *Presupernova Evolution of Differentially Rotating Massive Stars Including Magnetic Fields*, *ApJ* **626** 350, eprint: astro-ph/0409422 (cit. on pp. 14, 30, 104).
- Hellings, P. (1983), *Phenomenological study of massive accretion stars*, *Ap&SS* **96** 37 (cit. on p. 107). – (1984), *The post-RLOF structure of the secondary components in close binary systems, with an application to masses of Wolf-Rayet stars*, *Ap&SS* **104** 83 (cit. on p. 107).
- Herrero, A. et al. (1992), *Intrinsic parameters of galactic luminous OB stars*, *A&A* **261** 209 (cit. on p. 10).
- Herschel, W. (1803), *Account of the Changes That Have Happened, during the Last Twenty-Five Years, in the Relative Situation of Double-Stars; With an Investigation of the Cause to Which They Are Owing*, Philosophical Transactions of the Royal Society of London Series I **93** 339 (cit. on pp. 2, 30).
- Hertzsprung, E. (1911), *Ueber die Verwendung photographischer effektiver Wellenlaengen zur Bestimmung von Farbenaequivalenten*, Publikationen des Astrophysikalischen Observatoriums zu Potsdam **63** (cit. on p. 4).
- Hewish, A. et al. (1968), *Observation of a Rapidly Pulsating Radio Source*, *Nature* **217** 709 (cit. on p. 9).
- Hills, J. G. (1983), *The effects of sudden mass loss and a random kick velocity produced in a supernova explosion on the dynamics of a binary star of arbitrary orbital eccentricity - Applications to X-ray binaries and to the binary pulsars*, *ApJ* **267** 322 (cit. on p. 133).
- Hjorth, J. et al. (2003), *A very energetic supernova associated with the  $\gamma$ -ray burst of 29 March 2003*, *Nature* **423** 847, eprint: astro-ph/0306347 (cit. on p. 16).
- Hobbs, G. et al. (2005), *A statistical study of 233 pulsar proper motions*, *MNRAS* **360** 974, eprint: astro-ph/0504584 (cit. on pp. 92, 131).
- Hofmeister, E., R. Kippenhahn and A. Weigert (1964a), *Sternentwicklung I. Ein Programm zur Lösung der zeitabhängigen Aufbaugleichungen. Mit 3 Textabbildungen*, Zeitschrift für Astrophysik **59** 215 (cit. on p. 102). – (1964b), *Sternentwicklung II. Die Wasserstoff-brennende Phase eines Sterns von 7.0 Sonnenmassen. Mit 6 Textabbildungen*, Zeitschrift für Astrophysik **59** 242 (cit. on p. 7).

- 
- Howell, S. B., L. A. Nelson and S. Rappaport (2001), *An Exploration of the Paradigm for the 2-3 Hour Period Gap in Cataclysmic Variables*, ApJ **550** 897 (cit. on pp. 39, 41).
- Hulse, R. A. and J. H. Taylor (1975), *Discovery of a pulsar in a binary system*, ApJ **195** L51 (cit. on pp. 23, 48).
- Hunter, I. et al. (2008), *The VLT FLAMES Survey of Massive Stars: Rotation and Nitrogen Enrichment as the Key to Understanding Massive Star Evolution*, ApJ **676**, L29 L29, arXiv: [0711.2267](#) (cit. on pp. 15, 102, 125).
- Hurley, J. R., C. A. Tout and O. R. Pols (2002), *Evolution of binary stars and the effect of tides on binary populations*, MNRAS **329** 897, eprint: [astro-ph/0201220](#) (cit. on pp. 36, 43, 44, 49, 72, 102, 104).
- Hut, P. (1981), *Tidal evolution in close binary systems*, ApJ **99** 126 (cit. on pp. 21, 36).
- Iben Jr., I. (1967), *Stellar Evolution Within and off the Main Sequence*, ARA&A **5** 571 (cit. on p. 102).
- Iglesias, C. A. and F. J. Rogers (1996), *Updated Opal Opacities*, ApJ **464** 943 (cit. on pp. 12, 49, 70, 103, 104).
- Israel, G. L., A. Belfiore et al. (2016), *ULX-1 in NGC5907: how bright can an accreting pulsar shine?*, ArXiv e-prints, arXiv: [1609.07375 \[astro-ph.HE\]](#) (cit. on p. 68).
- Israel, G. L., A. Papitto et al. (2016), *Discovery of a 0.42-s pulsar in NGC 7793 P13*, ArXiv e-prints, arXiv: [1609.06538 \[astro-ph.HE\]](#) (cit. on p. 68).
- Ivanova, N. et al. (2013), *Common envelope evolution: where we stand and how we can move forward*, A&A Rev. **21**, 59 59, arXiv: [1209.4302 \[astro-ph.HE\]](#) (cit. on pp. 22, 48, 135).
- Izzard, R. G. et al. (2006), *Population nucleosynthesis in single and binary stars. I. Model*, A&A **460** 565 (cit. on p. 102).
- Janka, H.-T. (2012), *Explosion Mechanisms of Core-Collapse Supernovae*, Annual Review of Nuclear and Particle Science **62** 407, arXiv: [1206.2503 \[astro-ph.SR\]](#) (cit. on p. 131).
- (2013), *Natal kicks of stellar mass black holes by asymmetric mass ejection in fallback supernovae*, MNRAS **434** 1355, arXiv: [1306.0007 \[astro-ph.SR\]](#) (cit. on p. 131).
- Japelj, J. et al. (2016), *Taking stock of superluminous supernovae and long gamma-ray burst host galaxy comparison using a complete sample of LGRBs*, A&A **593**, A115 A115, arXiv: [1607.01045 \[astro-ph.HE\]](#) (cit. on p. 16).
- Jiang, Y.-F. et al. (2015), *Local Radiation Hydrodynamic Simulations of Massive Star Envelopes at the Iron Opacity Peak*, ApJ **813**, 74 74, arXiv: [1509.05417 \[astro-ph.SR\]](#) (cit. on p. 13).
- Joss, P. C., E. E. Salpeter and J. P. Ostriker (1973), *On the "critical Luminosity" in Stellar Interiors and Stellar Surface Boundary Conditions . .*, ApJ **181** 429 (cit. on p. 12).
- Kaiser, N. et al. (2002), “Pan-STARRS: A Large Synoptic Survey Telescope Array”, *Survey and Other Telescope Technologies and Discoveries*, ed. by J. A. Tyson and S. Wolff, vol. 4836, Proc. SPIE 154 (cit. on pp. 16, 130).
- Kalogera, V. et al. (2004), *The Cosmic Coalescence Rates for Double Neutron Star Binaries*, ApJ **601** L179 (cit. on p. 48).
- Kasen, D. and L. Bildsten (2010), *Supernova Light Curves Powered by Young Magnetars*, ApJ **717** 245, arXiv: [0911.0680 \[astro-ph.HE\]](#) (cit. on p. 16).
- Kato, S. (1966), *Overstable Convection in a Medium Stratified in Mean Molecular Weight*, PASJ **18** 374 (cit. on p. 14).
- King, A. R. et al. (2001), *Ultraluminous X-Ray Sources in External Galaxies*, ApJ **552** L109, eprint: [astro-ph/0104333](#) (cit. on p. 68).
- King, A. and J.-P. Lasota (2016), *ULXs: Neutron stars versus black holes*, MNRAS **458** L10, arXiv: [1601.03738 \[astro-ph.HE\]](#) (cit. on pp. 68, 130).
- Kippenhahn, R., G. Ruschenplatt and H.-C. Thomas (1980), *The time scale of thermohaline mixing in stars*, A&A **91** 175 (cit. on pp. 14, 36, 103).

- Kippenhahn, R. and A. Weigert (1967), *Entwicklung in engen Doppelsternsystemen I. Massenaustausch vor und nach Beendigung des zentralen Wasserstoff-Brennens*, Zeitschrift für Astrophysik **66** 251 (cit. on pp. 20, 41).
- Kobulnicky, H. A. and C. L. Fryer (2007), *A New Look at the Binary Characteristics of Massive Stars*, ApJ **670** 747 (cit. on pp. 102, 129).
- Kobulnicky, H. A., D. C. Kiminki et al. (2014), *Toward Complete Statistics of Massive Binary Stars: Penultimate Results from the Cygnus OB2 Radial Velocity Survey*, ApJS **213**, 34 34, arXiv: [1406.6655 \[astro-ph.SR\]](#) (cit. on pp. 15, 18, 30, 102, 129).
- Koenigsberger, G. et al. (2014), *The HD 5980 Multiple System: Masses and Evolutionary Status*, AJ **148**, 62 62, arXiv: [1408.0556 \[astro-ph.SR\]](#) (cit. on p. 58).
- Köhler, K. et al. (2015), *The evolution of rotating very massive stars with LMC composition*, A&A **573**, A71 A71, arXiv: [1501.03794 \[astro-ph.SR\]](#) (cit. on pp. 48, 51, 56, 74, 79).
- Kolb, U. and H. Ritter (1990), *A comparative study of the evolution of a close binary using a standard and an improved technique for computing mass transfer*, A&A **236** 385 (cit. on pp. 34, 35).
- Kopal, Z. (1955), *The classification of close binary systems*, Annales d’Astrophysique **18** 379 (cit. on p. 20).
- Kopparapu, R. K. et al. (2008), *Host Galaxies Catalog Used in LIGO Searches for Compact Binary Coalescence Events*, ApJ **675** 1459, arXiv: [0706.1283](#) (cit. on p. 63).
- Körding, E., H. Falcke and S. Markoff (2002), *Population X: Are the super-Eddington X-ray sources beamed jets in microblazars or intermediate mass black holes?*, A&A **382** L13, eprint: [astro-ph/0112385](#) (cit. on p. 68).
- Kouveliotou, C. et al. (1993), *Identification of two classes of gamma-ray bursts*, ApJ **413** L101 (cit. on p. 16).
- Kramer, M. (2004), *Fundamental Physics with the SKA:Strong-Field Tests of Gravity Using Pulsars and Black Holes*, ArXiv Astrophysics e-prints, eprint: [astro-ph/0409020](#) (cit. on p. 92).
- Kramer, M., I. H. Stairs et al. (2006a), *Tests of General Relativity from Timing the Double Pulsar*, Science **314** 97 (cit. on p. 31).
- (2006b), *Tests of General Relativity from Timing the Double Pulsar*, Science **314** 97, eprint: [astro-ph/0609417](#) (cit. on p. 48).
- Kruckow, M. U. et al. (2016), *Common envelope ejection in massive binary stars - Implications for the progenitors of GW150914 and GW151226*, ArXiv e-prints, arXiv: [1610.04417 \[astro-ph.SR\]](#) (cit. on pp. 69, 89).
- Kulkarni, S. R. et al. (2007), *An unusually brilliant transient in the galaxy M85*, Nature **447** 458, arXiv: [0705.3668](#) (cit. on p. 130).
- Kurtz, D. W. et al. (2014), *Asteroseismic measurement of surface-to-core rotation in a main-sequence A star; KIC 11145123*, MNRAS **444** 102, arXiv: [1405.0155 \[astro-ph.SR\]](#) (cit. on p. 14).
- Landau, L. D. (1932), *To the Stars theory*, Phys. Zs. Sowjet., vol.1, p.285, 1932 (English and German) **1** 285 (cit. on p. 9).
- Langer, N. (1992), *Helium enrichment in massive early type stars*, A&A **265** L17 (cit. on p. 48).
- (1997), “The Eddington Limit in Rotating Massive Stars”, *Luminous Blue Variables: Massive Stars in Transition*, ed. by A. Nota and H. Lamers, vol. 120, Astronomical Society of the Pacific Conference Series 83 (cit. on p. 74).
- (1998), *Coupled mass and angular momentum loss of massive main sequence stars*, A&A **329** 551 (cit. on p. 104).
- (2012), *Presupernova Evolution of Massive Single and Binary Stars*, ARA&A **50** 107, arXiv: [1206.5443 \[astro-ph.SR\]](#) (cit. on pp. 10, 12, 55, 135).

- 
- Langer, N., M. Cantiello et al. (2008), “Rotation and Massive Close Binary Evolution”, *Massive Stars as Cosmic Engines*, ed. by F. Bresolin, P. A. Crowther and J. Puls, vol. 250, IAU Symposium 167, arXiv: [0803.0621](#) (cit. on pp. 102, 125).
- Langer, N., M. F. El Eid and K. J. Fricke (1985), *Evolution of massive stars with semiconvective diffusion*, *A&A* **145** 179 (cit. on p. 14).
- Langer, N., K. J. Fricke and D. Sugimoto (1983), *Semiconvective diffusion and energy transport*, *A&A* **126** 207 (cit. on pp. 49, 70, 103).
- Langer, N. and A. Maeder (1995), *The problem of the blue-to-red supergiant ratio in galaxies.*, *A&A* **295** 685 (cit. on p. 10).
- Langer, N. and C. A. Norman (2006), *On the Collapsar Model of Long Gamma-Ray Bursts: Constraints from Cosmic Metallicity Evolution*, *ApJ* **638** L63, eprint: [astro-ph/0512271](#) (cit. on pp. 64, 85, 86, 89, 90, 94).
- Langer, N., D. Sanyal et al. (2015), “The stellar Eddington limit”, *Wolf-Rayet Stars: Proceedings of an International Workshop held in Potsdam, Germany, 1-5 June 2015. Edited by Wolf-Rainer Hamann, Andreas Sander, Helge Todt. Universitätsverlag Potsdam, 2015.*, p.241-244, ed. by W.-R. Hamann, A. Sander and H. Todt 241 (cit. on p. 114).
- Langer, N., S. Wellstein and J. Petrovic (2003), *On the evolution of massive close binaries*, Proceedings of IAU Symposium **212** 275 (cit. on pp. 43, 45).
- Larsen, S. S. et al. (2011), *Resolved photometry of extragalactic young massive star clusters*, *A&A* **532**, A147 A147, arXiv: [1106.4560](#) (cit. on p. 10).
- Law, N. M. et al. (2009), *The Palomar Transient Factory: System Overview, Performance, and First Results*, *PASP* **121** 1395, arXiv: [0906.5350](#) [astro-ph.IM] (cit. on p. 30).
- Laycock, S. G. T., T. J. Maccarone and D. M. Christodoulou (2015), *Revisiting the dynamical case for a massive black hole in IC10 X-1*, *MNRAS* **452** L31, arXiv: [1506.03882](#) [astro-ph.HE] (cit. on p. 69).
- Lin, J. et al. (2011), *LMXB and IMXB Evolution: I. The Binary Radio Pulsar PSR J1614-2230*, *ApJ* **732** 70 (cit. on p. 30).
- Linden, T. et al. (2010), *The Effect of Starburst Metallicity on Bright X-ray Binary Formation Pathways*, *ApJ* **725** 1984, arXiv: [1005.1639](#) (cit. on p. 91).
- Liu, J.-F. et al. (2013), *Puzzling accretion onto a black hole in the ultraluminous X-ray source M 101 ULX-1*, *Nature* **503** 500, arXiv: [1312.0337](#) [astro-ph.HE] (cit. on p. 69).
- Long, K. S. and L. P. van Speybroeck (1983), “X-ray emission from normal galaxies”, *Accretion-Driven Stellar X-ray Sources*, ed. by W. H. G. Lewin and E. P. J. van den Heuvel 117 (cit. on pp. 19, 68).
- Luangtip, W. et al. (2015), *A deficit of ultraluminous X-ray sources in luminous infrared galaxies*, *MNRAS* **446** 470, arXiv: [1410.1569](#) [astro-ph.HE] (cit. on p. 68).
- Lubow, S. H. and F. H. Shu (1975), *Gas dynamics of semidetached binaries*, *ApJ* **198** 385 (cit. on p. 36).
- Lucy, L. B. and P. M. Solomon (1970), *Mass Loss by Hot Stars*, *ApJ* **159** 879 (cit. on p. 11).
- Mac Low, M.-M. et al. (2005), *The Distribution of Pressures in a Supernova-driven Interstellar Medium. I. Magnetized Medium*, *ApJ* **626** 864, eprint: [astro-ph/0410734](#) (cit. on p. 9).
- MacLeod, M., M. Trenti and E. Ramirez-Ruiz (2016), *The Close Stellar Companions to Intermediate-mass Black Holes*, *ApJ* **819**, 70 70, arXiv: [1508.07000](#) [astro-ph.HE] (cit. on p. 70).
- Madau, P. and M. Dickinson (2014), *Cosmic Star-Formation History*, *ARA&A* **52** 415, arXiv: [1403.0007](#) (cit. on p. 97).
- Madau, P. and M. J. Rees (2001), *Massive Black Holes as Population III Remnants*, *ApJ* **551** L27, eprint: [astro-ph/0101223](#) (cit. on p. 68).
- Madhusudhan, N., S. Justham et al. (2006), *Models of Ultraluminous X-Ray Sources with Intermediate-Mass Black Holes*, *ApJ* **640** 918 (cit. on p. 30).

- Madhusudhan, N., S. Rappaport et al. (2008), *Models for the Observable System Parameters of Ultraluminous X-Ray Sources*, *ApJ* **688**, 1235–1249 1235, arXiv: [0710.3854](#) (cit. on p. 91).
- Maeder, A. (1987), *Evidences for a bifurcation in massive star evolution. The ON-blue stragglers*, *A&A* **178** 159 (cit. on pp. 14, 48, 102).
- (2000), *Chemical enrichments by massive stars and the effects of rotation*, *New A Rev.* **44** 291 (cit. on pp. 15, 102).
- Maeder, A. and G. Meynet (2000), *The Evolution of Rotating Stars*, *ARA&A* **38** 143, eprint: arXiv: [astro-ph/0004204](#) (cit. on pp. 15, 30, 102).
- (2012), *Rotating massive stars: From first stars to gamma ray bursts*, *Reviews of Modern Physics* **84** 25 (cit. on p. 135).
- Manchester, R. N. and IPTA (2013), *The International Pulsar Timing Array*, *Classical and Quantum Gravity* **30**, 224010 224010, arXiv: [1309.7392 \[astro-ph.IM\]](#) (cit. on p. 23).
- Mandel, I. and S. E. de Mink (2016), *Merging binary black holes formed through chemically homogeneous evolution in short-period stellar binaries*, *MNRAS* **458** 2634, arXiv: [1601.00007 \[astro-ph.HE\]](#) (cit. on pp. 25, 48, 56, 64, 69, 92, 102, 129).
- Mapelli, M., E. Ripamonti et al. (2010), *Ultra-luminous X-ray sources and remnants of massive metal-poor stars*, *MNRAS* **408** 234, arXiv: [1005.3548](#) (cit. on pp. 19, 69).
- Mapelli, M. and L. Zampieri (2014), *Roche-lobe Overflow Systems Powered by Black Holes in Young Star Clusters: The Importance of Dynamical Exchanges*, *ApJ* **794**, 77, arXiv: [1408.1406 \[astro-ph.HE\]](#) (cit. on pp. 70, 91).
- Marchant, P. et al. (2016), *A new route towards merging massive black holes*, *A&A* **588**, A50 A50, arXiv: [1601.03718 \[astro-ph.SR\]](#) (cit. on pp. 25, 69–72, 75, 79, 81, 92, 98, 102, 104, 112, 129, 139).
- Marchenko, S. V. et al. (2007), *Spectroscopy of SMC Wolf-Rayet Stars Suggests that Wind Clumping Does Not Depend on Ambient Metallicity*, *ApJ* **656** L77, eprint: [astro-ph/0701516](#) (cit. on p. 11).
- Marsh, T. R., G. Nelemans and D. Steeghs (2004), *Mass transfer between double white dwarfs*, *MNRAS* **350** 113, eprint: [astro-ph/0312577](#) (cit. on p. 36).
- Martins, F., L. Mahy et al. (2012), *A quantitative study of O stars in NGC 2244 and the Monoceros OB2 association*, *A&A* **538**, A39 A39, arXiv: [1110.4509 \[astro-ph.SR\]](#) (cit. on p. 10).
- Martins, F. and A. Palacios (2013), *A comparison of evolutionary tracks for single Galactic massive stars*, *A&A* **560**, A16 A16, arXiv: [1310.7218 \[astro-ph.SR\]](#) (cit. on pp. 102, 105).
- Mauron, N. and E. Josselin (2011), *The mass-loss rates of red supergiants and the de Jager prescription*, *A&A* **526**, A156 A156, arXiv: [1010.5369 \[astro-ph.SR\]](#) (cit. on p. 11).
- Mayor, M. et al. (2003), *Setting New Standards with HARPS*, *The Messenger* **114** 20 (cit. on p. 18).
- McClintock, J. E., R. Narayan and J. F. Steiner (2014), *Black Hole Spin via Continuum Fitting and the Role of Spin in Powering Transient Jets*, *Space Science Reviews* **183** 295, arXiv: [1303.1583 \[astro-ph.HE\]](#) (cit. on p. 131).
- McCray, R. (1993), *Supernova 1987A revisited*, *ARA&A* **31** 175 (cit. on p. 9).
- McKee, C. F. and J. P. Ostriker (1977), *A theory of the interstellar medium - Three components regulated by supernova explosions in an inhomogeneous substrate*, *ApJ* **218** 148 (cit. on p. 102).
- Merloni, A. et al. (2012), *eROSITA Science Book: Mapping the Structure of the Energetic Universe*, ArXiv e-prints, arXiv: [1209.3114 \[astro-ph.HE\]](#) (cit. on p. 130).
- Mestel, L. (1968), *Magnetic braking by a stellar wind-I*, *MNRAS* **138** 359 (cit. on p. 33).
- Meynet, G. et al. (2015), *Impact of mass-loss on the evolution and pre-supernova properties of red supergiants*, *A&A* **575**, A60 A60, arXiv: [1410.8721 \[astro-ph.SR\]](#) (cit. on p. 130).
- Miller, M. C. and D. P. Hamilton (2002), *Production of intermediate-mass black holes in globular clusters*, *MNRAS* **330** 232, eprint: [astro-ph/0106188](#) (cit. on p. 68).

- 
- Moffat, A. F. J. et al. (1988), *Spectroscopic evidence for rapid blob ejection in Wolf-Rayet stars*, *ApJ* **334** 1038 (cit. on p. 11).
- Mohamed, S. and P. Podsiadlowski (2007), “Wind Roche-Lobe Overflow: a New Mass-Transfer Mode for Wide Binaries”, *15th European Workshop on White Dwarfs*, ed. by R. Napiwotzki and M. R. Burleigh, vol. 372, Astronomical Society of the Pacific Conference Series 397 (cit. on p. 21).
- Mokiem, M. R., A. de Koter, C. J. Evans et al. (2007), *The VLT-FLAMES survey of massive stars: wind properties and evolution of hot massive stars in the Large Magellanic Cloud*, *A&A* **465** 1003, arXiv: [0704.1113](#) (cit. on p. 10).
- Mokiem, M. R., A. de Koter, J. S. Vink et al. (2007), *The empirical metallicity dependence of the mass-loss rate of O- and early B-type stars*, *A&A* **473** 603, arXiv: [0708.2042](#) (cit. on p. 51).
- Moore, C. J., R. H. Cole and C. P. L. Berry (2015), *Gravitational-wave sensitivity curves*, *Classical and Quantum Gravity* **32**, 015014 015014, arXiv: [1408.0740 \[gr-qc\]](#) (cit. on p. 24).
- Morel, T., S. Hubrig and M. Briquet (2008), *Nitrogen enrichment, boron depletion and magnetic fields in slowly-rotating B-type dwarfs*, *A&A* **481** 453, arXiv: [0801.4491](#) (cit. on p. 102).
- Morton, D. C. (1960), *Evolutionary Mass Exchange in Close Binary Systems.*, *ApJ* **132** 146 (cit. on p. 20).
- (1967), *Mass Loss from Three OB Supergiants in Orion*, *ApJ* **150** 535 (cit. on p. 10).
- Mosser, B. et al. (2012), *Spin down of the core rotation in red giants*, *A&A* **548**, A10 A10, arXiv: [1209.3336 \[astro-ph.SR\]](#) (cit. on p. 14).
- Motch, C. et al. (2014), *A mass of less than 15 solar masses for the black hole in an ultraluminous X-ray source*, *Nature* **514** 198, arXiv: [1410.4250 \[astro-ph.HE\]](#) (cit. on p. 69).
- Muijres, L. E. et al. (2011), *Predictions of the effect of clumping on the wind properties of O-type stars*, *A&A* **526**, A32 A32 (cit. on p. 11).
- Müller, B. et al. (2016), *The Last Minutes of Oxygen Shell Burning in a Massive Star*, ArXiv e-prints, arXiv: [1605.01393 \[astro-ph.SR\]](#) (cit. on p. 13).
- Munari, U. et al. (2002), *The mysterious eruption of V838 Mon*, *A&A* **389** L51, eprint: [astro-ph/0205288](#) (cit. on p. 22).
- Nakar, E. (2007), *Short-hard gamma-ray bursts*, *Phys. Rep.* **442** 166, eprint: [astro-ph/0701748](#) (cit. on p. 16).
- Nelemans, G., T. M. Tauris and E. P. J. van den Heuvel (1999), *Constraints on mass ejection in black hole formation derived from black hole X-ray binaries*, *A&A* **352** L87, eprint: [astro-ph/9911054](#) (cit. on p. 131).
- Nelson, C. A. and P. P. Eggleton (2001), *A Complete Survey of Case A Binary Evolution with Comparison to Observed Algol-type Systems*, *ApJ* **552** 664 (cit. on p. 102).
- Neo, S. et al. (1977), *Effect of Rapid Mass Accretion onto the Main-Sequence Stars*, *PASJ* **29** 249 (cit. on p. 111).
- Nieuwenhuijzen, H. and C. de Jager (1990), *Parametrization of stellar rates of mass loss as functions of the fundamental stellar parameters M, L, and R*, *A&A* **231** 134 (cit. on pp. 72, 104).
- Nishizawa, A. et al. (2016), *eLISA eccentricity measurements as tracers of binary black hole formation*, *Phys. Rev. D* **94**, 064020 064020, arXiv: [1605.01341 \[gr-qc\]](#) (cit. on pp. 27, 92).
- Nomoto, K. et al. (2007), *Thermal Stability of White Dwarfs Accreting Hydrogen-rich Matter and Progenitors of Type Ia Supernovae*, *ApJ* **663** 1269 (cit. on p. 38).
- Oluseyi, H. M. et al. (2012), *Simulated LSST Survey of RR Lyrae Stars throughout the Local Group*, *AJ* **144**, 9 9 (cit. on pp. 30, 130).
- Öpik, E. (1938), *Stellar Structure, Source of Energy, and Evolution*, Publications of the Tartu Astrofizika Observatory **30** C1 (cit. on p. 5).

## Bibliography

---

- Oppenheimer, J. R. and H. Snyder (1939), *On Continued Gravitational Contraction*, Physical Review **56** 455 (cit. on p. 9).
- Orosz, J. A. et al. (2007), *A 15.65-solar-mass black hole in an eclipsing binary in the nearby spiral galaxy M 33*, Nature **449** 872, arXiv: 0710.3165 (cit. on p. 131).
- Owocki, S. P., K. G. Gayley and N. J. Shaviv (2004), *A Porosity-Length Formalism for Photon-Tiring-limited Mass Loss from Stars above the Eddington Limit*, ApJ **616** 525, eprint: astro-ph/0409573 (cit. on p. 13).
- Packet, W. (1981), *On the spin-up of the mass accreting component in a close binary system*, A&A **102** 17 (cit. on pp. 21, 107).
- Paczynski, B. (1976), “Common Envelope Binaries”, *Structure and Evolution of Close Binary Systems*, ed. by P. Eggleton, S. Mitton and J. Whelan, vol. 73, IAU Symposium 75 (cit. on pp. 21, 25).
- Paczyński, B. (1966), *Evolution of Close Binaries. I.*, Acta Astron. **16** 231 (cit. on p. 20).
- Pakull, M. W. and L. Mirioni (2003), “Bubble Nebulae around Ultraluminous X-Ray Sources”, *Revista Mexicana de Astronomia y Astrofisica Conference Series*, ed. by J. Arthur and W. J. Henney, vol. 15, Revista Mexicana de Astronomia y Astrofisica, vol. 27 197 (cit. on p. 68).
- Papadopoulos, A. et al. (2015), *DES13S2cmm: the first superluminous supernova from the Dark Energy Survey*, MNRAS **449** 1215, arXiv: 1501.07232 [astro-ph.HE] (cit. on p. 30).
- Pavlovskii, K. et al. (2016), *Stability of mass transfer from massive giants: double black-hole binary formation and ultra-luminous X-ray sources*, ArXiv e-prints, arXiv: 1606.04921 [astro-ph.HE] (cit. on p. 69).
- Pawlak, M. et al. (2013), *Eclipsing Binary Stars in the OGLE-III Fields of the Small Magellanic Cloud*, Acta Astron. **63** 323, arXiv: 1310.3272 [astro-ph.SR] (cit. on p. 18).
- Paxton, B., L. Bildsten et al. (2011), *Modules for Experiments in Stellar Astrophysics (MESA)*, ApJS **192**, 33, arXiv: 1009.1622 [astro-ph.SR] (cit. on pp. 27, 30, 31, 36, 49, 70, 103).
- Paxton, B., M. Cantiello et al. (2013), *Modules for Experiments in Stellar Astrophysics (MESA): Planets, Oscillations, Rotation, and Massive Stars*, ApJS **208**, 44, arXiv: 1301.0319 [astro-ph.SR] (cit. on pp. 27, 30, 31, 45, 49, 70, 103).
- Paxton, B., P. Marchant et al. (2015), *Modules for Experiments in Stellar Astrophysics (MESA): Binaries, Pulsations, and Explosions*, ApJS **220**, 15 15, arXiv: 1506.03146 [astro-ph.SR] (cit. on pp. 27, 49, 70, 103, 104).
- Payne, C. H. (1925), *Stellar Atmospheres; a Contribution to the Observational Study of High Temperature in the Reversing Layers of Stars.*, PhD thesis: RADCLIFFE COLLEGE. (cit. on p. 3).
- Peimbert, M., V. Luridiana and A. Peimbert (2007), *Revised Primordial Helium Abundance Based on New Atomic Data*, ApJ **666** 636, eprint: astro-ph/0701580 (cit. on pp. 50, 72).
- Pejcha, O. and T. A. Thompson (2015), *The Landscape of the Neutrino Mechanism of Core-collapse Supernovae: Neutron Star and Black Hole Mass Functions, Explosion Energies, and Nickel Yields*, ApJ **801**, 90 90, arXiv: 1409.0540 [astro-ph.HE] (cit. on p. 135).
- Peters, P. C. (1964), *Gravitational Radiation and the Motion of Two Point Masses*, Physical Review **136** 1224 (cit. on pp. 37, 131).
- Petrovic, J., N. Langer and K. A. van der Hucht (2005), *Constraining the mass transfer in massive binaries through progenitor evolution models of Wolf-Rayet+O binaries*, A&A **435** 1013 (cit. on pp. 14, 21, 30, 43, 102).
- Petrovic, J., N. Langer, S.-C. Yoon et al. (2005), *Which massive stars are gamma-ray burst progenitors?*, A&A **435** 247, eprint: astro-ph/0504175 (cit. on pp. 49, 70, 104).
- Pickering, E. C. (1890), *On the spectrum of zeta Ursae Majoris*, The Observatory **13** 80 (cit. on p. 17).
- Pietrukowicz, P. et al. (2013), *Eclipsing Binary Stars in the OGLE-III Galactic Disk Fields*, Acta Astron. **63** 115, arXiv: 1306.6324 [astro-ph.GA] (cit. on p. 18).

- 
- Pietrzyński, G. et al. (2013), *An eclipsing-binary distance to the Large Magellanic Cloud accurate to two per cent*, *Nature* **495** 76, arXiv: [1303.2063 \[astro-ph.GA\]](#) (cit. on p. 18).
- Piran, T. (2004), *The physics of gamma-ray bursts*, *Reviews of Modern Physics* **76** 1143, eprint: [astro-ph/0405503](#) (cit. on p. 16).
- Podsiadlowski, P., P. C. Joss and J. J. L. Hsu (1992), *Presupernova evolution in massive interacting binaries*, *ApJ* **391** 246 (cit. on p. 130).
- Podsiadlowski, P., S. Rappaport and Z. Han (2003), *On the formation and evolution of black hole binaries*, *MNRAS* **341** 385, eprint: [astro-ph/0207153](#) (cit. on pp. 73, 83, 89).
- Pols, O. R. (1994), *Case A evolution of massive close binaries: formation of contact systems and possible reversal of the supernova order*, *A&A* **290** 119 (cit. on p. 22).
- Pols, O. R. et al. (1995), *Approximate input physics for stellar modelling*, *MNRAS* **274** 964 (cit. on p. 37).
- Popham, R. and R. Narayan (1991), *Does accretion cease when a star approaches breakup?*, *ApJ* **370** 604 (cit. on pp. 21, 108).
- Portegies Zwart, S. F. and S. L. W. McMillan (2000), *Black Hole Mergers in the Universe*, *ApJ* **528** L17, eprint: [astro-ph/9910061](#) (cit. on p. 25).
- Postnov, K., L. Osokinova and J. M. Torrejón (2017), *A propelling neutron star in the enigmatic Be-star γ Cassiopeia*, *MNRAS* **465** L119, arXiv: [1610.07799 \[astro-ph.HE\]](#) (cit. on p. 128).
- Prestwich, A. H. et al. (2007), *The Orbital Period of the Wolf-Rayet Binary IC 10 X-1: Dynamic Evidence that the Compact Object Is a Black Hole*, *ApJ* **669** L21, arXiv: [0709.2892](#) (cit. on p. 131).
- Prokopenko, I. G. and M. R. Gilfanov (2009), *Normal galaxies in the all-sky survey by the eROSITA X-ray telescope of the Spectrum-X-Gamma observatory*, *Astronomy Letters* **35** 294 (cit. on p. 85).
- Rabe, W. (1958), *Bahnverbesserung durch Variationsbahnen für 8 Doppelsternsysteme*, *Astronomische Nachrichten* **284** 97 (cit. on p. 2).
- Raghavan, D. et al. (2010), *A Survey of Stellar Families: Multiplicity of Solar-type Stars*, *ApJS* **190** 1, arXiv: [1007.0414 \[astro-ph.SR\]](#) (cit. on p. 30).
- Rakavy, G. and G. Shaviv (1967), *Instabilities in Highly Evolved Stellar Models*, *ApJ* **148** 803 (cit. on p. 16).
- Ramírez-Agudelo, O. H. et al. (2015), *The VLT-FLAMES Tarantula Survey. XXI. Stellar spin rates of O-type spectroscopic binaries*, *A&A* **580**, A92 A92, arXiv: [1507.02286 \[astro-ph.SR\]](#) (cit. on p. 125).
- Rappaport, S. A., P. Podsiadlowski and E. Pfahl (2005), *Stellar-mass black hole binaries as ultraluminous X-ray sources*, *MNRAS* **356** 401, eprint: [astro-ph/0408032](#) (cit. on p. 69).
- Rappaport, S., P. C. Joss and F. Verbunt (1983), *A new technique for calculations of binary stellar evolution, with application to magnetic braking*, *ApJ* **275** 713 (cit. on pp. 33, 35, 39).
- Rappaport, S., P. C. Joss and R. F. Webbink (1982), *The evolution of highly compact binary stellar systems*, *ApJ* **254** 616 (cit. on p. 35).
- Rau, A. et al. (2009), *Exploring the Optical Transient Sky with the Palomar Transient Factory*, *PASP* **121** 1334, arXiv: [0906.5355 \[astro-ph.CO\]](#) (cit. on pp. 16, 98, 130).
- Repolust, T., J. Puls and A. Herrero (2004), *Stellar and wind parameters of Galactic O-stars. The influence of line-blocking/blanketing*, *A&A* **415** 349 (cit. on p. 10).
- Ricker, G. R. et al. (2015), *Transiting Exoplanet Survey Satellite (TESS)*, *Journal of Astronomical Telescopes, Instruments, and Systems* **1**, 014003 014003 (cit. on p. 30).
- Ritchie, B. W. et al. (2012), *The VLT-FLAMES survey of massive stars: NGC 346-013 as a test case for massive close binary evolution*, *A&A* **537**, A29 A29, arXiv: [1110.6325 \[astro-ph.SR\]](#) (cit. on p. 21).
- Ritter, H. (1988), *Turning on and off mass transfer in cataclysmic binaries*, *A&A* **202** 93 (cit. on p. 34).

- Robitaille, T. P. and B. A. Whitney (2010), *The Present-Day Star Formation Rate of the Milky Way Determined from Spitzer-Detected Young Stellar Objects*, *ApJ* **710** L11, arXiv: [1001.3672 \[astro-ph.GA\]](#) (cit. on p. 83).
- Rodriguez, C. L., S. Chatterjee and F. A. Rasio (2016), *Binary black hole mergers from globular clusters: Masses, merger rates, and the impact of stellar evolution*, *Phys. Rev. D* **93**, 084029 084029, arXiv: [1602.02444 \[astro-ph.HE\]](#) (cit. on p. 69).
- Rodriguez, C. L., C.-J. Haster et al. (2016), *Dynamical Formation of the GW150914 Binary Black Hole*, *ApJ* **824**, L8 L8, arXiv: [1604.04254 \[astro-ph.HE\]](#) (cit. on pp. 25, 27).
- Rodriguez, C. L., M. Morscher et al. (2015), *Binary Black Hole Mergers from Globular Clusters: Implications for Advanced LIGO*, *Physical Review Letters* **115**, 051101 051101, arXiv: [1505.00792 \[astro-ph.HE\]](#) (cit. on pp. 62, 137).
- Rodriguez, C. L., M. Zevin et al. (2016), *Illuminating Black Hole Binary Formation Channels with Spins in Advanced LIGO*, *ApJ* **832**, L2 L2, arXiv: [1609.05916 \[astro-ph.HE\]](#) (cit. on p. 27).
- Rogers, T. M. et al. (2013), *Internal Gravity Waves in Massive Stars: Angular Momentum Transport*, *ApJ* **772**, 21 21, arXiv: [1306.3262 \[astro-ph.SR\]](#) (cit. on p. 15).
- Russell, H. N. (1914), *Relations Between the Spectra and Other Characteristics of the Stars*, *Popular Astronomy* **22** 275 (cit. on p. 4).
- Ruszkowski, M. and M. C. Begelman (2003), *Eddington Limit and Radiative Transfer in Highly Inhomogeneous Atmospheres*, *ApJ* **586** 384, eprint: [astro-ph/0204256](#) (cit. on p. 68).
- Sacco, G. G. et al. (2015), *The Gaia-ESO survey: Discovery of a spatially extended low-mass population in the Vela OB2 association*, *A&A* **574**, L7 L7, arXiv: [1501.01330 \[astro-ph.SR\]](#) (cit. on p. 30).
- Sampson, R. A. (1895), *On the Rotation and Mechanical State of the Sun*, *MmRAS* **51** 123 (cit. on p. 5).
- Sana, H. et al. (2012), *Binary Interaction Dominates the Evolution of Massive Stars*, *Science* **444** 337 (cit. on pp. 15, 18, 22, 30, 102, 115, 125, 129).
- Sandage, A. R. and M. Schwarzschild (1952), *Inhomogeneous Stellar Models. II. Models with Exhausted Cores in Gravitational Contraction.*, *ApJ* **116** 463 (cit. on pp. 5, 102).
- Sandage, A. et al. (1966), *On the optical identification of SCO X-1*, *ApJ* **146** 316 (cit. on p. 17).
- Sanyal, D. et al. (2015), *Massive main-sequence stars evolving at the Eddington limit*, *A&A* **580**, A20 A20, arXiv: [1506.02997 \[astro-ph.SR\]](#) (cit. on pp. 13, 56).
- Schneider, F. R. N. et al. (2014), *Bonnsai: a Bayesian tool for comparing stars with stellar evolution models*, *A&A* **570**, A66 A66, arXiv: [1408.3409 \[astro-ph.SR\]](#) (cit. on p. 130).
- Schönberg, M. and S. Chandrasekhar (1942), *On the Evolution of the Main-Sequence Stars.*, *ApJ* **96** 161 (cit. on p. 5).
- Sesana, A. (2016), *Prospects for Multiband Gravitational-Wave Astronomy after GW150914*, *Physical Review Letters* **116**, 231102 231102, arXiv: [1602.06951 \[gr-qc\]](#) (cit. on pp. 25, 92).
- Shaviv, N. J. (2001), *The theory of steady-state super-Eddington winds and its application to novae*, *MNRAS* **326** 126, eprint: [astro-ph/0008489](#) (cit. on p. 13).
- Shen, K. J. and L. Bildsten (2007), *Thermally Stable Nuclear Burning on Accreting White Dwarfs*, *ApJ* **660** 1444 (cit. on p. 38).
- Siess, L. (2009), *Thermohaline mixing in super-AGB stars*, *A&A* **497** 463 (cit. on p. 14).
- Silverman, J. M. and A. V. Filippenko (2008), *On IC 10 X-1, the Most Massive Known Stellar-Mass Black Hole*, *ApJ* **678**, L17 L17, arXiv: [0802.2716](#) (cit. on p. 69).
- Skumanich, A. (1972), *Time Scales for CA II Emission Decay, Rotational Braking, and Lithium Depletion*, *ApJ* **171** 565 (cit. on p. 33).
- Smak, J. (1962), *Close Binaries. II. A Preliminary Discussion of the Subgiants in Close-binary Systems*, *Acta Astron.* **12** 28 (cit. on p. 21).

- 
- Smartt, S. J. (2015), *Observational Constraints on the Progenitors of Core-Collapse Supernovae: The Case for Missing High-Mass Stars*, PASA **32**, e016 e016, arXiv: [1504.02635 \[astro-ph.SR\]](#) (cit. on p. 130).
- Smith, N. (2014), *Mass Loss: Its Effect on the Evolution and Fate of High-Mass Stars*, ARA&A **52** 487, arXiv: [1402.1237 \[astro-ph.SR\]](#) (cit. on p. 10).
- Smith, N., R. D. Gehrz et al. (2003), *Mass and Kinetic Energy of the Homunculus Nebula around η Carinae*, AJ **125** 1458 (cit. on p. 12).
- Smith, N., W. Li et al. (2011), *Observed fractions of core-collapse supernova types and initial masses of their single and binary progenitor stars*, MNRAS **412** 1522, arXiv: [1006.3899 \[astro-ph.HE\]](#) (cit. on p. 130).
- Smith, R. M. et al. (2014), “The Zwicky transient facility observing system”, *Ground-based and Airborne Instrumentation for Astronomy V*, vol. 9147, Proc. SPIE 914779 (cit. on p. 98).
- Soberman, G. E., E. S. Phinney and E. P. J. van den Heuvel (1997), *Stability criteria for mass transfer in binary stellar evolution.*, A&A **327** 620 (cit. on pp. 21, 32, 34).
- Socrates, A. and S. W. Davis (2006), *Ultraluminous X-Ray Sources Powered by Radiatively Efficient Two-Phase Super-Eddington Accretion onto Stellar-Mass Black Holes*, ApJ **651** 1049, eprint: [astro-ph/0511549](#) (cit. on p. 68).
- Song, H. F. et al. (2016), *Massive star evolution in close binaries. Conditions for homogeneous chemical evolution*, A&A **585**, A120 A120, arXiv: [1508.06094 \[astro-ph.SR\]](#) (cit. on pp. 48, 69, 102).
- Sonneborn, G., B. Altner and R. P. Kirshner (1987), *The progenitor of SN 1987A - Spatially resolved ultraviolet spectroscopy of the supernova field*, ApJ **323** L35 (cit. on p. 9).
- Spera, M., M. Mapelli and A. Bressan (2015), *The mass spectrum of compact remnants from the PARSEC stellar evolution tracks*, MNRAS **451** 4086, arXiv: [1505.05201 \[astro-ph.SR\]](#) (cit. on p. 68).
- Spruit, H. C. (2002), *Dynamo action by differential rotation in a stably stratified stellar interior*, A&A **381** 923, eprint: [astro-ph/0108207](#) (cit. on pp. 14, 70, 104).
- Stancliffe, R. J., L. Fossati et al. (2015), *Confronting uncertainties in stellar physics: calibrating convective overshooting with eclipsing binaries*, A&A **575**, A117 A117, arXiv: [1501.05322 \[astro-ph.SR\]](#) (cit. on p. 13).
- Stancliffe, R. J. and E. Glebbeek (2008), *Thermohaline mixing and gravitational settling in carbon-enhanced metal-poor stars*, MNRAS **389** 1828, arXiv: [0807.1758](#) (cit. on p. 14).
- Stancliffe, R. J. and J. J. Eldridge (2009), *Modelling the binary progenitor of Supernova 1993J*, MNRAS **396** 1699 (cit. on p. 37).
- Stanway, E. R., J. J. Eldridge and G. D. Becker (2016), *Stellar population effects on the inferred photon density at reionization*, MNRAS **456** 485, arXiv: [1511.03268](#) (cit. on p. 102).
- Suijs, M. P. L. et al. (2008), *White dwarf spins from low-mass stellar evolution models*, A&A **481** L87, arXiv: [0802.3286](#) (cit. on p. 14).
- Sukhbold, T. et al. (2016), *Core-collapse Supernovae from 9 to 120 Solar Masses Based on Neutrino-powered Explosions*, ApJ **821**, 38 38, arXiv: [1510.04643 \[astro-ph.HE\]](#) (cit. on pp. 68, 91, 92).
- Sutton, A. D., T. P. Roberts, J. C. Gladstone et al. (2015), *The hyperluminous X-ray source candidate in IC 4320: another HLX bites the dust*, MNRAS **450** 787, arXiv: [1503.01711 \[astro-ph.HE\]](#) (cit. on p. 69).
- Sutton, A. D., T. P. Roberts, D. J. Walton et al. (2012), *The most extreme ultraluminous X-ray sources: evidence for intermediate-mass black holes?*, MNRAS **423** 1154, arXiv: [1203.4100 \[astro-ph.HE\]](#) (cit. on p. 69).
- Swartz, D. A. et al. (2011), *A Complete Sample of Ultraluminous X-ray Source Host Galaxies*, ApJ **741**, 49 49, arXiv: [1108.1372 \[astro-ph.HE\]](#) (cit. on pp. 19, 68, 69, 83–85).

- Szécsi, D. et al. (2015), *Low-metallicity massive single stars with rotation. Evolutionary models applicable to I Zwicky 18*, *A&A* **581**, A15 A15, arXiv: [1506.09132 \[astro-ph.SR\]](#) (cit. on pp. 48, 51, 56, 79).
- Taam, R. E. and E. L. Sandquist (2000), *Common Envelope Evolution of Massive Binary Stars*, *ARA&A* **38** 113 (cit. on pp. 22, 48).
- Tauris, T. M., R. P. Fender et al. (1999), *Circinus X-1: survivor of a highly asymmetric supernova*, *MNRAS* **310** 1165, eprint: [astro-ph/9909148](#) (cit. on p. 92).
- Tauris, T. M., N. Langer and P. Podsiadlowski (2015), *Ultra-stripped supernovae: progenitors and fate*, *MNRAS* **451** 2123, arXiv: [1505.00270 \[astro-ph.SR\]](#) (cit. on p. 73).
- Tauris, T. M. and E. P. J. van den Heuvel (2006), “Formation and evolution of compact stellar X-ray sources”, *Compact stellar X-ray sources*, ed. by W. H. G. Lewin and M. van der Klis 623 (cit. on pp. 17, 22, 37, 135).
- Tauris, T. M., E. P. J. van den Heuvel and G. J. Savonije (2000), *Formation of Millisecond Pulsars with Heavy White Dwarf Companions: Extreme Mass Transfer on Subthermal Timescales*, *ApJ* **530** L93, eprint: [astro-ph/0001013](#) (cit. on p. 89).
- Taylor, P. and C. Kobayashi (2015), *Quantifying AGN-driven metal-enhanced outflows in chemodynamical simulations*, *MNRAS* **452** L59, arXiv: [1506.08957](#) (cit. on p. 64).
- The LIGO Scientific Collaboration et al. (2016a), *Binary Black Hole Mergers in the first Advanced LIGO Observing Run*, ArXiv e-prints, arXiv: [1606.04856 \[gr-qc\]](#) (cit. on pp. 23, 24).
- (2016b), *The Rate of Binary Black Hole Mergers Inferred from Advanced LIGO Observations Surrounding GW150914*, ArXiv e-prints, arXiv: [1602.03842 \[astro-ph.HE\]](#) (cit. on p. 129).
- Thorne, K. S. (1974), *Disk-Accretion onto a Black Hole. II. Evolution of the Hole*, *ApJ* **191** 507 (cit. on p. 74).
- Torres, G., J. Andersen and A. Giménez (2010), *Accurate masses and radii of normal stars: modern results and applications*, *A&A Rev.* **18** 67, arXiv: [0908.2624 \[astro-ph.SR\]](#) (cit. on pp. 13, 30).
- Tout, C. A. et al. (1997), *Rapid binary star evolution for N-body simulations and population synthesis*, *MNRAS* **291** 732 (cit. on p. 33).
- Tutukov, A. V. and L. R. Yungelson (1993), *The merger rate of neutron star and black hole binaries*, *MNRAS* **260** 675 (cit. on p. 25).
- Tylenda, R. et al. (2011), *V1309 Scorpii: merger of a contact binary*, *A&A* **528**, A114 A114, arXiv: [1012.0163 \[astro-ph.SR\]](#) (cit. on p. 22).
- Tyson, J. A. (2002), “Large Synoptic Survey Telescope: Overview”, *Survey and Other Telescope Technologies and Discoveries*, ed. by J. A. Tyson and S. Wolff, vol. 4836, Proc. SPIE 10, eprint: [astro-ph/0302102](#) (cit. on p. 98).
- Ugliano, M. et al. (2012), *Progenitor-explosion Connection and Remnant Birth Masses for Neutrino-driven Supernovae of Iron-core Progenitors*, *ApJ* **757**, 69 69, arXiv: [1205.3657 \[astro-ph.SR\]](#) (cit. on p. 135).
- Ulrich, R. K. and H. L. Burger (1976), *The accreting component of mass-exchange binaries*, *ApJ* **206** 509 (cit. on p. 36).
- Valsecchi, F. et al. (2010), *Formation of the black-hole binary M33 X-7 through mass exchange in a tight massive system*, *Nature* **468** 77, arXiv: [1010.4809 \[astro-ph.SR\]](#) (cit. on p. 135).
- van den Heuvel, E. P. J. (1976), “Late Stages of Close Binary Systems”, *Structure and Evolution of Close Binary Systems*, ed. by P. Eggleton, S. Mitton and J. Whelan, vol. 73, IAU Symposium 35 (cit. on p. 21).
- van Rensbergen, W. et al. (2008), *Spin-up and hot spots can drive mass out of a binary*, *A&A* **487** 1129, arXiv: [0804.1215](#) (cit. on p. 21).

- 
- Verbunt, F. and C. Zwaan (1981), *Magnetic braking in low-mass X-ray binaries*, A&A **100** L7 (cit. on p. 33).
- Vink, J. S. and A. de Koter (2005), *On the metallicity dependence of Wolf-Rayet winds*, A&A **442** 587, eprint: [astro-ph/0507352](#) (cit. on pp. 11, 51).
- Vink, J. S., A. de Koter and H. J. G. L. M. Lamers (2001), *Mass-loss predictions for O and B stars as a function of metallicity*, A&A **369** 574, eprint: [astro-ph/0101509](#) (cit. on pp. 11, 49, 72, 104).
- Vogel, H. C. (1890), *Spectrographische Beobachtungen an Algol*, Astronomische Nachrichten **123** 289 (cit. on p. 17).
- Voss, R. and T. M. Tauris (2003), *Galactic distribution of merging neutron stars and black holes - prospects for short gamma-ray burst progenitors and LIGO/VIRGO*, MNRAS **342** 1169, eprint: [astro-ph/0303227](#) (cit. on p. 61).
- Vreeswijk, P. M. et al. (2014), *The Hydrogen-poor Superluminous Supernova iPTF 13ajg and its Host Galaxy in Absorption and Emission*, ApJ **797**, 24 24, arXiv: [1409.8287 \[astro-ph.HE\]](#) (cit. on p. 30).
- Webster, B. L. and P. Murdin (1972), *Cygnus X-1-a Spectroscopic Binary with a Heavy Companion ?*, Nature **235** 37 (cit. on p. 17).
- Weisberg, J. M., D. J. Nice and J. H. Taylor (2010), *Timing Measurements of the Relativistic Binary Pulsar PSR B1913+16*, ApJ **722** 1030, arXiv: [1011.0718 \[astro-ph.GA\]](#) (cit. on p. 48).
- Weisberg, J. M. and J. H. Taylor (2005), *The Relativistic Binary Pulsar B1913+16: Thirty Years of Observations and Analysis*, ASP Conference Series **328** 25 (cit. on p. 31).
- Wellstein, S. and N. Langer (1999), *Implications of massive close binaries for black hole formation and supernovae*, A&A **350** 148, eprint: [astro-ph/9904256](#) (cit. on pp. 14, 21, 102).
- Wellstein, S., N. Langer and H. Braun (2001), *Formation of contact in massive close binaries*, A&A **369** 939 (cit. on pp. 14, 22, 38, 42, 102, 111).
- Wheeler, J. C. (1977), *Final evolution of stars in the range 1,000 to 10,000 solar masses*, Ap&SS **50** 125 (cit. on p. 16).
- Whyte, C. A. and P. P. Eggleton (1980), *Comments on the evolution and origin of cataclysmic binaries*, MNRAS **190** 801 (cit. on p. 35).
- Wickramasinghe, D. T., C. A. Tout and L. Ferrario (2014), *The most magnetic stars*, MNRAS **437** 675, arXiv: [1310.2696 \[astro-ph.SR\]](#) (cit. on pp. 22, 130).
- Willson, L. A. (2000), *Mass Loss From Cool Stars: Impact on the Evolution of Stars and Stellar Populations*, ARA&A **38** 573 (cit. on p. 11).
- Wood, T. S., P. Garaud and S. Stellmach (2013), *A New Model for Mixing by Double-diffusive Convection (Semi-convection). II. The Transport of Heat and Composition through Layers*, ApJ **768**, 157 157, arXiv: [1212.1218 \[astro-ph.SR\]](#) (cit. on p. 14).
- Woosley, S. E. (1993), *Gamma-ray bursts from stellar mass accretion disks around black holes*, ApJ **405** 273 (cit. on pp. 16, 58, 59, 69, 76, 129).
- (2016), *Pulsational-Pair Instability Supernovae*, ArXiv e-prints, arXiv: [1608.08939 \[astro-ph.HE\]](#) (cit. on pp. 16, 72, 76, 91).
- Woosley, S. E., S. Blinnikov and A. Heger (2007), *Pulsational pair instability as an explanation for the most luminous supernovae*, Nature **450** 390, arXiv: [0710.3314](#) (cit. on pp. 16, 59, 129).
- Woosley, S. E. and A. Heger (2006), *The Progenitor Stars of Gamma-Ray Bursts*, ApJ **637** 914, eprint: [astro-ph/0508175](#) (cit. on pp. 14, 16, 48, 102).
- Yoon, S.-C., A. Dierks and N. Langer (2012), *Evolution of massive Population III stars with rotation and magnetic fields*, A&A **542**, A113 A113, arXiv: [1201.2364 \[astro-ph.SR\]](#) (cit. on pp. 14, 56, 102).
- Yoon, S.-C. and N. Langer (2005), *Evolution of rapidly rotating metal-poor massive stars towards gamma-ray bursts*, A&A **443** 643, eprint: [astro-ph/0508242](#) (cit. on pp. 14, 48, 102).

- Yoon, S.-C., N. Langer and C. Norman (2006), *Single star progenitors of long gamma-ray bursts. I. Model grids and redshift dependent GRB rate*, *A&A* **460** 199, eprint: [astro-ph/0606637](#) (cit. on pp. 14, 16, 48, 49, 56, 70, 74, 75, 102, 104).
- Yuan, F. et al. (2015), *OzDES multi-fibre spectroscopy for the Dark Energy Survey: first-year operation and results*, ArXiv e-prints, arXiv: [1504.03039](#) (cit. on p. 30).
- Yungelson, L. (1973), *Evolution of the secondary component of a close binary system*, *Nauchnye Informatsii* **27** 93 (cit. on p. 20).
- Zahn, J.-P. (1975), *The dynamical tide in close binaries*, *A&A* **41** 329 (cit. on pp. 21, 72, 104). – (1977), *Tidal friction in close binary stars*, *A&A* **57** 383 (cit. on pp. 21, 43–45, 72, 104).
- Zampieri, L. and T. P. Roberts (2009), *Low-metallicity natal environments and black hole masses in ultraluminous X-ray sources*, *MNRAS* **400** 677, arXiv: [0909.1017 \[astro-ph.HE\]](#) (cit. on p. 68).
- Zaussinger, F. and H. C. Spruit (2013), *Semiconvection: numerical simulations*, *A&A* **554**, A119 A119, arXiv: [1303.4522 \[astro-ph.SR\]](#) (cit. on p. 14).
- Zorotovic, M., M. R. Schreiber and B. T. Gänsicke (2011), “Post-Common-Envelope Binaries from SDSS: Constraining the Common-Envelope Efficiency”, *Evolution of Compact Binaries*, ed. by L. Schmidtobreick, M. R. Schreiber and C. Tappert, vol. 447, Astronomical Society of the Pacific Conference Series 113 (cit. on p. 48).
- Zorotovic, M., M. R. Schreiber, B. T. Gänsicke and A. Nebot Gómez-Morán (2010), *Post-common-envelope binaries from SDSS. IX: Constraining the common-envelope efficiency*, *A&A* **520**, A86 A86, arXiv: [1006.1621 \[astro-ph.SR\]](#) (cit. on p. 22).

---

## Publication list

- M. Kruckow, T. Tauris, N. Langer, D. Szecsi, P. Marchant, P. Podsiadlowski. Common envelope ejection in massive binary stars. Implications for the progenitors of GW150914 and GW151226, *A&A*, in press, December 2016.
- A. Istrate, G. Fontaine, A. Gianninas, L. Grassitelli, P. Marchant, T.M. Tauris, N. Langer. Asteroseismic test of rotational mixing in low-mass white dwarfs, *A&A*, 595:L12, November 2016.
- A. Istrate, P. Marchant, T. M. Tauris, N. Langer, R. J. Stancliffe and L. Grassitelli. Models of low-mass helium white dwarfs including gravitational settling, thermal and chemical diffusion, and rotational mixing, *A&A*, 595:A35, October 2016.
- P. Marchant, N. Langer, P. Podsiadlowski, T. M. Tauris, and T. J. Moriya. A new route towards merging massive black holes. *A&A*, 588:A50, April 2016.
- B. Paxton, P. Marchant, J. Schwab, E. B. Bauer, L. Bildsten, M. Cantiello, L. Dessart, R. Farmer, H. Hu, N. Langer, R. H. D. Townsend, D. M. Townsley, and F. X. Timmes. Modules for Experiments in Stellar Astrophysics (MESA): Binaries, Pulsations, and Explosions. *ApJS*, 220:15, September 2015.
- J. Brooks, L. Bildsten, P. Marchant, and B. Paxton. AM Canum Venaticorum Progenitors with Helium Star Donors and the Resultant Explosions. *ApJ*, 807:74, July 2015.
- J. Vos, R. H. Østensen, P. Marchant, and H. Van Winckel. Testing eccentricity pumping mechanisms to model eccentric long-period sdB binaries with MESA. *A&A*, 579:A49, July 2015.
- F. Valsecchi, S. Rappaport, F. A. Rasio, P. Marchant, and L. A. Rogers. Tidally-driven Roche-Lobe Overflow of Hot Jupiters with MESA. *ApJ*, 813:101, June 2015.
- P. Marchant, A. Reisenegger, J. Alejandro Valdivia, and J. H. Hoyos. Stability of Hall Equilibria in Neutron Star Crusts. *ApJ*, 796:94, December 2014.
- C. Armaza, A. Reisenegger, J. A. Valdivia, and P. Marchant. On magnetic fields in barotropic stars. In *Revista Mexicana de Astronomia y Astrofisica Conference Series*, volume 44 of *Revista Mexicana de Astronomia y Astrofisica*, vol. 27, pages 147–148, October 2014.
- C. Armaza, A. Reisenegger, J. A. Valdivia, and P. Marchant. Magnetohydrodynamic equilibria in barotropic stars. In P. Petit, M. Jardine, and H. C. Spruit, editors, *IAU Symposium*, volume 302 of *IAU Symposium*, pages 419–422, August 2014.
- T. Akgün, A. Reisenegger, A. Mastrano, and P. Marchant. Stability of magnetic fields in non-barotropic stars: an analytic treatment. *MNRAS*, 433:2445–2466, August 2013.
- P. Marchant, Reisenegger. A., and T. Akgün. Formal proof of the Flowers-Ruderman instability mechanism in magnetic stars. *Boletin de la Asociacion Argentina de Astronomia La Plata Argentina*, 54:81–84, 2011.
- P. Marchant, A. Reisenegger, and T. Akgün. Revisiting the Flowers-Ruderman instability of magnetic stars. *MNRAS*, 415:2426–2438, August 2011.